

# Theories of topologically-induced phenomena in skyrmion-hosting magnetoelectric insulators

THÈSE N° 8163 (2017)

PRÉSENTÉE LE 13 NOVEMBRE 2017  
À LA FACULTÉ DES SCIENCES DE BASE  
LABORATOIRE DE MAGNÉTISME QUANTIQUE  
PROGRAMME DOCTORAL EN PHYSIQUE

ÉCOLE POLYTECHNIQUE FÉDÉRALE DE LAUSANNE

POUR L'OBTENTION DU GRADE DE DOCTEUR ÈS SCIENCES

PAR

Oleksandr KRIUCHKOV

acceptée sur proposition du jury:

Prof. O. Schneider, président du jury  
Prof. H. M. Rønnow, directeur de thèse  
Prof. S. Seki, rapporteur  
Prof. J. Zang, rapporteur  
Prof. F. Carbone, rapporteur



ÉCOLE POLYTECHNIQUE  
FÉDÉRALE DE LAUSANNE

Suisse  
2017



# THEORIES OF TOPOLOGICALLY-INDUCED PHENOMENA IN SKYRMION-HOSTING MAGNETOELECTRIC INSULATORS

## ABSTRACT

There once was a harsh competition between different computer memory technologies, and now we cheer triumph for the Random Access-Memory (RAM) devices, – cheap, fast, tiny, stable. The competing Magnetic Bubble Memory had faded away as magnetic bubbles are undesirably large and pretty much not robust, manifesting both low data density and high operational costs. However, what we do possess now are nanosize objects of topological nature, *magnetic skyrmions*, which are protected from continuous field variations and take very little energy cost to be moved. Thus, skyrmions are considered as promising information carriers for future memory devices and ultradense data storage, while skyrmion phases in bulk materials are interesting from fundamental point of view in exploring topological states of matter.

In this thesis, I develop and advance several effective theoretical approaches, diverse both in their methods and use, which were of appeal for several skyrmionic experiments in our lab (LQM/EPFL). We were and are primarily interested in the open issues in the applied field of *skyrmionics*, which may be taken under the umbrella of creation, stabilization and control of magnetic skyrmions under electric fields, mechanical strains, thermal gradients, etc. For the goals achieved and yet to be achieved, the *magnetoelectric insulator*  $\text{Cu}_2\text{OSeO}_3$ , which uniquely responses to all the above mentioned fields, is a highly advantageous candidate. *Magnetoelectric* here means that the spins of a magnetic material are coupled to external electric fields, while insulating properties are very advantageous to preserve both the state and the very existence of skyrmions by eliminating the Joule heating.

The novel results in this thesis are calculations for both individual and arrayed skyrmions under electric fields, mechanical strains and uniform pressures, and thermal gradients. Furthermore, several fundamental questions were addressed by developing an extended formalism for calculation skyrmion-pocket phase diagrams, studying the topologically-governed crossover between skyrmions and magnetic bubbles, and dis-

cussing the possible role of merons (half-skyrmions) in skyrmion phase formation. The result with the most immediate appeal is probably the theoretical and experimental study of skyrmion lattices in electric fields, with a direct demonstration of writing and erasing of the full skyrmion phase under electric fields of few Volts per micrometer, as compatible with modern microelectronic devices.

**Keywords:** *magnetism, skyrmions, topology, chiral magnets, magnetoelectricity, magnetic memory, phase diagrams, effective field theories, quasiparticle formalism, physical modelling.*



# THEORIEN TOPOLOGISCH INDUZierter PHÄNOMENE IN SKYRMIONENTRAGENDEN MAGNETOELEKTRISCHEN ISOLATOREN

## ZUSAMMENFASSUNG

Nachdem es einst einen harten Wettbewerb zwischen verschiedenen Computerspeichertechnologien gab, feiern wir mittlerweile den Triumph von günstigen, schnellen, kleinen und stabilen Geräten mit Random Access Memory (Direktzugriffsspeicher, RAM). Der Magnetblasenspeicher als Konkurrent geriet bald ins Hintertreffen, da magnetische Blasen einerseits unerwünscht gross und andererseits nicht sehr robust sind, was zu sowohl niedriger Datendichte als auch zu hohen Unterhaltskosten führt. Jedoch verfügen wir jetzt über Nanoobjekte topologischer Natur, *magnetische Skyrmionen*, die vor kontinuierlichen Feldänderungen geschützt sind und mit geringen Energieaufwand bewegt werden können. Daher werden die Skyrmionenphasen als vielversprechende Informationsträger für künftige Speichergeräte und ultradichte Datenspeicher betrachtet, wobei Skyrmionenphasen im Festkörper aus fundamentalen Gesichtspunkten in der Erforschung topologischer Materiezustände ebenso interessant sind.

In dieser Arbeit werden verschiedene effektive theoretische Zugänge entwickelt, jeweils mit mannigfaltigen Methoden und Anwendungen, welche verschiedenen aktuellen skyrmionischen Experimenten in unserem Labor (LQM/EPFL) zugutekamen. Wir waren und sind vor allem interessiert an offenen Fragen im angewandten Feld der *Skyrmionik*, welche unter anderem die Erzeugung, Stabilisierung und Kontrolle magnetischer Skyrmionen mittels einfacher und nicht-flüchtiger Methoden unter dem Einfluss von z.B. elektrischem Feld, mechanischer Belastung und Temperaturgradienten umfasst. Für die erreichten und zu erreichenden Ziele ist der *magnetoelektrische Isolator*  $\text{Cu}_2\text{OSeO}_3$ , welcher einzigartigerweise auf alle oben erwähnten Felder anspricht, ein sehr vorteilhafter Kandidat. *Magnetoelektrisch* bedeutet in diesem Falle, dass die Spins des magnetischen Materials mit externen elektrischen Feldern koppeln, während die isolatorischen Eigenschaften sehr vorteilhaft zur Erhaltung sowohl des Zustandes als auch der blossen Existenz des Skyrmions sind, da sie die Effekte joulescher Wärme eliminieren.

Die neuen Resultate dieser Arbeit sind Berechnungen sowohl an individuellen als

auch an Anordnungen von Skyrmionen unter elektrischen Feldern, mechanischer Belastung, uniformem Druck und Temperaturgradienten. Es wurde weiterhin ein erweiterter Formalismus eingeführt, welcher verschiedene fundamentale Fragen betrachtet: die Berechnung von Skyrmionenträger-Phasendiagrammen, die Untersuchung des topologisch beherrschten Übergangs zwischen Skyrmionen und magnetischen Blasen und eine Diskussion der möglichen Rolle von Meronen (*halber* Skyrmionen) bei der Schmelze von Skyrmionenkristallen. Das eindrucksvollste Resultat ist wohl die theoretische und experimentelle Untersuchung von Skyrmionengittern in elektrischen Feldern, mit einer direkten Demonstration des Schreibens und Löschens der kompletten Skyrmionenphase mittels einer Spannung von einigen Volt pro Mikrometer, einem typischen Wert für moderne mikroelektronische Geräte.

**Stichwörter:** *Magnetismus, Skyrmionen, Topologie, Chirale Magneten, Magnetische Speicher, Magnetoelektrizität, Phasendiagramme, effektive Feldtheorien, Quasiteilchen, Topologischer Schutz, physikalische Modellierung.*

# ÉTUDES THÉORIQUE DE PHÉNOMÈNES TOPOLOGIQUEMENT-INDUIT DANS DES ISOLANTS MAGNÉTOÉLECTRIQUES SKYRMIONIQUE

## RÉSUMÉ

Il y avait jadis une dure compétition entre différents systèmes de stockage de mémoire informatique - compétition remportée par la mémoire vive (ou RAM) qui a l'avantage d'être bon marché, rapide, compacte et stable. Les mémoires à bulles magnétique ont peu à peu disparu à cause de leur grande taille et leur manque de robustesse, impliquant une faible densité de stockage et des coûts de fonctionnement très élevés. Cependant, nous avons découvert des objets de nature topologique d'échelle nanoscopique, les *skyrmions magnétiques*, qui ont la particularité d'être insensibles aux variations continues de champ et dont la mise en mouvement requiert peu de coût en terme d'énergie. La communauté scientifique fonde ainsi de grands espoirs en ces skyrmions afin de créer une nouvelle génération de systèmes de stockage de mémoire ultradenses ainsi que de nouveaux moyens de transport de données. L'étude des skyrmions d'un point de vue purement fondamental a également connu un essort impressionnant ces dernières années, ceux-ci présentant un grand intérêt dans l'optique d'explorer les différents états topologiques de la matière.

Dans cette thèse, je développe et améliore plusieurs approches théoriques, différant de par leur méthode et leur application, qui ont été largement utilisées lors du développement d'expériences de pointe sur les skyrmions dans notre laboratoire (LQM/EPFL). Nous nous sommes particulièrement intéressés au domaine, encore en phase de développement, de la *skyrmionique*, plus précisément à la stabilisation et au contrôle de skyrmions magnétiques au travers de méthodes simples et non volatiles - sous l'application de champs électriques, contraintes mécaniques, gradients de température, etc. Pour atteindre nos objectifs expérimentaux, un candidat naturel a été l'*isolant magnetoélectrique*  $\text{Cu}_2\text{OSeO}_3$  qui possède une réponse unique à chacune des contraintes précédemment mentionnées. Par *magnetoélectrique*, il est entendu que les spins du matériau magnétique se couplent avec un champ électrique externe, tandis que ses propriétés isolantes permettent de préserver l'état du système ainsi que l'existence même des skyrmions en

éliminant l'effet Joule.

Les contributions que j'apporte à ce domaine au travers de ce travail de doctorat consistent en plusieurs développements théoriques décrivant à la fois des skyrmions isolés et des systèmes entiers soumis à des champs électriques, contraintes mécaniques et pressions uniformes, ainsi que des gradients thermiques. De plus, une série de questions fondamentales ont été soulevées en développant un formalisme avancé permettant de tracer le diagramme de phases de matériaux pouvant potentiellement accueillir des skyrmions. Ces nouvelles zones d'ombre sont apparues lors de l'étude du crossover, de nature topologiquement préservé, entre les skyrmions et les bulles magnétiques ainsi qu'en analysant l'influence potentielle des mereons (mi-skyrmions) dans la transition de la phase topologiquement triviale à la phase skyrmionique. Notre résultat le plus intéressant a sans doute été obtenu lors de l'étude théorique et expérimentale de réseaux de skyrmions dans un champ électrique, mettant en évidence la création et disparition totale de la phase skyrmionique sous l'effet d'une tension de quelques Volts par micromètre seulement, configuration présente dans les appareils microélectroniques modernes.

**Mots clés:** *magnétisme, skyrmions, topologie, aimants chiraux, mémoire magnétique, magnétoélectricité, diagrammes de phase, théories de champ effectifs, quasiparticules, protection topologique, modélisation physique.*

# Contents

<b>1</b>	<b>INTRODUCTION</b>	<b>1</b>
<b>2</b>	<b>MAGNETIC SKYRMIONS: TOPOLOGY, STABILITY AND QUASIPARTICLE PROPERTIES</b>	<b>9</b>
2.1	Topological invariants . . . . .	11
2.2	Skyrmion energetics: a variational approach . . . . .	18
2.3	Skyrmion tails . . . . .	24
2.4	Conclusions . . . . .	25
<b>3</b>	<b>UNIVERSALITY OF PHASE DIAGRAMS IN BULK SKYRMION-HOSTING MATERIALS</b>	<b>27</b>
3.1	Mean-field model and its limitations . . . . .	29
3.2	Solution in helical phase . . . . .	34
3.3	Solution in conical phase . . . . .	37
3.4	Solution in skyrmion lattice phase . . . . .	40
3.5	Importance of critical fluctuations . . . . .	46
3.6	Susceptibility tensor and mean-field fluctuation spectrum . . . . .	49
3.7	Free energy in non-interacting quasiparticle approach . . . . .	51
3.8	Conclusions . . . . .	55
<b>4</b>	<b>WRITING AND ERASING MAGNETIC SKYRMIONS WITH ELECTRIC FIELDS</b>	<b>57</b>
4.1	Energy of isolated skyrmions under electric fields . . . . .	58
4.2	Skyrmion lattice in electric fields . . . . .	60
4.3	Writing and erasing skyrmions . . . . .	74
4.4	Conclusions . . . . .	83
<b>5</b>	<b>MAGNETIC SKYRMIONS UNDER PRESSURE</b>	<b>85</b>
5.1	Stabilization of a single skyrmion under uniaxial mechanical strain . . . .	86
5.2	Dramatic pressure-induced stabilization of the skyrmion phase in Cu <sub>2</sub> OSeO <sub>3</sub> : Experiment and Theory . . . . .	90
5.3	Conclusions . . . . .	100

6	TOPOLOGICAL OBJECTS IN THIN FILMS: MAGNETIC SKYRMIONS, CHIRAL BUBBLES, MERONS AND BIMERONS	<b>101</b>
6.1	Magnetic skyrmions under thermal gradients . . . . .	102
6.2	Topologically-preserved crossover between skyrmions and magnetic bubbles in thin films . . . . .	108
6.3	Merons, bimerons and toy model of topological charge saturation . . . .	118
6.4	Conclusions . . . . .	123
7	CONCLUSIONS AND OVERVIEW	<b>125</b>
	REFERENCES	<b>139</b>

# List of Figures

1.1	Swiss Cheese Topology . . . . .	2
1.2	Haldane Gap . . . . .	3
1.3	Vortex-Antivortex Pair . . . . .	4
1.4	Magnetic Monopoles in Weyl Semimetals . . . . .	6
1.5	Magnetic Skyrmion . . . . .	7
2.1	Real-space Observation of Skyrmions . . . . .	10
2.2	Skyrmion Topology . . . . .	11
2.3	Unit-sphere Spin Parametrization . . . . .	13
2.4	Topological Invariant: Vorticity . . . . .	14
2.5	Bloch and Néel skyrmions . . . . .	16
2.6	Skyrmion Zoology . . . . .	17
2.7	What is Separatrix? . . . . .	21
2.8	Skyrmion Solution . . . . .	22
2.9	Skyrmion Energetics . . . . .	24
3.1	Skyrmion-hosting Magnetic Phase Diagram . . . . .	28
3.2	The Multispiral Skyrmion Lattice Ansatz . . . . .	30
3.3	Magnetic Modulation in Helical Phase . . . . .	36
3.4	Magnetic Modulation in Conical Phase . . . . .	38
3.5	The Hexagonal Skyrmion Lattice . . . . .	41
3.6	Mean-field Phase Diagram . . . . .	47
3.7	Fluctuation Footprint Below and Above the Ordering Temperature . . . . .	48
3.8	Appearance of the Brazovskii Sphere . . . . .	51
3.9	Fluctuation Strength of the Critical Modes . . . . .	52
3.10	Qualitative Phase Diagram . . . . .	54
4.1	Single Skyrmion Energy in Electric Fields . . . . .	59
4.2	The Hexagonal Lattice in Reciprocal Space . . . . .	62
4.3	Rotated Spin Frame . . . . .	63
4.4	Skyrmion Lattice under Voltage: Elastic Distortion . . . . .	66
4.5	Skyrmion Lattice under Voltage: Nonelastic Distortion . . . . .	69

4.6	Elastic vs. Nonelastic Distortions . . . . .	70
4.7	Applicability and Validity of the Perturbation Theory . . . . .	71
4.8	Experiment: Skyrmion Pockets in Electric Fields . . . . .	76
4.9	Skyrmion Phase Stability in Electric Fields: Experiment and Theory . .	79
4.10	Theory: Skyrmion Pockets in Electric Fields . . . . .	82
5.1	Skyrmions under Anisotropic Mechanical Stress . . . . .	88
5.2	Experiment: Magnetic Phase Diagram under Isotropic Pressure. . . . .	92
5.3	Detection of the Skyrmion Phase under Pressure . . . . .	94
5.4	Modelling of the Skyrmion Phase Evolution under Isotropic Pressure . .	98
5.5	Crystallographic Structure of $\text{Cu}_2\text{OSeO}_3$ . . . . .	99
6.1	Thermally-driven Rotation of Skyrmion Arrays . . . . .	103
6.2	Magnetization of $\text{Cu}_2\text{OSeO}_3$ in Field-Polarized Phase . . . . .	105
6.3	Skyrmion Energy vs. Local Magnetization . . . . .	107
6.4	Thermogradient Force vs. Temperature . . . . .	107
6.5	Magnetic Skyrmions and Chiral Bubbles: Topological Bloodline . . . . .	110
6.6	Topologically-preserved Crossover between Skyrmions and Magnetic Bubbles . . . . .	112
6.7	Moderate Stray Fields and Magnetic Bubbles . . . . .	113
6.8	Skyrmion-Bubble Crossover Revised . . . . .	116
6.9	Radii of Skyrmions, Chiral Bubbles, and Half-Breeds . . . . .	117
6.10	Topological Objects: Merons and Bimerons . . . . .	118
6.11	Meron Mechanism of Topological Charge Saturation . . . . .	121



TO MY FAMILY.



# Acknowledgments

First, I would like to thank Henrik Rønnow who over the past years advised me and guided towards this Ph.D. thesis. It was an incredible collaboration which I would say happens quite rarely: Henrik, being an experimentalist with a strong mathematical background, gave me interesting ideas for calculations, and I, as a theorist, implemented them computationally. Henrik was always open to discussions and helped me on various occasions when I had hard times, and without him it would be impossible for me to move further towards this thesis. Not only he mentored me in science, but he also supported me when I faced severe health problems, and I am cordially grateful him for that. Looking back, I should say that it was quite an unusual Ph.D. position opened for theoretical studies in the lab, and the four years spent in the Laboratory for Quantum Magnetism (LQM) were rich with experience which brought me so close to the real physics I could taste it. I think it is an important step for every theorist to be in a skin contact with experiments, with the real-life physics, as very often a particular mathematical formalism is *just one* of the possible ways to distill the observed phenomenon and describe it to a broader community.

I would further like to thank Ivica Živković, who upon joining LQM fuelled my interest towards this skyrmion thing. Ivica was always very friendly and open to explaining experiments on skyrmions he was working on and helped me to shape up my understanding on the skyrmion lattice for the very first calculation on that topic I've done (see chapter 5). I am thankful to Minki Jeong and Peter Babkevich who were my officemates and very good listeners over all these years, and of course, I am very thankful for their friendly support and all the advices they gave to me. I am thankful to Ping Huang for long discussions on experimental aspects of skyrmion physics, and, in particular, the real-time electric-field control of skyrmions embedded in the helical phase, as also I am thankful to Jonathan White for the very fruitful collaboration on writing and erasing skyrmions using electric fields under neutron scattering facility at PSI. Furthermore, I am for sure indebted to Albert Fert, Jiadong Zang and Achim Rosch for their numerous insightful discussions on the skyrmion physics during different occasions on conferences and in Lausanne; they did very much shape up my understanding for skyrmionics, and this thesis would be impossible without their valuable help. I

am thankful to Jiadong Zang, Fabrizio Carbone and Shinichiro Seki for their valuable suggestions on this manuscript.

A separate word of gratitude goes to Vincenzo Savona, whom I assisted with lectures on diagrammatic techniques and learned very much of intricate methods which helped me to solve and publish problem on the one-dimensional condensation of photons. Vincenzo had built a very concise course of lectures on perturbation methods in Fermi and Bose systems. Before this, I, of course, studied these methods during my Master years by following "the Bible" (the book by Abrikosov, Gorkov, Dzyaloshinskii), however only after the lectures of Vincenzo I finally mastered this witchcraft and started diagrammatically calculate each and every thing I need. I am also cordially grateful to Vincenzo for that he allowed me to get a good experience in lecturing on the advanced level. I am cordially thankful to Sergiy Katrych for multiple friendly advices on science and life, and all the gallons of coffee we have drunk together. Without his help, it would be impossible to finish this thesis. I am also thankful to László Forró and Petr Leiman for their friendly support. I would also like to thank Frédéric Mila, Mike Zhitomirsky, and Martin Mourigal, who were very friendly advising me during my first steps at the LQM, and in particular Frédéric Mila for that it was him who inspired me to study magnetism. I am thankful to Elahi, Ivan, Claudia, Luc, Virgile, and Namrata for wonderful years at LQM.

Very importantly, I am thankful to the Lindau Nobel Laureate Meeting committee for getting me in the 66th Meeting in 2016, and in particular to Nadine Gärber for her valuable support on different occasions. As for the very Lindau Meeting, I am thankful to Bill Phillips, David Wineland and Stephan Hell, with whom I spent very long hours discussing ideas in physics. This has influenced me very profoundly.

Finally, I am thankful to my family, as these were very hard years.

*Lausanne, 2017.*

# 1

## Introduction

The latest Nobel prize in physics (2016) was awarded to Thouless, Haldane, and Kosterlitz for their contribution to diverse topological concepts carefully developed and tested in condensed matter through three decades. Clearly now, topology had evolved from an obscure mathematical concept to something useful, measurable, practical. Graphene, topological superconductors, and skyrmion memory for computers are just some examples where the fundamental research in emergent topological phenomena is fuelled by the technological potential. However more to be done as the field is extensively growing.

Historically, topology appeared as a study of shapes of different objects and relations between them as abstract entities without physical density, rigidity, and ultimate tensile strength. A good – but far from being full – analogy is imaging a children’s toy made of plasticine. Clearly, if you have a ball rolled out of plasticine, it is very easy to deform it smoothly into an ellipsoid or a pancake-like disk or another rather arbitrary shape without holes: we say, a sphere is *homeomorphic* to any closed 2D figure without holes. The *continuity*, – which mathematically is the existence and regularity of derivatives, – is the key concept in topology. In fact, singularities (such as holes in the shape) often serve for topological classification of the objects under study (see Figure 1.1). For a long time though topology remained quite an obscure and metaphysical discipline not affecting the direct experimental data. As an anecdote, in 1961 George Gamow even wrote in his book [1], ”only number theory and topology (analysis situs) still remain purely mathematical disciplines without any application to physics”. In fact, just two decades after, topology was called upon to explain integer quantum Hall effect - a phenomenon where the electric conductance of material is *exactly quantized* in units of  $e^2/h$ , - it can be only  $1 \frac{e^2}{h}$ ,  $2 \frac{e^2}{h}$ ,



Figure 1.1: **Topology in real life:** Rolex Learning Center at EPFL is topologically equivalent to a slice of cheese. [Figure from EPFL website]

$3\frac{e^2}{h}$ ,  $4\frac{e^2}{h}$ , etc., – in the same topological spirit as there can be 1,2,3,4, etc. holes in the swiss cheese, but never e.g.  $\sqrt{2}$  holes or anything else too irrational for the cheese industry. The importance of this discovery (awarded with Nobel prize to von Klitzing in 1985) is such that it had impacted the standards of precise measurements: the definition of a standard electrical resistance is the von Klitzing constant  $R_K = h/e^2 \approx 25.8\text{k}\Omega$ . In fact, this year (2017) is expected to be the last when we still use the approximate set of fundamental constants.

Topology is an elegant and a very powerful tool which allows constructing effective condensed-matter models without much going into details of complicated microscopic physics. In fact, many theories on both classical conductivity (e.g. metals, insulators) and more recent advances in the field (e.g. topological insulators, Dirac and Weyl semimetals, superconductors) are built very extensively on the topological notions; a good example here is the Fermi surface, which is a topologically stable quantized vortex in reciprocal space; conceptually, it can be further broken into Fermi arcs (for example, as in Weyl semimetals), and further on even shrunk into a Fermi point (as in the superconductive  $^3\text{He-A}$ ). Thus it is currently believed that most of the conductive features of the *macroscopic systems* can be captured by the topology of the reciprocal space itself, while further material-specific properties can be sufficiently calculated by merging microscopic calculations with topology ideas [2, 3].

The content of this thesis is however devoted to another rapidly expanding branch of condensed matter physics where magnetism meets topology, in particular to *skyrmionics*, - the study of properties of individual and arrayed magnetic skyrmions, their creation, annihilation, and control in the prospect of magnetic memory applications. In one sentence, the skyrmions are vortices made of spins in such a way that there is a sense of rotation: normally, the spin points "down" at the very center of a skyrmion and gradually twists "up" at its periphery. Below I very briefly review several important notions for topological magnetic physics to place magnetic skyrmions in a broader theoretical

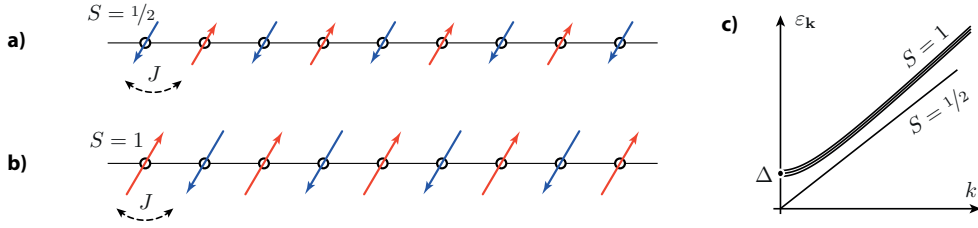


Figure 1.2: **Haldane gap: a "hydrogen atom" of topological matter physics.** a) Spin- $1/2$  chain with antiferromagnetic coupling  $J$ . b) Spin-1 chain with the same antiferromagnetic coupling  $J$ . c) The schematic spectrum of elementary excitations. Surprisingly, the spin-1 chain develops a gapped triplet while the spin- $1/2$  chain elementary excitations are gapless. Once having a finite *Haldane gap*  $\Delta$ , the spin-1 chain cannot be continuously mapped onto the spin- $1/2$  chain, – the two systems are *topologically non-equivalent*.

background.

**HALDANE GAP.** The "hydrogen atom" of topological magnetic matter physics is the appearance of the *Haldane gap* in a 1D spin-1 chain, – in the way it had influenced the development of the field. Historically, a general algorithm was to start treating a phenomenon from the lowest possible dimension (1D or 2D), and only after generalizing the solution towards a 3D case. However, this was not the case with the Haldane problem, even though the *spin chains* appeared more like a toy model of theoretical physics, as the exact solution for  $S = 1/2$  chain and the quasiclassical asymptotes for  $S \gg 1$  were already known. It however turns out that for non-perturbative  $1/S$ , the properties of a 1D spin chain with antiferromagnetic exchange interaction depend crucially on whether the spin is integer or half-integer. For a naked eye it may seem rather strange, as in a naïve picture the Heisenberg Hamiltonian may seem rather "scalable" in terms of the spin magnitudes  $S$ . In fact, for a long time people thought the model has a continuous dependence on the spin quantum number. However, as it was reported by Haldane back in 1988 [4], in contrast to a 1D spin- $1/2$  chain which produces gapless elementary excitations (pairs of spinons), the spin-1 chain manifests a gapped triplet for low-energy quasiparticles. This observation is topologically nontrivial as once the spin-1 chain has a finite gap in its spectrum it cannot be continuously mapped on the gapless spin- $1/2$  chain. This apparent paradox has been a subject of long discussion. Nontrivially, the spin is an operator with either integer or half-integer values, which cannot be transformed into each other, – and this is a topological statement.

**TOPOLOGICAL ORDER.** Another crucial aspect is the concept of *topological order*, – a type of ordering in a system when it is hard to introduce the local order parameter (write down a formula describing the field at every point), however the hidden order is indeed present in terms of algebraic correlations between the different points in space.

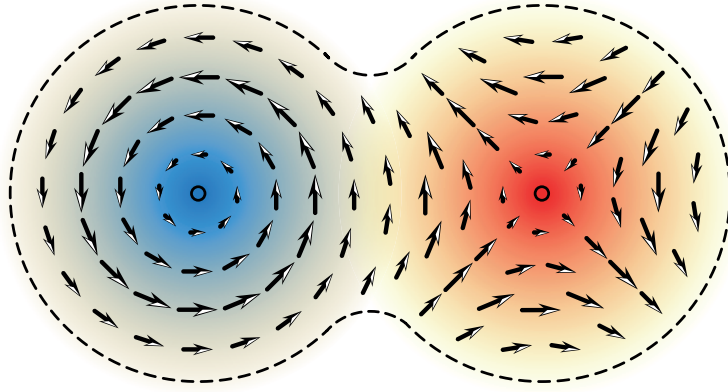


Figure 1.3: **Vortex-antivortex pair (VAP)**: an important object in many condensed matter systems. In Kosterlitz-Thouless physics, a dense packing of VAPs contribute to the topologically-ordered state, i.e. when it is impossible to mathematically formulate the *local* order parameter, however the hidden order is present in terms of algebraic correlations. Upon heating the system, the process known as unbinding of VAPs takes place, and the system transforms to a topologically-trivial phase with well-separated vortices.

It was shown by Kosterlitz and Thouless in several simple models that this could be due to the formation and unbinding of vortex-antivortex pairs. Imagine a two-dimensional charged gas, cooled down to zero Kelvin. If it was a typical three-dimensional gas, at low temperatures, it would overpass the known transitions, such as Bose–Einstein condensation (if bosons), or Fermi liquid (if fermions). However, it was considered for a long time that for flat (two-dimensional and uniform) systems, such phase transitions are forbidden (the so-called Mermin–Wagner theorem [5, 6]). However, even though early numerical studies of such systems showed no singularities, there was an indication that something strange is going on: the correlation functions (the functions which show how much a small part of the system knows about the other parts) behaved differently above and below some critical temperature  $T_C$ , the signature that one would normally expect for phase transitions! This was striking as it opposed the Mermin–Wagner theorem, which had been proven in different contexts. The apparent contradiction was first qualitatively explained in the 1972 paper of Kosterlitz and Thouless [7] in which they argue that below some  $T_C$ , it is very easy to create vortices, but only in pairs – a vortex and an antivortex. Of course, the evolution of the vortex pairs is complex, but intuitively one could expect that if we heat the system, we can destroy these vortex pairs. Indeed, the calculations show that above  $T_C$ , all the vortex pairs unbind into single (uncorrelated) vortices. Such a subtle topological mechanism gives no physically measurable singularities at  $T_C$  in thermodynamic properties, however it does, indeed, change the correlation functions of the system below and above  $T_C$ . The corresponding order in the system is a topological order, which supports this quite strange (topological) phase transition. It is interesting that in mathematically similar earlier arguments of Berezinskii [8, 9], there



was no mention of superconductivity or vortex–antivortex physics at all.<sup>1</sup>

SKYRME MECHANISM. An interesting concept here, be it not from condensed matter physics, but closely related to this thesis, is the so-called Skyrme mechanism for explaining baryon (and later, meson) stability [11–18]. *Baryons* are quite a large group of *elementary particles*, including, in particular, *nucleons*, - the constituents of atomic nuclei: protons and neutrons. According to Skyrme’s idea, a nucleon can be represented as a whirl in *pion* liquid, leading to a so-called *hedgehog* solution of field equations on a sphere. In fact, Skyrme had introduced a topological classification of solutions of nonlinear field equations and introduced the topological (homotopic) conservation laws. The new conserved quantity, the *topological charge*, was interpreted as baryonic charge, and baryons themselves were interpreted as topological solitons. The Skyrme’s mechanism was based on rather deep topological ideas which were quite distant to most of the physicists those days, and for a long time the simple and beautiful Skyrme’s model was relatively little explored, while the quark theory became a mainstream tool in the particle physics theory. This *status quo* changed in the 1980s when it was shown that the Skyrme’s model can be considered as a  $N_c \rightarrow \infty$  limiting case<sup>2</sup> of quantum chromodynamics [19, 20], and the conceptual model got progressively more attention in other fields of physics, such as ultracold gases, superconductivity and magnetism. As an anecdote, Skyrme mentioned [18] being influenced by an interesting yet terribly wrong vortex model of atoms by W. Thomson (Lord Kelvin) who in 1867 proposed a toy model [21] in which atoms were considered as vortex objects in hypothetical *aether* filling all the universe (in fact, not).

QUANTIZATION OF ELECTRIC CHARGE AND MAGNETIC MONOPOLES. The symmetry of Maxwell equations is somewhat disturbed by the absence of magnetic charges, – analogs of electric charges such as the one carried by electrons. For a long time a field-theoretical reverie was to find the hypothetical particle which supports a monopole term in magnetic field multipole expansion, – the so-called *magnetic monopole*, – but all in vain.<sup>3</sup> It could be of course just an *idée fixe*, if not a remarkable observation made by Paul Dirac in 1931 [23]: if a magnetic monopole exists in nature, all electric charges should be quantized. So here we are: Electric charge is, in fact, quantized:  $\pm 1e$ ,  $\pm 2e$ ,  $\pm 3e$ , etc. Should we thus await for Dirac monopoles? Well, at least that appears to be the only more-or-less reasonable explanation on why the electric charge is quantized, so far. The real magnetic monopoles, if they exist(ed), – and I bet they do, – are currently unreachable for experiments as they have an estimated mass of order  $M_o \sim 10^{16} \text{ GeV}$  (after renormalizations made on that mass scale, see [24]). For

---

<sup>1</sup>This paragraph is reused from my publication Ref.[10].

<sup>2</sup> $N_c$  is the number of "colours" in quantum chromodynamics.

<sup>3</sup>For a detailed but rather pedagogical review of magnetic monopole physics, see Ref.[22]. In particular, special attention should be paid to the Wu-Yang monopole, which, similar to an electron, is a point-like particle with a  $1/r$  potential field everywhere.

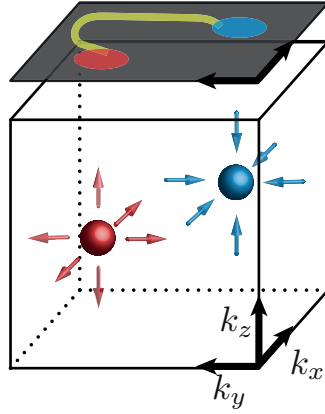


Figure 1.4: Magnetic monopoles in Weyl semimetals (in reciprocal space): elementary excitations near the linear band crossings (Weyl nodes) in Weyl semimetals follow the Dirac equation for *massless* electrons, which act as left-polarized and right-polarized chiral particles. The positive and negative Weyl nodes (red and blue in this figure) can be interpreted as magnetic monopoles of Berry magnetic (pseudo)field, and are connected with the Dirac string in bulk. Being projected on the surface, the Dirac string is seen as a *Fermi arc*, i.e., topologically nontrivial "slice" of a Fermi loop.

comparison, the Higgs boson is only 125 GeV and according to Forbes it had cost \$13.25 billion to make it discovered. Condensed matter systems are amazing in the way they can incorporate nontrivial field-theoretical concepts in a measurable way. To date, the condensed matter community found several systems with low-energy *analogs* of magnetic monopoles, such as, for example, in "spin ices" [25], Weyl semimetals [26], skyrmion-hosting chiral magnets [27], etc. Topologically, magnetic monopole can be visualized as a solenoid with magnetic flux  $2\pi/e$  and one ending point. This infinitesimal line solenoid, also called a *Dirac string*, links a monopole and antimonopole together, thus forming a magnetic dipole. One of the most beautiful condensed matter analogs of this concept is observation of *Fermi arcs* in Weyl semimetals, which are surface projections of Dirac strings (in reciprocal space); the Weyl nodes are magnetic monopoles of pseudo-magnetic (Berry curvature) field in reciprocal space, see Fig. 1.4

**MAGNETIC SKYRMIONS.** - Magnetic skyrmions is a class of several nontrivial spin configurations in chiral magnets. They are mainly distinguished by their topological charge, chirality and helicity. The lowest-charged skyrmions observed in the bulk chiral magnets and thin magnetic films are the Bloch-type and Néel-type skyrmions, topologically equivalent (through a continuous map) to a hedgehog-like "hairy sphere". In context of magnetization vortices, the magnetic skyrmions were introduced in 1989 by Bogdanov [28] and Ivanov [29, 30], as also indirectly mentioned in some earlier studies [31–33]. The skyrmion crystalline in MnSi was introduced around 2006 in studies of Vishwanath and Binz [34–37], which very shortly lead to experimental discovery of magnetic skyrmions in MnSi [38, 39], and later in many other systems, including other chiral-lattice fer-

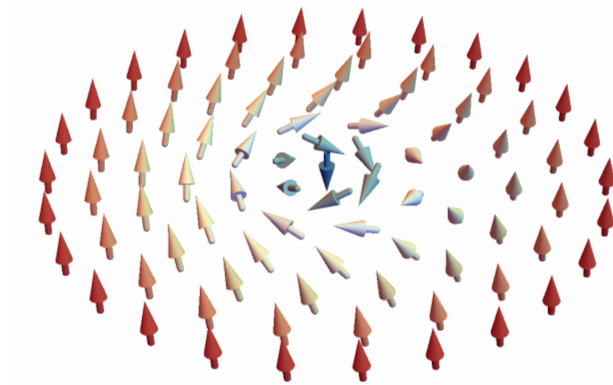


Figure 1.5: Magnetic skyrmions are topologically-protected quasiparticle-like vortices of spins in chiral magnets, typically of a nanoscale size. On the figure: a radially-symmetric Bloch-type skyrmion. The spin points "down" (against magnetic field) in the very center and gradually rotates towards pointing "up" at the periphery (along the external magnetic field). Skyrmionics is a study of creation, stabilization and control of magnetic skyrmions in the viewpoint of magnetic data applications.

romagnets [40–45], centrosymmetric ferromagnets [46, 47], iterfaced systems [48, 49] and systems with confined geometry [50–52]. Experimentally, the topological nature of individual skyrmions was confirmed by predicting and observing the *skyrmion Hall effect* [53–57]. To a known extent, magnetic skyrmions can be considered topologically and energetically protected against continuous perturbations. To this point, magnetic skyrmions are promising information carriers for future memory devices and ultradense data storage, while skyrmion phases in bulk materials are interesting from a fundamental point of view in exploring topological states of matter.

The novel results of this thesis are calculations for both individual and arrayed skyrmions under electric fields, mechanical strains and uniform pressures, and thermal gradients. Furthermore, several fundamental questions were addressed by developing an extended formalism for calculation skyrmion-hosting magnetic-phase diagrams, studying the topologically-governed crossover between skyrmions and magnetic bubbles, and discussing the possible role of merons (half-skyrmions) in skyrmion crystal melting. The most immediately appealing result is probably the theoretical and experimental study of skyrmion lattices in electric fields, with a direct demonstration of writing and erasing of the full skyrmion phase under voltages of few Volts per micrometer, compatible with modern microelectronics.

This thesis is organized as follows: in the next chapter (Chapter 2) I introduce important skyrmionics concepts and present a rather pedagogical description of diverse skyrmionic ideas which are otherwise scattered over multiple research papers only. In Chapter 3 I discuss possible magnetic phases in bulk skyrmion-hosting materials, and present a refined method for calculating bulk magnetic phase diagrams on the basis

of fluctuation-induced stabilization of the skyrmionic phase with respect to the conical phase. In Chapter 4, I consider the effective way of creation and annihilation of single skyrmions and stabilization and destabilization of the skyrmion phase (in bulk) by applying mechanical strains and uniform pressure. In Chapter 5, I present two different models: for single skyrmion in electric fields, as also for the skyrmion lattice stabilization in electric fields, including results of experiments for writing and erasing magnetic skyrmions with moderate voltages. In Chapter 6, I consider several models for different aspects of topological physics in magnetic thin films, namely (i) mechanism for moving magnetic skyrmions with thermal gradients; (ii) topologically-preserved crossover between fast and mobile skyrmions and slow magnetic bubbles; (iii) a simple model that tracks topological charge saturation in thin films by tracing the pairs of merons (half-skyrmions) in the system. The concluding chapter is made in the form of an overview as the field is very rapidly growing.

# 2

## Magnetic Skyrmions: Topology, Stability and Quasiparticle Properties

Skyrmions were first introduced in 1950s-1960s in the context of topologically protected states to explain the empirical stability of hadrons [17], by Tony Skyrme. Although the quark theory proved to be more constructive, the concept of both the 3D and 2D<sup>1</sup> skyrmions and related topologically-induced phenomena have found deep roots in diverse subfields of many-body physics, such as in 2D electron gases [58, 59], superconductors [60–68], spinor Bose-Einstein condensates [69–75] and, remarkably, quasiclassical magnetic systems as described below. Initially, magnetic skyrmions were theoretically proposed as topologically-protected microscopic analogs of chiral magnetic bubbles Bogdanov in 1989 [28] and Ivanov in 1986 [29, 30], and for years were mainly called *magnetic vortices* and *topological solitons*.<sup>2</sup> It is hard to trace when the term *magnetic skyrmion* coined its modern shape, however for a 2D magnetic skyrmion in ferromagnetic (uniform) background one would probably name the paper on a skyrmion in ferromagnetic thin films by Abanov in 1998 [78] and Bogdanov in 2002 [79]; throughout this thesis, an effectively two-dimensional magnetic skyrmion (or a skyrmion tube) will be simply referred to as *the skyrmion* if not stated otherwise. The experimental discovery of magnetic skyrmions in form of a hexagonal long-range-order lattice was reported by a joint group of Pfleiderer, Böni and Rosch [38, 54, 80] in metallic chiral-lattice ferromagnet MnSi (see also the real-space observation [39, 41], and Figure 2.1 in this regard), and

---

<sup>1</sup>In some papers 2D skyrmions are also called "baby" skyrmions.

<sup>2</sup>Similar magnetic objects were also treated in some earlier studies, see Refs.[31–33, 76]. See also the 1989's paper [77] for a single-vortex model.

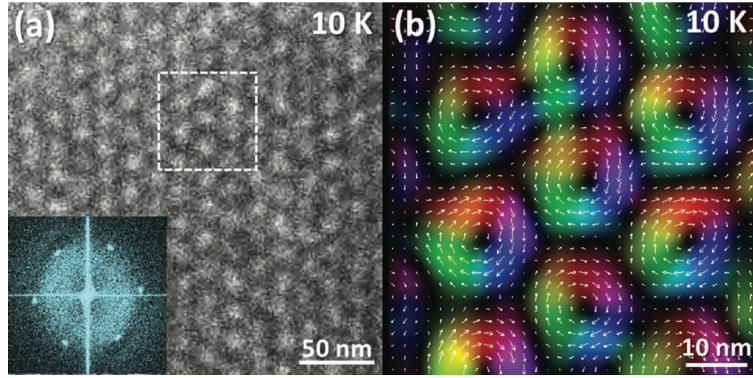


Figure 2.1: Observation of the skyrmion phase in real space with transmission electron microscopy. Figure from Ref.[39].

later found in several other chiral-lattice ferromagnets [40–45], layered centrosymmetric ferromagnets [46, 47], and interfaced systems [48, 49]. This discovery was preceded by two independent theoretical proposals (2006) for the skyrmion phase as a possible candidate for the partially-ordered A-crystal in MnSi,<sup>3</sup> by Binz and Vishwanath [34–37] and Rössler, Bogdanov and Pfleiderer [81]. In acknowledgement for masterminding the seminal works [28, 34, 38, 54, 80, 81], Böni, Bogdanov, Pfleiderer, Rosch and Vishwanath were awarded with 2016 EPS CMD Europhysics Prize “for the theoretical prediction, the experimental discovery and the theoretical analysis of a magnetic skyrmion phase in MnSi, a new state of matter.”

Because a topological barrier stabilizes the skyrmion [29, 30, 82], robust quasiparticle properties can be assigned, together with a quantized topological charge (see next section). Furthermore, skyrmions require very little energy cost to be moved with electric currents in metallic environment [46, 80, 83–89], or, surprisingly, with thermal gradients in insulating samples [90, 91]; a topologically interesting twist for skyrmionics is the conjectured existence of charged skyrmions on the surface of topological insulators [92]. Several methods for creating (“writing”) and destroying (“erasing”) skyrmions were proposed [49, 88, 93–98], depending on the specificities of the system. As quasiparticles, the skyrmions can interact with each other [99–103], as also condense to and melt back from a crystal made of quasiparticles, the skyrmion lattice [38, 99, 104, 105]. To this point, magnetic skyrmions are promising information carriers for future memory devices and ultradense data storage, while skyrmion phases in bulk materials are interesting from a fundamental point of view in exploring topological states of matter [78, 106–111].

In this chapter, I mainly review some pivotal properties of the skyrmions, such as topological numbers and their underlying connections with crystal symmetries, and sketch a controllable numerical scheme for variational minimization of the energy func-

---

<sup>3</sup>Before understanding the skyrmion nature of the strange phase in MnSi, the skyrmion lattice was mainly nicknamed as an “A-phase” or “A-crystal”.

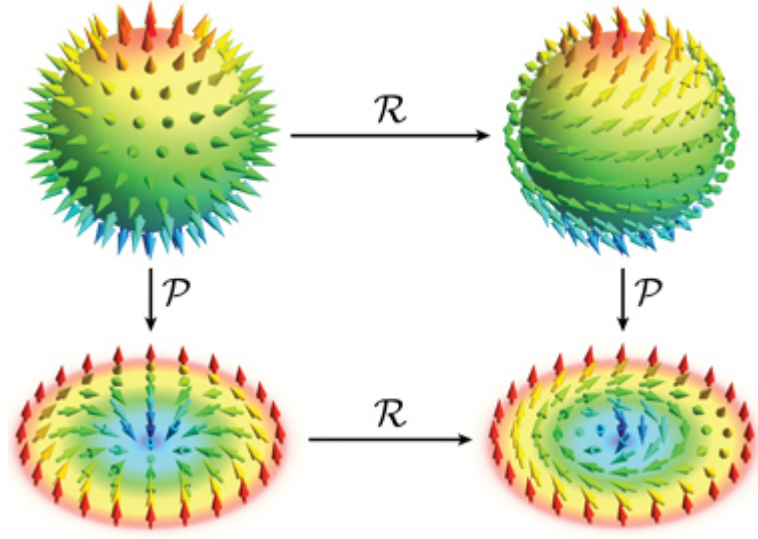


Figure 2.2: **Skyrmion topology.** Skyrmion is topologically equivalent to a "hedgehog sphere". *Top left:* a "hedgehog" spin configuration on a 3D sphere. Upon stereographic projection  $P$  it gives a **nonchiral (Néel-type) skyrmion** (*bottom left*). The "south pole" of the hedgehog sphere is projected into the center of a skyrmion, and the spin points down. The "north pole" of the hedgehog sphere is projected on the periphery of a skyrmion, where thus the spins point up. *Top right:* One can further wrap spins around the hedgehog sphere with a rotation  $R$  in order-parameter space, and the **topological charge remains invariant**. Being projected on the plane, the wrapped configuration gives a **chiral (Bloch-type) skyrmion** (*bottom right*). **Topological protection:** Note that it is impossible to continuously tilt spins on the hedgehog sphere so that they all point in the same direction. In other words, the model skyrmion cannot be continuously transformed into a topologically-trivial state (e.g. ferromagnetic). Illustration taken from Ref.[112].

tional. In the last section of the chapter, I re-derive the skyrmion field afar from the core (which is responsible for the low-energy skyrmion-skyrmion interaction vertex), as it is unfortunately often shown wrongly in the literature.

## 2.1 TOPOLOGICAL INVARIANTS

Skyrmions are characterized by a few topological invariants, which are integer numbers relatively robust against moderate perturbations unless a specific way for collapsing a skyrmion is chosen [82]. The two main topological numbers are the *topological charge*, which encapsulates how many times the spins winds around an order-parameter sphere, and the *helicity*, which is responsible for how exactly do the spins twist from "spin down" at the very center of a skyrmion towards "spin up" at the periphery, see illustration on the bottom of Figure 2.2.

The topological charge of a skyrmion<sup>4</sup> shows the order of a topological knot formed

<sup>4</sup>a.k.a. skyrmion number, winding number, Chern number, topological number - in different sources.

by spins, and in continuous-field approximation is given conventionally as<sup>5</sup>

$$Q = \frac{1}{4\pi} \int dx dy \mathbf{m} \cdot \left( \frac{\partial \mathbf{m}}{\partial x} \times \frac{\partial \mathbf{m}}{\partial y} \right), \quad (2.1)$$

where we have introduced the orientation of local magnetization  $\mathbf{m}(x, y) = \mathbf{M}(x, y)/|\mathbf{M}|$ . By construction, the topological charge is an integer number – the number of times the field wraps around the sphere – which for topologically nontrivial smoothly-varying field configurations attains values  $\pm 1, \pm 2, \pm 3$ , etc. One can also introduce the emergent Berry field

$$\mathfrak{B} = \frac{1}{2} \mathbf{m} \cdot \left( \frac{\partial \mathbf{m}}{\partial x} \times \frac{\partial \mathbf{m}}{\partial y} \right), \quad (2.2)$$

that the emergent magnetic flux  $\Phi$  associated with a skyrmion is  $2\pi Q$ .

**Natural parametrization of a skyrmion in a uniform background.** – It is as a general rule rather handy to parametrize a skyrmion field in spherical coordinates (in spin space), as this field is homeomorphic to a "hedgehog" spin configuration on a 3D sphere, see Figure 2.2. Thus for unit-lengthed vector  $|\mathbf{m}| = 1$ , we write

$$\mathbf{m} = \begin{pmatrix} \sin\theta \cos\psi \\ \sin\theta \sin\psi \\ \cos\theta \end{pmatrix}, \quad (2.3)$$

where the the angles are introduced on the figure 2.3. We define a model skyrmion as  $\theta(0) = \pi$  ("spin down" in the center of a skyrmion) and  $\theta(\infty) = 0$  ("spin up" on remote periphery), if not mentioned otherwise. In case of the axially-symmetric (perfect, non-distorted) skyrmion, one may further simplify calculations by introducing real-space cylindrical frame  $(r, \phi, z)$ ,

$$\theta = \theta(r), \quad \psi = \psi(\phi). \quad (2.4)$$

We now perform implicitly the integration in (2.1). The straightforward algebra gives

---

<sup>5</sup>Here and in general, the magnetic skyrmions are two-dimensional or effectively two-dimensional (skyrmion tubes), thus we consider a 3D spin space  $\mathbf{M} = (M_x, M_y, M_z)$  defined on the 2D real space  $\mathbf{r} = (x, y)$ , unless stated otherwise.



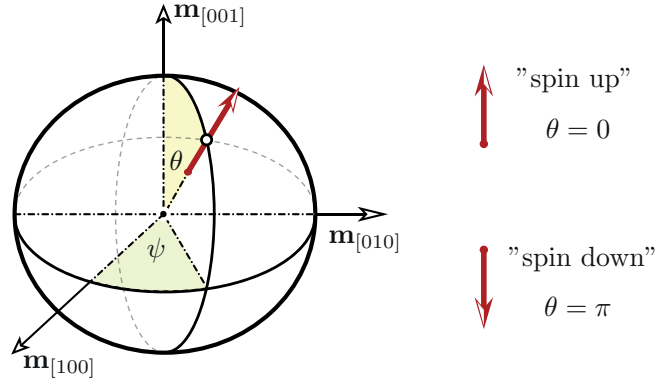


Figure 2.3: **Unit-sphere spin parametrization:** a normalized continuous-limit local magnetization  $\mathbf{m}(\mathbf{r}) = (\sin\theta(\mathbf{r})\cos\psi(\mathbf{r}), \sin\theta(\mathbf{r})\sin\psi(\mathbf{r}), \cos\theta(\mathbf{r}))$  is handy in the spherical spin frame. Note that for the spatial coordinates, it is often more convenient to proceed in the polar (cylindrical) frame, where  $\theta = \theta(r)$ ,  $\psi = \psi(\phi)$ .

$$\frac{\partial \mathbf{m}}{\partial x} = \mathbf{v}_1 \frac{\partial \theta}{\partial x} + \mathbf{v}_2 \frac{\partial \psi}{\partial x}, \quad (2.5)$$

$$\frac{\partial \mathbf{m}}{\partial y} = \mathbf{v}_1 \frac{\partial \theta}{\partial y} + \mathbf{v}_2 \frac{\partial \psi}{\partial y}, \quad (2.6)$$

where we have introduced auxiliary vectors  $\mathbf{v}_1, \mathbf{v}_2$ ,

$$\mathbf{v}_1 = (\cos\theta \cos\psi, \cos\theta \sin\psi, -\sin\theta), \quad (2.7)$$

$$\mathbf{v}_2 = (-\sin\theta \sin\psi, \sin\theta \cos\psi, 0), \quad (2.8)$$

which are handy to keep written down for further calculations. Using the properties  $\mathbf{v}_1 \times \mathbf{v}_1 = 0$ ,  $\mathbf{v}_2 \times \mathbf{v}_2 = 0$ , and  $\mathbf{v}_1 \times \mathbf{v}_2 = -\mathbf{v}_2 \times \mathbf{v}_1 = \mathbf{m} \sin\theta$ , and proceeding to polar frame, we have

$$\frac{\partial \theta}{\partial x} = \frac{d\theta}{dr} \cos\phi, \quad \frac{\partial \psi}{\partial x} = -\frac{1}{r} \frac{d\psi}{d\phi} \sin\phi, \quad (2.9)$$

$$\frac{\partial \theta}{\partial y} = \frac{d\theta}{dr} \sin\phi, \quad \frac{\partial \psi}{\partial y} = \frac{1}{r} \frac{d\psi}{d\phi} \cos\phi, \quad (2.10)$$

thus the emergent Berry field is

$$\mathfrak{B} = \frac{1}{2} \mathbf{m} \cdot \left( \frac{\partial \mathbf{m}}{\partial x} \times \frac{\partial \mathbf{m}}{\partial y} \right) = \frac{\sin\theta}{2r} \frac{d\theta}{dr} \frac{d\psi}{d\phi}. \quad (2.11)$$

which corresponds to a two-dimensional magnetic monopole with topological charge

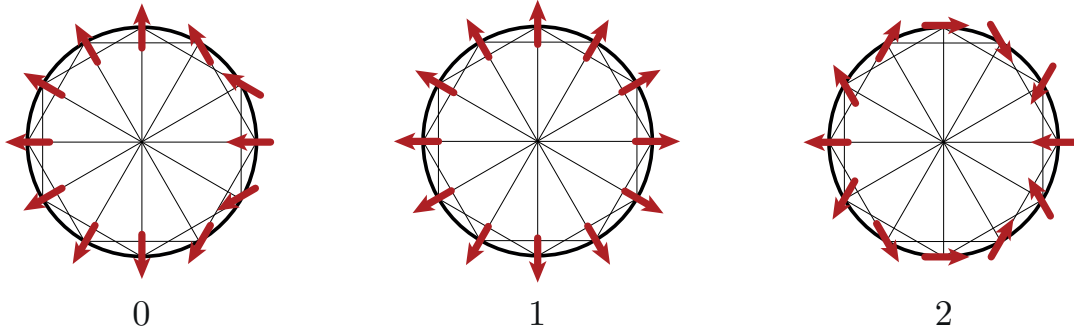


Figure 2.4: **Vorticity**  $w$  shows how many times a continuous vector field makes a full (anti)clockwise turn. **0**: the vector field (red arrows) can be continuously transformed to a uniform field (all arrows point the same direction). **1**: such a field configuration cannot be continuously transformed into  $w = 0$ . **2**: such a double-twisted flow cannot be mapped neither on  $w = 0$  nor  $w = 1$ .

$$Q = \frac{1}{2\pi} \int \mathfrak{B} d^2\mathbf{r} = \frac{1}{4\pi} \int_0^{2\pi} d\phi \frac{d\psi}{d\phi} \int_0^\infty dr \frac{d\theta}{dr} \sin\theta = -\frac{1}{4\pi} \psi(\phi)|_0^{2\pi} \cos\theta(r)|_0^\infty. \quad (2.12)$$

Assuming a skyrmion in the ferromagnetic background,  $\theta(0) = \pi$ ,  $\theta(\infty) = 0$ , gives  $\cos\theta(r)|_0^\infty = 2$ . If the function  $\psi(\phi)$  is a smooth continuous function defined mod  $2\pi$ , for the axially-symmetric skyrmion one has

$$\psi(\phi) = w\phi + \gamma. \quad (2.13)$$

Thus the topological charge of a skyrmion in this definition is

$$Q = -w, \quad w \in \mathbb{Z}, \quad (2.14)$$

where  $w$  is an integer-valued vorticity of a vector field (the number of times a vector field twists around a closed loop, see Figure 2.4) and  $\gamma$  is, in principle, an arbitrary phase, which may or may not be defined by the underlying crystallographic symmetry. Thus, even minimally charge skyrmions ( $Q = \pm 1$ ) represent a very broad family of topological defects. Several most important of them are discussed in the next subsection. The variables  $w$  and  $\gamma$  are called *vorticity* and *helicity*. The first one accounts for the topological charge of the skyrmion ( $\pm 1, \pm 2, \pm 3, \dots$ , see figure 2.4, and helicity reflects the angle between the normal to the chosen contour and magnetization vectors. The topologically trivial field configurations are given by  $Q = 0$ .

Note that even though we used a particular symmetry of a skyrmion when wrote down the ansatz (2.4), in the real life a skyrmion may or may not follow this idealization. In fact, in most of the cases skyrmions are observed rather deformed, – because of their dynamics or imperfections of the sample, – and sometimes even with an ameboid form. This, however, does not matter, as they can be rather easily deformed into other topologically equal shapes, – at least while they still possess the topological charge and can be thus distinguished from the background. Moreover, in the skyrmion crystalline, the skyrmions are in fact shaped up more like hexagons, and only the very core maintains the cylindrical symmetry itself. The axisymmetric model of a skyrmion, presented in this subsection, is a however very important toy model allowing both classification of magnetic skyrmions, – as they can be continuously distorted without changing their topological charge, – and direct calculations of the skyrmionic (free) energy in case when the distortions from the cylindricity is not important. This works well for skyrmions in the ferromagnetic (field-polarized) phase in sufficiently large magnetic fields, and, surprisingly, for long-range-ordered skyrmion arrays in the thin films. One however shouldn't misuse the good model outside the area of its validity.

#### SKYRMION ZOOLOGY

In the most cases, skyrmions can be distinguished by their topological charge. As a general rule, the lowest-energy field configurations correspond to the lowest topological charge,  $Q = \pm 1$ , depending on the explicit form of the spin Hamiltonian. The underlying crystallographic symmetry determines the type of helicity  $\gamma$  in the system. Among the several types of 2D skyrmion patterns the two most significant are the Néel-type skyrmion and the Bloch-type skyrmion (see figure 2.5).

In order to observe a unique chirality and thus the topological charge for skyrmions, one usually needs an inversion-breaking mechanism in the Hamiltonian. As such a mechanism, Dzyaloshinskii-Moriya interaction (DMI)<sup>6</sup> is present in non-centrosymmetric magnets, and magnetic systems such as thin films with complex surface interactions and interfaces with inversion breaking. The physics of chiral ("twisted") spin structures dates back to 1960s to the works of Dzyaloshinskii and Moriya [113–116]. In the most general case, the DMI can be summarized as a microscopic Hamiltonian,

$$\mathcal{H}_{\text{DMI}} = \sum_{i,j} \mathbf{D}_{ij} \cdot (\mathbf{S}_i \times \mathbf{S}_j), \quad (2.15)$$

where  $\mathbf{D}_{ij}$  is the Dzyaloshinskii vector.<sup>7</sup> In the two most common cases, this expression

---

<sup>6</sup>Also called an "antisymmetric exchange" exchange, in analogy with symmetric (Heisenberg) exchange.

<sup>7</sup>Even centrosymmetric crystal structures can have DMI along noncentrosymmetric bonds, but the

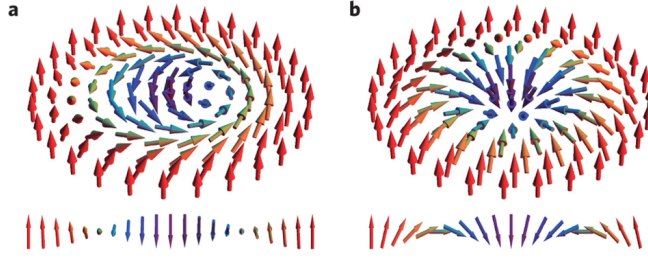


Figure 2.5: Bloch and Néel skyrmions: (a) In a *Bloch-type skyrmion*, the spin projections in a diagonal cut (below) make a full twist like in a Bloch domain wall. On contrary, in in a *Néel-type skyrmion*, the spins projections make a "salto" across the diagonal. Figure from Ref.[117]

further simplifies depending on the underlying symmetry of the lattice (see further), as

$$\mathcal{H}_{\text{DMI}}^{\text{Bloch}} = -D \sum_i \mathbf{S}_i \times \mathbf{S}_{i+\hat{x}} \cdot \hat{x} + \mathbf{S}_i \times \mathbf{S}_{i+\hat{y}} \cdot \hat{y}, \quad (2.16)$$

$$\mathcal{H}_{\text{DMI}}^{\text{Néel}} = -D \sum_i \mathbf{S}_i \times \mathbf{S}_{i+\hat{x}} \cdot \hat{y} - \mathbf{S}_i \times \mathbf{S}_{i+\hat{y}} \cdot \hat{x}, \quad (2.17)$$

Originally, Dzyaloshinskii analyzed the anisotropic interaction in terms of *Lifshitz invariants* - the lowest order inversion-breaking terms which contain spatial derivatives

$$\mathcal{L}_{\alpha\beta}^\gamma = m_\alpha \frac{\partial m_\beta}{\partial x_\gamma} - m_\beta \frac{\partial m_\alpha}{\partial x_\gamma}, \quad (2.18)$$

here  $\alpha, \beta = x, y, z$  are covariant coordinates and  $\gamma$  contra-variant coordinates for convenience. Note that  $\mathcal{L}_{\alpha\beta}^\gamma$  is an antisymmetric tensor with respect to  $\alpha \leftrightarrow \beta$ .

One can show that for uniaxial crystallographic classes, such as  $C_{nv}$  (gives Néel-type skyrmion) and  $D_n$  (gives Bloch-type skyrmion), the corresponding continuous-limit DMI energies are given by

$$W_{\text{DMI}}^{\text{Néel}} = \langle D(\mathcal{L}_{xz}^x - \mathcal{L}_{yz}^y) \rangle, \quad (2.19)$$

$$W_{\text{DMI}}^{\text{Bloch}} = \langle D_1(\mathcal{L}_{yz}^x + \mathcal{L}_{xz}^y) + D_2 L_{xy}^z \rangle. \quad (2.20)$$

In particular, the Bloch-type skyrmions are favoured if  $D_1 = D_2 = D$ , which is also the case for the metallic cubic helimagnets such as MnSi, FeGe and in magnetoelectric insulator Cu<sub>2</sub>OSeO<sub>3</sub>. Thus one obtains

$$W_{\text{DMI}}^{\text{Bloch}} = \langle D(\mathcal{L}_{yx}^z + \mathcal{L}_{xz}^y + \mathcal{L}_{zy}^x) \rangle = D \langle \mathbf{m} \cdot (\nabla \times \mathbf{m}) \rangle, \quad (2.21)$$

---

DMI effect averages to zero over the unit cell except for noncentrosymmetric structures.

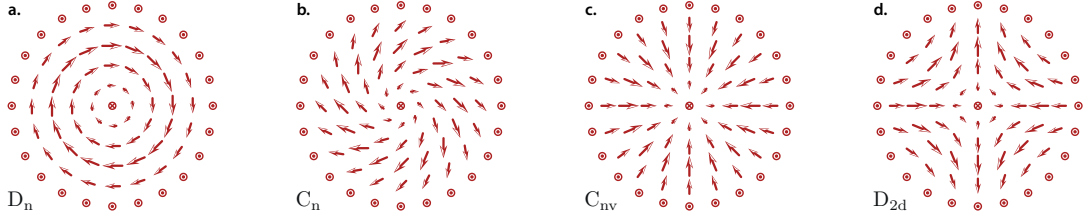


Figure 2.6: **Skyrmion zoology**: depending on the underlying symmetry of the crystal, which promotes the shape of the chiral (DM) interaction, the skyrmion may look differently. On figure: spin projections of different skyrmions on the basal plane (a)  $D_n$  skyrmion (Bloch skyrmion,  $\gamma = 0$ ); (b)  $C_n$  skyrmion; (c)  $C_{nv}$  skyrmion (Néel skyrmion,  $\gamma = \pi/2$ ); (d)  $D_{2d}$  skyrmion.

where  $\langle \dots \rangle$  denotes bulk averaging. Introducing dimensionless  $\tilde{W} = W/D$ , and using the axisymmetric form of a skyrmion (2.3)-(2.4), one thus obtains:

$$\tilde{W}_{\text{DMI}}^{\text{Néel}} = \theta'_r \cos(\psi - \phi) - \frac{1}{2} \psi'_r \sin 2\theta \sin(\psi - \phi) - \frac{1}{r} \theta'_\phi \sin(\psi - \phi) + \frac{1}{2r} \psi'_\phi \sin 2\theta \cos(\psi - \phi), \quad (2.22)$$

$$\tilde{W}_{\text{DMI}}^{\text{Bloch}} = \theta'_r \sin(\psi - \phi) - \frac{1}{2} \psi'_r \sin 2\theta \cos(\psi - \phi) - \frac{1}{r} \theta'_\phi \cos(\psi - \phi) + \frac{1}{2r} \psi'_\phi \sin 2\theta \sin(\psi - \phi). \quad (2.23)$$

In particular, the energetics considerations on basis of Eqs. (2.22) and (2.23) give that for  $\psi = w\phi + \gamma$ , the helicity is  $\gamma = 0$  for a Néel-type skyrmion and  $\gamma = \pi/2$  for a Bloch-type skyrmion, see Figure 2.6. Thus, for a minimally topologically charged skyrmion ( $|Q| = 1$ ), the Eqs. (2.22) and (2.23) are both reduced to

$$W_{\text{DMI}}^{\text{Néel}} = D \left( \frac{d\theta}{dr} + \frac{\sin 2\theta}{2r} \right), \quad W_{\text{DMI}}^{\text{Bloch}} = D \left( \frac{d\theta}{dr} + \frac{\sin 2\theta}{2r} \right). \quad (2.24)$$

Finally, we note that a further symmetry analysis can guide the systematic search for the new skyrmion hosts (see Refs.[118]). The analysis is based on considering which point groups can provide a Fourier-transformed DMI term of from  $iD\mathbf{S}_{\mathbf{k}} \cdot (\mathbf{k} \times \mathbf{S}_{-\mathbf{k}})$ , which has broken inversion symmetry, and also broken mirror symmetry. A detailed analysis presented in [118] shows that the non-vanishing DMI contribution appears in following point groups, class-I:  $C_1, C_2, D_2$ ; class-II:  $C_3, D_3, C_4, D_4, C_6, D_6$ ; class-III:  $S_4, D_{2d}$ ; class-IV:  $T$ ; class-V:  $O$ . Based on this approach, new skyrmion hosts were reportedly found [118, 119].

## 2.2 SKYRMION ENERGETICS: A VARIATIONAL APPROACH

In this section we consider a variational calculation for an axisymmetric skyrmion in a ferromagnetic background. For definiteness, in this section we consider a Bloch-type skyrmion with unitary topological charge. The minimal model in a coarse-grained case reads

$$w_0[\mathbf{M}(\mathbf{r})] = J(\nabla \mathbf{M})^2 + D \mathbf{M} \cdot (\nabla \times \mathbf{M}) - \mathbf{M} \cdot \mathbf{H}, \quad (2.25)$$

where  $J$  is the Heisenberg stiffness resulting from a ferromagnetic exchange, and shortcut  $(\nabla \mathbf{M})^2$  means  $\sum_{i,j} (\partial M_i / \partial x_j)^2$ . Here  $D$  is a DMI constant and  $H$  external magnetic field. If DMI is absent, the ground state of (2.25) is a ferromagnet; with small but finite DMI the ground state is the helical phase, where spin structure is periodically modulated with wave vector  $k_0 = D/2J$ , and the ferromagnetic (field-polarized) state exists only in strong magnetic fields  $H$  (see Chapter 3 for further details). The averaged energy is thus defined by

$$\langle W_0[\mathbf{M}(\mathbf{r})] \rangle = \int d^2 \mathbf{r} w_0[\mathbf{M}(\mathbf{r})], \quad (2.26)$$

which is a functional of the local magnetization field  $\mathbf{M}$ . Thus the value of  $\langle W_0 \rangle$  will depend crucially on the field configuration chosen. Provided there is a local minimum (which may or may not be a ground state), it is possible to address the variational problem: if the skyrmion is present, what is its the most stable field configuration?

It can be shown that, *statically*, an isolated axisymmetric skyrmion in *homogeneous* background is energetically more favourable than an isolated ameboid skyrmion; we thus work in the framework of Eqs.(2.3)-(2.4). For this, we first rewrite the functional in convenient variables. We consider sufficiently smooth, monotonous  $\theta(r)$  in single-skyrmion parametrization  $\mathbf{m} = \mathbf{M}/M_s$ , where  $M_s$  is the saturation magnetization. Taking explicitly Eq.(2.3), we thus have

Now, using the explicit definition of the cross product in 3D space

$$\nabla \times \mathbf{m} = \left( \frac{\partial m_z}{\partial y} - \frac{\partial m_y}{\partial z}, \frac{\partial m_x}{\partial z} - \frac{\partial m_z}{\partial x}, \frac{\partial m_y}{\partial x} - \frac{\partial m_x}{\partial y} \right), \quad (2.27)$$

so the DMI term simply reads

$$\mathbf{m} \cdot (\nabla \times \mathbf{m}) = \sin(\psi - \phi) \left[ \frac{d\theta}{dr} + \frac{\sin 2\theta}{2r} \frac{d\psi}{d\phi} \right], \quad (2.28)$$

For Heisenberg stiffness, we obtain (see Eqs.(2.5),(2.6))

$$(\nabla \mathbf{m})^2 = \mathbf{v}_1^2 (\nabla \theta)^2 + \mathbf{v}_2^2 (\nabla \psi)^2 = \left( \frac{d\theta}{dr} \right)^2 + \frac{\sin^2 \theta}{r^2} \left( \frac{d\psi}{d\phi} \right)^2. \quad (2.29)$$

Thus, for a Bloch-type skyrmion with  $|Q| = 1$ ,  $\psi = \phi - \pi/2$ , and

$$\mathbf{m} \cdot (\nabla \times \mathbf{m}) = - \left[ \frac{d\theta}{dr} + \frac{\sin 2\theta}{2r} \right], \quad (\nabla \mathbf{m})^2 = \left( \frac{d\theta}{dr} \right)^2 + \frac{\sin^2 \theta}{r^2}, \quad (2.30)$$

where we have used properties  $\mathbf{v}_1^2 = 1$ ,  $\mathbf{v}_2^2 = \sin^2 \theta$ ,  $\mathbf{v}_1 \cdot \mathbf{v}_2 = 0$  of auxiliary vectors defined in Eqs. (2.7)-(2.8). The skyrmion energy with respect to a field-polarized (ferromagnetic) background therefore reads

$$\Delta W = 2\pi M^2 \int dr r \left\{ J \left[ \left( \frac{d\theta}{dr} \right)^2 + \frac{\sin^2 \theta}{r^2} \right] + D \left( \frac{d\theta}{dr} + \frac{\sin 2\theta}{2r} \right) + \frac{H}{M} (1 - \cos \theta) \right\}. \quad (2.31)$$

For numerical calculations, it is more convenient to introduce dimensionless variables by measuring rest energy of a skyrmion in units of  $JM^2$  and radial distance in units of lattice parameter,  $x = \rho/a$ ,

$$\frac{\Delta W}{JM^2} = 2\pi \int_0^\infty dx x \underbrace{\left[ \theta_x'^2 + \frac{\sin^2 \theta}{x^2} + 2k_0 \left( \theta_x' + \frac{\sin 2\theta}{2x} \right) + 2\mathfrak{h}(1 - \cos \theta) \right]}_{\equiv \Omega(\theta, \theta'; x)}, \quad (2.32)$$

where we have introduced the dimensionless quantity  $k_0 = Da/2J$  (this is modulation vector times lattice constant), and magnetic field  $\mathfrak{h} = Ha^2/2JM$ . After that, we solve the variational problem with respect to the configuration  $\theta(r)$  which minimizes the rest energy for given  $k_0$  and  $\mathfrak{h}$ . Namely, we write<sup>8</sup>

$$\frac{\partial \Omega(\theta, \theta'; x)}{\partial \theta} = 2x \left[ \frac{\sin 2\theta}{2x^2} + \frac{k_0 \cos 2\theta}{x} + \mathfrak{h} \sin \theta \right], \quad (2.33)$$

$$\frac{\partial \Omega(\theta, \theta'; x)}{\partial \theta'} = 2x [\theta' + k_0], \quad (2.34)$$

$$\frac{d}{dx} \frac{\partial \Omega(\theta, \theta'; x)}{\partial \theta'} = 2x \left[ \theta'' + \frac{\theta'}{x} + \frac{k_0}{x} \right], \quad (2.35)$$

Therefore, the Euler-Lagrange equation which extremizes the skyrmion configuration

---

<sup>8</sup>For a generalized action  $A = \int_{t_1}^{t_2} L(q, \dot{q}; t) dt$ , the Euler-Lagrange equation reads  $\frac{\partial L}{\partial q} - \frac{d}{dt} \frac{\partial L}{\partial \dot{q}} = 0$ , here  $q$ ,  $\dot{q}$ ,  $t$  are the generalized coordinates, velocity, time. See e.g. Principle of Least Action in Ref.[120].

reads

$$\theta''(x) + \frac{1}{x}\theta'(x) - \frac{\sin 2\theta}{2x^2} + 2k_0 \frac{\sin^2 \theta}{x} - \mathfrak{h} \sin \theta = 0, \quad (2.36)$$

with boundary conditions:  $\theta(0) = \pi$ ,  $\theta(\infty) = 0$ , corresponding to the “spin down” in the very center of the skyrmion and “spins up” on its periphery. In general case, the solution of the nonlinear differential equation (2.36) can be done only numerically. The long-scale asymptote to this equation can be found analytically; as  $x \rightarrow \infty$ , it is  $\theta(x) \sim \frac{e^{-\mathfrak{h}x}}{\sqrt{\mathfrak{h}x}}$  (see next section).

It is the boundary conditions who dictate the exact form of a skyrmion and, in many cases, the very existence of solution of the *skyrmionic equation* of type Eq.(2.36)<sup>9</sup>. We stress here that the equation (2.36) with these boundary conditions should be solved very cautiously. In particular, due to the structure of the equation, the second boundary condition at infinity,  $\theta(\infty) = 0$ , should be implemented with a reliable and controllable method. Setting some finite  $L$  such that  $\theta(L) = 0$  is not only wrong, but deeply unphysical as the skyrmion radius in such a case becomes strongly dependent on the choice of  $L$  and the function  $\theta(x > L)$  is dramatically divergent.<sup>10</sup> In other words, one needs to satisfy both  $\theta(\infty) = 0$  and an intuitive  $\theta'(\infty) = 0$ , – which follows from the long-scale asymptote  $\frac{e^{-\mathfrak{h}r}}{\sqrt{\mathfrak{h}r}}$ , – so the (numerical) solution is physically reasonable at infinity. To my experience, there are just a few numerical methods with a controllable output at  $x \gg 1/k_0$ , and probably the best combination of both the speed and reliability is secured by solving an *auxiliary Cauchy problem*.<sup>11</sup>

The idea of solution is following: instead of solving the Dirichlet boundary value problem with  $\theta(0) = \pi$ ,  $\theta(\infty) = 0$ , we try to reformulate the boundary value problem (BVP) in such a way that we can easily address it numerically. One of the ways of doing it is to formulate a set of “initial conditions” at some point, so the integration would be straightforward. In general, there are two locations when we supposedly know something about the skyrmion: at the very center or at the very periphery. Clearly, we cannot address it from the periphery, as  $\infty$  is not accessible numerically. Thus we focus on the very center of the skyrmion, where we know that the spin points down ( $\theta(0) = \pi$ ), however, we do not know how fast it twists from that direction (i.e., what is  $\theta'(0)$ ). We can however make an educated guess. We start from a small negative slope (in order of  $k_0$ ), and look how the trajectory behaves in the phase space  $\{\theta(x), \varkappa(x) \equiv \theta'(x)\}$ , by solving a system of first-order differential equations,

<sup>9</sup>There could be further modifications to the skyrmionic equation by including e.g. anisotropies.

<sup>10</sup>The same stands for  $\theta(L) = \epsilon \ll 1$ , as the radius of the skyrmion in this case strongly depends on the choice of  $\epsilon$  and  $L$ .

<sup>11</sup>In differential calculus, the Cauchy problem is a type of a boundary value problem, for which the boundary conditions are given at the same point, e.g. by defining both the function and its derivative at the “starting” point for the second order ordinary differential equation.



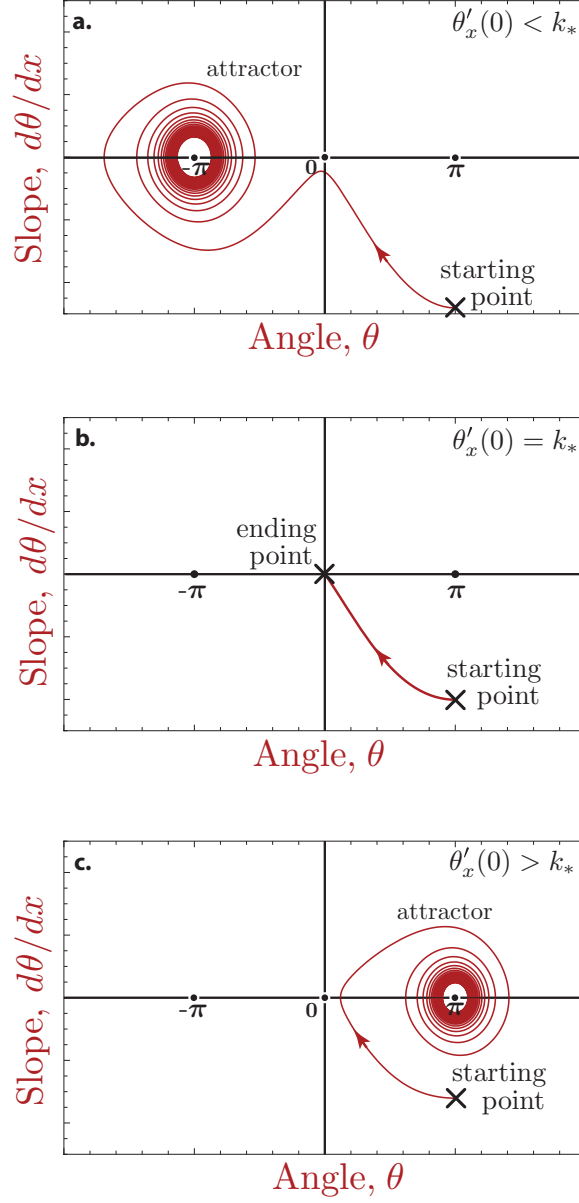


Figure 2.7: Phase portraits analysis of Euler-Lagrange Equation (2.36) to determine the skyrmion solution. We look for a phase portrait which satisfies the skyrmion boundary conditions on infinity ( $\theta(\infty) = 0$ ,  $\theta'(\infty) = 0$ ), which corresponds to crossing point  $(0,0)$  on these plots. (a) The phase trajectory winds around *attractor*  $(-\pi, 0)$  and does not cross the plot origin; (c) The phase trajectory winds around attractor  $(\pi, 0)$  and does not cross  $(0,0)$ ; (b) The phase trajectory crosses  $(0,0)$  for one and only one initial  $\theta'(0)$  with  $\theta(0) = \pi$  fixed. This curve is called a *separatrix*, as it separates two unphysical branches of solutions. There are others attractors (not shown), e.g.  $\pm 3$ ,  $\pm 5$ , with separatrices corresponding to skyrmions of higher topological charges.

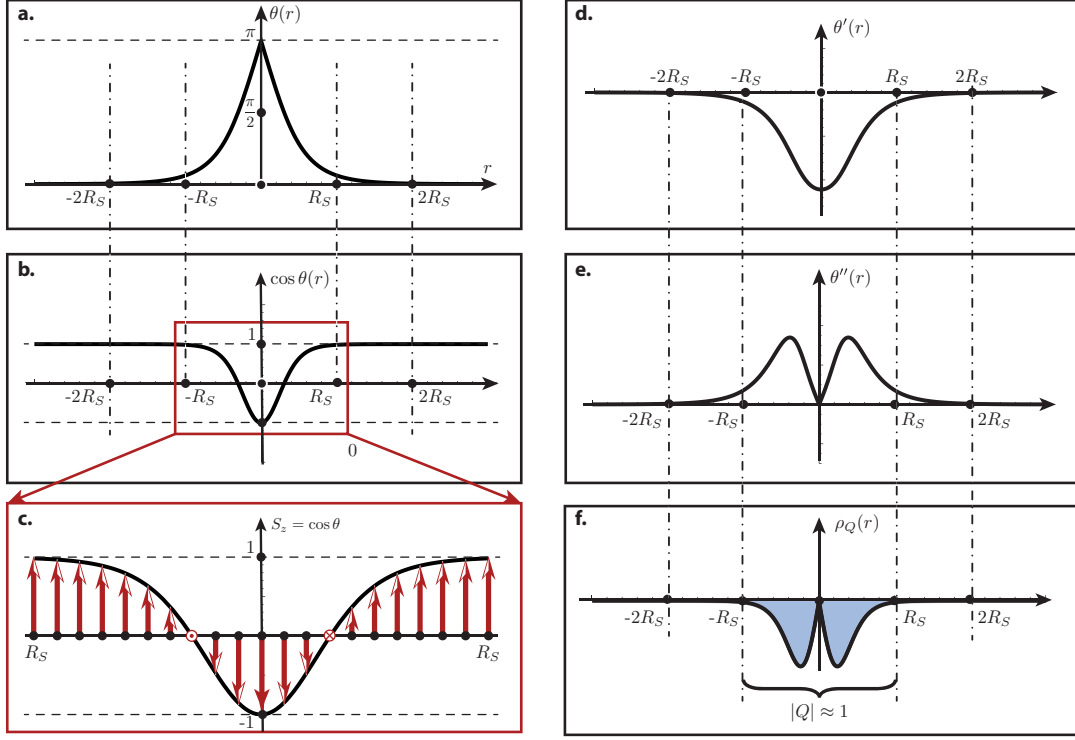


Figure 2.8: A typical skyrmionic solution of Euler-Lagrange equation (2.36). a) Angular profile  $\theta(r)$  corresponding to unitary topological charge; b)  $\cos\theta(r)$  represents the z-projection of local magnetization, showing the  $2\pi$  spin twist (c). d) and e): the skyrmionic angular slope and angular curvature; f) radial topological charge density,  $Q \equiv \int \rho_Q dr$ . We define skyrmion radius such as integrated skyrmion charge is  $\left| \int_0^{R_S} \rho_Q dr \right| \approx 1$ .

$$\varkappa'(x) = -\frac{\varkappa(x)}{x} + \frac{\sin 2\theta}{2x^2} - 2k_0 \frac{\sin^2 \theta}{x} + \mathfrak{h} \sin \theta = 0, \quad (2.37)$$

$$\theta'(x) = \varkappa(x), \quad (2.38)$$

$$\theta(0) = \pi, \quad \varkappa(0) = k < 0. \quad (2.39)$$

We thus treat  $\varkappa(x)$  and  $\theta(x)$  as independent functions and look iteratively for such  $k$  that the phase trajectory goes through  $\varkappa = 0$ ,  $\theta = 0$ . Depending on the starting point, the trajectory in phase space winds around one of the attractors<sup>12</sup> see figure 2.7. The line which separates the two attractors is called *separatrix* and in our case it passes through  $\{\theta(\infty) = 0, \theta'(\infty) = 0\}$ . The value of  $k_* = \theta'(0)$  corresponding to the separatrix depends crucially on  $\mathfrak{h}$  and  $k_0$ ; for  $\theta'(0) < k_*$ , the phase trajectory winds around  $\theta'(0) > k_*$ . It is

<sup>12</sup>An attractor is a state towards which a system evolves around for a wide region of initial conditions. The definition of an attractor uses metrics of a given system, but as a general rule the resulting notion depends only on topology of the phase space.

thus possible to find iteratively the value  $k_*$  with any beforehand given accuracy (maybe limited by the computational power), and thus the behavior of  $\theta(x)$  for large distances is fully controllable. The value of a skyrmion radius does not depend on ultimate accuracy of  $k_*$ , and for most calculations with skyrmions 3-4 digits is sufficiently enough.<sup>13</sup> Note that the solution of auxiliary Cauchy problem of (2.37)-(2.39) acquires a total twist  $\Delta\theta = \int_0^\infty \theta'(x)dx = \pi$ . However, the equation of form (2.36) allows other topologically distinct solutions: the acquired phase  $\theta(0) - \theta(\infty)$  can be  $\pm\pi, \pm3\pi, \pm5\pi$ , etc., reflecting topological charge  $Q$ .

The energetics of a skyrmion follows from substituting the solution to Euler-Lagrange equation(2.36) in the energy density  $\Omega(\theta, \theta'; x)$  in Eq.(2.32), see Figures 2.8 and 2.9. In our minimal model (2.25), the skyrmion experiences only three types of interactions: Heisenberg exchange  $J$ , chiral interaction  $D$ , and Zeeman energy. The Heisenberg exchange, crucial at the very short scales where the system is effectively a ferromagnet, tends to destabilize the skyrmion as a non-collinear field configuration; on contrary, chiral interaction  $D$  not only promotes the tilting spins, but also stabilizes the skyrmion energy density on moderate distances; finally, the Zeeman term (which is energetically unfavorable for flipped spins) ensures the skyrmion solution in strong magnetic fields<sup>14</sup> however, the skyrmion is not thermodynamically stable as the integrated energy is positive with respect to the field-polarized phase. This means that under such conditions a skyrmion can appear only as a field excitation with probability of order  $e^{-\Delta W/T}$ , and thus with a finite lifetime; this situation is seen in many experiments, where skyrmions appear and vanish over the sample (see e.g. [96]). It is however possible to enrich the minimal model (2.25) with other terms which lead to proliferation and even to thermodynamic stability of skyrmions, be it in a weakly-interacting skyrmion gas or a skyrmion lattice form. One further needs, for example, a rather strong uniaxial anisotropy [28] or "higher-order" terms of different nature (including those of magnetocrystalline origin) to thermodynamically stabilize skyrmions in bulk chiral magnets [34, 38].

The interplay of the energy terms, together with both the existence or non-existence of skyrmionic solution to variational equation (2.36) determines the **stability category** for a skyrmion. In a rather simple classification, the continuous-field skyrmions can be stable, metastable and unstable, depending on the existence of skyrmionic solution to (2.36) and the energy sign of the energy gap  $\Delta W$ : **unstable** if no skyrmionic solution exists; **metastable**, if the skyrmionic solution exists but the (free) energy barrier with respect to the surrounding phase is positive,  $\Delta W > 0$ ; **stable** if both the solution exists and  $\Delta W < 0$ , – often referred to as a thermodynamically stable skyrmion [28, 38]. Because the role of topology in the latest case is in providing a skyrmionic state being

<sup>13</sup>This is of course not the case for chiral magnetic bubbles, which have a wide flat core ( $\theta'(0) \approx 0$ ), however the method is still applicable in full.

<sup>14</sup>Beautiful it is: we supposed in Eq.(2.31) a skyrmion being embedded in the field-polarized phase, – the phase which itself requires strong magnetic fields. The skyrmion solution is also present only in strong magnetic fields with the minimal model (2.25).

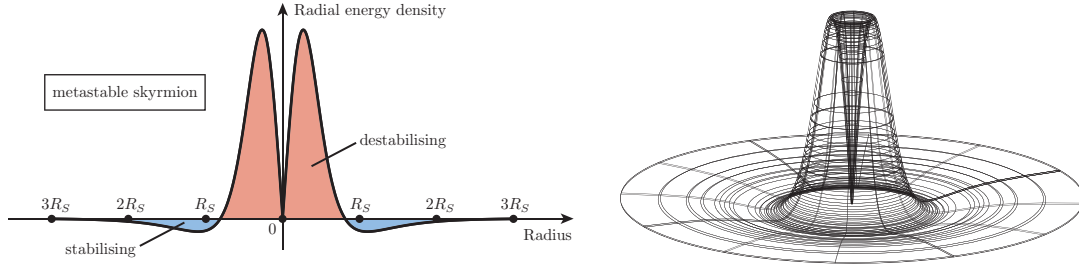


Figure 2.9: An energy profile of a metastable skyrmion: even though a skyrmionic solution of a minimal model (2.25) exists in field-polarized phase (very strong magnetic fields), it is metastable as the integrated energy is higher than the energy of the underlying phase; short-scale Heisenberg interaction, as a general rule, destabilizes the skyrmion (red), while DMI and Zeeman interaction tend to stabilize the skyrmion (see discussion in main text), however, only with a partial success. One thus further needs either a uniaxial anisotropy or "higher-order" terms of different nature (including those of magnetocrystalline origin) to stabilize a skyrmion in chiral magnets. Radial energy density is  $\Omega(\theta, \theta'; x)$  in Eq.(2.32) upon substitution of skyrmionic solution to Euler-Lagrange equation(2.36).

energetically lower than the surrounding phase, such skyrmions are protected due to the topologically-induced energetic barrier. However, in real systems, magnetization field is discrete (magnetic moments are localized on atoms), so, as a general rule, the topological protection is not strict; recent studies indicate the existence of a topological energy barrier for dynamical skyrmion creation in order of  $J < \Delta W < 2J$  [98], and different channels for topological charge dissipation are possible.<sup>15</sup>

### 2.3 SKYRMION TAILS

As another quasiparticle property, skyrmion-skyrmion interactions are pivotal in a number of both theoretical and applied studies for skyrmionic behavior. In the general case, because of the nontrivial topology and often deformed shapes and the presence of impurities, this question may be in general addressed only numerically. However, in a number of problems, – such as for the systems where skyrmions can be considered as weakly non-ideal two-dimensional gas, – the crucial characteristic is the low-energy ( $k \rightarrow 0$ ) asymptote of skyrmion-skyrmion interaction. Thus, to obtain an effective low-energy skyrmion-skyrmion interaction vortex, I re-derive here the long-scale asymptote of the skyrmion field, the "skyrmion tail".

The general procedure for finding the asymptote of 2nd-order ordinary differential equation is following: (i) linearize the ODE  $F(y(x); y'(x); y''(x); x) = 0$  with respect to  $y(x)$  and its derivatives; (ii) reduce the linearized equation to the oscillatory form  $u''(x) + k^2(x)u(x) = 0$ ; (iii) solve the resulting equation and restore  $y(x)$  [124–126].

<sup>15</sup>See e.g. Refs.[82, 121–123].

We thus consider a remote asymptote of the skyrmion in a uniform background. We start from the Euler-Lagrange equation as derived above from the minimal model,

$$\theta''(x) + \frac{1}{x}\theta'(x) - \frac{\sin 2\theta(x)}{2x^2} + 2k_0 \frac{\sin^2 \theta(x)}{x} - \mathfrak{h} \sin \theta(x) = 0, \quad (2.40)$$

Linearization of this equations yields formally  $\theta(x \rightarrow \infty) \rightarrow 0$ , thus one gets

$$\theta''(x) + \frac{1}{x}\theta'(x) - \frac{1}{x^2}\theta(x) - \mathfrak{h}\theta(x) = 0, \quad (2.41)$$

Now, we get rid of the term with first derivatives by proceeding to a new variable  $u(x) = \sqrt{x}\theta(x)$ , which gives

$$u''(x) - \kappa^2(x)u(x) = 0, \quad \kappa^2(x) = \mathfrak{h} + \frac{3}{4x^2}. \quad (2.42)$$

As  $\kappa(x)$  is slowly varying at  $x \rightarrow \infty$ , the long-scale asymptote is thus given by (see e.g. Ref.[124–126])

$$u(x) \simeq \frac{e^{-\int \kappa(x) dx}}{\sqrt{\kappa(x)}} \simeq \text{Const} \times \frac{e^{-\mathfrak{h}x}}{\sqrt{\mathfrak{h}}}. \quad (2.43)$$

Restoring the dimensional units, as also using  $\theta(x) = u(x)/\sqrt{x}$ ,  $r = xa$  the long-scale asymptote is given by

$$\theta(r) \propto \sqrt{\frac{2JM}{Ha^2r}} \exp\left[-\frac{Ha^2r}{2JM}\right]. \quad (2.44)$$

Thus the skyrmion tail, at least in ferromagnetic background, decays faster than exponentially,  $e^{-\mathfrak{h}x}/\sqrt{x}$ . Note that in many papers there is a confusion about that: the skyrmion tail is said to behave as  $e^{-\mathfrak{h}x}$  – apparently by inheriting from Ref.[127] and some later papers of Bogdanov. The way it was obtained is by dropping all the terms in (2.40), but  $\theta''(x) - \mathfrak{h}\theta(x) = 0$ . This is simply wrong. You cannot drop terms in a differential equation just because they are small.<sup>16</sup>

## 2.4 CONCLUSIONS

In this chapter, I mainly reviewed the crucial properties of a skyrmion in chiral magnets. A skyrmion is, simply speaking, a quasiclassical magnetic vortex; however its *nanoscale*

---

<sup>16</sup>One of the most known manifestation of that is probably Navier-Stokes equations and turbulence.

*size* and *strict topological charge* make the skyrmion a rather robust quasiparticle, with a moderate lifetime even if it is energetically metastable. The skyrmion field is, as a general rule, incommensurate with the atomic lattice (magnetic moments not pinned to certain atoms), which allows the skyrmion to move rather freely through the sample. The topological charge is independent of the underlying crystallographic symmetry, however a particular helicity of a skyrmion (e.g. Bloch-type or Néel-type) is mainly influenced by the particular form of chiral interactions (DMIs), which in the bulk materials is indeed induced by the crystallographic symmetry. The axisymmetric skyrmions have a rather fast-decaying (*faster-than-exponentially*) tails, through which they may weakly interact with each other at moderate distances. In experiments, however, the shape of skyrmions is somewhat distorted by random-field fluctuations, making them more amoeboid, especially in case those large skyrmions ("skyrmion bubbles") which are rather soft in thin films and at interfaces. One thus should very carefully interpret any links between the axisymmetric skyrmion model and direct experimental data, and, – in some desperate cases, – shouldn't at all.

Furthermore, if existence of a long-range order in the skyrmion phase is established,<sup>17</sup> one then needs to keep in mind that condensed matter techniques may serve as a better descriptive tool for herding the skyrmion arrays as a thermodynamically stable magnetic phase. In particular, this is crucial for the bulk systems, where the skyrmion phase is stable only in a very narrow window near the ordering temperature, - mainly due to the long-range-order critical fluctuations, without which the conical phase competes better in free energies [38]. In thin films, however, due to a very rich sets of DMIs, dipolar interactions and anisotropies, the skyrmions are well described even at the level of abstraction of a "skyrmion gas" or a "skyrmion liquid", and usually a single-skyrmion solution translated through the 2D space benefits in good results (see e.g. [105, 128], and references therein).

---

<sup>17</sup>For example, by probing with neutron scattering or X-ray imaging.

# 3

## Universality of Phase Diagrams in Bulk Skyrmion-hosting Materials

Experimentally, the study of skyrmions is very much shaped by the conditions under which skyrmions exist or may exist under proper tuning. In this regard, a typical characteristic of a skyrmion host material is a magnetic phase diagram, - a graphical summary on how the spin order is influenced by magnetic field and temperature. The phase diagram of the most bulk skyrmion hosting materials reveals a remarkable universality in its constitutional components and their arrangement. The phase diagram typically consists of the four main magnetic phases, a disordered paramagnetic phase, which is replaced by one of three ordered phases, - helical, conical, and SkL, - as one cools down the sample. Below the ordering temperature  $T_C$  the thermal ground state (the ground state in terms of  $H = 0$ ,  $0 \leq T \leq T_C$ ) is a helical phase, with spins rotating within a plane that is perpendicular to the propagation vector  $Q$ , usually set by magnetocrystalline anisotropy. Upon the application of magnetic field  $H > H_{C1}(T)$  the magnetic structure polarizes into a conical phase, where spins precess within a surface of a cone, axially-aligned with the direction of magnetic field. Going higher in magnetic fields, namely  $H > H_{C2}$ , the spin structure is the so-called field-polarized ferromagnet (all spins are aligned up towards the direction of magnetic field). In bulk, the skyrmion phase is placed very close to the order-disorder line, usually within just a few % of  $T_C$ , in terms of temperature range. A first-order phase transition separates the skyrmion phase from the paramagnetic state at the high temperature side, while on the low temperature side the skyrmion phase is surrounded with the conical phase. From the specific heat measurements on MnSi it

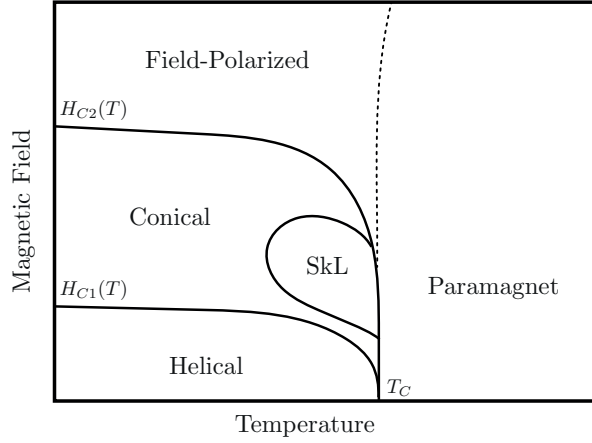


Figure 3.1: A sketch of a bulk phase diagram: the five distinct magnetic phases are usually present. At high temperatures ( $T > T_C$ ), the system exists in a disordered paramagnetic state. Upon cooling down, the ordered phases appear: the ground state is the helical phase which is observed at low magnetic fields. With increasing magnetic fields, the helical phase polarizes into the conical phase which is defined for  $H_{C1}(T) < H < H_{C2}(T)$ , but not in the vicinity of the  $T_C$  where the bulk critical modes promote the Skyrmion Lattice phase (SkL), which is a thermodynamically stable long-range topological phase. For even higher magnetic fields, all the spins are polarized into a forced ferromagnetic state (all spins are aligned), which is labelled as the Field-Polarized (FP) magnetic phase.

has been established that this transition is also first-order while recent AC susceptibility measurements on  $\text{Cu}_2\text{OSeO}_3$  showed a more complex behavior [129] with a wide dissipation region and a double-peak feature at low frequencies. This field-temperature region, where the skyrmion phase is stable, is often referred to as a *skyrmion pocket*.

The skyrmion lattice can to some approximation be considered as a regular, long-range ordered hexagonal arrangement of individual skyrmions. For each of the skyrmions in the vortex lattice, the central spin points in the opposite direction of the applied magnetic field and there is a sense of rotation of spins around the central spin, thus allowing to introduce the topological charge. The appearance of the hexagonal structure can be illustrated by applying a modified closed packing theorem. The close-packing of equal spheres is a mathematical problem which has been solved only in several finite dimensions, see e.g. recent studies [130, 131]. For a 2D spheres (circles), the closest packing is achieved for a hexagonal lattice, giving the surface occupancy  $\pi/2\sqrt{3} \approx 0.9069$ .<sup>1</sup> It can be shown that this theorem also applies towards the solid-core 2D circles with thin-walled soft borders, thus fulfilling a qualitative explanation of why we have hexagonal skyrmions in bulk. Thus the energetics of the skyrmion lattice could be, to some extent, captured by considering many skyrmions with radially symmetric cores glued together. This approach may work for a number of purposes, but in general is not qualified for capturing phase transitions - in the same way as considering individual atoms cannot

<sup>1</sup>The square lattice packing is  $\pi/4 \approx 0.7854$ .



capture the physics of crystallization and lattice melting.

In bulk materials, the role of critical fluctuations is very important in the skyrmion phase. In fact, from the condensed matter point of view, the phase with lower symmetry is more sensitive to thermal fluctuations, simply because the higher symmetry usually means breaking restrictions on thermal fluctuations propagation. For example, the paramagnetic phase is essentially made up of thermal fluctuations and is of the highest symmetry in the phase diagram on Figure 3.1. The skyrmion phase has lower symmetry than both the conical and helical phases, so that the entropy of the critical fluctuations could be high enough to drive the free energy down, allowing the stabilization of the skyrmion phase near  $T_C$ , where the SkL is closely competing with the conical phase already in the mean-field sense.

This chapter is constructed as follows: first, we discuss the mean-field approach which allows to qualitatively distinguish the transition between paramagnetic/field-polarized and conical phases, and, in principle, the crossover between the helical and conical if spatially anisotropic terms are added in the model. This approach, however, does not allow to establish the phase diagram even qualitatively because the skyrmion phase is always higher in free energy. It does however compete very closely with the conical phase near  $T_C$ . Thus the next model I very briefly review in this section is the path-integral formulation (also referred here as Rosch model). This model allows now to qualitatively calculate the phase diagram, including the conical and skyrmion phase. However, the qualitative criterion of the breakdown of the ordered phases near  $T_C$  does not allow quantitative comparison with experimental phase diagrams. In the next section, I described the new model developed on the basis of the existing model in a more self-consistent way and reviewing the role of critical fluctuations in the system. The developed approach allows a deeper understanding of the role of the critical fluctuations near  $T_C$ , which in the first approach can be viewed as noninteracting quasiparticles. Adding these quasiparticles on top of the mean-field solution cost more entropy in the skyrmion phase, which drives the stability of the skyrmion phase close to  $T_C$ . Additionally, the model allows relatively easy expansion towards the interacting critical modes and qualitatively captures the almost vertical (magnetic-field-independent) breakdown of ordered phases near  $T_C$ , as observed in experiments.

### 3.1 MEAN-FIELD MODEL AND ITS LIMITATIONS

#### 3.1.1 FREE ENERGY IN THE COARSE-GRAINED MODEL

The Skyrmion Lattice (SkL) is a long-range-order spin configuration and thus the condensed-matter description here is more appropriate as it naturally encapsulates emergent many-body phenomena. Conventionally, it is thus primarily important to establish the corresponding order parameter of the skyrmion phase, and thus it is easier to work within a continuous-limit order parameter of coarse-grained local magnetization.

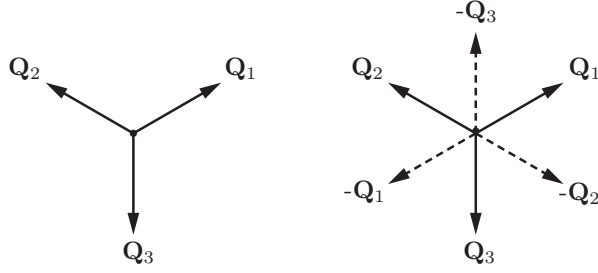


Figure 3.2: The multispiral ("3Q") SkL structure in reciprocal space. Right-hand side of the figure shows the auxiliary negative reflexes, so that the hexagonal real-space SkL is built on the six wave vectors  $\{\mathbf{Q}_1, -\mathbf{Q}_3, \mathbf{Q}_2, -\mathbf{Q}_1, \mathbf{Q}_3, -\mathbf{Q}_2\}$ , see the main text.

Experimentally, the hallmark of the SkL phase is appearance of a six-fold reflection pattern in reciprocal space, as sketched in Fig. 3.2, each of the wave vectors are rotated by  $2\pi/3$  (see e.g. Refs. [38, 132] for SANS patterns). In this study, we describe the skyrmion lattice by a coarse-grained local magnetization vector  $\mathbf{S}(\mathbf{r})$ , which can be built on the three  $\mathbf{Q}$ -vectors (Fig. 3.2). With a good accuracy the SkL phase can be approximated by the multispiral spin structure [37, 38]

$$\mathbf{S}(\mathbf{r}) = \mathbf{m} + \mu \sum_{\mathbf{Q}_n} \mathbf{S}_{\mathbf{Q}_n} e^{i\mathbf{Q}_n \mathbf{r} + i\varphi_n} + \mathbf{S}_{\mathbf{Q}_n}^* e^{-i\mathbf{Q}_n \mathbf{r} - i\varphi_n}, \quad (3.1)$$

where  $\mathbf{m} \equiv \langle \mathbf{S}(\mathbf{r}) \rangle$  is a uniform magnetization, with (spatial) average defined as  $\langle \dots \rangle = \int \frac{dV}{V} (\dots)$  throughout the study, and  $\mu$  is the weight of the SkL helical modulations. The sum in (3.1) runs over the "3Q-structure" (Figure 3.2), the relative phases  $\varphi_n$  in (3.1) are important for minimization of the SkL energy.

The expectation of energy density in the coarse-grained model is given by calculating the spatial average  $\langle \mathcal{H} \rangle$  with energy function

$$\mathcal{H} = \mathcal{H}_{JDh} + \mathcal{H}_A + \mathcal{H}_{\alpha E}, \quad (3.2)$$

where the helimagnetic term

$$\mathcal{H}_{JDh} = J(\nabla \mathbf{S})^2 + D \mathbf{S} \cdot (\nabla \times \mathbf{S}) - \mathbf{h} \cdot \mathbf{S} \quad (3.3)$$

where the shortcut  $(\nabla \mathbf{M})^2$  means  $\sum_{i,j} (\partial M_i / \partial x_j)^2$  and takes into account Heisenberg stiffness ( $J$ ),  $D$  is strength of Dzyaloshinskii-Moriya interaction and magnetic field  $\mathbf{h}$  Zeeman coupling to the external magnetic field.<sup>2</sup> We have already shown in the previous chapter that this minimal model provides a necessary but not sufficient set of conditions allowing

<sup>2</sup>For practical reasons, it is easier to proceed to "partially-dimensionless" formalism, where the local magnetization is  $\mathbf{S}(\mathbf{r}) = \mathbf{M}(\mathbf{r})/M_s$ , with  $M_s$  being the saturation magnetization (magnetization limit in strong magnetic fields), thus we introduce  $W_0 = F_0/(M_s^2 a^3)$ , and dimensionless magnetic field  $\mathbf{h} = \mathbf{H}/M_s$

the topologically-nontrivial skyrmionic solution.

This coarse-grained model for magnetic energy works well when the following hierarchy of energies is respected: (1) the strongest is Heisenberg exchange  $J$  which favours the ferromagnetic alignment; (2) the Dzyaloshinskii-Moriya interaction (DMI) is slightly tilting two adjacent spins thus resulting in helical modulations. (3) The cubic magnetocrystalline anisotropy  $\mathcal{H}_A$  together with the higher order terms of different nature plays the role for stabilization of the skyrmion lattice, and locks the helical modulation in cubic  $[1\ 1\ 1]$  direction, but in principle can be relatively weak. The spatial modulation of the ordered phase (the wavelength of the helices in the ground state) is given by a wave length of order  $\lambda/a \sim J/D \gg 1$ , i.e. much larger than the crystal lattice parameter  $a$ : for example, in  $\text{Cu}_2\text{OSeO}_3$ ,  $\lambda = 630\text{\AA}$ ,  $a = 8.9\text{\AA}$ , which gives  $\lambda/a \sim 70$ . In such case, the magnetization on neighbouring lattice sites is varying very slowly and the physics of the system in the ordered phase is appropriately described by a continuous-limit model as assumed in (3.7).

In this study, we consider the fourth-order anisotropy as it represents the essential physics of the problem by stabilizing the SkL phase[38, 132]. The symmetry of  $\text{Cu}_2\text{OSeO}_3$  is described by the  $P2_13$  space group, which allows a fourth-order magnetocrystalline anisotropy of the form  $A_1(S_x^4 + S_y^4 + S_z^4) + A_2(S_x^2 S_y^2 + S_y^2 S_z^2 + S_z^2 S_x^2)$ . Proceeding to the unitary parametrization  $\mathbf{S}/|\mathbf{S}| = (\sin\theta \cos\psi, \sin\theta \sin\psi, \cos\theta)$ , one obtains  $S_x^2 S_y^2 + S_y^2 S_z^2 + S_z^2 S_x^2 = -\frac{1}{2}(S_x^4 + S_y^4 + S_z^4) + \frac{1}{2}$ , we thus have:

$$\mathcal{H}_A = A(S_x^4 + S_y^4 + S_z^4) + U\mathbf{S}^4. \quad (3.4)$$

with  $A = A_1 - A_2/2$  and  $U = A_2/2$ . Thus, there could be two qualitatively distinct situations, first with  $A_1 \gg A_2$ , for which the anisotropy of the bulk is important, and the opposite case with  $A_1 \sim A_2/2$ , where the role of anisotropy is reduced to providing mode-mode coupling  $U \sim A_1, A_2$ . In this section, following my paper [133], we consider the first case, while the second case will be presented in the next section as it provides a qualitatively universal picture for bulk skyrmion hosts.

Finally, we make a remark on the importance of the anisotropy terms. The appearance of the six-fold set  $\{\mathbf{Q}_1, -\mathbf{Q}_3, \mathbf{Q}_2, -\mathbf{Q}_1, \mathbf{Q}_3, -\mathbf{Q}_2\}$  of helices phased in such a way as to form the two-dimensional skyrmion crystalline can occur only as a consequence of higher-order energy terms represented in the model. A third-order term like  $\mathbf{S}^3$  is however forbidden by a symmetry promoted by magnetic field. Therefore, the anisotropy of at least the fourth order can be considered as the source of the skyrmion lattice order parameter (3.1) in bulk chiral ferromagnets.<sup>3</sup> Indeed, we can consider the fourth order anisotropy which contains - fully or partially - the term  $\mathbf{S}^4(\mathbf{r}) = S_x^4 + S_y^4 + S_z^4 + 2(S_x^2 S_y^2 + S_y^2 S_z^2 + S_z^2 S_x^2)$ . After decoupling the uniform component,  $\mathbf{S}(\mathbf{r}) = \langle \mathbf{S} \rangle + \mathbf{s}(\mathbf{r})$ , the expansion will contain the

---

<sup>3</sup>In metallic chiral magnets such as  $\text{MnSi}$ , the  $\mathbf{S}^4$  term may appear as the result of conductive mode-mode interaction [38].

cubic term

$$\mathbf{S}^4(\mathbf{r}) = [\mathbf{s}(\mathbf{r}) + \langle \mathbf{S}(\mathbf{r}) \rangle]^4 = \dots + 4\mathbf{s}^2(\mathbf{r}) \mathbf{s}(\mathbf{r}) \cdot \langle \mathbf{S}(\mathbf{r}) \rangle + \dots, \quad (3.5)$$

which thus generates a third-order term with momentum-conserving 3-helix condition  $\mathbf{Q}_1 + \mathbf{Q}_2 + \mathbf{Q}_3 = 0$ ,

$$\langle \mathbf{s}^2(\mathbf{r}) \mathbf{s}(\mathbf{r}) \rangle = \sum_{\mathbf{Q}_i} (\mathbf{S}_{\mathbf{Q}_1} \cdot \mathbf{S}_{\mathbf{Q}_2}) \mathbf{S}_{\mathbf{Q}_3} \delta(\mathbf{Q}_1 + \mathbf{Q}_2 + \mathbf{Q}_3). \quad (3.6)$$

One can show that the solution of a higher symmetry phase (SkL) can be expressed through the three in-plane  $\mathbf{Q}$  vectors, equirotated by  $2\pi/3$ , with an arbitrary rotation  $\phi$  in the plane,<sup>4</sup> as it can be already guessed from the right illustration in Fig. 3.2. Therefore, the multispiral phase (SkL) is supposed to minimize the terms which include the form of (3.6) after an appropriate variational choice of order parameter components.

We note that the effective description of the skyrmion-host magnetic phase diagram in bulk materials is already possible within the  $US^4$  formalism. The remarkable universality in phase diagrams of different materials, and qualitatively-invariant constitution of the phase diagram under sample rotation, leads us to conjecture that the rotationally-invariant  $US^4$  term is responsible for most of the qualitative physics related with the skyrmion lattices in bulk. Moreover, the observed *Brazovskii sphere* of critical fluctuations at  $T_C$  [134] indicate that the fluctuation-induced phase transition in these systems is of isotropic nature [135] (see also further discussion in the end of the chapter). Thus we consider the effective Hamiltonian function as

$$\mathcal{H}_{J Dh} = J(\nabla \mathbf{S})^2 + D \mathbf{S} \cdot (\nabla \times \mathbf{S}) + U \mathbf{S}^4 - \mathbf{h} \cdot \mathbf{S}, \quad (3.7)$$

and work within this effective model unless required otherwise.

**LANDAU-LIKE FREE ENERGY** To compare directly different thermodynamic phases, one needs however to consider not the energy of the phase  $\mathcal{E}$ , but the free energy  $F = \mathcal{E} - TS$ . Thus the entropy of the phase, – which also includes the entropy of phase-promoted elementary excitations at finite temperatures, – is important as it may play the key role in stabilization of one phase with respect to others. In this respect, Ginsburg

---

<sup>4</sup>Indeed, rewriting the equation  $\mathbf{k}_1 + \mathbf{k}_2 + \mathbf{k}_3 = 0$  in the complex form gives two equations:  $\rho_1 e^{i\phi_1} + \rho_2 e^{i\phi_2} + \rho_3 e^{i\phi_3} = 0$  plus a conjugated equation. Looking now for a lowest Fourier harmonic,  $|\mathbf{k}_1| = |\mathbf{k}_2| = |\mathbf{k}_3| = k_0$ , gives two equations  $1 + e^{\pm i\Delta\phi_{21}} + e^{\pm i\Delta\phi_{31}} = 0$ , where  $\Delta\phi_{21} = \phi_2 - \phi_1$ ,  $\Delta\phi_{31} = \phi_3 - \phi_1$  are the relative rotations of the wave vectors. Solution of these equations gives  $\cos\Delta\phi_{31} - \cos\Delta\phi_{21} = -1/2$ , or  $\Delta\phi_{32} = \Delta\phi_{31} - \Delta\phi_{21} = \pm 2\pi/3$ . Now, because this treatment is independent of how we label the initial momenta, we get the threesome of vectors with  $\phi$ ,  $\phi + 2\pi/3$ ,  $\phi + 4\pi/3$ , and the rotational parameter  $\phi$  to be determined further from the variational principle.

and Landau came up with a phenomenological free energy functional of coarse-grained local magnetization  $\mathbf{M}(\mathbf{r})$  to address the spontaneous symmetry breaking, which for a ferromagnet in its minimal set is given by

$$F_{\text{ferro}}[\mathbf{M}(\mathbf{r})] = \langle \alpha_T \mathbf{M}^2 + J(\nabla \mathbf{M})^2 + U_0 \mathbf{M}^4 - \mathbf{H} \cdot \mathbf{M} \rangle, \quad (3.8)$$

where  $\langle \dots \rangle$  is the spatial average.<sup>5</sup> This functional is constructed by keeping lowest-order terms in  $\mathbf{M}$  which are not forbidden by the symmetry of the system, namely the inversion  $I$  ( $\mathbf{r} \rightarrow -\mathbf{r}$ ) and time-reversal  $\mathcal{T}$  ( $t \rightarrow -t$  plus complex conjugation), together with magnetic-field-induced symmetry ( $\mathbf{M} \rightarrow -\mathbf{M}$  if  $\mathbf{H} \rightarrow -\mathbf{H}$ ). It was shown that all the  $T$ -dependences can be encapsulated in phenomenological  $\alpha_T = \alpha_T(T)$ , so that the model (3.8) under minimization procedure gives either a paramagnetic  $\langle \mathbf{M} \rangle = 0$  for  $\alpha_T > 0$  or a uniform  $\mathbf{M} \neq 0$  for  $\alpha_T < 0$ , thus reproduces the ferromagnetic transition at ordering temperature  $T_C$  if  $\alpha_T = 0$  at  $T_C$ . As a general rule, the exact dependence  $\alpha_T(T)$  is not known and it is usually very hard to establish it microscopically; in some particular cases it could be guessed indirectly from typical experimental features; otherwise, the linear-like expansion  $\alpha_T \sim (T - T_C^{\text{m.f.}})$  is acceptable. Note also that as the magnetic moment is a normalizable quantity, one can in principle add an arbitrary term of form  $\text{const} \times \mathbf{M}^2$  to (3.8) as a Lagrange-multiplied term to adjust the model  $T_C^{\text{m.f.}}$  to the experimentally observed  $T_C$ .

We note that the free energy of a ferromagnet resembles our model (3.7), however one thing is missing: the DMI. In chiral magnets (such as skyrmion-hosting MnSi and Cu<sub>2</sub>OSeO<sub>3</sub>) the atomic unit cell lacks inversion symmetry. The lack of this symmetry relaxes the above stated requirements for the Ginsburg-Landau-like free energy functional and allows terms with an odd number of spatial derivatives to appear, – as they are odd under inversion symmetry. The lowest-order such terms were already considered in the previous chapter (Lifshitz invariants), which give the explicit form of DMI coupling in chiral magnets as  $D\mathbf{M} \cdot (\nabla \times \mathbf{M})$ , thus

$$F[\mathbf{M}(\mathbf{r})] = \langle \alpha_T \mathbf{M}^2 + J(\nabla \mathbf{M})^2 + D\mathbf{M} \cdot (\nabla \times \mathbf{M}) + U_0 \mathbf{M}^4 - \mathbf{H} \cdot \mathbf{M} \rangle, \quad (3.9)$$

or in other units used for further calculations,

$$F[\mathbf{M}(\mathbf{r})]/M_s^2 = \langle \alpha_T \mathbf{S}^2 + J(\nabla \mathbf{S})^2 + D\mathbf{S} \cdot (\nabla \times \mathbf{S}) + U\mathbf{S}^4 - \mathbf{h} \cdot \mathbf{S} \rangle. \quad (3.10)$$

We note that the Ginsburg-Landau model, which appeared as a purely phenomenological concept in spirit of power-expansion in the middle of last century, actually managed

---

<sup>5</sup>For brevity, we will also refer to the mean-field spatial average  $\langle W \rangle$  as an *expectation value* of  $W$ .

not only to survive but also to produce a number of physically meaningful semi-quantitative results in different fields of physics, and has been enhanced with additional superstructures on top of it, such as, e.g., renormalization group formalism. It is also possible to establish an extended variational ("path-integral") representation, by introducing averaging over thermally-weighted contributions to free energy,

$$G = \frac{1}{Z} \int d\mathbf{M} e^{-F[\mathbf{M}(\mathbf{r})]/T}. \quad (3.11)$$

In the next sections I present a unified formalism for considering the modulated chiral magnetic phases (helical, conical, SkL), show the importance of critical fluctuation, and treat the critical fluctuations within this formalism, which will then allow to implement electric-field-induced perturbation theory, self-consistently. The novelty here is therefore the unification of several very different approaches existing in literature, in a more consistent model which enhances both the calculation capabilities and our understanding of the system, reduces the order of computational difficulty, as also allows to study new mechanisms for enhancing skyrmion pockets in the bulk (see e.g. next chapter).

### 3.2 SOLUTION IN HELICAL PHASE

It has been known for a while [136, 137] that the ground state of model (3.10) is the so-called *helical phase*, in which the spins make (in-plane) helical rotations with respect to the propagation vector  $\mathbf{k}$ , see Figure 3.3. Mathematically, it is thus given in compact form by

$$\mathbf{S}_{\text{hel}}(\mathbf{r}) = \mu \left( \mathbf{S}_{\mathbf{k}} e^{i\mathbf{k}\mathbf{r} + i\varphi_0} + \mathbf{S}_{-\mathbf{k}} e^{-i\mathbf{k}\mathbf{r} - i\varphi_0} \right), \quad (3.12)$$

defined up to normalization parameter  $\mu$ , which is the measure of order parameter in the helical phase; here  $\mathbf{S}_{\mathbf{k}}$  is a Fourier-transformed spin modulation state.

Experimentally, the helical phase is seen by appearance of the helical stripes in magnetic contrast Lorentz transmission electron microscopy (LTEM). With the wavelength between these stripes  $\lambda$  (the typical distance between two same-contrast parallel lines), the wave vector of the helical phase is naturally  $\mathbf{k} = 2\pi/\lambda$ . This wave vector is often addressed in literature as the *modulation wave vector*, in the sense it produces a long-range-periodic ("modulated") spin structure, as in the more recent skyrmion papers simply called "*the helix*". I thus shall use both of this terms here.

It is possible to deduce, in rather simple arguments, what shall the helix wave vector be. It is clear that in the mean-field, without more advanced renormalization as will be partially addressed further, the modulation wave vector is determined by the gradient terms of the model (3.10), and maybe by higher-order anisotropy terms containing

spatial derivatives (not taken into account here). We thus start from a minimal model containing<sup>6</sup>

$$W_0 = \langle J[\nabla \mathbf{S}(\mathbf{r})]^2 + D \mathbf{S}(\mathbf{r}) \cdot [\nabla \times \mathbf{S}(\mathbf{r})] \rangle = \sum_{\mathbf{k}}^{\pm \mathbf{k}} \mathbf{S}_{\mathbf{k}}^\dagger \hat{\mathcal{H}}_0 \mathbf{S}_{\mathbf{k}}, \quad (3.13)$$

where we have re-written the spatial average  $\langle \dots \rangle$  in the momentum space, with the matrix operator<sup>7</sup>  $\hat{\mathcal{H}}_0$  given in the general case as

$$\hat{\mathcal{H}}_0 = \begin{pmatrix} Jk^2 & -iDk_z & iDk_y \\ iDk_z & Jk^2 & -iDk_x \\ -iDk_y & iDk_x & Jk^2 \end{pmatrix}. \quad (3.14)$$

In the real samples, it is the anisotropy of material properties who picks up a helix direction, – the feature undefined in the effective model (3.10). The physics of the helical ground state was studied in past and we will not focus on it much here. For simplicity, we denote  $\mathbf{k}/|\mathbf{k}| = [100]$  as the helical direction, thus

$$\hat{\mathcal{H}}_0 = \begin{pmatrix} Jk^2 & 0 & 0 \\ 0 & Jk^2 & -iDk \\ 0 & iDk & Jk^2 \end{pmatrix}. \quad (3.15)$$

For positive  $D, J$ , the *normalized* eigenvectors of this Hamiltonian matrix are

$$\mathbf{S}_k^{(0)} = \frac{1}{\sqrt{2}} \begin{pmatrix} 0 \\ i \\ 1 \end{pmatrix}, \quad \mathbf{S}_k^{(1)} = \begin{pmatrix} 1 \\ 0 \\ 0 \end{pmatrix}, \quad \mathbf{S}_k^{(2)} = \frac{1}{\sqrt{2}} \begin{pmatrix} 0 \\ -i \\ 1 \end{pmatrix}, \quad (3.16)$$

with corresponding eigenvalues

$$\varepsilon_k^{(0)} = Jk^2 - Dk, \quad \varepsilon_k^{(1)} = Jk^2, \quad \varepsilon_k^{(2)} = Jk^2 + Dk, \quad (3.17)$$

We note that for positive  $J, D$ , the lowest energy is favoured by  $S_k^0$ , which we will simply call the helix. From now, we intentionally drop "0" superscript and notice that due to the form of matrix (3.15), one has the eigen vector of the lowest energy ("the ground state") as

---

<sup>6</sup>The Zeeman term can be dropped due to zero net magnetization.

<sup>7</sup>I will call it "Hamiltonian" for brevity.

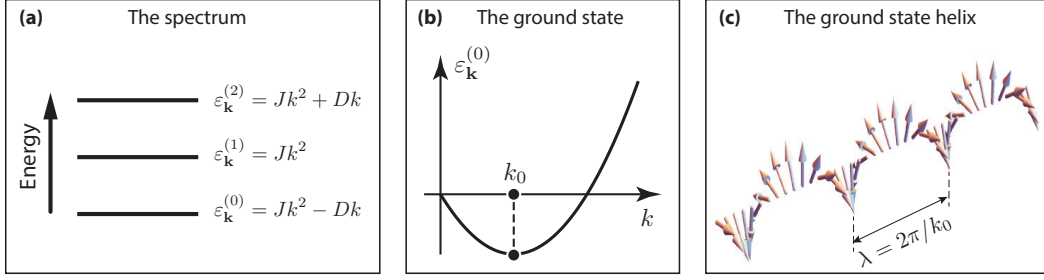


Figure 3.3: Appearance of the helical modulation: (a) The spectrum of  $3 \times 3$  energy matrix  $\hat{\mathcal{H}}_0$ . (b) Minimization of the state with lowest energy  $\epsilon_{\mathbf{k}}^{(0)} = Jk^2 - Dk$  gives helix wave vector  $\mathbf{k}_0 = D/2J$ . (c) Real-space visualization of the helix with  $\lambda = 2\pi/k_0$ .

$$\mathbf{S}_{\pm k} = \frac{1}{\sqrt{2}} (0 \ \pm i \ 1)^\top. \quad (3.18)$$

This corresponds to the real-space helix

$$\mathbf{S}_{\text{hel}}(x) = \mu \left( \mathbf{S}_k e^{ikx} + \mathbf{S}_{-k} e^{-ikx} \right) = \sqrt{2}\mu (0, \sin kx, \cos kx), \quad (3.19)$$

where  $\varphi_0$  is set to zero for simplicity. Finally, before proceeding further, we note that in the limit  $k \rightarrow 0$  (that is, as we shall see,  $D = 0$ ), the model degenerates into a uniform (ferromagnetic) magnetic phase.

With the ground state helix  $\mathbf{S}_{\pm k}^{(0)}$ , the eigenvalue  $\epsilon_k^{(0)} = Jk^2 - Dk$  is minimized at  $k_0 = D/2J$ ; indeed,

$$\frac{d}{dk} \epsilon_k^{(0)} = 2Jk - D = 0, \quad \text{at local minimum.} \quad (3.20)$$

Within the absence of higher-order spatial derivatives in effective model (3.10), the free energy gets

$$W[\mathbf{S}_{\text{hel}}(\mathbf{r})] = 2\alpha_T \mu^2 + 2Jk_0^2 \mu^2 - 2Dk_0 \mu^2 + 4U\mu^4, \quad (3.21)$$

in the helical phase.<sup>8</sup> The mean-field temperature dependence of magnetization is thus regulated by  $\alpha_T$ , by solving  $\mu(T) = \mu(\alpha_T)$  from

<sup>8</sup>We used the normalization condition  $\langle \mathbf{S}(\mathbf{r})^2 \rangle = \mu^2 \sum_{\pm k} \mathbf{S}_k^\dagger \mathbf{S}_k = 2\mu^2$ , which can be identically deduced from directly (3.19) by implying periodic boundary conditions.



$$\frac{dw}{d\mu} = 4(\alpha_T - Jk_0^2)\mu + 16U\mu^3 = 0. \quad (3.22)$$

where we used straightforward identity  $Jk_0^2 = Dk_0/2$ . The nonvanishing solution of (3.22) is

$$\mu_{\text{hel}} = \left( \frac{Jk_0^2 - \alpha_T}{4U} \right)^{1/2}, \quad \text{in the mean-field.} \quad (3.23)$$

Restoring now  $M_s$  and  $a$ , the mean-field free energy in this phase is therefore given by<sup>9</sup>

$$\frac{F_{\text{hel}}}{M_s^2 a^3} = 2(\alpha_T - Jk_0^2) \mu_{\text{hel}}^2 + 4U \mu_{\text{hel}}^4 = -\frac{(Jk_0^2 - \alpha_T)^2}{16U}. \quad (3.24)$$

The above calculation is valid for arbitrary  $\mathbf{k}$ -direction with respect to external (uniform) magnetic field, as  $\langle \mathbf{h} \cdot \mathbf{S}_{\text{hel}}(\mathbf{r}) \rangle = 0$  according to (3.12).

### 3.3 SOLUTION IN CONICAL PHASE

Experimentally, the helical phase is favourable in the low magnetic fields, for the anisotropic samples - below some first critical magnetic field  $H_{C1}(T)$ , which is roughly determined by the cubic magnetocrystalline anisotropy. In higher fields one would expect the local spins to align with magnetic field, thus going to the phase of higher symmetry. In bulk materials and low temperatures, this process is two-step: first, the helical phase transforms into a conical phase, and then the conical phase degenerates into a field-polarized ferromagnet (all spins aligned with the field). In this subsection, we will capture the essential physics of the conical phase without focusing on deeper details which had been studied elsewhere.

The conical phase simply took its name as spins are orbiting the surface of a cone along the propagation of  $\mathbf{k}$ -vector,

$$\mathbf{S}_{\text{con}}(\mathbf{r}) = m\hat{e}_z + \mu \left( \mathbf{S}_{\mathbf{k}} e^{i\mathbf{k}\mathbf{r} + i\varphi_0} + \mathbf{S}_{-\mathbf{k}} e^{-i\mathbf{k}\mathbf{r} - i\varphi_0} \right), \quad (3.25)$$

where  $\hat{e}_z$  is unit vector in direction of magnetic field, which is also the new direction of spin modulation  $\mathbf{k}$ , giving the cone converging to the ferromagnetic state at high fields.<sup>10</sup>

---

<sup>9</sup>By the "mean-field" I here mean the expectation value given under assumption that  $\mathbf{S}_{\mathbf{k}}$  can be approximated with (3.16), i.e. without further renormalization by critical fluctuations or high-order anisotropies.

<sup>10</sup>Here  $\mu$ ,  $\varphi_0$ ,  $\mathbf{k}$  have, of course, different values than that in Eq. (3.12), but carry the same mean-

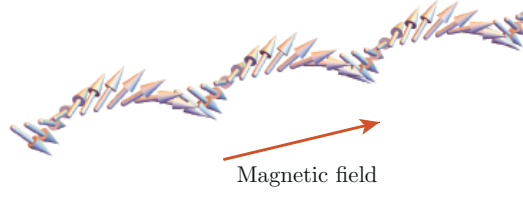


Figure 3.4: Conical phase: spins tend to tilt towards external magnetic field. In saturated state ( $H > H_{c2}$ ), all the spins aligned with the magnetic field.

We firstly consider, again, the core model

$$W_0 = \langle J [\nabla \mathbf{S}(\mathbf{r})]^2 + D \mathbf{S}(\mathbf{r}) \cdot [\nabla \times \mathbf{S}(\mathbf{r})] \rangle = \sum_{\mathbf{k}} \mathbf{S}_{\mathbf{k}}^\dagger \hat{\mathcal{H}}_0 \mathbf{S}_{\mathbf{k}}, \quad (3.26)$$

and the matrix operator  $\hat{\mathcal{H}}_0$  now reflecting the conical symmetry ( $\mathbf{k} \parallel \mathbf{h} \parallel \hat{e}_z$ ),

$$\hat{\mathcal{H}}_0 = \begin{pmatrix} Jk^2 & -iDk & 0 \\ iDk & Jk^2 & 0 \\ 0 & 0 & Jk^2 \end{pmatrix}. \quad (3.27)$$

For positive  $D, J$ , the *normalized* eigenstates of this Hamiltonian operator are given similar to those in Eq.(3.16)

$$\mathbf{S}_k^{(0)} = \frac{1}{\sqrt{2}} \begin{pmatrix} i \\ 1 \\ 0 \end{pmatrix}, \quad \mathbf{S}_k^{(1)} = \begin{pmatrix} 0 \\ 0 \\ 1 \end{pmatrix}, \quad \mathbf{S}_k^{(2)} = \frac{1}{\sqrt{2}} \begin{pmatrix} -i \\ 1 \\ 0 \end{pmatrix}, \quad (3.28)$$

corresponding to essentially the same helix-eigenvalues

$$\varepsilon_k^{(0)} = Jk^2 - Dk, \quad \varepsilon_k^{(1)} = Jk^2, \quad \varepsilon_k^{(2)} = Jk^2 + Dk, \quad (3.29)$$

which leaves  $k_0 = D/2J$  unaffected – the same as in the helical phase. Taking into account  $S_{\pm k}^0 = \frac{1}{\sqrt{2}}(\pm i \ 1 \ 0)$ , the real-space representation of the conical phase (3.25) is given simply by

$$\mathbf{S}_{\text{con}}(z) = \left( \sqrt{2}\mu \sin k_0 z, \sqrt{2}\mu \cos k_0 z, m \right), \quad (3.30)$$

or, in a more familiar notation

---

ing.

$$\mathbf{S}_{\text{con}}(\mathbf{r}) = m\hat{e}_z + \sqrt{2}\mu(\hat{e}_x \sin k_0 z + \hat{e}_y \cos k_0 z). \quad (3.31)$$

We note that in this notation the conical phase is normalized as

$$\langle \mathbf{S}_{\text{con}}^2(\mathbf{r}) \rangle = m^2 + 2\mu^2, \quad (3.32)$$

thus the free energy is now given by<sup>11</sup>

$$W[\mathbf{S}_{\text{con}}(\mathbf{r})] = \alpha_T(m^2 + 2\mu^2) - 2Jk_0^2\mu^2 - hm + U(m^2 + 2\mu^2)^2, \quad (3.33)$$

The local minimum in mean-field free energy (3.33) is satisfied if

$$\frac{\partial W}{\partial m} = 2m\alpha_T - h + 4Um(m^2 + 2\mu^2) = 0, \quad (3.34)$$

$$\frac{\partial W}{\partial \mu} = 4\mu\alpha_T - 4Jk_0^2\mu + 8U\mu(m^2 + 2\mu^2) = 0, \quad (3.35)$$

Solution of this system of equations yields

$$m_{\text{con}} = \frac{h}{Dk_0}, \quad \mu_{\text{con}} = \left( \frac{Jk_0^2 - \alpha_T}{4U} - \frac{h^2}{2D^2k_0^2} \right)^{1/2}, \quad \text{in the mean-field.} \quad (3.36)$$

The mean-field free energy of the conical phase is thus given by

$$\frac{F_{\text{con}}}{M_s^2 a^3} = \alpha_T(m_{\text{con}}^2 + 2\mu_{\text{con}}^2) - 2Jk_0^2\mu_{\text{con}}^2 - hm_{\text{con}} + U(m_{\text{con}}^2 + 2\mu_{\text{con}}^2)^2 \quad (3.37)$$

$$= -\frac{h^2}{2Dk_0} - \frac{(Jk_0^2 - \alpha_T)^2}{4U}. \quad (3.38)$$

Note that the conical phase within effective model (3.10) is continuously transformed into the helical phase in zero magnetic field (compare formulas (3.36) and (3.23)). Thus, in this model, the pure helical phase exists only at  $h = 0$ , giving preference to the conical phase in the finite fields. This artefact is, of course, lifted, upon extending model (3.10) with weak anisotropic terms, which give the first critical field (helical-conical phase boundary)  $H_{C1} \sim A$ .

Finally, we can draw the mean-field value of the upper critical field  $H_{C2}$ , - the field

---

<sup>11</sup>We again used  $Dk_0 = 2Jk_0^2$ .

when the conical phase (3.25) collapse into the field-polarized ("ferromagnetic") phase. For this, we set  $\mu = 0$  in (3.36), which gives

$$h_{C2} = Dk_0 \sqrt{\frac{Jk_0^2 - \alpha_T}{2U}}, \quad (3.39)$$

or, restoring the units

$$H_{c2}(T) = M_s Dk_0 \sqrt{\frac{Jk_0^2 - \alpha_T}{2U}}. \quad (3.40)$$

this mean-field argument sketches the conical phase boundary with paramagnetic and ferromagnetic phase (see section 3.5 and Figure 3.7).

### 3.4 SOLUTION IN SKYRMION LATTICE PHASE

The Skyrmion Lattice (SkL) is a long-range-ordered spin configuration which can be visualized as a hexagonal lattice of magnetization vortices, see Figure 3.5). Experimentally, it is seen as a sixfold scattering pattern with momenta  $|\mathbf{Q}| = k_0$  (see e.g. Refs. [38, 132] for SANS patterns), and weaker higher-order scattering reflexes indicating  $|\mathbf{Q}| > k_0$ . In a general case, any periodic long-range-ordered spin structure can be expanded into Fourier series as

$$\mathbf{S}(\mathbf{r}) = m\hat{e}_z + \mu \sum_{\mathbf{k}_n} \mathbf{S}_{\mathbf{k}_n} e^{i\mathbf{k}_n \mathbf{r} + i\varphi_n} + \mathbf{S}_{-\mathbf{k}_n} e^{-i\mathbf{k}_n \mathbf{r} - i\varphi_n}, \quad (3.41)$$

which mathematically reminds topologically-trivial single-helix phases such as conical (3.25) and helical (3.12).

We start here from empirical observation (see e.g. [38, 132] for SANS measurements), that the hallmark of the SkL long-range order is a six-fold scattering pattern in reciprocal space, each of the wave vectors are rotated by  $2\pi/3$ , while the higher-order harmonics are neglectibly weaker in their intensities [38, 132]. Thus to a good approximation, the skyrmion lattice is determined by

$$\mathbf{S}(\mathbf{r}) = m\hat{e}_z + \mu \sum_{\mathbf{k}_n = \mathbf{Q}_{1,2,3}} \mathbf{S}_{\mathbf{k}_n} e^{i\mathbf{k}_n \mathbf{r} + i\varphi_n} + \mathbf{S}_{-\mathbf{k}_n} e^{-i\mathbf{k}_n \mathbf{r} - i\varphi_n}, \quad (3.42)$$

The sum in (3.42) runs over the  $\mathbf{Q}_1, \mathbf{Q}_2, \mathbf{Q}_3$ , with properties  $|\mathbf{Q}_i| = k_0 = D/2J$  (in the mean-field – critical fluctuation renormalize this value) and  $\mathbf{Q}_1 + \mathbf{Q}_2 + \mathbf{Q}_3 = 0$ , compare with Figure (3.2). The relative phases  $\varphi_n$  in (3.42) are important for minimization of the SkL

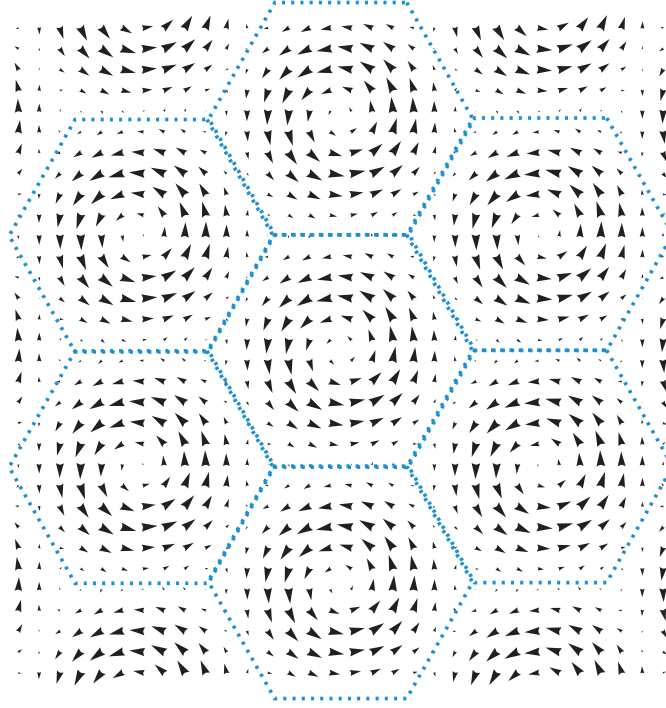


Figure 3.5: The hexagonal skyrmion lattice (projection on the basal plane)

(free) energy.

We start again from the minimal model

$$W_0 = \langle J [\nabla \mathbf{S}(\mathbf{r})]^2 + D \mathbf{S}(\mathbf{r}) \cdot [\nabla \times \mathbf{S}(\mathbf{r})] \rangle = \sum_{\mathbf{k}} \mathbf{S}_{\mathbf{k}}^\dagger \hat{\mathcal{H}}_0 \mathbf{S}_{\mathbf{k}}, \quad (3.43)$$

Here, again,  $\hat{\mathcal{H}}_0$  is written in spin representation  $\mathbf{S}_{\mathbf{k}} = (S_{\mathbf{k}}^x, S_{\mathbf{k}}^y, S_{\mathbf{k}}^z)^T$  as a matrix operator

$$\hat{\mathcal{H}}_0 = \begin{pmatrix} Jk^2 & -iDk_z & iDk_y \\ iDk_z & Jk^2 & -iDk_x \\ -iDk_y & iDk_x & Jk^2 \end{pmatrix}. \quad (3.44)$$

However we now direct the  $z$ -axis along the magnetic field. The  $\mathbf{Q}$ -vectors of the skyrmion lattice lie in the plane which is perpendicular to the magnetic field  $\mathbf{h}$ . Consequently, each of the six helices of the skyrmion lattice is parametrized as  $\mathbf{k} = (k_z, k_y, 0)$  in the rotated frame, thus the problem is effectively two-dimensional. The energy matrix ("hamiltonian")

nian”) (3.44) is

$$\hat{\mathcal{H}}_0 = \begin{pmatrix} Jk^2 & 0 & iDk_y \\ 0 & Jk^2 & -iDk_x \\ -iDk_y & iDk_x & Jk^2 \end{pmatrix}, \quad (3.45)$$

and is diagonalized on the eigenstates

$$|\mathbf{S}_{\mathbf{k}}^{(0)}\rangle = \frac{1}{\sqrt{2}}(-i\hat{k}_y, i\hat{k}_x, 1)^\top, \quad (3.46)$$

$$|\mathbf{S}_{\mathbf{k}}^{(1)}\rangle = (\hat{k}_x, \hat{k}_y, 0)^\top, \quad (3.47)$$

$$|\mathbf{S}_{\mathbf{k}}^{(2)}\rangle = \frac{1}{\sqrt{2}}(i\hat{k}_y, -i\hat{k}_x, 1)^\top, \quad (3.48)$$

where  $\hat{k}_{x,y,z} = k_{x,y,z}/|\mathbf{k}|$  and we introduced ”bra” and ”ket” notations as shortcuts to write the perturbation formulas of the matrix mechanics [138] in a familiar way. Consistent with our previous notations, we denote  $\langle \mathbf{S}_{\mathbf{k}} | \dots | \mathbf{S}_{\mathbf{k}} \rangle = \sum_{\mathbf{k}} \mathbf{S}_{\mathbf{k}}^\dagger \dots \mathbf{S}_{\mathbf{k}}$ , which is just a Fourier-transform of the corresponding spatial averaging  $\langle \dots \rangle$  as in Eq.(3.43).

The spectrum of matrix  $\hat{\mathcal{H}}_0$  consists of the three equidistant energy solutions, with the energy separation  $\pm Dk$ ,

$$\varepsilon_{\mathbf{k}}^{(0)} = Jk^2 - Dk, \quad \varepsilon_{\mathbf{k}}^{(1)} = Jk^2, \quad \varepsilon_{\mathbf{k}}^{(2)} = Jk^2 + Dk, \quad (3.49)$$

For the positive  $J, D$  the lowest energy solution is the helix

$$|\mathbf{S}_{\mathbf{k}}^{(0)}\rangle = \frac{1}{\sqrt{2}} \begin{pmatrix} -i\hat{k}_y \\ i\hat{k}_x \\ 1 \end{pmatrix}, \quad (3.50)$$

which corresponds to the eigenvalue  $\varepsilon_{\mathbf{k}}^{(0)}$ . The modulation vector  $\mathbf{k}_0$  is determined by further minimization of the energy,  $\partial \varepsilon_{\mathbf{k}}^{(0)} / \partial \mathbf{k} = 0$ . Consequently, the minimum of the dispersion  $\varepsilon_{\mathbf{k}}^{(0)} = Jk^2 - Dk$  is satisfied if

$$k_0 = \frac{D}{2J}, \quad (3.51)$$

see also Fig. 3.3a,b. Finally, it is instructive to rewrite one more time the eigenspectrum of  $\mathcal{H}_0$  as we use it in perturbation formulas further,

$$\varepsilon_{\mathbf{k}_0}^{(0)} = -Dk_0/2, \quad \varepsilon_{\mathbf{k}_0}^{(1)} = Dk_0/2, \quad \varepsilon_{\mathbf{k}_0}^{(2)} = 3Dk_0/2. \quad (3.52)$$

As a remark, it is usually convenient to measure the energy of the system in units of  $Dk_0$ .

Next we consider the superposition of helices into a skyrmion lattice. Neglecting higher-order harmonics, the skyrmion lattice is approximated as uniform magnetization  $m\hat{e}_z$  along magnetic field and a  $3Q$  multispiral configuration,

$$\mathbf{S}(\mathbf{r}) \simeq \mu \sum_{i=1}^3 (\mathbf{S}_{\mathbf{Q}_i} e^{i\mathbf{Q}_i \cdot \mathbf{r}} + c.c.) + m\hat{e}_z. \quad (3.53)$$

In the "braket" notation, the real-space skyrmion phase has a shortcut notation

$$|\mathbf{S}(\mathbf{r})\rangle = \mu \sum_{\mathbf{k}}^{\{\pm\mathbf{Q}_1, \dots, \pm\mathbf{Q}_3\}} |\mathbf{S}_{\mathbf{k}}^{(0)}\rangle e^{i\mathbf{k}\cdot\mathbf{r} + i\varphi_{\mathbf{k}}} + m|\mathbf{S}_0\rangle, \quad (3.54)$$

where  $|\mathbf{S}_{\mathbf{k}}^{(0)}\rangle$  is given by Eq.(4.21) and the ferromagnetic component is  $|\mathbf{S}_0\rangle \equiv (001)^\top$ .

The skyrmion lattice possess some interesting properties. First, using the explicit form (3.53), the first-order moments are

$$\langle S_x(\mathbf{r}) \rangle = 0, \quad \langle S_y(\mathbf{r}) \rangle = 0, \quad \langle S_z(\mathbf{r}) \rangle = m, \quad (3.55)$$

so the uniform magnetization (the "ferromagnetic component")  $\mathbf{m} \equiv \langle \mathbf{S}(\mathbf{r}) \rangle = m\hat{e}_z$  is the only non-vanishing first-order moment. The second-order in-plane moments are

$$\langle S_x^2(\mathbf{r}) \rangle = \sum_{\mathbf{k}}^{\{\pm\mathbf{Q}_1, \dots, \pm\mathbf{Q}_3\}} S_{\mathbf{k}}^x S_{-\mathbf{k}}^x = 3\mu^2/2, \quad (3.56)$$

$$\langle S_y^2(\mathbf{r}) \rangle = \sum_{\mathbf{k}}^{\{\pm\mathbf{Q}_1, \dots, \pm\mathbf{Q}_3\}} S_{\mathbf{k}}^y S_{-\mathbf{k}}^y = 3\mu^2/2, \quad (3.57)$$

while the longitudinal (z) second-order moment is

$$\langle S_z^2(\mathbf{r}) \rangle = m^2 + \sum_{\mathbf{k}}^{\{\pm\mathbf{Q}_1, \dots, \pm\mathbf{Q}_3\}} S_{\mathbf{k}}^z S_{-\mathbf{k}}^z = m^2 + 3\mu^2. \quad (3.58)$$

One can verify that all the mixed moments vanish,

$$\langle S_\alpha S_\beta \rangle = 0, \quad \alpha \neq \beta, \quad (3.59)$$

so, in general, one has

$$\langle S_\alpha S_\beta \rangle = \frac{3}{2} \mu^2 \delta_{\alpha,\beta} [1 + (1 + 2m^2/3\mu^2) \delta_{\alpha,z}], \quad (3.60)$$

where  $\alpha, \beta = x, y, z$ . Formula (3.60) is handy for further expectation value calculations. For a fixed temperature one can use normalization  $\langle \mathbf{S}^2(\mathbf{r}) \rangle = 1$ , thus the following constraint holds[132]

$$\langle \mathbf{S}^2 \rangle = m^2 + 6\mu^2 = 1. \quad (3.61)$$

Finally, it is interesting to note that in this approximation the fourth-order moment for the skyrmion lattice is surprisingly  $\langle \mathbf{S}^4 \rangle \neq \langle \mathbf{S}^2 \rangle^2$ , i.e. the magnetization field is “soft”.

We now calculate the free energy corresponding to the skyrmion lattice. For this we directly find that (3.10) gives

$$W_{\text{SkL}} = \alpha_T(m^2 + 6\mu^2) - 3Dk_0\mu^2 - hm + U(m^4 + 51\mu^4 + 24m^2\mu^2 - 18\sqrt{2}m\mu^3) \quad (3.62)$$

We show in details the appearance of the last term for pedagogical reasons. It comes from

$$W_{\text{SkL}}^{(U)} = \langle U \mathbf{S}^4(\mathbf{r}) \rangle \quad (3.63)$$

upon substitution of (3.1). More detailly, we first decouple the ferromagnetic component  $\mathbf{m} = m\hat{e}_z$  from  $\mathbf{S}(\mathbf{r}) \equiv \mathbf{m} + \mathbf{s}(\mathbf{r})$ ,

$$\mathbf{S}^4 = \mathbf{m}^4 + 4\mathbf{m}^2(\mathbf{m} \cdot \mathbf{s}) + 4(\mathbf{m} \cdot \mathbf{s})(\mathbf{m} \cdot \mathbf{s}) + 2\mathbf{m}^2\mathbf{s}^2 + 4(\mathbf{m} \cdot \mathbf{s})\mathbf{s}^2 + \mathbf{s}^4. \quad (3.64)$$

Taking the expectation value, the second term vanishes as  $\langle \mathbf{s}(\mathbf{r}) \rangle = 0$ , and the further simplification gives

$$\langle \mathbf{S}^4(\mathbf{r}) \rangle = m^4 + 2m^2 \langle s_x^2 + s_y^2 + 3s_z^2 \rangle + 4m \langle s_z(s_x^2 + s_y^2 + s_z^2) \rangle + \langle (s_x^2 + s_y^2 + s_z^2)^2 \rangle \quad (3.65)$$

The second term here gives simply



$$2m^2 \langle s_x^2 + s_y^2 + 3s_z^2 \rangle = 24m^2 \mu^2 \quad (3.66)$$

due to relations (3.56)-(3.58). The third term in (3.65) gives

$$\begin{aligned} \langle s_z(s_x^2 + s_y^2 + s_z^2) \rangle &= \mu^3 \sum_{\mathbf{k}_1}^{\{\mathbf{q}_1 \dots \mathbf{q}_6\}} \sum_{\mathbf{k}_2}^{\{\mathbf{q}_1 \dots \mathbf{q}_6\}} \sum_{\mathbf{k}_3}^{\{\mathbf{q}_1 \dots \mathbf{q}_6\}} \left( S_{\mathbf{k}_1}^z S_{\mathbf{k}_2}^x S_{\mathbf{k}_3}^x + S_{\mathbf{k}_1}^z S_{\mathbf{k}_2}^y S_{\mathbf{k}_3}^y + S_{\mathbf{k}_1}^z S_{\mathbf{k}_2}^z S_{\mathbf{k}_3}^z \right) \\ &\quad \times e^{i(\varphi_{\mathbf{k}_1} + \varphi_{\mathbf{k}_2} + \varphi_{\mathbf{k}_3})} \delta(\mathbf{k}_1 + \mathbf{k}_2 + \mathbf{k}_3), \end{aligned} \quad (3.67)$$

where we relabelled  $\{\mathbf{q}_1 \dots \mathbf{q}_6\} = \{\pm \mathbf{Q}_1 \dots \pm \mathbf{Q}_3\}$  for convenience (the order does not matter). Note that this term is responsible for skyrmion lattice formation (see section 3.1). In the basic (4.21), one thus obtains:

$$4m \langle s_z(s_x^2 + s_y^2 + s_z^2) \rangle = 18\sqrt{2}m\mu^3 \cos(\varphi_{\mathbf{k}_1} + \varphi_{\mathbf{k}_2} + \varphi_{\mathbf{k}_3}) \quad (3.68)$$

The minimum of this expression is given for  $\varphi_{\mathbf{k}_1} = \varphi_{\mathbf{k}_2} = \varphi_{\mathbf{k}_3} = \pm\pi/3 \pmod{2\pi/3}$ , which reflects the symmetry of three-spiral modulation),

$$4m \langle s_z(s_x^2 + s_y^2 + s_z^2) \rangle = -18\sqrt{2}m\mu^3. \quad (3.69)$$

Finally,

$$\begin{aligned} \langle (s_x^2 + s_y^2 + s_z^2)^2 \rangle &= \mu^4 \sum_{\mathbf{k}_1}^{\{\mathbf{q}_1 \dots \mathbf{q}_6\}} \sum_{\mathbf{k}_2}^{\{\mathbf{q}_1 \dots \mathbf{q}_6\}} \sum_{\mathbf{k}_3}^{\{\mathbf{q}_1 \dots \mathbf{q}_6\}} \sum_{\mathbf{k}_4}^{\{\mathbf{q}_1 \dots \mathbf{q}_6\}} \left( S_{\mathbf{k}_1}^x S_{\mathbf{k}_2}^x S_{\mathbf{k}_3}^x S_{\mathbf{k}_4}^x + S_{\mathbf{k}_1}^y S_{\mathbf{k}_2}^y S_{\mathbf{k}_3}^y S_{\mathbf{k}_4}^y + S_{\mathbf{k}_1}^z S_{\mathbf{k}_2}^z S_{\mathbf{k}_3}^z S_{\mathbf{k}_4}^z \right. \\ &\quad \left. + 2S_{\mathbf{k}_1}^x S_{\mathbf{k}_2}^x S_{\mathbf{k}_3}^y S_{\mathbf{k}_4}^y + 2S_{\mathbf{k}_1}^y S_{\mathbf{k}_2}^y S_{\mathbf{k}_3}^z S_{\mathbf{k}_4}^z + 2S_{\mathbf{k}_1}^z S_{\mathbf{k}_2}^z S_{\mathbf{k}_3}^x S_{\mathbf{k}_4}^x \right) \\ &\quad \times e^{i(\varphi_{\mathbf{k}_1} + \varphi_{\mathbf{k}_2} + \varphi_{\mathbf{k}_3} + \varphi_{\mathbf{k}_4})} \delta(\mathbf{k}_1 + \mathbf{k}_2 + \mathbf{k}_3 + \mathbf{k}_4), \end{aligned} \quad (3.70)$$

After some lengthy but rather hackneyed algebra one obtains

$$\langle (s_x^2 + s_y^2 + s_z^2)^2 \rangle = 51\mu^4. \quad (3.71)$$

Thus, taking everything together, one gets:

$$W_{skL}^{(U)} = \langle U \mathbf{S}^4(\mathbf{r}) \rangle = U \left( m^4 + 51\mu^4 + 24m^2\mu^2 - 18\sqrt{2}m\mu^3 \right) \quad (3.72)$$

if  $U$  is a constant.

Therefore, the skyrmion lattice in the mean-field can be approximated as a multi-spiral spin structure with a "soft magnetization", i.e. with its norm slightly varying over space. In fact, the skyrmion lattice has the lowest mean-field energy when these fluctuations are minimized. It however costs very much energy (several J) to suppress the SkL magnetization locally to zero. In this regard, the multi-spiral skyrmion lattice on one hand and single-spiral helical and conical phases on the other hand belong to different topological classes. It is impossible to continuously transform a skyrmion lattice into the conical phase, as it would require to crush magnetization locally to zero. We further note that approximation (3.41) can be further improved with higher order Fourier harmonics, which still respect the skyrmion lattice formation condition  $\mathbf{k}_1 + \mathbf{k}_2 + \mathbf{k}_3 = 0$ . Upon this procedure, the topology of the skyrmion lattice remains unmodified. There is an experimental evidence (see e.g. [132]) that higher-order reflexes are of negligibly lower intensity, which indirectly implies that they are also energetically less important.

### 3.5 IMPORTANCE OF CRITICAL FLUCTUATIONS

Critical fluctuations are thermodynamic fluctuations near the critical point of phase transitions. In contrast to the role of thermal fluctuations in a high-symmetry phase, where the conventional thermodynamics can be sufficiently carried out by considering statistical averages which make fluctuations unimportant, the critical fluctuations very often are pivotal for phase-phase competition near the ordering temperature.

To illustrate the role of critical fluctuations for stabilization of the skyrmion phase (in bulk), we plot a mean-field magnetic phase diagram (see also [38]). Considering  $\alpha_T \propto (T - T_c)$ , we obtain a qualitative phase diagram (a typical one is shown on Figure 3.7). We thus implement numerically the mean-field (fluctuation-free) calculations on the basis of the model described above. As we know from experiments, the skyrmions pocket appears embedded in the conical phase, thus we directly compare the variationally-minimized skyrmion phase free energy (3.62) with the conical phase free energy (3.37).

A typical phase diagram consists of conical and helical phases<sup>12</sup> + magnetically trivial phases (paramagnetically-disordered and field-polarized). The skyrmion lattice phase is always higher in free energies than the conical phase, if critical fluctuations are not included. However, near the critical temperature, the skyrmion phase is competing very closely to the conical. It was shown in Ref [38] that inclusion of even of the Gaussian (=noninteracting) fluctuations helps to stabilize the skyrmion lattice phase as the resulting fluctuative contribution is negative and more significant in the skyrmion phase. Thus the skyrmion lattice free energies shifts down with respect to the conical (see Figure 3.7). To elaborate the other possible mean-field effects, it was shown that further

---

<sup>12</sup>The helical phase appears only if adding the anisotropic term  $A$ . If it is absent, the conical phase continuously transforms into the helical at  $H=0$ .

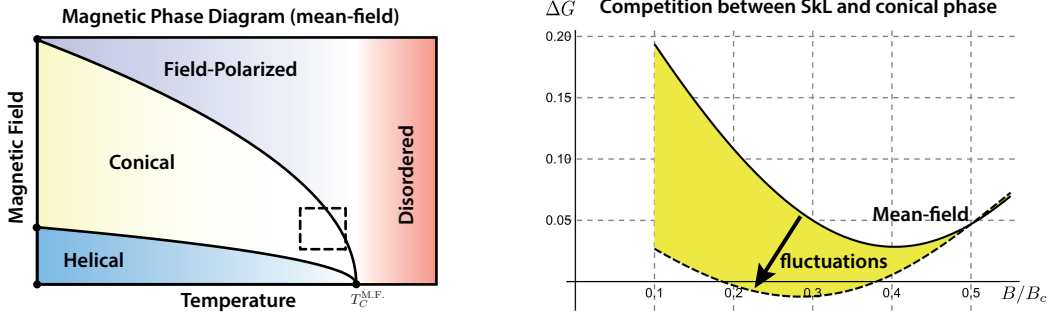


Figure 3.6: Mean-field phase diagram (a) consists of helical, conical, field-polarized and paramagnetic phases (The conical phase transforms continuously to the helical phase at  $H = 0$  if anisotropy is vanishing  $A = 0$ ). The skyrmion phase is however not present: it's free energy is higher than in the conical phase (b). However, in the region denoted with dashed line (qualitatively), the skyrmion phase is competing very tight with conicals. Upon inclusion of the critical fluctuations, the skyrmion crystalline is stabilized [38].

inclusion of higher order harmonics (i.e.  $k = nk_0$ ,  $k_0 = D/2J$ ,  $n > 1$ ) even though helps to shape up the SkL order parameter, however does not contribute significantly to the mean-field free energy [38]. However, the skyrmion lattice is observed as a thermodynamically stable phase with neutron scattering, and the other parts of the phase diagram are captured by the existing mean-field-theoretical formalism; it is on basis of this it is believed that the critical fluctuations are responsible for stabilizing the skyrmion phase in the form of skyrmion crystal.

A further twist on importance of critical fluctuations and stabilization of the skyrmion lattice phase have been done in Ref.[134]. In particular, the authors of Ref.[134] directly report the fluctuation-induced phase transition by observing appearance of Brazovskii-like sphere exactly at  $T_C$ . Brazovskii in his seminal works [135, 139] proposed a mechanism of first-order phase transition, for which the fluctuations become "soft" <sup>13</sup> not only for a single value of momentum (e.g.  $k = 0$  for a ferromagnet,  $k = k_0$  for a helical phase of a ferromagnet), but rather on a closed manifold, which for isotropic systems is a sphere, the *Brazovskii sphere*. This crucially leads to the singularity in density-of-states of these critical modes. For example, for a critical mode with  $\epsilon_{\mathbf{k}} \simeq \Delta + u^2(\mathbf{k} - \mathbf{k}_*)^2$ , the squared field-amplitude of these thermal fluctuations is [135]

$$\langle \psi^*(r)\psi(r) \rangle \propto \int \frac{d^3\mathbf{k}}{(2\pi)^3} \frac{T}{\epsilon(\mathbf{k})} = \frac{k_*^2 T}{2\pi u \Delta^{1/2}} \propto \frac{1}{\sqrt{\Delta}}, \quad (3.73)$$

thus, the fluctuation field for a soft mode ( $\Delta = 0$ ) diverges as  $\Delta^{-1/2}$ , which eventually leads to the fluctuation-induced discontinuous phase transition [135]. The critical mode

<sup>13</sup>In this terminology, the fluctuations are considered to be soft if their dispersion relation  $\epsilon = \epsilon(\mathbf{k})$  becomes zero at one or more points in reciprocal space  $\{\mathbf{k}\}$ , i.e.  $\epsilon(\mathbf{k}_*) = 0$  denotes a soft mode at  $\mathbf{k} = \mathbf{k}_*$ .

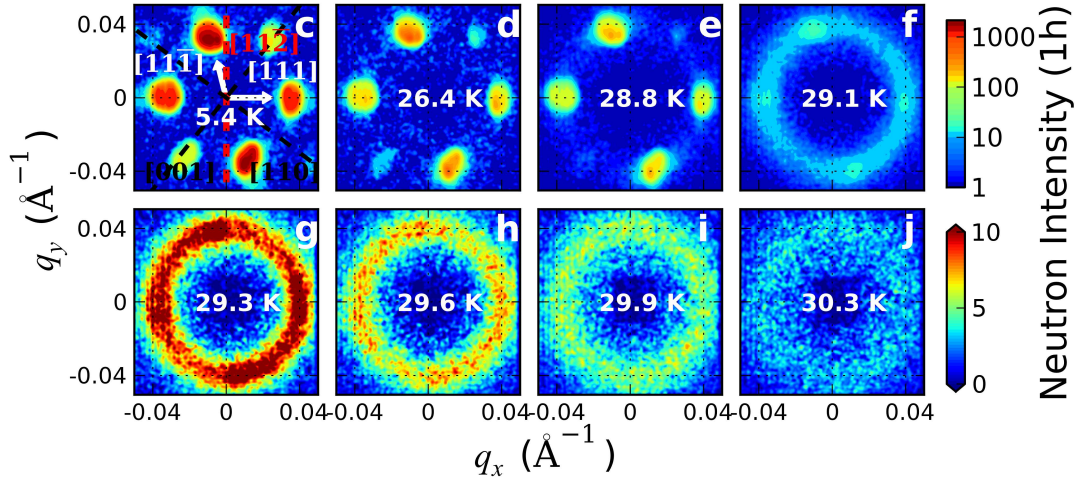


Figure 3.7: Fluctuations intensity (in reciprocal space) in skyrmion-hosting MnSi near  $T_c$ . Below critical temperature [(c)–(e)]: countable scattering reflexes indicate the helical phase. Above  $T_c$  [(g)–(j)]: the excitations are continuously presented on a *Brazovskii sphere*  $|\mathbf{k}| = k_0$ . The black broken lines in (c) indicate weak reflections due to multiple scattering effects along the [001] and [110] directions. Intensity in (c)–(f) is plotted in the logarithmic scale for better comparison. Figure from [134].

which exhibits  $\Delta(T_*) = 0$  is called a dangerous mode as it leads to abrupt breakdown of the ordered phases at  $T = T_*$  (or vice versa, depending from which side of  $T_*$  you are considering the effect).

The main result of study [134] is that they have proved that at  $T = T_C$  the fluctuations indeed emerge on the (three-dimensional) Brazovskii sphere  $|\mathbf{k}| = k_0 = D/2J$ , at least in zero magnetic fields. The intensity of the critical fluctuations distributed at  $|\mathbf{k}| = k_0$  was shown to be almost homogeneous, with some small corrections due to the cubic anisotropies.<sup>14</sup> In paramagnetic phase (well above  $T_C$ ), the collective modes are absent (see Figure); when temperature is lowered to  $\approx T_C$ , the fluctuations concentrate a sphere  $|\mathbf{k}| = k_0$  in reciprocal space. Finally, lowering temperature below, the correlation lengths associated with cubic anisotropies favour the fluctuations along crystallographic [111] direction (corresponding to the orientation of the helical phase) [134].

This, to my current understanding, have a substantial importance on understanding of the multispiral physics and skyrmion lattice physics in this system, in particular it addresses following questions: (i) why the periodicity of both the helical and skyrmion lattice phase are given by  $2\pi/k_0$ ,  $k_0 = D/2J$ ? (ii) what makes the system choosing between a single-helix and three-helix solution? (iii) why does this selection happens at  $T_C$ ? The order-generating critical fluctuations appear firstly at  $T_C$  at the surface  $|\mathbf{k}| = k_0$ , which has a spherical symmetry, however the further evolution breaks this symmetry towards

<sup>14</sup>one more time confirms that the  $US^4$  physics is predominant and neglecting the truly anisotropic contribution  $A(S_x^4 + S_y^4 + S_z^4)$  is for *magnetic phase diagram calculations* is qualitatively correct; see also Ref.[135].

either a plane (the three SkL helices form a plane,  $(\mathbf{k}_1 + \mathbf{k}_2 + \mathbf{k}_3 = 0)$ , or a line ( $\mathbf{k}$  in helical and conical phase), however still this vectors are touching the Brazovskii sphere, i.e.  $|\mathbf{k}_i| = k_0$  for all helices. Thus, the *skyrmion lattice phase*, as the long-range-ordered phase which promotes *collective excitations*, exists in bulk systems ( $U \neq 0$ ) only due the fluctuative-governed symmetry breaking and the other mechanisms (such as e.g. glueing individual skyrmions together as in Ref.[81]) are eliminated.<sup>15</sup>

On the quasiparticle language, the large entropy produced by the critical fluctuations results in the significant change in free energies, which is important especially near  $T = T_C$  where several phases meet. In this sense, the quasiparticle approach is often useful as it allows to depict the very complicated underlying mechanisms on the level of pictorial understanding and diagrammatic techniques. It is for this reasons I reformulated the only existing before formalism for semi-analytical calculation of magnetic phase diagrams with skyrmion lattices [38] on the quasiparticle language, which allows not only to operate the magnetic phase diagram computationally, but also to address the underlying physical mechanisms on the different stages of calculation on the level of order-of-magnitude estimates, when the real physics is so close I can taste it. Less importantly in general, however important here, I also restored all the dimensional units. Finally, this new approach allowed to incorporate several newly discovered features of the skyrmion lattice (e.g. [134]) and join the phase-diagram calculation with the other mechanisms for studying the skyrmion lattices (e.g. electric fields); thus in the next sections I present a concise description for the synthesized model for semi-quantitative phase-diagram calculation which I condensed on the basis of reformulated mean-field language of the previous sections and several heterogeneous theoretical approaches as described in Refs.[35, 38, 81, 105, 132, 134].

### 3.6 SUSCEPTIBILITY TENSOR AND MEAN-FIELD FLUCTUATION SPECTRUM

The noninteracting (Gaussian) critical fluctuations around the mean-field solution are described by the generalized susceptibility tensor  $\chi_{ij}(\mathbf{r}, \mathbf{r}')$  [140], defined as

$$\chi_{\alpha\beta}^{-1}(\mathbf{r}, \mathbf{r}') = \frac{1}{T} \frac{\delta^2 F}{\delta M^\alpha(\mathbf{r}) \delta M^\beta(\mathbf{r}')} \quad (3.74)$$

To calculate it explicitly for our effective free energy (3.10), we use auxiliary expressions

---

<sup>15</sup>This is not to say that the same is valid for magnetic thin films where  $U\mathbf{S}^4$ -term promoting the formation of the skyrmion crystalline is generally unimportant; instead, in thin films the skyrmion phase exists in a somehow disordered state so the critical fluctuations are suppressed; the skyrmion physics their is sufficiently captured within Bogdanov-like calculations for both interacting and non-interacting skyrmions ("skyrmion gas"). For the thin-film discussion, see Chapter 6.

$$\mathbf{M}^2(\mathbf{r}) = \delta_{\alpha\beta} M^\alpha(\mathbf{r}) M^\beta(\mathbf{r}), \quad \mathbf{M}^4(\mathbf{r}) = \delta_{\alpha\beta} \delta_{\alpha'\beta'} M^\alpha(\mathbf{r}) M^\beta(\mathbf{r}) M^{\alpha'}(\mathbf{r}) M^{\beta'}(\mathbf{r}), \quad (3.75)$$

which thereafter leads to susceptibility in spin variables  $\mathbf{S}(\mathbf{r})$  as

$$T\chi_{\alpha\beta}^{-1}(\mathbf{r}, \mathbf{r}') = \delta(\mathbf{r} - \mathbf{r}') \left[ (\alpha_T - J\nabla^2) \delta_{\alpha\beta} - D\varepsilon_{\alpha\beta\gamma} \partial_\gamma + 4US^\alpha(\mathbf{r}) S^\alpha(\mathbf{r}) \delta_{\alpha\beta} + 8US^\alpha(\mathbf{r}) S^\beta(\mathbf{r}) \right]. \quad (3.76)$$

Even though it is formally possible to proceed in the real space, it will be more comfortable in several ways to work in the reciprocal space, thus the Fourier-transformed susceptibility reads

$$T\chi_{\alpha\beta}^{-1}(\mathbf{k}, \mathbf{k}') = \Theta_{\alpha\beta}(\mathbf{k}) \delta_{\mathbf{k}\mathbf{k}'} + 4U \sum_{\mathbf{k}''} \left( \delta_{\alpha\beta} S_{-\mathbf{k}''}^\alpha S_{\mathbf{k}-\mathbf{k}'+\mathbf{k}''}^\alpha + 2S_{-\mathbf{k}''}^\alpha S_{\mathbf{k}-\mathbf{k}'+\mathbf{k}''}^\beta \right), \quad (3.77)$$

with  $\Theta_{\alpha\beta}(\mathbf{k}) = (Jk^2 + \alpha_T) \delta_{\alpha\beta} - iD\varepsilon_{\alpha\beta\gamma} k_\gamma$ . The spectrum of Gaussian fluctuations is thus given by poles of the susceptibility  $\chi_{\alpha\beta}(\mathbf{k}, \mathbf{k}')$ , and the eigenvalue equation reads

$$T \sum_{\mathbf{k}} \chi_{ij}^{-1}(\mathbf{k}, \mathbf{k}') v_i(-\mathbf{k}) = \omega_{\mathbf{k}} v_i(\mathbf{k}) \quad (3.78)$$

where  $v_i(-\mathbf{k})$  are eigenvectors. It is fruitful to firstly consider the mean-field fluctuation spectrum in the paramagnetic phase ( $\langle M_i \rangle = 0$ ,  $\langle M_i^2 \rangle = 0$ ) close to the critical point. The corresponding spectrum has three branches<sup>16</sup>

$$\omega_{\mathbf{k}}^{(0)} = J(k - k_0)^2 + \delta(T), \quad \omega_{\mathbf{k}}^{(1)} = J(k^2 + k_0^2) + \delta(T), \quad \omega_{\mathbf{k}}^{(2)} = J(k + k_0)^2 + \delta(T), \quad (3.79)$$

where  $\delta(T)$  is the detuning parameter, see Ref[134] for more details. The dangerous mode is  $\omega_{\mathbf{k}}^{(0)}$  which is soft at  $k_0 = D/J$  at  $T_c$  where  $\delta(T_c) = 0$ . This results to fluctuations on the 3D Brazovskii sphere  $\mathbf{k} = k_0$ , which leads to field amplitude-squared singularity seen by neutron scattering as a uniform scattering ring at  $T = T_c$ . This symmetry on the 3D sphere  $\mathbf{k} = k_0$  is broken further below the critical point, either into a 3Q-helices defining a plane (the skyrmion phase:  $\mathbf{k}_1 + \mathbf{k}_2 + \mathbf{k}_3 = 0$ , i.e. the sixfold scattering pattern with  $k = k_0$ ), or a 1-helix defining a line (helical or conical phase, two-fold scattering pattern). The dispersions  $\omega_{\mathbf{k}}^{(0)}$ ,  $\omega_{\mathbf{k}}^{(1)}$ ,  $\omega_{\mathbf{k}}^{(2)}$  are changed as below  $T_c$  as the average magnetization is not vanishing, and thus anisotropy-induced terms (e.g. those with  $U$  in (3.77)) come into a play, however the limiting case  $k \rightarrow \infty$  for all the branches is  $\omega_{\mathbf{k}} \sim Jk^2$ , which

---

<sup>16</sup>Here  $J$  and  $D$  are in proper-energetical units, i.e. with restored  $M$  and  $a$ .

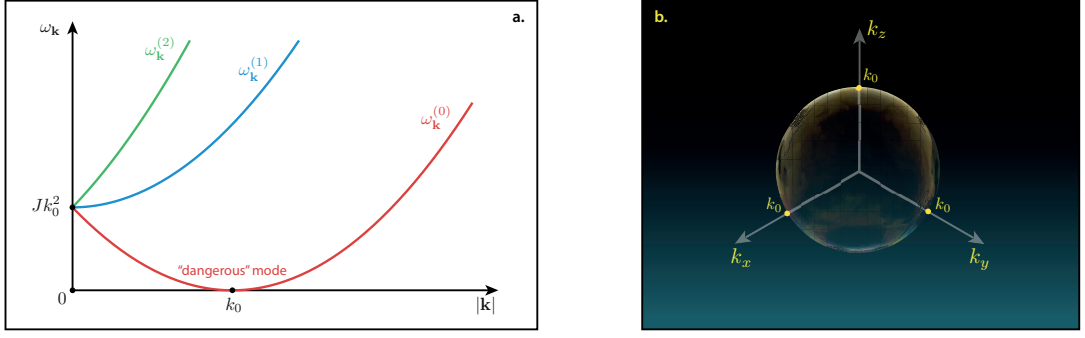


Figure 3.8: Appearance of the Brazovskii sphere: (a): Critical modes at  $T = T_C$  (mean-field approximation). The dangerous mode is  $\omega_{\mathbf{k}}^{(0)}$  which becomes soft at the sphere  $|\mathbf{k}| = k_0$ , leading to Van-Hove-like singularity in the density of states. The squared field amplitude of these thermal fluctuations thus diverges giving rise to the Brazovskii sphere in the reciprocal space (b).

physically means that on the short scales the chiral magnet has ferromagnetic nature.

### 3.7 FREE ENERGY IN NON-INTERACTING QUASIPARTICLE APPROACH

The surprising finding of the study [38] is that the main contribution to the fluctuative free energy is given by the short scale fluctuations, which was also verified numerically [38]. Here we consider a different way of deriving this result, which is more self-consistent with quasiparticle picture of fluctuation-induced ordering transition. In the approximation of Gaussian (noninteracting) fluctuations, the fluctuative free energy is given by

$$F_{\text{fluct}} = \sum_i \sum_{\mathbf{k}}^{|k| < \Lambda} \omega_{\mathbf{k}}^{(i)} f_{\mathbf{k}}^{(i)} - T S_{\text{fluct}}, \quad (3.80)$$

where  $\Lambda \approx 2\pi/a$  is the natural cutoff and  $f_{\mathbf{k}}^{(i)}$  is equilibrium distribution function and  $S_{\text{fluct}}$  is the entropy of the noninteracting gas of fluctuations,

$$S_{\text{fluct}} = \sum_i \sum_{\mathbf{k}}^{|k| < \Lambda} \left\{ (1 + f_{\mathbf{k}}^{(i)}) \ln(1 + f_{\mathbf{k}}^{(i)}) - f_{\mathbf{k}}^{(i)} \ln f_{\mathbf{k}}^{(i)} \right\}. \quad (3.81)$$

Note that this approach can be extended to the case of the interacting fluctuations. As a general rule, the excitation energy is  $\omega_{\mathbf{k}} \ll T_C$ , thus the free energy (3.80) allows further simplification; for low-energy collective excitations (Bose-Einstein statistics), one has

$$\ln(1 + f_{\mathbf{k}}^{(i)}) \simeq \beta \omega_{\mathbf{k}}^{(i)} - \ln \beta \omega_{\mathbf{k}}^{(i)}, \quad \ln f_{\mathbf{k}}^{(i)} \simeq -\ln \beta \omega_{\mathbf{k}}^{(i)}, \quad (3.82)$$

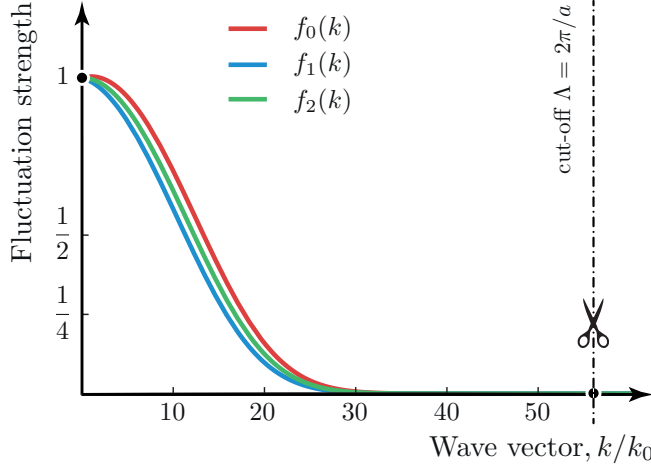


Figure 3.9: Occupation  $f_{\mathbf{k}}^{(0)}$ ,  $f_{\mathbf{k}}^{(1)}$ ,  $f_{\mathbf{k}}^{(2)}$  of the three critical modes at  $T_C$  (without showing the divergent accumulation of  $\omega_{\mathbf{k}_0}^{(0)}$ ). Note that the fluctuation *energy* does not depend on the choice of the momentum cut-off  $\Lambda \gg k_0$ ; however the entropy carried by fluctuations does indeed depends however is naturally restricted by the short-scale grid  $a$ .

where we took into account that the cut-off energy is smaller than ordering temperature. Thus asymptotically one has

$$F_{\text{fluct}} \simeq T \sum_{\mathbf{k}}^{\mathbf{k} < \Lambda} \ln \beta \omega_{\mathbf{k}} \quad (3.83)$$

At short length-scales, the collective excitations merge to a single effectively ferromagnetic mode  $\omega_{\mathbf{k}} \sim Jk^2$ , which gives the main contribution to the free energy. To take effect of mode-mode interactions, which below  $T_C$  promote propagation of collective excitations in (3.77) only along the symmetry-broken directions of the underlying phase, we thus keep main non-vanishing terms as

$$F_{\text{fluct}}^{\text{short}} \simeq T \sum_{\mathbf{k}} \ln \beta Jk^2 (1 + \Gamma/Jk^2) \simeq T \sum_{\mathbf{k}} (\ln \beta Jk^2 + \Gamma/Jk^2). \quad (3.84)$$

where

$$\Gamma = \Gamma_1 + \Gamma_2, \quad \Gamma_1 = 4U \sum_{\mathbf{k}', \mathbf{k}''} \delta_{\alpha\beta} S_{-\mathbf{k}''}^{\alpha} S_{\mathbf{k}-\mathbf{k}'+\mathbf{k}''}^{\beta}, \quad \Gamma_2 = 8U \sum_{\mathbf{k}', \mathbf{k}''} S_{-\mathbf{k}''}^{\alpha} S_{\mathbf{k}-\mathbf{k}'+\mathbf{k}''}^{\beta}. \quad (3.85)$$

The first term in (3.84),  $\ln \beta Jk^2$ , does not contribute to free energy difference if helical and skyrmion phase are treated on the same volume in momentum space. The second term gives the fluctuative contribution dependent on the mean-field values of magnetization



in two phases,<sup>17</sup>

$$\Delta F_{\text{fluct}} \approx \Delta F_{\text{fluct}}^{\text{short}} \simeq \frac{5\Lambda UT}{2\pi^2 J k_0} (\langle M_{\text{sk}}^2 \rangle - \langle M_{\text{con}}^2 \rangle) = \frac{10}{\pi} \frac{UT}{Da} (\langle M_{\text{sk}}^2 \rangle - \langle M_{\text{con}}^2 \rangle). \quad (3.86)$$

The phase diagram is plotted with the fluctuative energy (3.86) on top of the mean-field solution. The described formalism is expected to capture the qualitative physics of the system.

**Order-Breakdown estimate.** It is further possible to draw a qualitative criterion on breakdown of ordered phase by considering the stability of the Brazovskii sphere. Below we estimate the temperature range fluctuation  $\delta T$  which could break down the Brazovskii sphere into paramagnetic phase. Accurately it should be done by studying stability of the Brazovskii sphere surface with respect to surface distortions (in reciprocal space), but below I present a simplified order-of-magnitude estimate by comparing the typical involved energies. For this, we first estimate energy associated with fluctuations on Brazovskii sphere. Only the soft modes are important here,  $\omega_{\mathbf{k}}^{(0)}$ , and contributions of the other two  $\omega_{\mathbf{k}}^{(1)}$ ,  $\omega_{\mathbf{k}}^{(2)}$  are neglectable. However, the integrals can be taken analytically if we consider contributions from  $\omega_{\mathbf{k}}^{(0)}$  together with  $\omega_{\mathbf{k}}^{(2)}$  modes, therefore

$$E_{\text{Br.sph.}}(T \approx T_C) \simeq V \int \frac{d^3 \mathbf{k}}{(2\pi)^3} \left\{ \frac{J(k-k_0)^2}{e^{J(k-k_0)^2/T} - 1} + \frac{J(k+k_0)^2}{e^{J(k+k_0)^2/T} - 1} \right\}. \quad (3.87)$$

The integral can be taken by proceeding to the dimensionless momenta  $\kappa = k/k_0$  and dimensionless critical temperature  $\theta = T_C/Jk_0^2$ . Then the energy density is given by:

$$\left. \frac{E_{\text{Br.sph.}}}{V} \right|_{T_C} = \frac{Jk_0^5}{2\pi^2} \int_0^\infty d\kappa \kappa^2 \left\{ \frac{(\kappa-1)^2}{e^{(\kappa-1)^2} - 1} + \frac{(\kappa+1)^2}{e^{(\kappa+1)^2} - 1} \right\}. \quad (3.88)$$

After some algebra, one obtains

$$\left. \frac{E_{\text{Br.sph.}}}{V} \right|_{T=T_C} = \frac{Jk_0^5}{2\pi^2} [c_1 \theta^{3/2} + c_2 \theta^{5/2}], \quad (3.89)$$

where  $c_1 = \frac{\sqrt{\pi}}{2} \zeta(3/2) \approx 2.31$  and  $c_2 = \frac{3\sqrt{\pi}}{4} \zeta(5/2) \approx 1.78$ . Thus we have

$$\left. \frac{E_{\text{Br.sph.}}}{V} \right|_{T=T_c} = \frac{Jk_0^5}{2\pi^2} \left[ c_1 \left( \frac{T_C}{JQ^2} \right)^{3/2} + c_2 \left( \frac{T_C}{JQ^2} \right)^{5/2} \right]. \quad (3.90)$$

---

<sup>17</sup>Here we used the discrete summation approximation  $\sum_{\mathbf{k}} |\mathbf{k}| < \Lambda \frac{1}{k^2} \approx \int_0^{\Lambda/k_0} \frac{d^3 \mathbf{q}}{(2\pi)^3} \frac{1}{q^2} = \frac{\Lambda}{2\pi^2 k_0}$ .

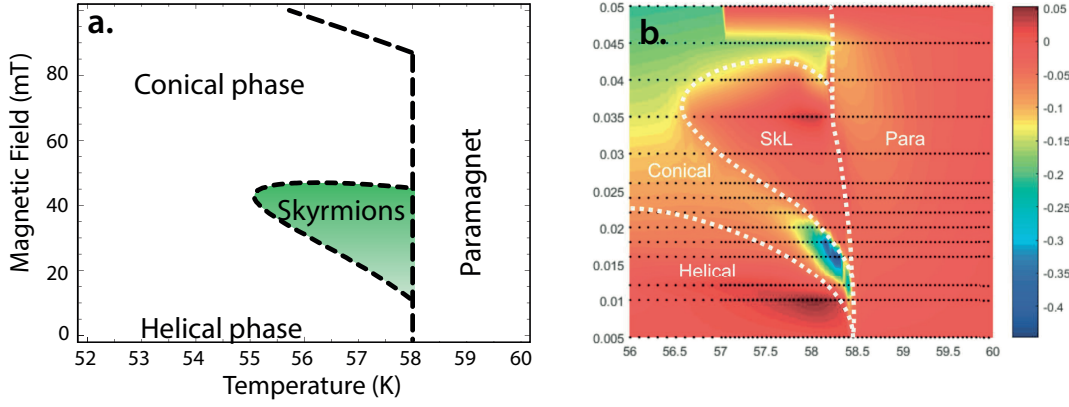


Figure 3.10: A typical calculated phase diagram (a) and a typical experimental phase diagram (b). Figure (b) taken from Ref. [141]

Thus a temperature fluctuation of order

$$\delta T_C \sim \frac{Jk_0^5}{2\pi^2\alpha} \left[ c_1 \left( \frac{T_c^{\text{mf}}}{Jk_0^2} \right)^{3/2} + c_2 \left( \frac{T_c^{\text{mf}}}{JQ^2} \right)^{5/2} \right], \quad (3.91)$$

will destroy the Brazovskii sphere by throwing system into a (more heated) disordered state. This of course may or may not mean that each of the ordered phases (helical, conical and SkL) always follows this criterion as more detailed analysis involves considering both the conical and skyrmionic phase independently, however it (very) qualitatively sketches the width of precursor region near  $T_C$ . Experimentally, this can be seen as an abrupt breakdown of the ordered phases (conical or SkL) into a paramagnetic phase. Restoring now the dimensional units, one obtains

$$\delta T_C \sim \frac{Jk_0^5 a^3}{2\pi^2\alpha} \left[ c_1 \left( \frac{k_B T_c^{\text{mf}}}{Jk_0^2 M_s^2 a^3} \right)^{3/2} + c_2 \left( \frac{k_B T_c^{\text{mf}}}{Jk_0^2 M_s^2 a^3} \right)^{5/2} \right] \quad (3.92)$$

Using now numerical values  $J = 4.85 \times 10^{-23} \text{ Jm/A}^2$ ,  $D = 1.22 \times 10^{-14} \text{ J/A}^2$ ,  $k_0 = \frac{D}{2J} = 1.26 \times 10^8 \text{ m}^{-1}$ ,  $a = 8.91 \times 10^{-10} \text{ m}$ ,  $k_B = 1.38 \times 10^{-23} \text{ J/K}$ ,  $M_s = 1.11 \times 10^5 \text{ A/m}$ ,  $T_c^{\text{mf}} \approx T_c = 58 \text{ K}$ ,  $\alpha \approx 10^{-5} \text{ Tm/AK}$ , one obtains  $\delta T_C \sim 1.5 \text{ K}$ , which is in a reasonable agreement with precursor phenomenon temperature width in experiments [134]. Note that the only free parameter here is  $\alpha$ , which is unknown. However, a similar value  $\alpha \sim 10^{-6} \div 10^{-5} \text{ Tm/AK}$  was reported in Ref.[142] as a good fit with experiment. Thus the line  $T = T_C - \delta T_C$ , roughly denotes the breakdown of the ordered state (in general, it is weakly magnetic-field-dependent).

Phase diagram. Above I have sketched the underlying mechanisms leading to stabi-

lization of a topologically-nontrivial Skyrmion Lattice phase with respect to competing conical phase in bulk chiral magnets. A typical phase diagram within approximation of Gaussian (non-interacting) critical modes is shown on Figure 3.10. For simplicity, we consider the framework of  $M^4$  theory within which the conical phase is continuously transformed into the helical phase exactly at  $H = 0$ .

### 3.8 CONCLUSIONS

In this chapter, I presented a synthesized model for semi-quantitative phase-diagram calculation on the basis of several heterogeneous theoretical approaches as described in Refs.[35, 38, 81, 105, 132, 134]. I tried to maintain the best physical features of each of those approaches. In particular, an implementation of experimentally proved [134] Brazovskii-like physics of broken symmetry of critical fluctuations, namely, the existence of a soft mode on sphere  $k = k_0$  around  $T = T_C$  and further "breaking" of this spherical- $k$  symmetry into phase-dependent sixfold or twofold long-range critical fluctuations. These implementations allowed not only to treat the phase fluctuations in a more consistent way with the mean-field model, but also to establish a more substantiated criterion for the abrupt breakdown of the modulated magnetic order near  $T_C$ , which was absent in previous models [38, 81]. I would like to emphasize that this feature is an intrinsically collective concept and thus it is impossible to capture it via a single skyrmion approach (see e.g. Ref.[81] and references therein). Note however that the reduced dimensionality (thin films and interfaces) may lead to qualitatively different physics by either appearance of higher-order terms due to dipolar interactions (a.k.a. "demagnetizing" or stray field), or a stabilizations of skyrmion arrays in a skyrmion liquid, where the single-skyrmion model translated over the space may work well.



# 4

## Writing and Erasing Magnetic Skyrmions with Electric Fields

An ultimate goal of skyrmionics is the usage of skyrmions as bits of data, which would require a controlled and reliable mechanism of skyrmion writing, erasing and reading at room temperature and small magnetic fields. For this, an external field is in general required. As such a field, one possibility would be the electric field as being often employed in electronics. In this respect, the discovery of skyrmions in a magnetoelectric insulator  $\text{Cu}_2\text{OSeO}_3$  opened dramatically new ways for exploiting topologically non-trivial magnetic phases under electric fields [44, 143, 144]. Thus, a natural question rises: under which conditions writing and erasing of skyrmions with applied voltages is possible. One of the first proposals in this direction was a usage of magnetoelectric insulator  $\text{Cu}_2\text{OSeO}_3$  where relatively moderate fields may support a dynamical nucleation of skyrmions [94, 145], however recent progress was also demonstrated in substantially different system manufactured with conducting thin films for the so-called skyrmion-bubbles (huge skyrmions) [96].

In this chapter, I calculate the effect of electric field on the energy of skyrmions and phase stability of skyrmions in insulating  $\text{Cu}_2\text{OSeO}_3$ . Using neutron scattering, we have demonstrated that the skyrmion pocket either expands or shrinks significantly depending on the direction of electric fields, allowing us to write or erase the skyrmion phase in bulk [95]. To explain the observed phenomena, the effect is addressed theoretically by using the framework of fluctuation-induced phase transitions and the first order perturbation theory in electric fields [95, 132, 133]. As the electric field is almost not heating the

insulating  $\text{Cu}_2\text{OSeO}_3$  samples, our study provides further perspectives for dissipation-free electrical control of skyrmions in insulators.

This chapter is organized as follows. In the first section I consider the energy of a single skyrmion under electric fields in the field-polarized phase (strong magnetic fields). In the next section, I push further the existing theory for the skyrmion lattice in electric fields [132] in several ways, in particular by calculating implicitly all the terms of the first order perturbation theory, developing the second-order corrections, and establishing the link with phase diagram calculation by considering  $M^4$  term, etc. To keep consistency in the first two orders of the perturbation theory, we introduce the inelastic distortion vector, and write down all the terms in first and second orders in dimensionless electric fields coming from both elastic and inelastic contributions. The third section considers experiments and theory on the writing and erasing the skyrmion phase all over the bulk. The last two sections are mainly based on my papers [133] and [95], while the manuscript containing calculation from the first part of the chapter is under preparation.

#### 4.1 ENERGY OF ISOLATED SKYRMIONS UNDER ELECTRIC FIELDS

In this section we consider the energy of isolated skyrmions emerged in the magnetic-field-polarized phase of magnetoelectric insulator  $\text{Cu}_2\text{OSeO}_3$ . The magneto-electric coupling in  $\text{Cu}_2\text{OSeO}_3$  arises due to the weak  $p$ - $d$  hybridization mechanism (see Refs. [44, 146–148]), which gives rise to an electric dipole moment  $\mathbf{P} = \alpha_\lambda(S_y S_z, S_z S_x, S_x S_y)$ , i.e. the *electric dipole moment* coupled to the spin variables  $S_x, S_y, S_z$ . Therefore, in external electric fields the ordered phase is perturbed by a dipole energy  $-\mathbf{P} \cdot \mathbf{E}$ , or

$$\mathcal{H}_\text{ae} = \alpha E_x S_y S_z + \text{cyclic permutations}, \quad (4.1)$$

where  $\mathbf{E} = (E_x, E_y, E_z)$  is the external electric field and for simplicity we absorbed the minus sign into  $\alpha = -\alpha_\lambda$ . For  $\text{Cu}_2\text{OSeO}_3$  the strength of magneto-electric coupling is estimated as  $|\alpha| \sim 10^{-33} \text{ Jm/V}$ , see Ref.[149].

We consider now electric field along  $[1\ 1\ 1]$  (we put  $\mathbf{E} = E[1\ 1\ 1]$  for simplicity<sup>1</sup>), which coincides with an anisotropy axis. Proceeding to rotated spin frame,

$$\mathbf{S}_\text{F} = \mathcal{R}_{[111]} \mathbf{S}_\text{F}, \quad \mathcal{R}_{[111]} = \begin{pmatrix} -\frac{1}{\sqrt{2}} & -\frac{1}{\sqrt{6}} & \frac{1}{\sqrt{3}} \\ \frac{1}{\sqrt{2}} & -\frac{1}{\sqrt{6}} & \frac{1}{\sqrt{3}} \\ 0 & \sqrt{\frac{2}{3}} & \frac{1}{\sqrt{3}} \end{pmatrix}, \quad (4.2)$$

so that the ME coupling (4.1) in the new frame reads:

$$\mathcal{H}_\text{ae} = \frac{1}{2} \alpha E \left( -S_{x'}^2 - S_{y'}^2 + 2S_{z'}^2 \right), \quad (4.3)$$

---

<sup>1</sup>In this notation,  $E = |\mathbf{E}|/\sqrt{3}$

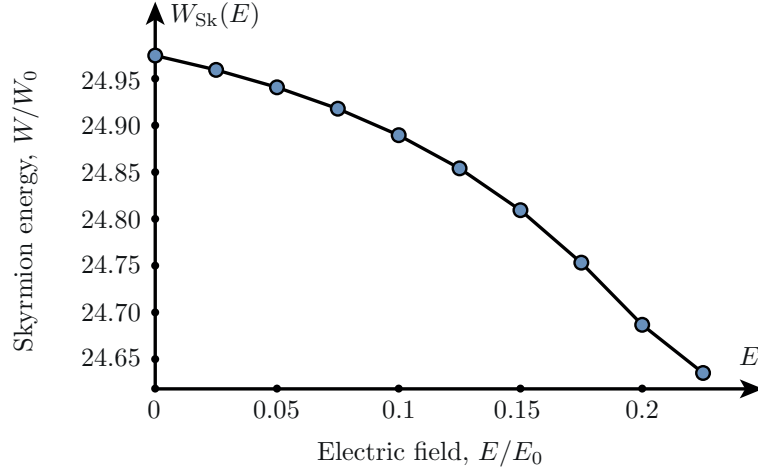


Figure 4.1: Stabilization of a single skyrmion emerged in the field-polarized phase (strong magnetic fields) with the external electric field aligned as  $\mathbf{E}||\mathbf{H}||[111]$ . The skyrmion energy is calculated for  $k_0 = 0.2/a$  and with respect to the field-polarized phase ensured by strong magnetic field  $\mathfrak{h} = 0.5$ ; here  $W_0 = 2JM^2$  and  $E_0 = 4JM_3^2/3\sqrt{3}|\alpha_\lambda|$ . The decrease in the skyrmion energy is tiny as it is assumed in the field-polarized phase. However it still indicates that the  $E$ -field-operated skyrmion stabilization mechanism is qualitatively valid even under such extreme conditions. Note also that in strong electric fields ( $E \sim E_0$ ) the skyrmion topology breaks down (the skyrmion solution no longer exists).

or in the spin-vector basis,

$$\mathcal{H}_\infty = \frac{1}{2}\alpha E \begin{pmatrix} -1 & 0 & 0 \\ 0 & -1 & 0 \\ 0 & 0 & 2 \end{pmatrix}, \quad (4.4)$$

By using parametrization  $S_{x'} = \sin\theta \cos\psi$ ,  $S_{y'} = \sin\theta \sin\psi$ ,  $S_{z'} = \cos\theta$ , one obtains

$$H_\infty = \frac{1}{2}\alpha E (3\cos^2\theta - 1) = \alpha E (1 - \frac{3}{2}\sin^2\theta). \quad (4.5)$$

The constant here can be dropped if comparing between two phases. Thus, the effect of electric field in this particular case reduces to renormalizing the uniaxial anisotropy. Thus, the energy functional reads:

$$W = \langle J(\nabla S)^2 + D\mathbf{S} \cdot (\nabla \times \mathbf{S}) - hS_{z'} + KS_{z'}^2 + \frac{3}{2}\alpha ES_{z'}^2 \rangle \quad (4.6)$$

In this chapter we consider, for simplicity, a skyrmion in the field-polarized phase, that is for  $H > H_{C2}(T)$ . Thus the energy functional reads

$$\frac{W_{\text{Sk}}}{JM_s^2} = 2\pi \int_0^\infty dr r \left[ \left( \frac{d\theta}{dr} + k_0 \right)^2 - k_0^2 + \frac{\sin^2 \theta}{r^2} + k_0 \frac{\sin 2\theta}{r} + \kappa_E (1 - \cos^2 \theta) + \mathfrak{h} (1 - \cos \theta) \right], \quad (4.7)$$

with parameters

$$k_0 = \frac{D}{2J}, \quad \kappa_E = \frac{K + 3\alpha E/2}{J}, \quad \mathfrak{h} = \frac{H}{JM_s}. \quad (4.8)$$

At finite temperatures, probability for a thermodynamical appearing of a skyrmion in the field-polarized phase is thus

$$\rho = e^{-W_{\text{Sk}}/T}. \quad (4.9)$$

This approximation is good for a low density of isolated skyrmions, or non-interacting skyrmion gas limit. If interactions are important, the meron and bimeron energy considerations are however modified [150]. We solve the Euler-Lagrange equation corresponding to the energy functional (4.7) (see Chapter 2 for further details), and consider for simplicity case with  $K = 0$ . We choose the conditions ensuring the field-polarized phase (strong magnetic fields),  $\mathfrak{h} = 0.5$ , and model helical wave vector  $k_0 = 0.2/a$  (thus helical period is  $\lambda = 2\pi/a \approx 31a$ ). After the skyrmion solution  $\theta(r)$  is variationally found for each of the electric fields  $E/E_0$ ,  $E_0 = 4JM_s^2/3\sqrt{3}|\alpha_\lambda|$ , it is further substituted to the energy functional (4.7), and the integration is carried out numerically. The results of these calculations are summarized on Figure 4.1. Thus we see that a single skyrmion, which appears as a metastable exited state, can be stabilized by applying external electric fields  $\mathbf{E}||\mathbf{H}||[111]$ , which lower its energy. Consequently, the probability of observing isolated skyrmions will depend on the strength (and, in general, polarity) of electric field. The effect in the field-polarized phase is however not dramatic, as according to my calculations, it never stabilizes the skyrmion thermodynamically, and the skyrmion remains a metastable stable of the field-polarized background. We will see however in the next sections that even the moderate electric fields dramatically tune the *skyrmion lattice stability* with respect to the conical phase, enabling to "write" or "erase" the skyrmion phase all over the bulk.

## 4.2 SKYRMION LATTICE IN ELECTRIC FIELDS

Manipulation and control of skyrmions have become an active topic of skyrmionics. Recent experiments succeeded manipulation of skyrmions with moderate electric fields, electric currents, and thermal gradients [46, 80, 91, 93, 132, 151–153]. To avoid Ohmic



heating effects which are undesirable for electronics, the application of moderate electric fields to insulating skyrmion-host compounds (such as  $\text{Cu}_2\text{OSeO}_3$  [44]) is potentially more advantageous for the current-driven devices. These observations motivated theoretical proposals for creation (“writing”) skyrmions in insulating helimagnets with the help of external electric field, [94, 145, 153, 154] and subsequent electric-field guiding. [155] To date, a key experimental challenge in this direction is stabilization and control of the skyrmion lattice by an electric field. Therefore, there is a need for simple theories of skyrmion lattice response to the  $E$ -field. In particular, what is of interest is the shift of skyrmion lattice energy in electric field, with subsequent stabilization of the skyrmion lattice.[154]

We treat the physics of the skyrmion lattice upon application of  $E$ -field to an insulating skyrmion-host compound, such as  $\text{Cu}_2\text{OSeO}_3$ . In this material, the effect of magnetoelectric coupling arises due to a hybridization mechanism originating from relativistic spin-orbit interaction (see Refs. [44, 146–148]), which gives rise to an electric dipole moment which can be expressed in terms of the local spin variables. The strength of the effect is however relativistically small, which allows us to build an accurate perturbation theory in  $E$ -fields.

In this paper, we treat the effect of electric field on skyrmion lattices in the two first orders of perturbation theory. The skyrmion lattice in electric fields becomes slightly distorted, and we introduce the elastic and inelastic distortion vectors. The shift of SkL energy comes from expectation values of the electromagnetic coupling and anisotropic contributions.

#### 4.2.1 ENERGY DENSITY IN A COARSE-GRAINED MODEL

The Skyrmion Lattice (SkL) is a long-range-order spin configuration which can be visualized as a triangular (hexagonal) lattice of vortices. Experimentally, the hallmark of the SkL phase is appearance of a six-fold reflection pattern in reciprocal space, as sketched in Figure 4.2, each of the wave vectors are rotated by  $2\pi/3$  (see e.g. Refs. [38, 132] for SANS patterns). In this study, we describe the skyrmion lattice by a coarse-grained local magnetization vector  $\mathbf{S}(\mathbf{r})$ , which can be built on the three  $\mathbf{Q}$ -vectors (Fig. 4.2). With a good accuracy the SkL phase can be approximated by the multispiral spin structure [37, 38]

$$\mathbf{S}(\mathbf{r}) = \mathbf{m} + \mu \sum_{\mathbf{Q}_n} \mathbf{S}_{\mathbf{Q}_n} e^{i\mathbf{Q}_n \mathbf{r} + i\varphi_n} + \mathbf{S}_{\mathbf{Q}_n}^* e^{-i\mathbf{Q}_n \mathbf{r} - i\varphi_n}, \quad (4.10)$$

where  $\mathbf{m} \equiv \langle \mathbf{S}(\mathbf{r}) \rangle$  is a uniform magnetization, with (spatial) average defined as  $\langle \dots \rangle = \int \frac{dV}{V} (\dots)$  throughout the study, and  $\mu$  is the weight of the SkL helical modulations. The sum in (3.1) runs over the “3Q-structure” (Fig. 4.2), the relative phases  $\varphi_n$  in (3.1) are important for minimization of the SkL energy. The expectation of energy density in the

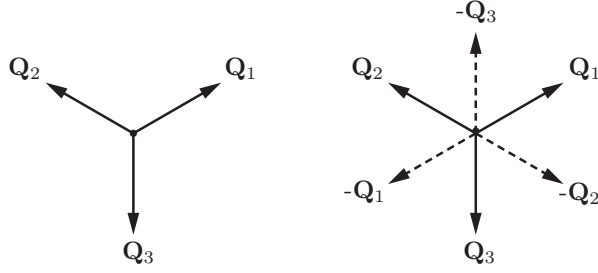


Figure 4.2: The hexagonal Skyrmin Lattice in reciprocal space. Right-hand side of the figure shows the auxiliary negative reflexes, so that the hexagonal real-space SkL is built on the six wave vectors  $\{\mathbf{Q}_1, -\mathbf{Q}_3, \mathbf{Q}_2, -\mathbf{Q}_1, \mathbf{Q}_3, -\mathbf{Q}_2\}$ , see the main text.

coarse-grained model is given by calculating the spatial average  $\langle \mathcal{H} \rangle$  with spin function

$$\mathcal{H} = \mathcal{H}_{JDh} + \mathcal{H}_A + \mathcal{H}_{\alpha E}, \quad (4.11)$$

where the helimagnetic term

$$\mathcal{H}_{JDh} = J(\nabla \mathbf{S})^2 + D\mathbf{S} \cdot (\nabla \times \mathbf{S}) - \mathbf{h} \cdot \mathbf{S} \quad (4.12)$$

takes into account Heisenberg interaction ( $J$ ), Dzyaloshinskii-Moriya interaction ( $D$ ) and the Zeeman coupling to the external magnetic field  $\mathbf{h}$ .

In this study, we consider the fourth-order anisotropy as it represents the essential physics of the problem by stabilizing the SkL phase.[38, 132] The symmetry of  $\text{Cu}_2\text{OSeO}_3$  is described by the  $P2_13$  space group, which allows a fourth-order magneto-crystalline anisotropy of the form  $A_1(S_x^4 + S_y^4 + S_z^4) + A_2(S_x^2 S_y^2 + S_y^2 S_z^2 + S_z^2 S_x^2)$ . Proceeding to the unitary parametrization  $\mathbf{S}/|\mathbf{S}| = (\sin\theta \cos\psi, \sin\theta \sin\psi, \cos\theta)$ , one obtains  $S_x^2 S_y^2 + S_y^2 S_z^2 + S_z^2 S_x^2 = -\frac{1}{2}(S_x^4 + S_y^4 + S_z^4) + \frac{1}{2}$ , we thus have:

$$\mathcal{H}_A = A(S_x^4 + S_y^4 + S_z^4) + U\mathbf{S}^4. \quad (4.13)$$

with  $A = A_1 - A_2/2$  and  $U = A_2/2$ . Thus, there could be too distinct situations, first with  $A_1 \gg A_2$ , for which the anisotropy of the bulk is important, and the opposite case with  $A_1 \sim A_2/2$ , where the role of anisotropy is reduced to providing mode-mode coupling  $U \sim A_1, A_2$ . In this section, following my paper [133], we consider the first case, while the second case will be presented in the next section as it provides a qualitatively universal picture for bulk skyrmion hosts.

The above expressions (3.7)-(4.1) are written in the natural frame. Experimentally, one often needs to apply magnetic and electric fields along directions where particular properties of the system are better revealed. In particular, in some  $E$ -field rotation experiments,[132] the magnetic field  $\mathbf{h}$  is parallel to  $[1\bar{1}0]$ , while the electric field is parallel to  $[111]$  or  $[\bar{1}\bar{1}\bar{1}]$ , with  $|E_x| = |E_y| = |E_z| \equiv E$  for simplicity of notations (thus the

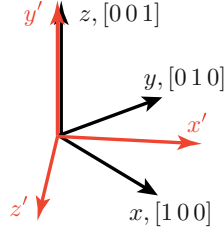


Figure 4.3: Rotated spin frame (red) for the magnetic field orientation  $[1\bar{1}0]$ .

magnitude is  $|\mathbf{E}| = \sqrt{3}E$ ). It is easier to carry out calculations in the rotated spin frame  $(x', y', z')$ , with  $\hat{z}'$  set by the direction of magnetic field  $\mathbf{h}$ , see Fig. 4.3. In the case of above-mentioned geometry (Fig. 4.3), the transformation of the rotated spin frame is given by the rotation matrix

$$\mathcal{R} = \frac{1}{\sqrt{2}} \begin{pmatrix} 1 & 0 & 1 \\ 1 & 0 & -1 \\ 0 & \sqrt{2} & 0 \end{pmatrix}. \quad (4.14)$$

While the helimagnetic term (3.7) is a Lifshitz invariant, the fourth-order anisotropy (4.13) is transformed under rotation (4.14) into

$$\mathcal{H}_A = A \left( \frac{1}{2} S_{x'}^4 + S_{y'}^4 + 3 S_{x'}^2 S_{z'}^2 + \frac{1}{2} S_{z'}^4 \right), \quad (4.15)$$

The  $E$ -field perturbation (4.1) also transforms under rotation  $\mathcal{R}$ ,

$$\mathcal{H}_{\text{ae}} = \frac{\alpha E}{2} \left( S_{x'}^2 + 2\sqrt{2} S_{x'} S_{y'} - S_{z'}^2 \right), \quad (4.16)$$

and the electric field is directed along  $\hat{e}_{x'} + \hat{e}_{y'}$ . For simplicity, we drop the prime signs in the subsequent calculations.

#### 4.2.2 UNPERTURBED STATE

In this section I very briefly remind the concepts of the mean-field treatment of the skyrmion lattice (Chapter 3), which will be important for the perturbation theory which follows. First, we find the single-helix eigenstates, which give rise to a modulated spin structures with wave length  $\lambda = 2\pi/k_0 = 4\pi J/D$ . After that, we construct the skyrmion lattice order parameter, and calculate the mean-field energy of the skyrmion lattice.

We start from considering the interplay between the Heisenberg term and the DMI

coupling,

$$W_0 = \langle J[\nabla \mathbf{S}(\mathbf{r})]^2 + D \mathbf{S}(\mathbf{r}) \cdot [\nabla \times \mathbf{S}(\mathbf{r})] \rangle = \sum_{\mathbf{k}} \mathbf{S}_{\mathbf{k}}^\dagger \hat{\mathcal{H}}_0 \mathbf{S}_{\mathbf{k}}, \quad (4.17)$$

where in we used the Fourier transform of the spatial average to reciprocal space. Here  $\hat{\mathcal{H}}_0$  is written in spin representation  $\mathbf{S}_{\mathbf{k}} = (S_{\mathbf{k}}^x, S_{\mathbf{k}}^y, S_{\mathbf{k}}^z)^T$  as a matrix operator

$$\hat{\mathcal{H}}_0 = \begin{pmatrix} Jk^2 & 0 & iDk_y \\ 0 & Jk^2 & -iDk_x \\ -iDk_y & iDk_x & Jk^2 \end{pmatrix}, \quad (4.18)$$

and is diagonalized on the eigenvectors

$$|\mathbf{S}_{\mathbf{k}}^{(0)}\rangle = \frac{1}{\sqrt{2}}(-i\hat{k}_y, i\hat{k}_x, 1)^\top, \quad |\mathbf{S}_{\mathbf{k}}^{(1)}\rangle = (\hat{k}_x, \hat{k}_y, 0)^\top, \quad |\mathbf{S}_{\mathbf{k}}^{(2)}\rangle = \frac{1}{\sqrt{2}}(i\hat{k}_y, -i\hat{k}_x, 1)^\top, \quad (4.19)$$

where  $\hat{k}_{x,y,z} = k_{x,y,z}/|\mathbf{k}|$  and we introduced "bra" and "ket" notations as shortcuts to write the perturbation formulas of the matrix mechanics [138] in a familiar way. Consistent with our previous notations, we denote  $\langle \mathbf{S}_{\mathbf{k}} | \dots | \mathbf{S}_{\mathbf{k}} \rangle = \sum_{\mathbf{k}} \mathbf{S}_{\mathbf{k}}^\dagger \dots \mathbf{S}_{\mathbf{k}}$ , which is just a Fourier-transform of the corresponding spatial averaging  $\langle \dots \rangle$  as in Eq.(4.17). The spectrum of matrix  $\hat{\mathcal{H}}_0$  consists of the three equidistant energy solutions, with the energy separation  $\pm Dk$ ,

$$\varepsilon_{\mathbf{k}}^{(0)} = Jk^2 - Dk, \quad \varepsilon_{\mathbf{k}}^{(1)} = Jk^2, \quad \varepsilon_{\mathbf{k}}^{(2)} = Jk^2 + Dk, \quad (4.20)$$

For the positive  $J, D$  the lowest energy solution is the helix

$$|\mathbf{S}_{\mathbf{k}}^{(0)}\rangle = \frac{1}{\sqrt{2}} \begin{pmatrix} -i\hat{k}_y \\ i\hat{k}_x \\ 1 \end{pmatrix}, \quad (4.21)$$

which corresponds to the eigenvalue  $\varepsilon_{\mathbf{k}}^{(0)}$ . The modulation vector  $\mathbf{k}_0$  is determined by further minimization of the energy,  $\partial \varepsilon_{\mathbf{k}}^{(0)} / \partial \mathbf{k} = 0$ . Consequently, the minimum of the dispersion  $\varepsilon_{\mathbf{k}}^{(0)} = Jk^2 - Dk$  is satisfied if  $\mathbf{k}_0 = \frac{D}{2J}$ . Finally, I remind that the energies spectrum under considerations is

$$\varepsilon_{\mathbf{k}_0}^{(0)} = -Dk_0/2, \quad \varepsilon_{\mathbf{k}_0}^{(1)} = Dk_0/2, \quad \varepsilon_{\mathbf{k}_0}^{(2)} = 3Dk_0/2, \quad (4.22)$$

which is used in the following calculations.

#### 4.2.3 SKYRMION LATTICE IN ELECTRIC FIELDS: ELASTIC PERTURBATION

In this section we consider the shift in the SkL energy caused by distortion of the skyrmion vectors. We start by re-writing the magneto-electric coupling in the rotated frame (4.16) in symmetrized form, which in units  $Dk_0$  is simply

$$\hat{\mathcal{H}}_{\mathfrak{a}}/Dk_0 = 2\mathfrak{a} \begin{pmatrix} 1 & \sqrt{2} & 0 \\ \sqrt{2} & 0 & 0 \\ 0 & 0 & -1 \end{pmatrix}, \quad (4.23)$$

where we have introduced the *dimensionless electric field*  $\mathfrak{a}$ ,

$$\mathfrak{a} \equiv \frac{\alpha E}{4Dk_0}, \quad (4.24)$$

which plays the role of the small parameter of the theory. To illustrate its smallness, we use typical electric fields  $E = 5 \times 10^6 \text{ V/m}$ , and  $\text{Cu}_2\text{OSeO}_3$  parameters as  $J = 4.85 \times 10^{-23} \text{ Jm/A}$ ,  $k_0 = D/2J = 10^8 \text{ m}$ , and ME coupling [94] is  $\alpha \sim 10^{-14} \text{ J/m}^2\text{V}$ . This gives  $\mathfrak{a} \sim 0.01$ . Thus throughout this study, we build the perturbation theory in orders of  $\mathfrak{a}^1$  and  $\mathfrak{a}^2$ , which is sufficient for describing both the symmetric and asymmetric responses in  $E$ -fields.

First, we consider the helix vectors in external electric field. Considering  $E$ -field as a small perturbation (4.23) on top of the  $JD$ -matrix (4.18), matrix perturbation theory gives[138]

$$|\mathbf{S}_{\mathbf{k}}^{(\mathfrak{a})}\rangle = |\mathbf{S}_{\mathbf{k}}^{(0)}\rangle + \sum_{n \neq 0} |\mathbf{S}_{\mathbf{k}}^{(n)}\rangle \frac{\langle \mathbf{S}_{\mathbf{k}}^{(n)} | \hat{\mathcal{H}}_{\mathfrak{a}} | \mathbf{S}_{\mathbf{k}}^{(0)} \rangle}{\epsilon_{\mathbf{k}}^{(0)} - \epsilon_{\mathbf{k}}^{(n)}} + \mathcal{O}(\mathfrak{a}^2). \quad (4.25)$$

where  $\epsilon_{\mathbf{k}}^{(n)}$  are given by Eq.(4.22) and  $|\mathbf{S}_{\mathbf{k}}^{(n)}\rangle$ ,  $n = 0, 1, 2$ , are eigenstates of  $\mathcal{H}_0$  as given by Eqs.(14-16). The perturbed helix (4.25) is by construction normalized on unity up to terms of order  $\mathcal{O}(\mathfrak{a}^2)$ ,

$$\langle \mathbf{S}_{\mathbf{k}}^{(\mathfrak{a})} | \mathbf{S}_{\mathbf{k}}^{(\mathfrak{a})} \rangle = 1 + \mathcal{O}(\mathfrak{a}^2). \quad (4.26)$$

A direct calculation for the new helix, using formulas (4.25), (4.23), (3.46)-(4.19), gives

$$|\mathbf{S}_{\mathbf{k}}^{(\mathfrak{a})}\rangle = |\mathbf{S}_{\mathbf{k}}^{(0)}\rangle - \mathfrak{a} |\mathbf{F}_{\mathbf{k}}\rangle + \mathcal{O}(\mathfrak{a}^2), \quad (4.27)$$

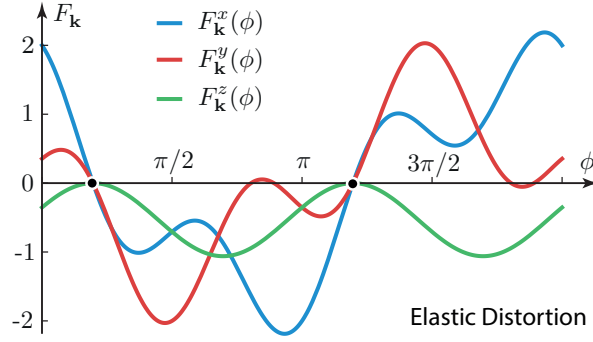


Figure 4.4: Components of elastic distortion vector  $\mathbf{F}_{\mathbf{k}}$  as functions of the helix angle  $\phi$ .  $F_{\mathbf{k}}^{x,y}$  are  $2\pi$ -periodic while  $F_{\mathbf{k}}^z$  is  $\pi$ -periodic. The dots denote stationary points which are not effected by  $E$ -field.

where  $\mathbf{F}_{\mathbf{k}} = \mathbf{F}(\hat{k}_x, \hat{k}_y) \equiv \mathbf{F}_{\mathbf{k}}(\phi)$  is the elastic distortion vector (here for each helix  $\hat{k}_x = \cos\phi$ ,  $\hat{k}_y = \sin\phi$ , that is  $\phi$  is angle between  $\mathbf{k}$  and  $\hat{x}$ ), so that

$$|\mathbf{F}_{\mathbf{k}}\rangle = (iF_{\mathbf{k}}^x(\phi), iF_{\mathbf{k}}^y(\phi), F_{\mathbf{k}}^z(\phi))^{\top}, \quad (4.28)$$

with angle-dependent components

$$F_{\mathbf{k}}^x(\phi) = -\frac{\sin\phi}{\sqrt{2}} + 2\cos^3\phi - \frac{3\sin\phi\cos^2\phi}{2\sqrt{2}} - \sin^2\phi\cos\phi, \quad (4.29)$$

$$F_{\mathbf{k}}^y(\phi) = \frac{\cos\phi}{2\sqrt{2}} - 2\sin^3\phi + \sin\phi\cos^2\phi - \frac{3\sin^2\phi\cos\phi}{2\sqrt{2}}, \quad (4.30)$$

$$F_{\mathbf{k}}^z(\phi) = -\frac{1}{2\sqrt{2}} - \frac{\sin^2\phi}{2\sqrt{2}} + \sin\phi\cos\phi. \quad (4.31)$$

The components  $F_{\mathbf{k}}^x$ ,  $F_{\mathbf{k}}^y$ ,  $F_{\mathbf{k}}^z$  of the elastic distortion vector are  $\pi$  and  $2\pi$  periodic functions, and are illustrated in Fig. 4.4. Note that the  $x$  and  $y$  components of both  $\mathbf{S}_{\mathbf{k}}^{(0)}$  and  $\mathbf{S}_{\mathbf{k}}^{(\text{ae})}$  are imaginary, and  $z$  component is real for both  $\mathbf{S}_{\mathbf{k}}^{(0)}$  and  $\mathbf{S}_{\mathbf{k}}^{(\text{ae})}$ . Physically it means that the field-induced distortion of the skyrmion lattice does not change the orientation of the skyrmion plane. One can verify both analytically and numerically that Eqs.(4.29)-(4.30) together with (4.28) satisfy normalization (4.26).

#### 4.2.4 ENERGY SHIFT OF THE SKYRMION LATTICE IN ELECTRIC FIELDS

In this section, we calculate the shift of the SkL energy in the first two orders in terms of dimensionless electric field  $\text{ae}$ . This shift is contributed by the expectation value of the magnetoelectric coupling, and the anisotropic contributions due to the skyrmion lattice distortion.

## MAGNETO-ELECTRIC RESPONSE

The first contribution to the energy shift of the skyrmion lattice in electric field comes from taking the expectation value of (4.23) in the appropriate order in  $\mathfrak{a}$ . In this study, we consider  $\mathfrak{a}$  to be small, thus the second order is sufficient for capturing the essential physics in both antisymmetric (field reversion  $E \rightarrow -E$  gives the energy shifts of different signs) and symmetric (field reversion  $E \rightarrow -E$  gives the energy shifts of same signs) cases of interest. Using the explicit expression (4.27)–(4.31), one obtains

$$\frac{\langle \hat{\mathcal{H}}_{\mathfrak{a}} \rangle}{Dk_0} = \sum_{\mathbf{k}} \frac{\langle \mathbf{S}_{\mathbf{k}} | \hat{\mathcal{H}}_{\mathfrak{a}} | \mathbf{S}_{\mathbf{k}} \rangle}{Dk_0} = -(2m^2 + 3\mu^2)\mathfrak{a} - \frac{189}{4}\mu^2\mathfrak{a}^2 + \mathcal{O}(\mathfrak{a}^3). \quad (4.32)$$

The expression (4.32) is the leading contribution in case if the anisotropy of the system is small. Restoring the dimensional units, the shift of the SkL energy  $W$  in electric field  $E$  is therefore given by

$$\Delta W_1(E) = -\frac{\alpha(2m^2 + 3\mu^2)M_s^2 a^3}{4}E - \frac{189\alpha^2\mu^2 M_s^2 a^3}{64Dk_0}E^2 + \mathcal{O}(E^3). \quad (4.33)$$

where  $M_s$  is saturation magnetization (in A/m),  $a$  is the lattice constant. Note that the helimagnetic term  $H_{JDh}$  is not giving shift contributions to this order.

## ANISOTROPY RESPONSE

Now, we calculate the direct contribution of anisotropy to the energy shift. The main physical mechanism here is the distortion of SkL in electric field, which results to perturbation in the anisotropic energy. To proceed, we explicitly use formulas (4.27)–(4.31) to calculate the expectation value of the anisotropic term in the new ground state. In the leading order one therefore obtains

$$\begin{aligned} \langle \mathcal{H}_A \rangle_1 = \langle \mathbf{S}^{(\mathfrak{a})} | \hat{\mathcal{H}}_A | \mathbf{S}^{(\mathfrak{a})} \rangle &\simeq \frac{9}{8}Am^2\mu^2\mathfrak{a} + \frac{99}{32}A\mu^4\mathfrak{a} + \frac{81}{64}A\mu^4\mathfrak{a}(\cos 6\phi_0 + 2\sqrt{2}\sin 6\phi_0) \\ &+ \frac{27}{4\sqrt{2}}A\mathfrak{a}m\mu^3\cos(\varphi_1 + \varphi_2 + \varphi_3). \end{aligned} \quad (4.34)$$

Here  $\phi_0$  is the angle between the first skyrmion helix and  $\hat{x}$  (note that due to  $2\pi/3$  symmetry in SkL rotation, and  $6\phi$ -arguments in Eq.(4.34), one can take  $\phi_0$  as the angle between any of the skyrmion helices and  $\hat{x}$ ). The same angular dependence [third term in Eq.(4.34)] were reported in study [132], where the minimization of SkL energy in electric fields leads to the SkL rotation in real space with respect to  $\hat{x}$ , if six-order anisotropy is considered, however all the angular-independent anisotropic contributions were there neglected.[132] We notice that expression (4.34) is dependent on the relative phases of the

helices  $\varphi_i$ . The same situation occurs in (3.67), when the mean-field energy is dependent on phase. We take again  $\cos(\varphi_1 + \varphi_2 + \varphi_3) = -1$ , which minimizes the mean-field energy for fixed positive  $m, \mu$ , therefore

$$\langle \mathcal{H}_A \rangle_1 = \frac{9}{8} A \mu^4 \left( \frac{11}{4} - 3\sqrt{2} \frac{\mu}{m} + \frac{\mu^2}{m^2} \right) \mathfrak{x} + \frac{81}{64} A \mu^4 (\cos 6\phi_0 + 2\sqrt{2} \sin 6\phi_0) \mathfrak{x} + \mathcal{O}(\mathfrak{x}^2). \quad (4.35)$$

This contribution gives the linear anisotropic response to the external field. However, for the completeness of discussion, we need to take into account further terms  $\mathcal{O}(\mathfrak{x}^2)$ , which come both from the elastic distortion of the SkL and the inelastic (quadratic in  $\mathfrak{x}$ ) distortion of the SkL.

#### MIXED INELASTIC RESPONSE

To consider the nonlinear anisotropic response, we re-define the perturbed helix eigenstates up to the second order, which are given by a perturbative expansion

$$\begin{aligned} |\mathbf{S}_{\mathbf{k}}^{(\mathfrak{x})}\rangle &= |\mathbf{S}_{\mathbf{k}}^{(0)}\rangle + \sum_{n \neq 0} |\mathbf{S}_{\mathbf{k}}^{(n)}\rangle \frac{\langle \mathbf{S}_{\mathbf{k}}^{(n)} | \hat{\mathcal{H}}_{\mathfrak{x}} | \mathbf{S}_{\mathbf{k}}^{(0)} \rangle}{\varepsilon_{\mathbf{k}}^{(0)} - \varepsilon_{\mathbf{k}}^{(n)}} \\ &+ \sum_{n \neq 0} \sum_{m \neq 0} |\mathbf{S}_{\mathbf{k}}^{(n)}\rangle \frac{\langle \mathbf{S}_{\mathbf{k}}^{(n)} | \hat{\mathcal{H}}_{\mathfrak{x}} | \mathbf{S}_{\mathbf{k}}^{(m)} \rangle \langle \mathbf{S}_{\mathbf{k}}^{(m)} | \hat{\mathcal{H}}_{\mathfrak{x}} | \mathbf{S}_{\mathbf{k}}^{(0)} \rangle}{(\varepsilon_{\mathbf{k}}^{(0)} - \varepsilon_{\mathbf{k}}^{(n)}) (\varepsilon_{\mathbf{k}}^{(0)} - \varepsilon_{\mathbf{k}}^{(m)})} \\ &- \sum_{n \neq 0} |\mathbf{S}_{\mathbf{k}}^{(n)}\rangle \frac{\langle \mathbf{S}_{\mathbf{k}}^{(n)} | \hat{\mathcal{H}}_{\mathfrak{x}} | \mathbf{S}_{\mathbf{k}}^{(0)} \rangle \langle \mathbf{S}_{\mathbf{k}}^{(0)} | \hat{\mathcal{H}}_{\mathfrak{x}} | \mathbf{S}_{\mathbf{k}}^{(0)} \rangle}{(\varepsilon_{\mathbf{k}}^{(0)} - \varepsilon_{\mathbf{k}}^{(n)})^2} \\ &- \sum_{n \neq 0} |\mathbf{S}_{\mathbf{k}}^{(0)}\rangle \frac{\langle \mathbf{S}_{\mathbf{k}}^{(0)} | \hat{\mathcal{H}}_{\mathfrak{x}} | \mathbf{S}_{\mathbf{k}}^{(n)} \rangle \langle \mathbf{S}_{\mathbf{k}}^{(n)} | \hat{\mathcal{H}}_{\mathfrak{x}} | \mathbf{S}_{\mathbf{k}}^{(0)} \rangle}{2(\varepsilon_{\mathbf{k}}^{(0)} - \varepsilon_{\mathbf{k}}^{(n)})^2} + \mathcal{O}(\mathfrak{x}^3). \end{aligned} \quad (4.36)$$

This expansion leads to re-definition of (4.27) by adding a nonelastic distortion of the skyrmion lattice,

$$|\mathbf{S}_{\mathbf{k}}^{(\mathfrak{x})}\rangle = |\mathbf{S}_{\mathbf{k}}^{(0)}\rangle - \mathfrak{x} |\mathbf{F}_{\mathbf{k}}\rangle + \mathfrak{x}^2 |\mathbf{G}_{\mathbf{k}}\rangle + \mathcal{O}(\mathfrak{x}^3), \quad (4.37)$$

where  $\mathbf{G}_{\mathbf{k}} = \mathbf{G}(\hat{k}_x, \hat{k}_y) \equiv \mathbf{G}_{\mathbf{k}}(\phi)$  is the main inelastic distortion vector,

$$|\mathbf{G}_{\mathbf{k}}\rangle = (iG_{\mathbf{k}}^x(\phi), iG_{\mathbf{k}}^y(\phi), G_{\mathbf{k}}^z(\phi))^T. \quad (4.38)$$

The direct calculation of the inelastic distortion vector, by using (4.36), (4.23), (3.46)-



(4.19), gives

$$\begin{aligned}
G_{\mathbf{k}}^x(\phi) &= -\frac{39}{64\sqrt{2}}\sin\phi + \frac{131}{128\sqrt{2}}\sin 3\phi + \frac{273}{128\sqrt{2}}\sin 5\phi + \frac{33}{16}\cos\phi + \frac{119}{32}\cos 3\phi + \frac{39}{32}\cos 5\phi, \\
G_{\mathbf{k}}^y(\phi) &= -\frac{33}{16}\sin\phi + \frac{37}{32}\sin 3\phi + \frac{39}{32}\sin 5\phi - \frac{93}{64\sqrt{2}}\cos\phi + \frac{443}{128\sqrt{2}}\cos 3\phi - \frac{273}{128\sqrt{2}}\cos 5\phi, \\
G_{\mathbf{k}}^z(\phi) &= \frac{3}{8}\sin 2\phi + \frac{15}{16}\sin 4\phi + \frac{3}{16\sqrt{2}}\cos 2\phi - \frac{105}{64\sqrt{2}}\cos 4\phi - \frac{171}{64\sqrt{2}}.
\end{aligned} \tag{4.39}$$

These dependencies are shown in Fig. 4.5. The comparison between the elastic and inelastic distortion vectors is shown on Figure 4.6. Finally, for the numerical consistence of calculations, one can verify that the new ground state is normalized on unity,

$$\langle \mathbf{S}_{\mathbf{k}}^{(\mathfrak{a})} | \mathbf{S}_{\mathbf{k}}^{(\mathfrak{a})} \rangle = 1 + \mathcal{O}(\mathfrak{a}^3). \tag{4.40}$$

Therefore, the mixed elastic-inelastic response  $\mathcal{O}(\mathfrak{a}^2)$  is obtained by calculating the expectation value in the new basis (4.37). The direct calculation gives

$$\langle \mathcal{H}_A \rangle_2 = \frac{27}{64} A \mu^4 (f_0 + f_1 \cos 6\phi_0 + f_2 \sin 6\phi_0) \mathfrak{a}^2, \tag{4.41}$$

where we have introduced the following dimensionless factors

$$f_0 = -\frac{191}{8} + 62\sqrt{2}\frac{m}{\mu} - 16\frac{m^2}{\mu^2}, \quad f_1 = 29 - 14\sqrt{2}\frac{m}{\mu} + 56\frac{m^2}{\mu^2}, \quad f_2 = -59\sqrt{2} + 16\frac{m}{\mu} - 32\sqrt{2}\frac{m^2}{\mu^2}. \tag{4.42}$$

The mixed elastic-inelastic contribution (4.41) gives the second-order correction in  $\mathfrak{a}$  which may be important in some particular cases, for example, when the first order correction vanishes. Then, the electric field response does not depend on the field polarity

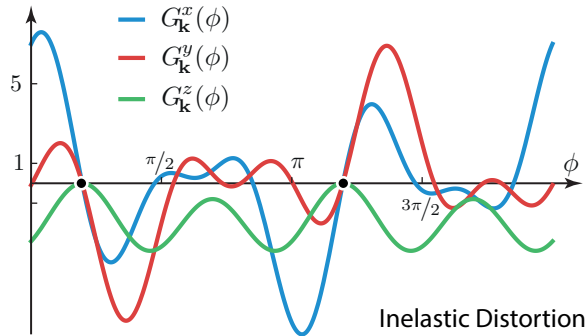


Figure 4.5: Components of the nonelastic distortion vector  $\mathbf{G}_{\mathbf{k}}$  as a function of the helix direction angle  $\phi$ .  $G_{\mathbf{k}}^{x,y}$  are  $2\pi$ -periodic while  $G_{\mathbf{k}}^z$  is  $\pi$ -periodic. The dots denote stationary points which are not effected by  $E$ -field.

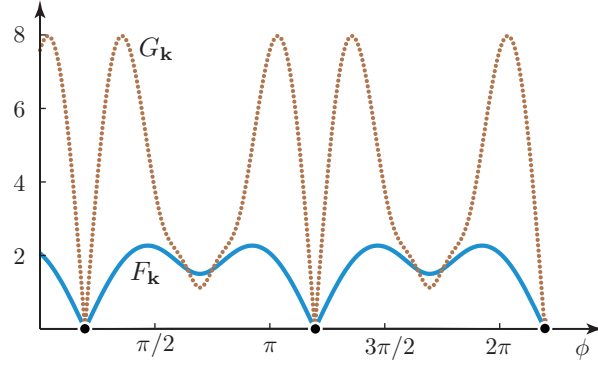


Figure 4.6: Comparison between magnitudes of elastic  $F_{\mathbf{k}} = |\mathbf{F}_{\mathbf{k}}|$  and nonelastic  $G_{\mathbf{k}} = |\mathbf{G}_{\mathbf{k}}|$  distortion vectors as the function of the helix angle  $\phi$ . There  $\pi$ -periodic stationary points, which indicate the direction along which the helices are not disturbed,  $F_k = G_k = 0$ .

( $\pm E$  is absorbed in  $E^2$ ).

Thus we have three contributions to the shift in the SkL mean-field energy:

$$\Delta W_1(E) = -\frac{\alpha(2m^2 + 3\mu^2)M_s^2 a^3}{4}E - \frac{189\alpha^2 \mu^2 M_s^2 a^3}{64 D k_0}E^2, \quad (4.43)$$

$$\Delta W_2(E) = \frac{9\alpha A \mu^4 M_s^2 a^3}{32 D k_0}E \left[ \frac{11}{4} - 3\sqrt{2}\frac{\mu}{m} + \frac{\mu^2}{m^2} + \frac{9}{8}(\cos 6\phi_0 + 2\sqrt{2}\sin 6\phi_0) \right], \quad (4.44)$$

$$\Delta W_3(E) = \frac{27\alpha^2 A \mu^4 M_s^2 a^3}{1024 D^2 k_0^2}E^2 \times (f_0 + f_1 \cos 6\phi_0 + f_2 \sin 6\phi_0). \quad (4.45)$$

Together, formulas (4.43)-(4.45) give the contribution up to the second order in electric field  $E$ . In case of the weak anisotropy  $A \ll D^2/J$ , the term (4.45) can be usually neglected. Note also that in the main-order approximation ( $\propto^1$ ) the  $E$ -field induced shift in energy is also the shift in free energy of the skyrmion lattice for a fixed temperature near  $T_C$ . We note that if combining a weaker six-order anisotropy, which contains field-independent terms as  $\mu^6 \cos 6\phi_0$ , together with  $6\phi_0$ -dependencies in (4.43)-(4.45), one will get minimization of skyrmion lattice energy for  $\phi_0 = \phi_0(E)$ , that is, the electric-field rotation of the skyrmion lattice discovered recently. [132]

Finally, we plot the dependence  $\Delta W(E)$  for for magnetoelectric  $\text{Cu}_2\text{OSeO}_3$  (see Fig. 4.7). We use  $J = 4.85 \times 10^{-23} \text{ Jm/A}^2$ ,  $D = -9.85 \times 10^{-15} \text{ J/A}^2$ ,  $M_s = 1.11 \times 10^5 \text{ A/m}$ ,  $A = 6.2 \times 10^{-6} \text{ Jm}^{-1} \text{ A}^{-2}$ , and  $\alpha/Dk_0 = 9.23 \times 10^{-9} \text{ m/V}$ . We also restore  $\sqrt{3}$  coming from notations introduced in paragraph under Eq.(4.1) (recall for  $\mathbf{E}||[111]$  it was convenient to set  $|\mathbf{E}| = \sqrt{3}E$ ), and we fix for simplicity the skyrmion lattice orientation as  $\phi_0 = 0$ . As indicated with a red bar on Fig. 4.7, the electric field ranges accessed in recent literature [132, 151, 154] is well within the validity of first order perturbation theory calculations. We come to conclusion that it is possible to stabilize (if  $\Delta W_{\text{total}} < 0$ ) or destabilize (if  $\Delta W_{\text{total}} > 0$ ) the skyrmion lattice by choosing the appropriate magnitudes and polarities

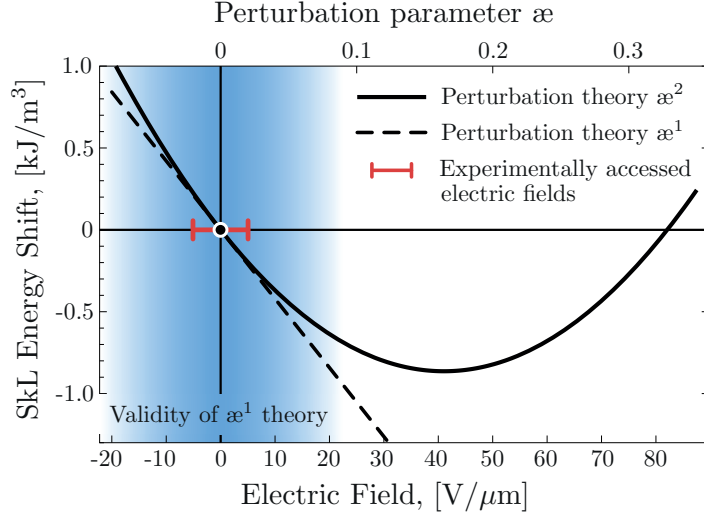


Figure 4.7: Shift in the skyrmion lattice (free) energy in electric fields. Solid line: first + second order (i.e. up to  $\mathfrak{a}^2$ ) perturbation theory, dashed line: contribution of the first order ( $\mathfrak{a}^1$ ) perturbation theory only. We sketch validity of the  $\mathfrak{a}^1$  perturbation theory as around  $|\mathfrak{a}| \sim 0.1$ , which for  $\text{Cu}_2\text{OSeO}_3$  converts to approximately  $\pm 20 \text{ V}/\mu\text{m}$ . Experimentally accessed range of electric fields is of order  $\pm 5 \text{ V}/\mu\text{m}$ , which is sufficiently captured with the  $\mathfrak{a}^1$  theory.

of electric fields. This coincides with the previous idea of Mochizuki [145] of creating *single* magnetic skyrmions with external  $E$ -fields in multiferroic  $\text{Cu}_2\text{OSeO}_3$ . The present study is therefore a bridge towards this idea in the bulk samples, where the skyrmions usually exist in the form of long-range-ordered or partially-disordered skyrmion arrays.

An interesting output of the calculation is the existence of the stationary points if a helix is directed in a proper way (Fig. 4.6). This feature comes both in the elastic and nonelastic distortions of the skyrmion lattice. However, as the SkL is constructed on the three helices, the mean-field energy of the SkL is still shifted.

We sketch the limitations of the calculation. First, this study describes the first two perturbative corrections to the mean-field energy of the skyrmion lattice in the multi-spiral approximation, without comparing the free energies of different possible phases (helical, conical) in the system. Second, the energy functional is taken in the quasiclassical continuous-field limit, which limits the use of the model only to the sufficiently low DMI parameter ( $D/J \ll 1$ ) and excludes the quantum regime (low  $T$ ). Third, the effect of electric field on critical fluctuations on top of the mean-field SkL solution is not considered as it comes as a higher-order contribution in the critical correlation length.

#### 4.2.5 EFFECTIVE $M^4$ MODEL

To capture universal physics of phase diagrams, we consider the effective  $M^4$  model, that is the asymptote of (4.13) where the main contribution is given by  $M^4$ .

$$F_0[\mathbf{M}(\mathbf{r})]/V = \langle \alpha_T \mathbf{M}^2 + J(\nabla \mathbf{M})^2 + D \mathbf{M} \cdot (\nabla \times \mathbf{M}) - \mathbf{H} \cdot \mathbf{M} + U_0 \mathbf{M}^4 \rangle, \quad (4.46)$$

or

$$W_0[\mathbf{S}(\mathbf{r})] = \langle \alpha_T \mathbf{S}^2 + J(\nabla \mathbf{S})^2 + D \mathbf{S} \cdot (\nabla \times \mathbf{S}) - \mathbf{h} \cdot \mathbf{S} + U \mathbf{S}^4 \rangle. \quad (4.47)$$

The importance of this model was already discussed in the previous chapter.

We consider now the other field geometry, namely,  $\mathbf{E}||\mathbf{H}||[111]$ , as it will be important for discussing experiments in the next section. The rotated spin frame, – in which the skyrmion tubes are aligned with the new  $z'$  axis, – is given by a unitary linear transform

$$\mathbf{S}_{\mathbf{r}} = \mathcal{R}_{[111]} \mathbf{S}_{\mathbf{r}'}, \quad \mathcal{R}_{[111]} = \begin{pmatrix} -\frac{1}{\sqrt{2}} & -\frac{1}{\sqrt{6}} & \frac{1}{\sqrt{3}} \\ \frac{1}{\sqrt{2}} & -\frac{1}{\sqrt{6}} & \frac{1}{\sqrt{3}} \\ 0 & \sqrt{\frac{2}{3}} & \frac{1}{\sqrt{3}} \end{pmatrix}, \quad (4.48)$$

for which the ME coupling reads

$$\mathcal{H}_{\mathfrak{x}}/Dk_0 = 2\mathfrak{x} \begin{pmatrix} -1 & 0 & 0 \\ 0 & -1 & 0 \\ 0 & 0 & 2 \end{pmatrix}, \quad \mathfrak{x} = \frac{\alpha E}{4Dk_0}, \quad \mathbf{E} = (E, E, E), \quad E = \frac{|\mathbf{E}|}{\sqrt{3}}. \quad (4.49)$$

In this section, we will be primarily interested in the first order perturbation theory, thus only the higher-order terms contribute. We thus use

$$|\mathbf{S}_{\mathbf{k}}^{(\mathfrak{x}^1)}\rangle = |\mathbf{S}_{\mathbf{k}}^{(0)}\rangle + \sum_{n \neq 0} |\mathbf{S}_{\mathbf{k}}^{(n)}\rangle \frac{\langle \mathbf{S}_{\mathbf{k}}^{(n)} | \hat{\mathcal{H}}_{\mathfrak{x}} | \mathbf{S}_{\mathbf{k}}^{(0)} \rangle}{\varepsilon_{\mathbf{k}}^{(0)} - \varepsilon_{\mathbf{k}}^{(n)}}. \quad (4.50)$$

where  $\varepsilon_{\mathbf{k}}^{(n)}$  are given by Eq.(4.22) and  $|\mathbf{S}_{\mathbf{k}}^{(n)}\rangle$ ,  $n = 0, 1, 2$ , are eigenstates of  $\mathcal{H}_0$  as given by Eqs.(3.46) -(3.47). The direct calculation for perturbation (4.49) is

$$|\mathbf{S}_{\mathbf{k}}^{(\mathfrak{x}^1)}\rangle = |\mathbf{S}_{\mathbf{k}}^{(0)}\rangle - \mathfrak{x} |\mathbf{F}_{\mathbf{k}}\rangle, \quad (4.51)$$

with the elastic vector of form

$$|\mathbf{F}_{\mathbf{k}}\rangle = \frac{3}{2\sqrt{2}} \begin{pmatrix} -i \sin \phi \\ +i \cos \phi \\ -1 \end{pmatrix} = \frac{3}{2} |\mathbf{S}_{\mathbf{k}}^{(0)}\rangle - 2 |\mathbf{S}_0^{(0)}\rangle, \quad (4.52)$$

where  $|\mathbf{S}_{\mathbf{k}}^{(0)}\rangle$  is given by (3.46) and  $|\mathbf{S}_0^{(0)}\rangle \equiv (0, 0, 1)^T$  is a field-polarized  $k=0$  component. Thus we have simply

$$|\mathbf{S}_{\mathbf{k}}^{(\text{æ}^1)}\rangle = \left(1 + \frac{3}{2}\text{æ}\right) |\mathbf{S}_{\mathbf{k}}^{(0)}\rangle - 2\text{æ} |\mathbf{S}_0^{(0)}\rangle, \quad (4.53)$$

Thus, similar to calculation (3.65), in the skyrmion phase we have

$$\begin{aligned} \langle \mathbf{S}^4(\mathbf{r}) \rangle &= m^4 + 2m^2\mu^2 \sum_{\mathbf{k}_1}^{\{\mathbf{q}_1 \dots \mathbf{q}_6\}} \sum_{\mathbf{k}_2}^{\{\mathbf{q}_1 \dots \mathbf{q}_6\}} \left( S_{\mathbf{k}_1}^x S_{\mathbf{k}_2}^x + S_{\mathbf{k}_1}^y S_{\mathbf{k}_2}^y + 3S_{\mathbf{k}_1}^z S_{\mathbf{k}_2}^z \right) \delta(\mathbf{k}_1 + \mathbf{k}_2) \\ &+ 4m\mu^3 \sum_{\mathbf{k}_1}^{\{\mathbf{q}_1 \dots \mathbf{q}_6\}} \sum_{\mathbf{k}_2}^{\{\mathbf{q}_1 \dots \mathbf{q}_6\}} \sum_{\mathbf{k}_3}^{\{\mathbf{q}_1 \dots \mathbf{q}_6\}} \left( S_{\mathbf{k}_1}^z S_{\mathbf{k}_2}^x S_{\mathbf{k}_3}^x + S_{\mathbf{k}_1}^z S_{\mathbf{k}_2}^y S_{\mathbf{k}_3}^y + S_{\mathbf{k}_1}^z S_{\mathbf{k}_2}^z S_{\mathbf{k}_3}^z \right) e^{i(\varphi_{\mathbf{k}_1} + \varphi_{\mathbf{k}_2} + \varphi_{\mathbf{k}_3})} \delta(\mathbf{k}_1 + \mathbf{k}_2 + \mathbf{k}_3) \\ &+ \mu^4 \sum_{\mathbf{k}_1}^{\{\mathbf{q}_1 \dots \mathbf{q}_6\}} \sum_{\mathbf{k}_2}^{\{\mathbf{q}_1 \dots \mathbf{q}_6\}} \sum_{\mathbf{k}_3}^{\{\mathbf{q}_1 \dots \mathbf{q}_6\}} \sum_{\mathbf{k}_4}^{\{\mathbf{q}_1 \dots \mathbf{q}_6\}} \left( S_{\mathbf{k}_1}^x S_{\mathbf{k}_2}^x S_{\mathbf{k}_3}^x S_{\mathbf{k}_4}^x + S_{\mathbf{k}_1}^y S_{\mathbf{k}_2}^y S_{\mathbf{k}_3}^y S_{\mathbf{k}_4}^y + S_{\mathbf{k}_1}^z S_{\mathbf{k}_2}^z S_{\mathbf{k}_3}^z S_{\mathbf{k}_4}^z \right. \\ &\quad \left. + 2S_{\mathbf{k}_1}^y S_{\mathbf{k}_2}^y S_{\mathbf{k}_3}^z S_{\mathbf{k}_4}^z + 2S_{\mathbf{k}_1}^x S_{\mathbf{k}_2}^x S_{\mathbf{k}_3}^z S_{\mathbf{k}_4}^z \right) \delta(\mathbf{k}_1 + \mathbf{k}_2 + \mathbf{k}_3 + \mathbf{k}_4). \end{aligned} \quad (4.54)$$

The direct substitution of (4.53) gives

$$W_{skL}^{(U)} = \langle U \mathbf{S}^4(\mathbf{r}) \rangle_{\text{æ}} = U \left( m^4 + 51\mu^4 + 24m^2\mu^2 - 18\sqrt{2}m\mu^3 \right) - 9U\mu^2 \left( 6\mu^2 + 4m^2 - 5\sqrt{2}\mu m \right) \text{æ}. \quad (4.55)$$

As a comparison, in the conical phase we only have

$$\begin{aligned} \langle \mathbf{S}^4(\mathbf{r}) \rangle &= m^4 + 2m^2\mu^2 \sum_{\mathbf{k}_1}^{\pm \mathbf{Q}} \sum_{\mathbf{k}_2}^{\pm \mathbf{Q}} \left( S_{\mathbf{k}_1}^x S_{\mathbf{k}_2}^x + S_{\mathbf{k}_1}^y S_{\mathbf{k}_2}^y + S_{\mathbf{k}_1}^z S_{\mathbf{k}_2}^z \right) \delta(\mathbf{k}_1 + \mathbf{k}_2) \\ &+ \mu^4 \sum_{\mathbf{k}_1}^{\pm \mathbf{Q}} \sum_{\mathbf{k}_2}^{\pm \mathbf{Q}} \sum_{\mathbf{k}_3}^{\pm \mathbf{Q}} \sum_{\mathbf{k}_4}^{\pm \mathbf{Q}} \left( S_{\mathbf{k}_1}^x S_{\mathbf{k}_2}^x S_{\mathbf{k}_3}^x S_{\mathbf{k}_4}^x + S_{\mathbf{k}_1}^y S_{\mathbf{k}_2}^y S_{\mathbf{k}_3}^y S_{\mathbf{k}_4}^y + S_{\mathbf{k}_1}^z S_{\mathbf{k}_2}^z S_{\mathbf{k}_3}^z S_{\mathbf{k}_4}^z \right. \\ &\quad \left. + 2S_{\mathbf{k}_1}^y S_{\mathbf{k}_2}^y S_{\mathbf{k}_3}^z S_{\mathbf{k}_4}^z + 2S_{\mathbf{k}_1}^x S_{\mathbf{k}_2}^x S_{\mathbf{k}_3}^z S_{\mathbf{k}_4}^z \right) \delta(\mathbf{k}_1 + \mathbf{k}_2 + \mathbf{k}_3 + \mathbf{k}_4). \end{aligned} \quad (4.56)$$

as the cubic term is always zero, as also  $\langle \mathbf{m} \cdot \mathbf{s} \rangle = 0$  which results to only  $s_z^2$  instead of  $3s_z^2$  in the skyrmion phase.

To compare with the conical phase, we repeat the perturbation approach (4.36) for the conical phase (3.25). The calculation for the [111] E-field shows that the conical vectors (5.7) remain unperturbed. Thus for this field configuration, we have

$$W_{\text{con}}^{(U)} = \langle U \mathbf{S}^4(\mathbf{r}) \rangle_{\mathbf{\hat{e}}} = U(m^2 + 2\mu^2)^2. \quad (4.57)$$

Thus, in the main approximation the conical phase for  $\mathbf{E} \parallel \mathbf{H}$  [111] is not subjected to electric fields, thus allowing to observe a pure effect of electric field on the skyrmion lattice. This observation is used for planning studies described in the next section. Note however that the conical vectors will be indeed perturbed for  $\mathbf{H}$  [1 $\bar{1}$ 0], however not crucially.<sup>2</sup>

The present model describes the shift of the mean-field energy of the SkL, which is either positive or negative depending on the direction of the electric field. In a particular situation when the first order terms may vanish, the energy shift is of the same sign for both positive and negative voltage polarities.

The main physical consequence of the phenomenon under study is the field-induced *stabilization of the skyrmion phase in the bulk*, which has been so far indirectly observed in  $\text{Cu}_2\text{OSeO}_3$ . [154] This mechanism if further developed would allow one either to write or erase the skyrmion array over the full sample if it is properly placed in the  $H$ ,  $T$  phase diagram, and thus opens further routes for skyrmion-operating insulating logical elements and data storage devices.

### 4.3 WRITING AND ERASING SKYRMIONS

To realise skyrmion-based applications, research into creation, control and stabilisation of skyrmions is in an active phase [46, 80, 91, 93, 106, 132, 143, 151, 152]. In this context, it could seem problematic that in bulk materials the skyrmion phase is only stable in a finite temperature ( $T$ ) and applied magnetic field ( $\mu_0 H$ ) interval [38, 40, 45, 132, 156]. In  $\text{Cu}_2\text{OSeO}_3$  for example, the skyrmion pocket spreads downwards in  $T$  by just 3.5% of  $T_C$ , occupying no more than 1% of the total ordered phase space [143, 157]. This limited phase space is observed also in other known bulk skyrmion hosts [38, 40, 156, 158]. However, the finite extent of the skyrmion phase pocket is in fact an interesting advantage. It means that relatively small perturbations can dramatically influence the skyrmion phase stability. The ability to enhance or suppress the skyrmion phase space in a sample can provide a flexible platform for the respective creation or destruction of skyrmion states. Here we present a simple and reliable mechanism for the stabilisation

---

<sup>2</sup>The perturbed conical vector for this field configuration is given by  $S_{\mathbf{k}}^x = \frac{i}{\sqrt{2}} - \frac{i\mathbf{\hat{e}}}{2\sqrt{2}} - \mathbf{\hat{e}} - \frac{9i\mathbf{\hat{e}}^2}{8\sqrt{2}}$ ,  $S_{\mathbf{k}}^y = \frac{1}{\sqrt{2}} = -i\mathbf{\hat{e}} + \frac{\mathbf{\hat{e}}}{2\sqrt{2}} - \frac{9\mathbf{\hat{e}}^2}{8\sqrt{2}}$  and  $S_{\mathbf{k}}^z = 0$ . For such a perturbation, both  $U\langle S^4 \rangle$  and  $A\langle S_x^4 + S_y^4 + S_z^4 \rangle$  are not perturbed even in  $\mathbf{\hat{e}}^2$ . The magnetoelectric response is only  $\langle \mathcal{H} \rangle_{\mathbf{\hat{e}}} / 2Dk_0 = (\mu^2 - 2m^2)\mathbf{\hat{e}} - 9\mu^2\mathbf{\hat{e}}^2$ , which is of the smaller than in the SkL phase in the phase space under interest.

and destabilisation of the skyrmion phase exploiting electric ( $E$ ) fields applied to an insulating material.

To date, several approaches for skyrmion manipulation were demonstrated using either moderate electric currents, electric fields, or thermal gradients [46, 80, 91, 93, 94, 132, 133, 145, 151, 152, 154, 155]. Progress towards tuning the bulk skyrmion phase stability was also demonstrated using both applied uniaxial [159, 160] and hydrostatic pressure [157]. For possible applications of the insulating skyrmion host materials, the use of electric field to manipulate the skyrmions is a very promising option that remains relatively little explored.

Here we report a combined experimental and theoretical study of SkL phase stability under moderate  $E$ -fields ( $\text{V}/\mu\text{m}$ ) in the model insulating skyrmion host  $\text{Cu}_2\text{OSeO}_3$ . We use small-angle neutron scattering (SANS) to study microscopically how the  $E$ -field controls the extent of the equilibrium skyrmion phase in  $\text{Cu}_2\text{OSeO}_3$ . We find that both the magnetic field and temperature extent of the skyrmion phase respectively expands and shrinks dependent on the  $E$ -field polarity. Theoretically, the  $E$ -field effect is addressed using first order perturbation theory for the free energy of the underlying phases. This results in a small  $E$ -field driven shift of the SkL free energy that is nevertheless comparable with the energy difference between the skyrmion and conical phases. Furthermore, we develop a new approach for treating the fluctuative free energy by adding quasiparticle modes near  $T_C$  which prove to be pivotal in evaluating the free energy differences between the phases. The developed model describe well our experimental data and allows calculating phase diagrams for different magnetic and electric field orientations.

From recent bulk susceptibility  $\chi(E)$  measurements of  $\text{Cu}_2\text{OSeO}_3$  [154], it was suggested that skyrmions may be "created" or "annihilated" by applying a dc  $E$ -field in suitable parts of the  $(T, \mu_0 H)$  phase diagram. In that study [154] the skyrmion phase was identified as a small drop in  $\chi(E)$ , which served as an indirect indication for the existence of the skyrmion phase. Here we use the tool of small-angle neutron scattering (SANS) to directly observe the microscopic skyrmionic magnetism in  $\text{Cu}_2\text{OSeO}_3$ , and its response to an applied dc  $E$ -field. By SANS the skyrmion lattice phase is typically observed as a sixfold symmetric diffraction pattern, consistent with the so-called multispiral (triple- $\mathbf{q}$ ) magnetic structure described by three propagation ( $\mathbf{q}$ -)vectors rotated by  $120^\circ$  with respect to each other (note that both  $\pm\mathbf{q}$  each give a Bragg spot) [38, 44, 132]. To maximise the  $E$ -field effect, in our SANS experiments we oriented the sample so that  $E \parallel [\mu_0 H] \parallel [111]$  and, in comparison with the size of the skyrmion phase for  $E=0$ , succeeded in observing an expansion (contraction) of the skyrmion pockets for an  $E$ -field applied parallel (antiparallel) to the  $[111]$  axis. The changes in the phase diagram are summarised in Figure 4.8.

For the SANS experiment, we used a single crystal grown using chemical vapour transport [161]. The crystal was of mass 6 mg and volume  $3.0 \times 2.0 \times 0.50 \text{ mm}^3$

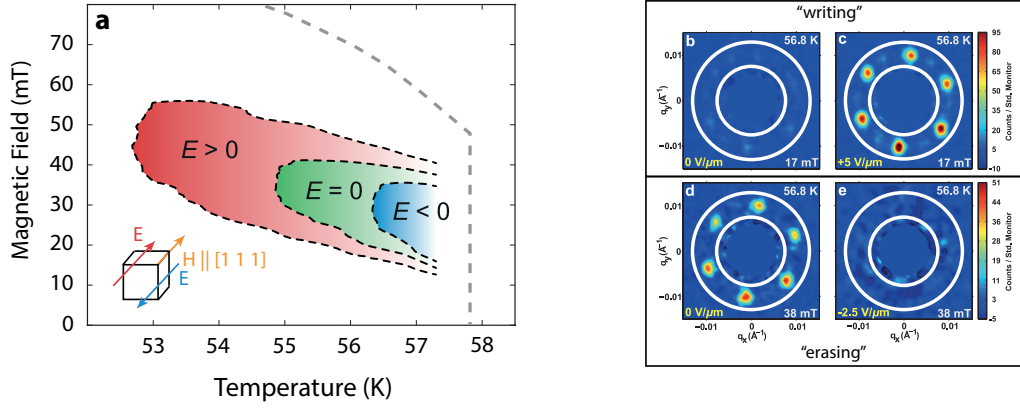


Figure 4.8: **Skyrmion phase tuning by electric fields.** (a) Phase diagram (skyrmion pockets) measured by small-angle neutron scattering (SANS) for  $E \parallel \mu_0 H \parallel [111]$ . The skyrmion pocket spreads almost doubles in the positive field  $+5.0 \text{ V}/\mu\text{m}$ , while shrinking to half under a negative field of  $-2.5 \text{ V}/\mu\text{m}$ . (b)-(g): Typical SANS diffraction patterns obtained from the SkL phase under various electric fields. Here the  $[111]$  direction is into the page. The black rings define an annular integration window used to evaluate the total scattered intensity due to the skyrmion phase on the detector. The hallmark six-fold symmetric scattering of the skyrmion lattice is clearly observed in (b),(d). At  $56.8 \text{ K}$ , applying  $E < 0$  suppresses both the SkL formation (compare (d) and (f)). In panels (c),(e),(f) the six-fold symmetric scattering signal is not clear, but it nevertheless arises from (orientationally-disordered) skyrmion arrays and displays the same  $|q|$  as the Bragg spots in six-fold patterns shown in (b) and (d). In panel (g) no SANS signal is observed above the background level.

with the thinnest axis  $\parallel [111]$ , and  $[\bar{1}\bar{1}2]$  vertical. The sample was mounted onto a bespoke sample stick designed for applying dc  $E$ -fields [162]. In our experiments we achieved  $E$ -fields ranging from  $+5.0 \text{ kV}/\text{mm}$  to  $-2.5 \text{ kV}/\text{mm}$ . Evidence of electrical breakdown was detected for  $E$ -fields outside this range.

The sample was loaded into a horizontal field cryomagnet at the SANS-II beam-line, SINQ, PSI. The magnetic field ( $\mu_0 H$ ) was applied parallel to both the  $[111]$  direction of the sample and the incident neutron beam to give the experimental geometry  $E \parallel \mu_0 H \parallel [111]$ . In this geometry, the SANS signal is only detected from the skyrmion phase, which typically presents as a hexagonal scattering pattern with propagation vectors  $\mathbf{q} \perp \mu_0 H$ . In this geometry, we avoid detecting any SANS signal due to either of the neighbouring helical ( $\mathbf{q} \parallel \langle 001 \rangle$ ) or conical phases ( $\mathbf{q} \parallel \mu_0 H$ ), since the propagation vectors of these phases lie well out of the SANS detector plane.

We used incident neutrons with a wavelength of  $10.8 \text{ \AA}$  ( $\Delta\lambda/\lambda = 10\%$ ). The scattered neutrons were detected using a position-sensitive multidetector. The SANS measurements were done by rotating (‘rocking’) the sample and cryomagnet ensemble over angles that brought the various SkL diffraction spots onto the Bragg condition at the detector. Data taken at  $70 \text{ K}$  in the paramagnetic state were used for background subtraction. Before starting each  $\mu_0 H$ -scan, the sample was initially zero field-cooled from  $70 \text{ K}$  to a target temperature, with the  $E$ -field applied when thermal equilibrium was achieved.



The  $E$ -field was maintained during the  $\mu_0 H$ -scan. At each  $T$  we define the  $\mu_0 H$  extent of the SkL phase as that over which SANS intensity is detected. We use this criterion to extract the parametric extent of the SkL phase for  $(\mu_0 H, T, E)$  as shown in Figures 4.8 and 4.9.

Figure 4.8 shows representative SANS data collected at various  $(T, \mu_0 H, E)$  conditions. The sixfold symmetric SANS patterns due to a skyrmion lattice most clearly seen in Figs. 4.8b,d. In these particular SANS patterns, weaker spots are also detected to lie between the six strongest spots. This indicates the co-existence at various  $(T, \mu_0 H, E)$  conditions of differently oriented skyrmion lattice domains around the  $\mu_0 H$ -axis, a phenomenon that has also been reported in other scattering studies of  $\text{Cu}_2\text{OSeO}_3$  [44, 163, 164]. For the patterns shown in Figs. 4.8c,e,f, each obtained near to an edge of the respective skyrmion phase as determined in the SANS experiment, the Bragg spots become ill-defined, and instead the intensity appears as azimuthally smeared patches, indicative of orientationally-disordered SkLs (hereafter termed ‘skyrmion arrays’). Since the origin of the SkL disordering is difficult to identify unambiguously, a systematic analysis of all SANS data is done by evaluating the the total scattered SANS intensity observed on the detector within the same annular integration window shown in each of Fig. 4.8b-g. From this approach we account for the scattering due to *all* the skyrmion arrays in the sample when determining the parametric extent of the skyrmion phase.

The main result of the SANS analysis is shown in Figure 4.8b. Importantly our results show how it is easier to destabilise the skyrmion phase than stabilise it; a positive  $E$ -field of  $+5.0 \text{ V}/\mu\text{m}$  is required to expand the skyrmion pocket so that it becomes almost twice larger, while a negative  $E$ -field of only  $E = -2.5 \text{ V}/\mu\text{m}$  is needed to shrink the pocket by approximately a factor of two. Since this controlled phase expansion and contraction can occur in general for an insulating magnetoelectric skyrmion phase at any temperature, our findings are very attractive for applications; for a device layer of thickness 100 nm the skyrmion phase in a sample can be almost entirely destabilised (erased) or restabilised (written) with less than 1 V, the voltage compatible with modern microelectronics.

Examining our SANS data more closely shows that at various points in the magnetic phase diagram, the moderate  $E$ -fields  $\text{V}/\mu\text{m}$  either fully destabilise or stabilise the skyrmion phase, when compared with data obtained at the same points but at  $E = 0$ . As shown in Fig. 4.9a, both of these effects are observed to occur over large  $T$  windows each roughly 1 K wide, corresponding to 2% bothway in  $\Delta T/T_C$  in  $\text{Cu}_2\text{OSeO}_3$ .

The total scattered SANS intensity is indicative of both the population and quality of the skyrmion arrays in the sample. As an example, consider the starting point when skyrmions are essentially absent from the system, such as on the conical/skyrmion phase border at the lower- $T$  boundary of the unperturbed skyrmion pocket ( $E=0$ ). Fig. 4.9b shows  $\mu_0 H$ -scan data obtained for this case at  $T = 54.8 \text{ K}$ . While at  $E=0$  the lack of SANS intensity indicates the skyrmion phase to be absent, the application of  $E = +5.0 \text{ V}/\mu\text{m}$  leads to an enhancement of the skyrmion stability such that significant SANS intensity

of the skyrmion phase is observed. In contrast, the destabilisation of skyrmion arrays requires an  $E$ -field of opposite sign. Fig. 4.9c shows that at  $T = 55.8$  K, a negative  $E = -2.5 \text{ V}/\mu\text{m}$  can completely destabilise the skyrmion arrays that were stable in the unperturbed state ( $E=0$ ).

We find that the  $T$ -window of 53-55.5 K is appropriate for enhancement of the skyrmion phase stability under  $E = +5.0 \text{ kV}/\text{mm}$ , while a  $T$ -window of 55-56.5 K is suitable for suppression of the skyrmion phase stability for  $E = -2.5 \text{ kV}/\text{mm}$ . Positioning a device at 55.5 K allows to demonstrate both a significant enhancement and suppression of the skyrmion phase by  $E$ -fields of opposite polarities.

The underlying mechanism for enhancing and suppressing the skyrmion phase stability by  $E$ -fields is mediated by the magnetoelectric (ME) coupling in insulating  $\text{Cu}_2\text{OSeO}_3$ . Microscopically, the ME coupling originates from the  $d$ - $p$  hybridisation mechanism (see Refs. [44, 146–148]). The emergent electric dipole moment  $\mathbf{P} = \lambda(S_y S_z, S_z S_x, S_x S_y)$  is linked to the underlying spin structure  $\mathbf{S}(\mathbf{r}) = (S_x, S_y, S_z)$  with the coupling parameter  $\lambda$  of relativistically small magnitude. Crucially, this effect results in a  $\mathbf{P} \cdot \mathbf{E}$  shift of energy in  $E$ -field because the skyrmion phase now has a nonvanishing electric-dipole moment. This perturbation renormalises the elementary helices upon which the skyrmion phase is built, and slightly distorts the skyrmion lattice [132].

In this study, we apply the ME perturbation to the free energy described by an effective Ginsburg-Landau functional with Dzyaloshinskii-Moriya interaction (DMI), and consider the critical fluctuations which in bulk samples favour the skyrmion phase with respect to the neighbouring conical phase. Due to the relativistically small size of  $\lambda$ , the dimensionless  $E$ -field is rather small so that,  $\alpha = \lambda E / D k_0 \ll 1$ , and we can build a perturbation theory in  $\alpha$  for the modified free energy neglecting all the terms of order  $\alpha^2$  and higher. Our finding is that the perturbations of fluctuative terms come in only at second order, while the mean-field energy already shifts in the first order due to the direct ME and nonlinear contributions. The corresponding shift in free energy of the skyrmion phase depends on the direction of  $E$ -field (see Fig. 4.10a), thus either enhancing the skyrmion phase stability ( $E > 0$ ) or destabilising ( $E < 0$ ) it. While at first sight it can be surprising that perturbatively small  $E$ -fields play a crucial role here, this is facilitated by the very close competition between the skyrmion and conical phases already in the mean-field.

To calculate the phase diagram in  $E$ -field, we use a new approach developed on the basis of effective models from Refs.[38, 132, 134]. Compared to these earlier studies the new approach is self-consistent in the way that it captures phase diagram, provides a deeper understanding of the role of quasiparticle modes near  $T_C$ , and covers the path-integral approach for calculating the fluctuative free energy [38] as a limiting case. We thus treat the first-order perturbation in  $E$ -fields on top of the mean-field solution, and add the fluctuative contributions that stabilise the skyrmion lattice in the bulk. The

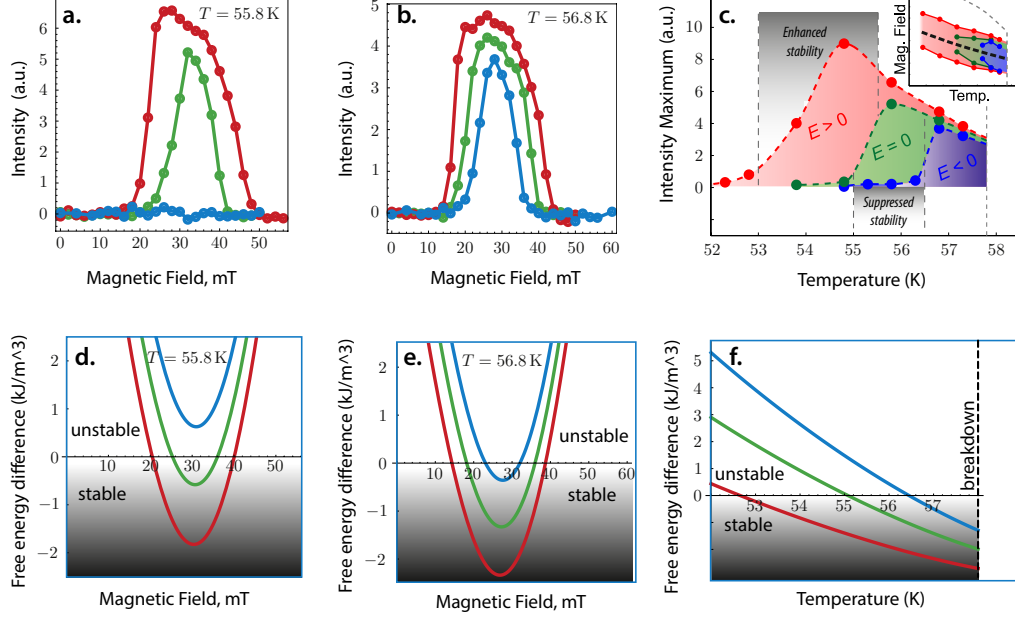


Figure 4.9: **Optimising skyrmion stability in electric fields.** (a)-(c): Experiments (a)-(b) SANS intensity versus magnetic field at (a) 55.8 K and (b) 56.8 K. Application of positive electric field  $5\text{V}/\mu\text{m}$  (red) enhances the stability and hence the neutron-scattering quality of the skyrmion lattice at (a) and (b), while application of a negative electric field  $2.5\text{V}/\mu\text{m}$  (blue) kills the skyrmion lattice at 55.8 K. (c) Summary for maximum SANS intensity versus temperature along the direction of the skyrmion pocket growth (dashed line on the inset). The zone favourable for enhancing the skyrmion phase stability ("writing" skyrmions) is 53 to 55.5 K, where the skyrmion array population is the highest for  $E > 0$  ( $+5.0\text{V}/\mu\text{m}$ ), while for  $E = 0$  the skyrmion phase is absent. For suppressing the skyrmion phase stability ("erasing" skyrmions), it is favourable to place the sample between 55 to 56.5 K, where the skyrmion phase is well populated under zero voltage, but becomes strongly suppressed under  $E < 0$  ( $-2.5\text{V}/\mu\text{m}$ ). (d-f): Theoretical calculation for free energy difference between skyrmion and conical phase neglecting the nonlinear ( $E^2$ ) effects. a) Free energy difference versus magnetic field at 55.8 K. b) Free energy difference versus magnetic field at 56.8 K. c) Free difference versus temperature along the direction of skyrmion pocket growth. Calculations are done neglecting second-order corrections i.e. for the same field-amplitude  $E = \pm 5\text{V}/\mu\text{m}$ , thus qualitative agreement is present.

main contribution to  $E$ -field effect here is given by the shift of the mean-field free energy difference between the two phases (conical and SkL), while the fluctuative shift under voltages can be considered quadratically small.

The effective mean-field theory is based on the coarse-grained magnetization approach  $M(\mathbf{r}) = M_s \mathbf{S}(\mathbf{r})$  as described in [38]; see also Chapter 3. One starts with the mean-field approach with free energy

$$F[\mathbf{M}] = \langle \Theta_T \mathbf{M}^2 + J(\nabla \mathbf{M})^2 + D \mathbf{M} \cdot (\nabla \times \mathbf{M}) + U \mathbf{M}^4 - \mathbf{H} \cdot \mathbf{M} \rangle \quad (4.58)$$

with spatial average  $\langle \dots \rangle = \int \frac{dV}{V} \dots$ , and  $\Theta_T \propto \alpha(T - T_C)$  near  $T_C$ ,  $J$  is the Heisenberg

stiffness and  $D$  is DMI,  $H$  is the magnetic field, and the higher-order term  $U$  grants the formation of the crystalline phase [38]. In the mean-field, the interplay between Heisenberg and DMI energies determines the helical vector as  $k_0 = D/2J$ . The long-range-ordered hexagonal skyrmion lattice is approximated as  $\mathbf{S}(\mathbf{r}) \simeq \mathbf{m} + \mu \sum_{\mathbf{q}_n} \mathbf{S}_{\mathbf{q}_n} e^{i\mathbf{q}_n \mathbf{r} + i\varphi_n} + \text{c.c.}$ , where the summation runs over the crystalline order vectors  $\mathbf{q}_1 + \mathbf{q}_2 + \mathbf{q}_3 = 0$ . In the mean-field, the skyrmion phase is slightly gapped with respect to the conical phase, however the two are closely competing. Further details of the mean-field theory described in Ref. [38].

**Perturbation theory in electric fields.** The magneto-electric coupling in  $\text{Cu}_2\text{OSeO}_3$  is relativistically small, so the perturbation parameter is  $\varkappa = \lambda E/4Dk_0 \ll 1$ . It is sufficient to use the first order perturbation theory on top of the non-perturbed free energy. We go to the rotated frame defined by the magnetic field direction along  $[1\ 1\ 1]$ , and re-write the free energy. The first order perturbation theory gives eigenvectors:

$$|\mathbf{S}_{\mathbf{k}}^{(\varkappa)}\rangle = |\mathbf{S}_{\mathbf{k}}^{(0)}\rangle + \sum_{n \neq 0} |\mathbf{S}_{\mathbf{k}}^{(n)}\rangle \frac{\langle \mathbf{S}_{\mathbf{k}}^{(n)} | \hat{\mathcal{H}}_{\varkappa} | \mathbf{S}_{\mathbf{k}}^{(0)} \rangle}{\varepsilon_{\mathbf{k}}^{(0)} - \varepsilon_{\mathbf{k}}^{(n)}} + \mathcal{O}(\varkappa^2), \quad (4.59)$$

which are now the basis for constructing the distorted skyrmion lattice. For other  $(\mathbf{H}, \mathbf{E})$ -field configurations, we re-do the calculations in the new rotated frames.

**Fluctuation-induced phase stabilisation.** We use a new approach, which captures as a limiting case the fluctuation free energy from [38], as described in Chapter 3. The essential physics is captured already in Gaussian (noninteracting) fluctuations with free energy density

$$F_{\text{fluct}} = \sum_i \sum_{|\mathbf{k}| < \Lambda} \omega_{\mathbf{k}}^{(i)} f_{\mathbf{k}}^{(i)} - T S_{\text{fluct}}, \quad (4.60)$$

where  $\Lambda = 2\pi/a$  is the natural cut-off,  $f_{\mathbf{k}}^{(i)}$  is the critical modes distribution, and the entropy of Gaussian fluctuations is

$$S_{\text{fluct}} = \sum_i \sum_{|\mathbf{k}| < \Lambda} \{(1 + f_{\mathbf{k}}^{(i)}) \ln(1 + f_{\mathbf{k}}^{(i)}) - f_{\mathbf{k}}^{(i)} \ln f_{\mathbf{k}}^{(i)}\} \quad (4.61)$$

in the case of bosons. Fluctuations around mean-field are described by the generalised susceptibility  $\chi_{ij}^{-1}(\mathbf{r}, \mathbf{r}') = \frac{1}{T} \frac{\delta^2 F}{\delta M_i(\mathbf{r}) \delta M_j(\mathbf{r})}$ , giving rise to several collective modes. On the local scale ( $k \gg J/D$ ), the chiral magnet is reminiscent of a ferromagnet, so the modes behave asymptotically  $\omega_{\mathbf{k}} \propto k^2$  for large  $k$ , thus asymptotically  $F_{\text{fluct}} \simeq \log \beta \omega_{\mathbf{k}} \propto \log k^2$ , which covers the model of Ref. [38]. The main contribution to (4.62) is given by the short

length-scale ("ferromagnetic") physics,

$$\Delta F_{\text{fluct}} \simeq \frac{10U}{\pi a J} \langle \mathbf{S}_{\text{SkL}}^2 - \mathbf{S}_{\text{con}}^2 \rangle T, \quad (4.62)$$

The electric field also slightly affects the fluctuative energy, because it modifies the correlation length near  $T_C$  and so renormalises  $J_{\text{eff}}$ , which is neglected here as a higher-order ( $\propto^2$ ) effect.

Our approach allows to understand the stability of the skyrmion lattice on the intuitive, pictorial level: the critical fluctuations (waves) are superposed on top of the variationally minimised free energies. There are three critical modes  $\omega_{\mathbf{k}}^{(0,1,2)}$  around the mean-field, with  $\omega_{\mathbf{k}}^{(0)}$  soft on the sphere  $|\mathbf{k}| = k_0$ , which means that it cost very little energy to add many such fluctuations if they are coherent with the helix  $\mathbf{k}_0$ . Thus  $\omega_{\mathbf{k}_0}^{(0)}$  is the so-called "dangerous" mode since it results in a Van-Hove-like singularity at  $T_C$  and eventually breaks down the ordered phases into the disordered (paramagnetic) phase [134]. Below  $T_C$  the breaking of symmetry can be observed by SANS with either a six-fold pattern (skyrmion phase) or two-fold pattern (helical or conical phase), both circumscribed by a sphere  $|\mathbf{k}| = k_0$  in reciprocal space. Our calculation shows that the skyrmion phase is favoured because adding fluctuations generates more entropy in the skyrmion phase. This analysis leads also to a qualitative criterion capturing magnetic-field-independent breakdown of the ordered phases at  $T_C$ . Asymptotically, the main contribution of the fluctuative free energy is given in the short-scale physics, where  $\text{Cu}_2\text{OSeO}_3$  is "almost" a ferromagnet, thus reproducing the result of the path-integral approach [38] as a limiting case. The model described here captures the qualitative physics of the system, as exemplified by the theoretical phase diagram shown in Fig. 4.10.

Experimentally, we have observed that the parametric extent (stability) of the skyrmion phase become enhanced under  $E > 0$ . This observation can be addressed theoretically by exploring the free energy density map across the phase space for different values of  $E$ -fields. We find that the free energy minimum deepens with an increasingly positive  $E$ -field. For example, if we sit at  $T = 54.8\text{K}$  at  $E=0$ , the free energy of the skyrmion phase has a gap with respect to the conical phase (see Figure 4.10a), which means that the skyrmion phase is not favoured. If we now apply the  $E$ -field, there is a finite range of  $\mu_0 H$  where the free energy difference is negative with respect to the conical phase and the skyrmion lattice can now exist.

For our numerical calculations we use  $T_C = 58\text{K}$ , which approximately sets the Heisenberg stiffness as  $J = 4.85 \times 10^{-23} \text{Jm/A}^2$ . From the SANS measurement we establish directly the modulation period of  $60\text{nm}$ , which estimatively differs by a few percents from the mean-field value  $2\pi/k_0$ , because the mean-field ordering vector  $\mathbf{k}_0 = D/2J$  is slightly renormalised by the fluctuations near  $T_C$ . This sets the "bare" DM interaction entering (4.58) as  $D = -9.85 \times 10^{-15} \text{J/A}^2$ . The lattice parameter is  $a = 8.91 \times 10^{-10} \text{m}$ , which gives the natural cutoff  $\Lambda = 2\pi/a \approx 70 k_0$ . The saturation magnetization in  $\text{Cu}_2\text{OSeO}_3$

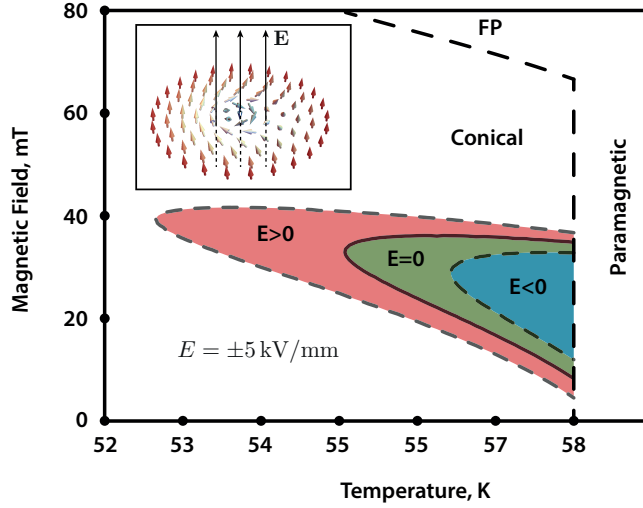


Figure 4.10: **Bulk stabilization of the skyrmion lattices under electric fields (theory):** Phase diagram (skyrmion pockets) for  $E$ -fields  $\pm 5 \text{ kV/mm}$ , for  $\mathbf{E} \parallel \mathbf{H} \parallel [111]$ .

is  $M_s = 1.11 \times 10^5 \text{ A/m}$  and scales with temperature as  $M_s(T) = M_s(1 - (T/T_C)^{\alpha_1})^{\alpha_2}$ , with  $\alpha_1 = 1.95$  and  $\alpha_2 = 0.393$  [165]. We choose the nonlinear coupling responsible for SkL formation  $K = 6.2 \times 10^{-6} \text{ Jm}^{-1} \text{ A}^{-2}$  and Landau parameter  $\alpha_T = \theta_T / Jk_0^2(T - T_C) = 3.5 \text{ K}^{-1}$ . For the qualitative phase diagram shown in Fig. 4.10, we use a symmetric-response model ( $\mathfrak{a}^1$ ), for which the best fit to SANS data is for  $\mathfrak{a} = 0.02$ , which corresponds here to  $E = \pm 5 \times 10^6 \text{ V/m}$  coupled with  $\lambda/Dk_0 = 1.6 \times 10^{-8} \text{ m/V}$  to the underlying spin structure through ME mechanism.

In some respects, the observed  $E$ -field effect on the skyrmion phase stability resembles that achieved due to either applied uniaxial [159, 160] or hydrostatic pressure [157]. However, integrating the pressure effect on skyrmion stability into a technological setting is very challenging. In contrast, the  $E$ -field effect is a versatile and reliable external parameter; providing an efficient control of both the skyrmion position [132, 149, 151] and the stability of the phase as a whole.

Our present study lays both theoretical and experimental foundations for fully exploring alternative  $\mu_0 H$ - and  $E$ -field configurations, not only in reciprocal-space measurements like SANS, but e.g. real-space imaging techniques such as cryo-Lorentz transmission electron microscopy (LTEM). The next steps shall be extending experimental and theoretical studies to out-of-equilibrium and metastable configurations and confined geometries, which can serve as platforms for skyrmion creation and annihilation in devices.

In conclusion, we have demonstrated experimentally and theoretically the mechanism by which a moderate electric field can enhance and suppress the stability of the skyrmion phase in the magnetoelectric chiral magnet  $\text{Cu}_2\text{OSeO}_3$ . In addition, we provide the parameters by which the theoretical approach achieves semi-qualitative agreement,

which can be extended towards describing the  $E$ -field effect on stable and metastable skyrmion states in devices, which are of paramount technological importance.

#### 4.4 CONCLUSIONS

In this chapter, I presented calculations which show stabilization of magnetic skyrmions under applied electric fields in a skyrmion-hosting magnetoelectric insulators. The first model calculation in Section 4.1, shows that even within the minimal model with absent anisotropies, under conditions when the skyrmions are, thermodynamically speaking, metastable, it is possible to lower their energy with respect to the ferromagnetic background upon applying external electric fields codirected with the magnetic field. This ideologically leads to the second model in use, for the calculation of the skyrmion lattices under electric fields in the bulk compounds. The essential formalism for this calculation was adopted from Ref.[132], and enhanced firstly towards calculating **all** the terms within the first order-perturbation theory; secondly, the second-order perturbation theory had been implemented, which is computationally more demanding [see Eq.(4.36)] as one needs to calculate analytically a plethora of momentum-conserved summations; thirdly, the range of validity of the present theory was sketched; fourthly, the calculations were repeated for the effective  $\mathbf{M}^4$  theory, which finally lead to the calculation of effective magnetic-phase diagram and helped to coin the understanding of the neutron scattering experiments for writing and erasing the skyrmion phase in bulk as shown in the last section.





# 5

## Magnetic Skyrmions under Pressure

Mechanical-strain and pressure-induced control of topological magnetic phases is a valuable and fruitful approach in skyrmionics [157, 159, 160, 166–168]. Among its advantages are the relatively cheap facility for establishing experiments, changing directions and intensity of the applied pressure force. Under mechanical strain, a material is pushed in volume so the distances between the constituting atoms are modified. This results to further interlapping between the local wave functions (in a rather nonlinear way), so the macroscopical properties, such as exchange stiffness, DMI, anisotropy is modified. Our experimental observations indicate that the  $J$  and  $D$  remain almost unchanged as the critical temperature and helix modulation wavelength have not noticeably modified even under pressure of several GPa (tens thousand of atmospheric pressure), however the  $H$ -field range of stability is shifted thus indicating on a very nonlinear change in anisotropy under such pressure, which we on the basis of this estimate to be in order of 20%. As a result, the stability of the skyrmion phase is tuned very dramatically - in more than 20 times comparing the initial phase space. Our findings thus provide a deeper understanding on mechanisms of stability of the skyrmion phase in bulk, as also sketch the possible route for pressure-controlled stabilization of topological magnetic phases in other systems, e.g. under uniaxial strains. Additionally, it provides further ideas for experiments towards increasing "chemical pressure", i.e. doping the sample with other atoms, which may lead to the discovery of bulk skyrmion hosts with better ranges of stability of the skyrmionic phases.

In the first section of this chapter I show theoretically stabilization of a skyrmion under uniaxial mechanical strain on the basis of the magnetoelastic effects on the spin-

density-wave phases in chiral magnets [169], which is important for relatively low strains (MPas) and in thin films; while in the second section I mainly follow the paper which I coauthor [157] on the study of effects of uniform pressure on bulk chiral magnet  $\text{Cu}_2\text{OSeO}_3$  and dramatic enhancement of the skyrmion phase therein.

## 5.1 STABILIZATION OF A SINGLE SKYRMION UNDER UNIAXIAL MECHANICAL STRAIN

Here we consider a generic mechanical-strain-induced change to magnetic anisotropy in the lowest order, valid for relatively weak mechanical strains of arbitrary directions, in particular, in thin films. The magnetoelastic perturbation by a generalized strain tensor<sup>1</sup>  $\varepsilon_{\alpha\beta}$  ( $\alpha, \beta = x, y, z$ ), to the lowest order can be represented by a quadratic form [169]

$$\begin{aligned} \delta W = & \frac{1}{2} L_0 \sum_{\alpha} \varepsilon_{\alpha\alpha} \mathbf{S} \cdot \mathbf{S} + L_1 (\varepsilon_{xx} |S_y|^2 + \varepsilon_{yy} |S_z|^2 + \varepsilon_{zz} |S_x|^2) + L_2 (\varepsilon_{xx} |S_z|^2 + \varepsilon_{yy} |S_x|^2 + \varepsilon_{zz} |S_y|^2) \\ & - \frac{1}{2} L_3 \sum_{\alpha \neq \beta} (S_{\alpha} S_{\beta}^* + S_{\alpha}^* S_{\beta}) \varepsilon_{\alpha\beta}, \end{aligned} \quad (5.1)$$

with all terms constructed invariant with respect to time-reversal symmetry and the operations of the space group  $P2_13$  of a chiral magnet (e.g. MnSi or  $\text{Cu}_2\text{OSeO}_3$ ). The coefficients  $L_{1,2,3}$ , responsible for lowest-order anisotropic effects under mechanical strain, are induced by spin-orbit coupling (including magnetic dipole-dipole interactions), while  $L_0 \propto J$  represents effective isotropic contribution. For simplicity, we further consider  $L_1 = L_2 \equiv L$ , and take into account Poisson's coefficient  $\nu \sim 1/3$  for most of materials<sup>2</sup> (e.g. for skyrmion-hosting MnSi,  $\nu = 0.28$  [172]). We consider for simplicity mechanical strain along  $[0\ 0\ 1]$  (and magnetic field  $[0\ 0\ 1]$ ). Upon application of the pressure tensor  $\sigma_{\alpha\beta}$  (with  $\sigma_{xx} = 0$ ,  $\sigma_{yy} = 0$ ,  $\sigma_{zz} = \sigma$ ) to material with elasticity modulus  $E$ , the strain tensor is defined by diagonal elements,

$$\varepsilon_{xx} = (\sigma_{xx} - \nu\sigma_{yy} - \nu\sigma_{zz})/E, \quad (5.2)$$

$$\varepsilon_{yy} = (\sigma_{yy} - \nu\sigma_{xx} - \nu\sigma_{zz})/E, \quad (5.3)$$

$$\varepsilon_{zz} = (\sigma_{zz} - \nu\sigma_{xx} - \nu\sigma_{yy})/E, \quad (5.4)$$

and thus we find  $\varepsilon_{xx} = \nu\sigma/E$ ,  $\varepsilon_{yy} = \nu\sigma/E$ ,  $\varepsilon_{zz} = (1 - \nu)\sigma/E$ . The direct substitution to (5.1) gives renormalization to uniaxial anisotropic contribution as

<sup>1</sup>On conventional theory of elasticity, see e.g. Ref.[170].

<sup>2</sup>Poisson's elastic coefficient  $\nu$  shows a dimensionless ratio between the transverse and axial strains. Theoretically, it cannot overflow values from range  $(-1; 1/2)$  [170]. Most of the real materials however fall into group  $1/5 \leq \nu < 1/2$ , with a very few exceptions; thus  $\nu \sim 1/3$  as a general rule. The underlying physical reasons for this has been only recently explained [171].

$$\delta W_{[001]} = -\mathfrak{L}\sigma \sum_{\mathbf{k}} \mathbf{S}_{\mathbf{k}}^T \hat{\Omega}_0 \mathbf{S}_{\mathbf{k}}, \quad \mathfrak{L} \approx \frac{4L}{3E}, \quad \hat{\Omega}_0 = \begin{pmatrix} 0 & 0 & 0 \\ 0 & 0 & 0 \\ 0 & 0 & 1 \end{pmatrix}, \quad (5.5)$$

and thus the surrounding conical phase becomes perturbed in the spin representation

$$\hat{\mathcal{H}}_0 = \begin{pmatrix} Jk^2 & -iDk & 0 \\ iDk & Jk^2 & 0 \\ 0 & 0 & Jk^2 - \mathfrak{L}\sigma \end{pmatrix}. \quad (5.6)$$

normalized eigenstates of this Hamiltonian operator are given similar to those in Eq.(3.16)

$$\mathbf{S}_k^{(0)} = \frac{1}{\sqrt{2}}(i, 1, 0)^T, \quad \mathbf{S}_k^{(1)} = (0, 0, 1)^T, \quad \mathbf{S}_k^{(2)} = \frac{1}{\sqrt{2}}(-i, 1, 0)^T, \quad (5.7)$$

corresponding to essentially the eigenvalues

$$\mathcal{E}_k^{(0)} = Jk^2 - Dk, \quad \mathcal{E}_k^{(1)} = Jk^2 - \mathfrak{L}\sigma, \quad \mathcal{E}_k^{(2)} = Jk^2 + Dk, \quad (5.8)$$

Thus for relatively small strain  $\|\varepsilon_{\alpha\beta}\| \ll 1$ ,  $\mathbf{S}_{\mathbf{k}}^{(0)}$  remains a groundstate, but under the stronger strains the ground state is  $\mathbf{S}_{\mathbf{k}}^{(1)}$ , so in general the conical helix is renormalized by  $\sigma_{\alpha\beta}$ , see also [160]. In this section we consider the former case, i.e. when  $0 < \mathfrak{L}\sigma < Dk$ , thus the conical phase is not perturbed, and the mean-field correction to the first order is simply  $\delta W_{\text{con}} = -\mathfrak{L}\sigma m^2$ .

We consider in this section a slab of a skyrmion-hosting material (a thick "thin film") such that the skyrmions are thermodynamically stable in some finite skyrmion pocket (see Figure 5.1), but the conical phase is still present at low temperatures. It is known that because of the surface-induced changes in anisotropies, DMI or stray field, the skyrmion phase can be stabilized in a much broader skyrmion pocket, in a form of a disordered skyrmion lattice or a skyrmion liquid. We choose the field-temperature conditions near the skyrmion-conical boundary (see figure 5.1) where a skyrmion is thermodynamically metastable, by a fixed free energy difference  $\Delta W_0$ , and imagine that we know the equipotential contour characterized by the same barrier energy  $\Delta W_0$  (see Figure 5.1). The probability of breaking a conical stripe and nucleating a skyrmion is, very roughly,

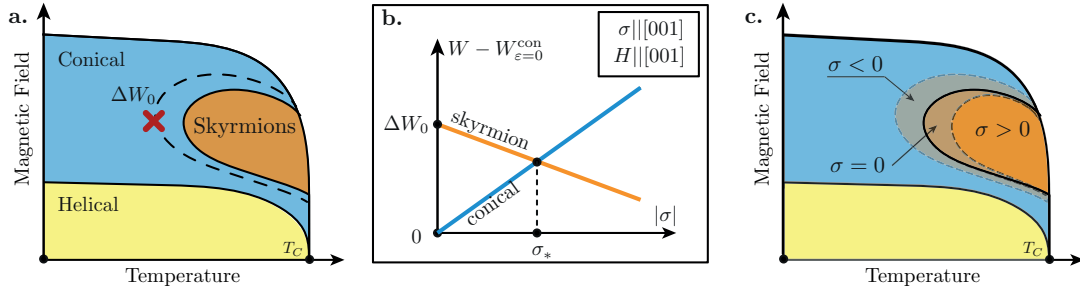


Figure 5.1: Stabilization and destabilization of (noninteracting) skyrmions with anisotropic mechanical stress ( $\sigma$ ). a) Qualitative phase diagram. Skyrmion positioning (red cross) near the skyrmion-conical boundary, where it is metastable. We assume that we know the equipotential contour (dashed line) characterized by a (2-meron) nucleation barrier  $\Delta W_0 > 0$ . b) By application a uniaxial stretching mechanical stress ( $\sigma < 0$ ) a randomly nucleated skyrmion (at  $\Delta W_0$  contour) becomes thermodynamically stable. c) Sketch of expected phase diagram under compressive ( $\sigma > 0$ ) and stretching ( $\sigma < 0$ ) uniaxial stress [001]; note that stretching  $\sigma < 0$  along [001] is physically equivalent to compressive  $\sigma > 0$  in direction [110] (see main text).

$$p \sim e^{-2\Delta W_0/T}, \quad (5.9)$$

(here 2 comes because nucleating a single skyrmion within a conical stripe requires putting 4 merons (half-skyrmions)). Thus, on an intuitive level we understand that at the red cross point on figure 5.1 there is always a finite probability that a skyrmion will appear, however, as it is in the metastable state, it will fast decay within lifetime of order  $1/\Delta W$ . Can we however ensure that it lives long enough, and eventually becomes thermodynamically stable, by applying the mechanical strain? Let's see.

The skyrmion energy in the helical phase, to a rather rough approximation, can be consider as axisymmetric, thus the model discussed in Chapter 2 can be applied for an order-of-magnitude estimate. Thus we write,

$$\Delta W = W_{\text{Sk}} - W_{\text{hel}}. \quad (5.10)$$

while a single-skyrmion energetics under the uniaxial strain (5.5) is

$$\langle W_{\text{Sk}} \rangle = 2\pi M^2 \int dr r \left\{ J \left[ \left( \frac{d\theta}{dr} \right)^2 + \frac{\sin^2 \theta}{r^2} \right] + D \left( \frac{d\theta}{dr} + \frac{\sin 2\theta}{2r} \right) + (K_U + \mathcal{L}\sigma) \sin^2 \theta - \frac{H}{M} \cos \theta \right\}, \quad (5.11)$$

where  $K_U$  represents the strength of this (second-order) uniaxial anisotropy<sup>3</sup>. Note that

<sup>3</sup>In "rather thin" slabs and thin films, the uniaxial anisotropy often comes from surface-induced

in Chapter 2 we consider  $K_u = 0$ , which leads to existence of the skyrmionic solution, however it is metastable. Including finite  $K_u > 0$  in moderate magnetic fields leads to proliferation of skyrmion lifetimes. Thus Euler-Lagrange equation in dimensionless  $x = r/a$  reads (see Chapter 2, Eq. (2.36)),

$$\theta''(x) + \frac{1}{x}\theta'(x) - \frac{\sin 2\theta}{2x^2} + 2k_0 \frac{\sin^2 \theta}{x} - (u_0 + u_{\mathcal{L}}\sigma) \sin 2\theta - \mathfrak{h} \sin \theta = 0, \quad (5.12)$$

with dimensionless uniaxial anisotropy  $u_0 = K_U a^2/2J$ , and strain-induced anisotropic rigidity  $u_{\mathcal{L}} = \mathcal{L}a^2/2J$ . Thus we fix a finite  $u_0$  and linearize the solution of (5.12) around  $u_0$  with a small perturbation  $u_{\mathcal{L}}\sigma \ll u_0$ . Thus for  $\sigma < 0$  (stretching strain), the effective value of  $u$  is decreased which upon reasonable set of parameters leads to proliferation of a skyrmion as a quasiparticle (for numerical calculations, we used e.g.  $\mathfrak{h} = 0.05$ ,  $u_0 = 1.0$ ,  $k_0/a = 2\pi/\lambda$ ,  $\lambda = 14a$ ); a typical situation is sketched on Figure 5.1. We see that there exists a critical strength  $|\sigma| = \sigma_*$  (with  $\varepsilon_* \approx \sigma_*/E \ll 1$ ) that leads to thermodynamical stabilization of a skyrmion. In other words, the skyrmions which are spontaneously nucleating with rate  $p \sim e^{-2\Delta W/T}$ , become long-live quasiparticles upon application of the critical strength  $\sigma_*$ . Thus  $\sigma_*$  is a continuous function of  $\Delta W_0$ , so the skyrmion pocket continuously expands upon application of arbitrary (but still rather small) strain  $\sigma_{zz} < 0$ . (see figure 5.1). This expansion is however a rather slow (roughly, linear) process.

Note that experimentally it is as a general rule not practical to apply stretching strains ( $\sigma < 0$ ), but much more natural to apply compressive strains ( $\sigma > 0$ ) by just pushing on the edges of the sample. Remarkably, within the above-described mechanism an application of the compressive stress along  $[0\ 0\ 1]$  leads to destabilization of the skyrmion phase, as is observed experimentally [160]. It is however possible to find another pressure geometry under which the compressive deformations lead to stabilization of the skyrmion phase. One of such options is by applying  $[1\ 1\ 0]$  strain, that is  $\sigma_{xx} = \sigma$ ,  $\sigma_{yy} = \sigma$ ,  $\sigma_{zz} = 0$ , which according to Eq. (5.2)- (5.4) leads to  $\varepsilon_{xx} = (1 - \nu)\sigma/E$ ,  $\varepsilon_{yy} = (1 - \nu)\sigma/E$ ,  $\varepsilon_{zz} = -2\nu\sigma/E$ . The direct substitution to (5.1) gives effective uniaxial contribution as

$$\delta W_{[110]} = +\mathcal{L}\sigma \sum_{\mathbf{k}} \mathbf{S}_{\mathbf{k}}^T \hat{\Omega}_0 \mathbf{S}_{\mathbf{k}}, \quad \mathcal{L} \approx \frac{4L}{3E}, \quad \hat{\Omega}_0 = \begin{pmatrix} 0 & 0 & 0 \\ 0 & 0 & 0 \\ 0 & 0 & 1 \end{pmatrix}, \quad (5.13)$$

i.e. like in (5.5) but with opposite sign. Thus the above-described physics is valid and the skyrmion is stabilized under a compressive strain  $\sigma > 0$ .

Thus we have qualitatively shown that upon application of some critical anisotropic stress  $\sigma_*$  (that is,  $\|\sigma_{\alpha\beta}\| = +\sigma_*$  for  $[0\ 0\ 1]$  and  $\|\sigma_{\alpha\beta}\| = -\sqrt{2}\sigma_*$ ), the skyrmion which if

---

phenomena, see also next Chapter 6.

spontaneously nucleated remains thermodynamically stable. This, to my understanding, leads to a situation when the conical phase starts "boiling" with topological charge (skyrmions and meron pairs), which ultimately leads to expansion of a skyrmion pocket in a richer phase space.<sup>4</sup> Because the critical stress  $\sigma_*$  is a continuous function of  $\Delta W_0$ , the skyrmion pocket continuously expands upon application of arbitrary (but still rather small) compressive strain  $\varepsilon_{zz} < 0$ . This expansion is a rather slow, mainly linear, process, as it is supported by uniaxial anisotropy only.

However, in bulk materials surface-induced anisotropy is negligible, and instead the cubic magnetocrystalline anisotropy is a key player for forming the skyrmion lattice. We show in the next section how applied uniform pressure to a bulk material dramatically expands the skyrmion pocket over a richer phase space.

## 5.2 DRAMATIC PRESSURE-INDUCED STABILIZATION OF THE SKYRMION PHASE IN $\text{Cu}_2\text{OSeO}_3$ : EXPERIMENT AND THEORY

So far the temperature width of the skyrmion pocket in bulk samples has been limited to  $\Delta T_{\text{SkL}}/T_C \sim 3\%$  in all investigated cubic chiral compounds. A substantial enhancement of the size of the skyrmion pocket has been demonstrated for thin films and ultra thin slabs of these materials [41, 44], with thickness  $d \lesssim 100$  nm. In these quasi-2D systems the anisotropy is considered to play a major role in the enhanced stabilization of the skyrmion lattice [173]. On the other hand, the resultant phase diagrams are not generic and depend on the material as well as on the method of preparation [39, 174]. Thus, finding a link between the universal phase diagram in bulk materials and the magnetocrystalline anisotropy presents a major challenge for the deeper understanding of the formation and stability of the skyrmion phase.

In the bulk skyrmion hosts, the cubic magnetocrystalline anisotropy, responsible for the stabilization of the skyrmion lattice as a long-range-order phase, is often the weakest of the energy scales present in skyrmion compounds  $A \ll D \ll J$ , where  $D$  and  $J$  are the Dzyaloshinskii-Moriya and the ferromagnetic exchange interactions, respectively.  $D$  favours a perpendicular orientation of neighbouring spins, and is responsible for the formation of the chiral helimagnet ground state with a long wavelength modulation  $\lambda \sim J/D \gg a$ ,  $a$  being the inter-atomic distance. The anisotropy  $A$  then pins the helices along preferred directions, and hence determines the value of the first critical magnetic field  $B_{C1}$  above which the conical structure is stabilized.

To further our understanding of the stability of the skyrmion lattice, it is imperative to establish the parameter range in which the skyrmion lattice is physically favourable with respect to other phases, and further how the size of the skyrmion phase depends on  $J$ ,  $D$  and  $A$ . In that context, the application of hydrostatic pressure is a well-known technique which allows fine-tuning of energy scales through tiny shifts in atomic positions.

---

<sup>4</sup>See also next Chapter.

Before the discovery of its skyrmion lattice phase, MnSi was intensively investigated [175, 176] due to a complete suppression of long-range magnetic order above a critical pressure ( $p_C \sim 1.5$  GPa) and the discovery of non-Fermi liquid behaviour for  $p > p_C$ . A similar suppression of magnetic order has been observed in FeGe [177] around 19 GPa. In contrast, the ordering temperature of  $\text{Cu}_2\text{OSeO}_3$  increases under pressure [178, 179], thus emphasizing the importance of detailed investigation of its pressure dependence.

In this section an extensive study of the phase diagram of  $\text{Cu}_2\text{OSeO}_3$  under hydrostatic pressure up to 2.3 GPa is presented ( $\sigma_{xx} = \sigma_{yy} = \sigma_{zz}$ ), and I follow Ref.[157] which I co-author on discovery of dramatical enhancement of bulk skyrmion phase stability, with some additional theoretical insights omitted in [157] due to length restrictions.

### 5.2.1 EXPERIMENTAL SETUP AND MEASUREMENTS

The single crystal sample was prepared by the chemical vapour transport technique. It was aligned by x-ray Laue backscattering and cut along the [111] direction with dimensions  $4 \times 1 \times 1 \text{ mm}^3$ . The ac susceptibility measurements were performed using a balanced coils setup. Two detection coils were wound on an inox tube 2 mm in diameter, with centers of the coils 2.5 mm apart. On top of each detection coil a driving coil was made for generation of ac magnetic field. AC current was supplied by a Keithley 6221 current source and the balance of the coils was achieved by changing a resistance in series with each driving coil. The amplitude of ac magnetic field was 0.1 mT. The detection of the ac signal was done by the lock-in amplifier Signal Recovery 7265. The measurements of the phase diagram for each pressure were performed in a slow temperature drift regime, where the sweeping rate has been controlled between  $100 \mu\text{K/s}$  around the skyrmion phase and  $700 \mu\text{K/s}$  below  $\sim 30$  K. The magnetic field was generated by a Cryomagnetics 9 T magnet with a sweep rate of 0.1 mT/s (the slowest available on the instrument) between zero and a maximum field value of  $B = 100$  mT. At higher temperatures the upper field value was regularly decreased in order to increase the density of the measured points inside the ordered part of the phase diagram.

The pressure for AC susceptibility study was generated using a non-magnetic piston cylinder pressure-cell with Daphne oil 7373 as a transmitting medium. Pressure was determined using the relative change of the resistance of a manganine wire compared to the zero-pressure case. The magnetization under pressure was measured in a Quantum Design SQUID magnetometer MPMS using a commercial EasyLab pressure cell. The sample used was  $1 \times 1 \times 1 \text{ mm}^3$  taken from the same batch.

High-quality magnetic ac susceptibility  $\chi = \text{Re } \chi + i \text{Im } \chi$  accurately traces the magnetic phases, as illustrated in Figure 5.2a for zero-pressure. As can be seen from the zoomed-in part in Figure 5.2e, the skyrmion phase is manifested as a region of lower susceptibility (yellow) compared to the surrounding conical phase (red). For  $p = 0$  it occupies a very small part of the phase diagram, adjacent to the order-disorder boundary, with a

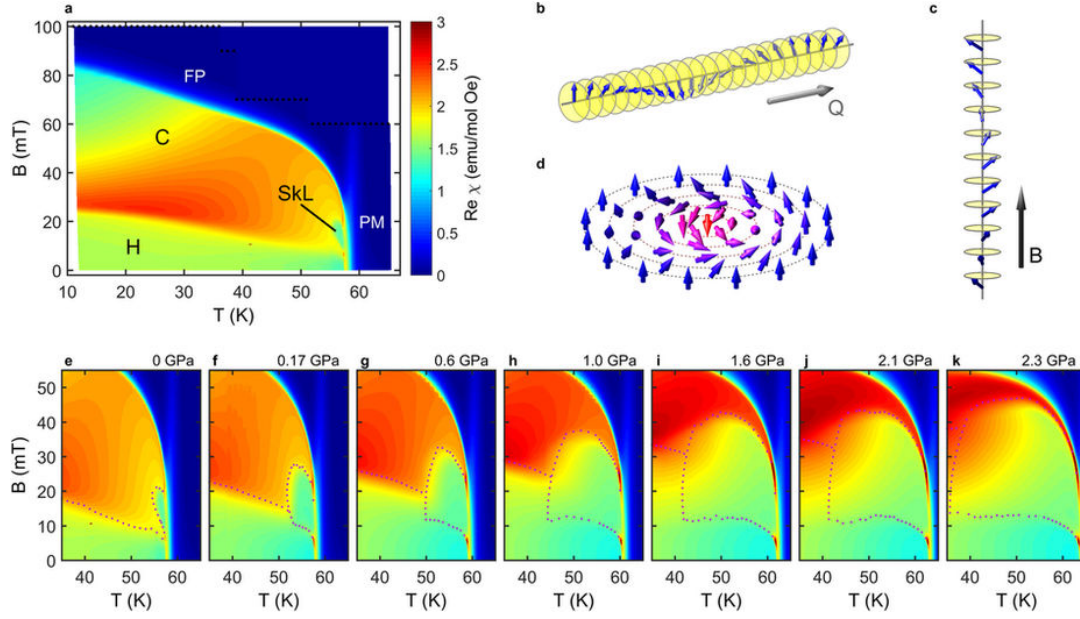


Figure 5.2: **Evolution of magnetic phase diagram of  $\text{Cu}_2\text{OSeO}_3$  under uniform pressure.** **a:** The phase diagram of  $\text{Cu}_2\text{OSeO}_3$  given by the real part of the magnetic susceptibility  $\text{Re } \chi$  taken while ramping magnetic field down. Black dots mark the upper boundary of scans. It consists of H - helical phase, C - conical phase, SkL - skyrmion lattice, FP - field polarized phase, PM - paramagnet. **b:** Helical spin arrangement. Magnetic moments rotate within the plane that is perpendicular to the direction of the wave vector  $Q$ . **c:** Conical spin arrangement. The precession of magnetic moments outlines the cone which is oriented along the direction of magnetic field  $B$ . **d:** Spin configuration of a single skyrmion. **e-g:** Pressure dependence of the phase diagram around the skyrmion pocket. One can see that the skyrmion phase stability was improved in more than 20 times by applying a moderate (for this material) pressure  $\sim 2$  GPa. From Ref.[157]



maximum extent in temperature of 2 K. The maximum field range amounts to around 15 mT, and at lower field values the skyrmion pocket becomes narrower, forming a shape of an inverted tear-drop. The situation drastically changes by the application of even a small hydrostatic pressure ( $p = 0.17$  GPa, Figure 5.2f). The skyrmion pocket increases in size, especially the low magnetic field region, more than doubling over the zero-pressure extent. In addition to the observed growth, one can notice a qualitative change in the way the phases are arranged in that part of the phase diagram. Namely, under pressure the skyrmion phase borders directly with the helimagnetic phase without the conical phase in-between. As shown in Figures 5.2g-k, further increase of the pressure evidences a continuation of the growth of the low-susceptibility region, both towards lower temperatures as well as towards larger magnetic fields.

Quantitatively, we can identify the phase boundaries and extract their pressure dependence from individual scans. Figures 5.3a-b show field scans of real and imaginary susceptibility at  $T = 57$  K, the middle of the skyrmion pocket at zero pressure. The phase boundaries are determined by maxima in the imaginary component, except for the transition between the conical (red) and the field polarized state (blue) where a kink in the real part marks the boundary. On the high-field side the skyrmion pocket (yellow) transforms into the conical phase by a steep increase of the real component, while the imaginary part exhibits a sharp peak. On the low-field side the presence of the conical phase between the helimagnetic (green) and the skyrmion phase at zero pressure is revealed by two peaks in the imaginary part, while at elevated pressures a single peak is observed. To our knowledge this represents the first experimental evidence that the helimagnetic phase and the skyrmion phase are thermodynamically distinct. In the real part this transition becomes less pronounced, because  $T_C$  increases with pressure, placing field scans at 57 K further away from the ordering temperature. We showed recently that the strength of the susceptibility anomaly marking the border of the skyrmion pocket becomes quickly suppressed for  $T < T_C$  [129].

In our experiment the temperature was slowly increased while magnetic field was continuously ramped between zero and a maximum value. Due to the slow temperature change ( $dT/dt < 100\mu\text{K/s}$ ) and reduced field range around the skyrmion pocket (black dots in Figure 5.2a), successive field scans were spaced by no more than 0.2 K, providing a very good resolution in temperature. This enables us to determine the temperature width of the skyrmion phase by plotting  $\chi(T, B)$  for fixed  $B$ . Extracted temperature profiles through the middle of the skyrmion pocket are displayed in Figure 5.3c. In Figure 5.3d we compare  $\chi(T)$  extracted from the  $\chi(T, B)$  maps to a temperature scan recorded on cooling using a standard susceptibility setup. The overlap of the two curves demonstrates that the extracted profiles presented in Figure 5.3c probe directly the thermodynamic phase boundaries.

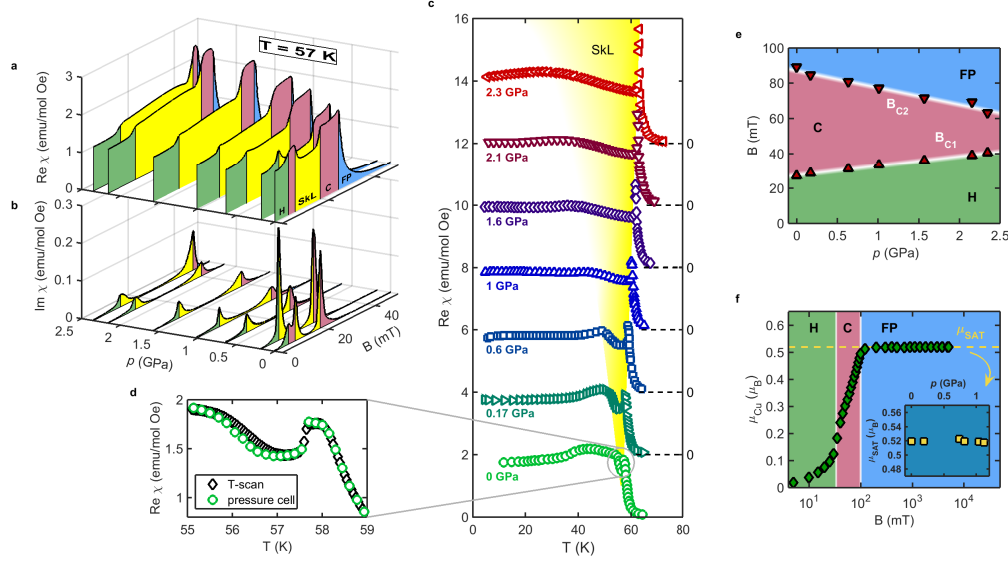


Figure 5.3: **Evolution of magnetic phases with pressure.** **a:** real part and **b:** imaginary part of the magnetic susceptibility  $\chi$  at  $T = 57$  K. **c:** Extracted temperature profiles through the middle of the skyrmion pocket at magnetic fields  $B = 15, 16.5, 18, 19.5, 21, 22.5$  and  $24$  mT (from  $0$  to  $2.3$  GPa). **d:** Comparison of the extracted temperature profile with a temperature scan taken in cooling measured on the same sample using a standard setup (without the pressure cell) at zero pressure and  $B = 15$  mT. A small difference is visible on the low temperature side of the skyrmion pocket ( $\leq 0.2$  K) where disintegration of the skyrmion lattice occurs and the exact path through the phase diagram becomes important. **e:** Pressure dependence of the helical-conical and conical-field polarized metamagnetic phase transitions in the  $T = 0$  K limit. **f:** Magnetic field dependence of magnetization at  $p = 1.0$  GPa and  $T = 10$  K. Inset: Pressure dependence of the saturation magnetization level. From Ref.[157].

### 5.2.2 PHYSICAL INTERPRETATION

First of all, we highlight that even at the smallest applied pressures an enhanced stability of the skyrmion phase is readily observed: compared to the zero pressure case, where  $\Delta T_{skL} \approx 2$  K (3% of  $T_C$ ), it reaches  $\Delta T_{skL} \approx 10$  K at 0.6 GPa, corresponding to 17% of  $T_C$ . If the same relative increase is achieved in the recently discovered skyrmion compound [156]  $\text{Co}_8\text{Zn}_9\text{Mn}_3$  with the ordering temperature at 322 K (49°C), the skyrmion lattice would be stable even below 0°C, this covering the usual operational temperature range for most electronic circuits.

With further increase of pressure the low-temperature boundary to the conical phase becomes less pronounced, transforming into a wide cross-over. At the highest pressure ( $p = 2.3$  GPa) the low susceptibility region extends almost to 30 K, indicating that skyrmions exist down to at least half of the ordered phase diagram in the high-magnetic field region. It remains an open question as to what kind of a spatial distribution is taken by skyrmions at high pressures and whether they still form a well-defined lattice.

Under mechanical strain, a material is pushed in volume so the distances between the constituting atoms are modified, which results to further interlapping between the local wave functions so the macroscopical properties, such as exchange stiffness, DMI, anisotropy is modified. Our experimental observations indicate that the  $J$  and  $D$  remain almost unchanged as the critical temperature and helix modulation wavelength have not noticeably modified even under pressure of several GPa. At low temperatures the helical and conical phases are thermodynamically stable, although with pressure the area covered by the conical phase is substantially reduced from both high and low field sides compared with ambient pressure, as revealed in Figure 5.3e. More importantly, we observe an increase of the first critical magnetic field  $B_{C1}$  that marks the transition from the helical to the conical phase. As has been introduced above,  $B_{C1}$  is linked directly to the anisotropy energy which determines the direction of the helical propagation vector in the absence of an applied magnetic field  $B$ . Therefore the  $B$ -field range of stability of the helical phase ( $B_{C1}$ ) is shifted thus indicating a very nonlinear change in anisotropy under such pressure, which we thus estimate to be in order of 15-20%.

In bulk samples of skyrmion host  $\text{Cu}_2\text{OSeO}_3$  (and similar materials with  $P2_13$  crystallographic group) the spin anisotropy  $\mathcal{H}_A$  arises in the form allowed by the effective T23 symmetry group as

$$\mathcal{H}_A \approx A_0(S_x^2 + S_y^2 + S_z^2) + A_1(S_x^4 + S_y^4 + S_z^4) + A_2(S_x^2 S_y^2 + S_y^2 S_z^2 + S_z^2 S_x^2) + \mathcal{O}(S^6), \quad (5.14)$$

the second-order effective "anisotropy" (first term in (5.14)) can be dropped as it does not contribute to the stability of the skyrmion lattice (see detailed discussion in Chapter 2). Note also that due to the same reason the isotropic terms in (5.1) can be also dropped.

The remaining fourth-order cubic anisotropy can be thus regrouped as

$$\mathcal{H}_A = A(S_x^4 + S_y^4 + S_z^4) + U\mathbf{S}^4. \quad (5.15)$$

with  $A = A_1 - A_2/2$  and  $U = A_2/2$ . Thus, there could be two qualitatively distinct situations, first with  $A_1 \gg A_2$ , for which the anisotropy of the bulk is important, and the opposite case with  $A_1 \sim A_2/2$ , where the role of anisotropy is reduced to providing mode-mode coupling  $U \sim A_1, A_2$ . However, taking into account the experimental observation that the magnetic phase diagram remains qualitatively invariant under bulk rotations in our experiments, we thus come to conclusion that the main role of the cubic anisotropy in this system is to provide the higher-order term  $U$  which allows to stabilize the magnetic crystalline, while the purely anisotropic properties reflected in  $A$  are actually of the lower importance. Furthermore, I would also like to stress one more time on the argument from Binz and Vishwanath [35] (which can be traced back as a very general condensed matter concept, see e.g. [180]) that one needs at least the fourth-order term  $\mathbf{S}^4(\mathbf{r})$  to stabilize the skyrmion crystalline in such a way that spin density waves for a hexagonal lattice (see also [38]). Indeed, after decoupling the uniform component, one has

$$U\mathbf{S}^4(\mathbf{r}) = [\mathbf{s}(\mathbf{r}) + \langle \mathbf{S}(\mathbf{r}) \rangle]^4 = \dots + 4U\mathbf{s}^2(\mathbf{r})\mathbf{s}(\mathbf{r}) \cdot \langle \mathbf{S}(\mathbf{r}) \rangle + \dots, \quad (5.16)$$

Thus it generates upon Fourier-transform the term

$$\langle \mathbf{s}^2(\mathbf{r})\mathbf{s}(\mathbf{r}) \rangle = \sum_{\mathbf{Q}_i} (\mathbf{S}_{\mathbf{Q}_1} \cdot \mathbf{S}_{\mathbf{Q}_2}) \mathbf{S}_{\mathbf{Q}_3} \delta(\mathbf{Q}_1 + \mathbf{Q}_2 + \mathbf{Q}_3), \quad (5.17)$$

which can be minimized (made strongly negative) if only  $\mathbf{Q}_1 + \mathbf{Q}_2 + \mathbf{Q}_3 = \mathbf{0}$ , which produces the hexagonal skyrmion lattice [38]. The magnetic phase diagram of is thus expected to be qualitatively captured by fluctuation-enriched Ginzburg-Landau formalism as discussed in Chapter 3. As this paper [157] was my first study of the skyrmion phases, I actually simply adopted the the effective (numerical) calculation described in Ref [38] for phase diagrams (before I developed and polished it further to the state as described in Chapter 3, so it became semi-analytical); thus for the detailed description of the numerical approach I hereby refer to Ref. [38] and just highlight here the main features of the formalism. The calculations are made in the continuous-field approximation justified by the large ratio of the skyrmion radius  $\lambda$  to the lattice constant  $a$ . The Ginzburg-Landau functional is taken up to fourth order in magnetization and second order in magnetization gradients, thus including both the Dzyaloshinskii-Moriya interaction and anisotropies. The magnetic structure is determined by minimization of the free energy, where the order parameter is naturally taken as the local magnetization reduced by the

average magnetization of the crystal. A mean-field treatment shows the conical phase to be energetically favourable, but the skyrmion phase lies only slightly higher in energy. By including the Gaussian fluctuations of the free energy the skyrmion phase becomes favourable in a certain range of finite magnetic fields. The fluctuations contribute mainly at the short-length scale and are calculated with the cut-off in the momentum space in order of  $2\pi/a$ . The transition to the paramagnetic state is expected to occur when the fluctuations become significant (around 20% of the mean-field value), which determines the ordered phase boundary through the relation  $B_{C2}(\tau) = \sqrt{2(\tau - \tau_0)}$ . For the calculation of the phase diagram at zero pressure we used the following parameters:  $\gamma = JD/U = 6.2$ ,  $\Lambda = \lambda/a = 28$ ,  $z_T = 3.4$  and  $\tau_0 = 3.1$ . The values of  $\gamma$  and  $\Lambda$  are in good agreement with a recent density functional calculation [142]. The Ginzburg-Landau approach is considered to break down away from  $T_C$  so we leave the field axis normalized to  $B_0 = \sqrt{(JQ^2)^3/U}$ .

We start from the magnetic path-integral approach with Ginzburg-Landau functional for modulated spin structure  $\mathbf{M}(\mathbf{r})$  (see Ref. [38]),

$$\mathfrak{Z} = \int \mathcal{D}\mathbf{M} e^{-F[\mathbf{M}(\mathbf{r})]/T}, \quad F[\mathbf{M}(\mathbf{r})] = \int dV [\alpha_T \mathbf{M}^2 + J(\nabla \mathbf{M})^2 + D\mathbf{M} \cdot (\nabla \times \mathbf{M}) + U\mathbf{M}^4 - \mathbf{B} \cdot \mathbf{M}], \quad (5.18)$$

where the  $M^2$  term is related to the temperature-dependent tuning parameter  $\tau(T) = 1 - \alpha_T J/D^2$ . Here,  $\alpha_T$  controls the transition and, in our approach, is adopted to reproduce the experimental  $T_C(p)$  and enable us to predict the phase diagram in absolute units of temperature. The microscopic parameters  $J$ ,  $D$  and  $U$  are related to experimental observables in a simple way:  $T_C \propto J$ ,  $k_0 = 2\pi/\lambda \approx D/2J$  while as mentioned previously we assume  $B_{C1} \propto A_1, A_2 \sim U$ . It has been shown [38] that when the (Gaussian) thermal fluctuations around the mean-field solution are included, the skyrmion lattice phase becomes stable close to  $T_C$ . However, it remained unknown as to the width of the temperature window over which the stabilization can be expected to occur. In order to address this question, first it is necessary to establish the functional relation between the tuning parameter  $\tau$  and the thermodynamic temperature  $T$ . Around the mean-field solution the upper-critical field  $B_{C2}$  is related to  $\tau$  through  $B_{C2}(\tau) \cong \sqrt{2(\tau - \tau_0)}$ , where  $\tau_0$  reflects the shift of the transition temperature away from its mean-field value due to the linear effects of fluctuations. In addition,  $B_{C2}(T)$  can itself be directly extracted from the experimentally established phase diagram, Figure 5.2a. We find that it follows the form of a critical behaviour  $\mathfrak{U}$

$$B_{C2}(T) = \mathfrak{B}(1 - T/T_C)^\kappa, \quad (5.19)$$

with critical exponent  $\kappa \cong 1/4$ , as presented in the inset of Figure 5.4. This leads to the

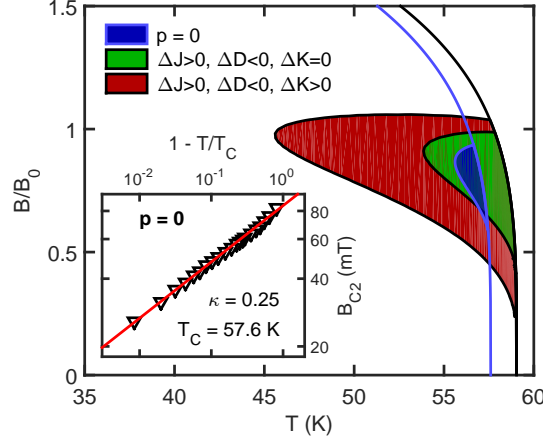


Figure 5.4: **Modelling of the size of the skyrmion pocket using the Ginzburg-Landau approach.** The width of the calculated skyrmion pocket ( $\sim 2$  K) for  $p = 0$  has been used to fix the values of all parameters within the model. To simulate the behaviour at elevated pressures, we change the values of  $J$ ,  $D$  and  $K$  as obtained at  $p = 0.6$  GPa:  $\Delta J/J = 2.5\%$ ,  $\Delta K/K = 15\%$  and  $\Delta D/D = -3.5\%$ . The size of the skyrmion pocket is significantly increased only if the change of anisotropy is incorporated in the calculation. Inset: critical behaviour of the upper metamagnetic transition between the conical and field-polarized phase  $B_{C2} \sim (1 - T/T_C)^\kappa$ . From Ref.[157]

phenomenological relation for  $\tau(T)$

$$\tau(T) - \tau_0 = \mathfrak{B}(1 - T/T_C)^{2\kappa} \simeq \mathfrak{B}\sqrt{1 - T/T_C}. \quad (5.20)$$

The square-root dependence is preserved across the pressure range investigated in this study [157].

Now we can proceed with the discussion of the size of the skyrmion pocket in terms of thermodynamic temperature  $T$ . As mentioned above, the inclusion of thermal fluctuations is necessary to stabilize the skyrmion lattice over the conical spin arrangement. However, it has been suggested recently [134] that the fluctuations close to  $T_C$  are strongly interacting, lowering the transition temperature and making it first-order. Within the effective model the reduction in  $T_C$  is implemented [38] by setting the corrections of the order parameter to be smaller than 20%. We keep this approach and in the main panel of Figure 5.4 plot the resultant order-disorder boundary with the outline of the skyrmion pocket for different values of  $J$ ,  $D$  and  $K$ . For the zero-pressure case we adjust the coefficients of the model so that the skyrmion pocket is limited to  $\sim 2$  K below  $T_C$ , as found in the experiment. To explore the effect of pressure we consider the particular case of  $p = 0.6$  GPa, where the skyrmion pocket is still well defined, and estimate  $\Delta J$ ,  $\Delta D$  and  $\Delta U$  from the experimental data:  $\Delta T_C/T_C = \Delta J/J = 2.5\%$ ,  $\Delta B_{C1}/B_{C1} = \Delta U/U = 15\%$ , while  $\Delta B_{C2}/B_{C2} = -9\%$  translates to  $\Delta D/D \approx -3.5\%$ . It can be shown that the skyrmion pocket grows (expands its thermodynamical stability over a larger phase diagram vol-

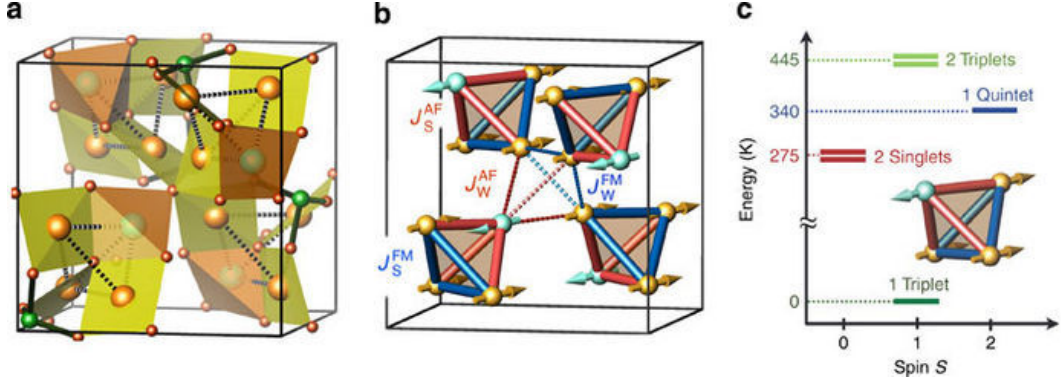


Figure 5.5:  **$\text{Cu}_2\text{OSeO}_3$  crystallographic structure (space group  $P2_13$ ).** (a) The crystal structure constitutes from  $\text{Cu}(2)\text{O}_4$  plaquettes (yellow) and  $\text{Cu}(1)\text{O}_5$  bipyramids (orange), and covalent Se-O bonds (thick lines), forming a sparse three-dimensional lattice. This lattice can be mapped as tetrahedra (dashed lines), each composed of one  $\text{Cu}(1)$  and three  $\text{Cu}(2)$  sites, depicted by large light brown and light cyan spheres, respectively. Small spheres denote the non-magnetic sites. (b) The magnetic  $\text{Cu}^{2+}$  ions form a distorted pyrochlore lattice, a network of corner-shared tetrahedra. (c) The energetics of a single tetrahedron ( $th$ ): magnetic spin ground state  $S_{th} = 1$  is separated from the closest energy excitation by a huge gap,  $\Delta \approx 5T_c$ . From Ref.[142]

ume) if the parameter  $JU/aD^2$  increases, indicating that all of the observed changes contribute positively. If we take into account only  $\Delta J$  and  $\Delta D$  ( $\Delta U = 0$ ) then we obtain a small increase of the skyrmion pocket. However, a more significant growth is obtained when the observed  $\Delta U$  is included, giving  $\Delta T_{SKL} \sim 10$  K. The temperature extent is here only indicative since it is known that even the well-modified Ginzburg-Landau approach is not valid far away from  $T_C$  [180]. Additionally,  $B_{C1} \sim U$  is only a crude approximation which is expected to hold only in a narrow range of parameters. Nevertheless, our analysis demonstrates the importance of anisotropy  $A_{1,2}$  which result into effective  $U$  in stabilizing the skyrmion lattice at temperatures far from the immediate proximity of the ordering temperature. Indeed just  $\sim 15\%$  change in effective anisotropy can expand the temperature range of the skyrmion stability by 600%, with conquering the overall phase space in more than 20 times.

While the above-presented model is applied as a continuous-field approximation, an important question is what qualitative changes occur with pressure on the level of the unit cell. This is especially important for  $\text{Cu}_2\text{OSeO}_3$  since there are two crystallographically distinct copper sites which couple strongly into tetrahedra with a quantum triplet ground state [142], see Figure 5.5. These triplets form a trillium lattice which is identical to the lattice of Mn ions in MnSi, and long-range order is then governed by the effective exchange and Dzyaloshinskii-Moriya interactions between the triplets. It follows that the effect of pressure on  $\text{Cu}_2\text{OSeO}_3$  can be two-fold: (i) changing the quantum nature of tetrahedrons and (ii) changing the inter-triplet interactions. In order to probe the former effect, we have performed measurements of the magnetization plateau under pres-



sure. The plateau occurs when the system enters the field polarized state for magnetic fields  $B > 100$  mT, see Figure 5.3f and inset. It turns out that within the error-bar the observed magnetization plateau does not change, at least for pressures  $p \lesssim 1$  GPa. This means that the tetrahedra remain relatively rigid, while pressure-induced shifts in atomic positions occur dominantly between the tetrahedrons, influencing the effective inter-triplet interactions and justifying the use of the continuous model.

### 5.3 CONCLUSIONS

In conclusion, we have manifested the pressure-induced tuning and control of the bulk skyrmion phase in  $\text{Cu}_2\text{OSeO}_3$ , which is carried out with a moderate pressure force. This offers a new insight on the role of cubic magnetocrystalline anisotropy and provides a further methodology for significant enhancement of skyrmion phase stability in laboratory conditions. As was explained from a semi-quantitative Landau-Ginsburg model, the proposed pressure-stabilized mechanism is valid in a broad range of skyrmion-hosting materials material with effective  $US^4$  anisotropy-induced bulk contribution.

The crucial role of (fourth-order) anisotropy terms has also been explored in Monte Carlo simulations [181] where it has been found that the correct phase diagram can be reproduced if additional anisotropy-compensation terms are added because of boundary effects. On the experimental side, in the recently discovered skyrmion compound  $\text{GaV}_4\text{S}_8$  the orientation of skyrmions is dictated by the magnetic easy axis and not by the direction of magnetic field [182]. At the same time, the relative size of the skyrmion pocket within the phase diagram of this polar magnet is substantially larger than in the family of chiral magnets such as  $\text{MnSi}$  and  $\text{Cu}_2\text{OSeO}_3$ .

The results presented in this chapter clearly demonstrate that although it is very often the weakest of the energy scales, anisotropy plays a decisive role in stabilization of the skyrmion lattice. Broadening the operational range for the skyrmion lattice and making it more resistant to external fluctuations provides a promising route for future investigations in order to enhance the potential of other skyrmion-supporting materials, especially around room temperature [156], where skyrmion-based applications are foreseen. The deeper theoretical understanding of the various mechanisms leading to skyrmion stability may also guide the rational design of new compounds with favourable characteristics for hosting stable skyrmion phases.



# 6

## Topological Objects in Thin Films: Magnetic Skyrmions, Chiral Bubbles, Merons and Bimerons

Thin films, – samples made of slabs of bulk materials by e.g. polishing down to a thickness of typically few interatomic distances, – provide a deeper understanding of the skyrmion host materials by implying specific boundary conditions, and thus allow to modify the relative strength of DMI and anisotropies in the system. Skyrmions in thin films behave somewhat differently, – rather like a gas or a liquid, in contrast to the skyrmions in bulk materials, which either prefer to group into a thermodynamically-stable crystalline (the skyrmion lattice) or, under certain conditions, to exist metastable and independent one of each other being isolated by stripes of the helical phase. One of the remarkable consequences of the thin film behaviour of skyrmions is the experimentally observed stability of the disordered-lattice skyrmion phase down to zero or very low temperatures, and achievable nucleating of skyrmions in ferromagnetic phase. As a general rule, there is a crucially different physics in skyrmion motion in thin films comparing to the bulk counterparts, including the broad dispersion in skyrmionic sizes, from nanometers to micrometers, thus skyrmion in thin films very often remind *chiral magnetic bubbles*, – the magnetic objects of the same topology but dynamically more inert. Furthermore, the conical phase is, as a general rule, conquered by the skyrmion phase fully or almost fully in the thin films. The ordered phase diagram hence simply consists of helical phase at low magnetic fields and skyrmion phase at moderate magnetic fields (the skyrmion phase further polarizes to the forced-ferromagnetic phase at the very strong fields). An interesting experimental (and theoretical) observation is

the presence of non-zero topological charge even in helical phase, due to relict merons (half-skyrmions) at the boundary where stripes of one helical domain merge with stripes of another helical domain. Thus the thin-film systems are topologically richer by the presence of merons and bimerons, which apparently play a distinct role in, – or at least somehow assess, – the helical-to-skyrmion transition.

In this chapter I consider three relatively simple models, describing (i) thin-film dynamics of magnetic skyrmions under thermal gradients, (ii) topologically-preserved crossover between skyrmion and magnetic chiral bubbles in thin films, and (iii) a toy model phenomenologically capturing the topological charge saturation due to spontaneous boiling of helical phase with (bi)merons. Despite its simplicity, the very last model in this thesis shows a qualitatively decent mechanism of the *topological charge saturation* at some critical magnetic field (that is, helical-to-skyrmion transition), in a resemblance with experimental feature  $H_{C1}(T)$ .

## 6.1 MAGNETIC SKYRMIONS UNDER THERMAL GRADIENTS

Normally, the Brownian motion and thermal diffusion in gases and liquids occurs in the direction of lowering temperature, which is intuitively captured by understanding that an average velocity of a particle or quasiparticle reflects the temperature in the local region. However, magnetic skyrmions have a counter-intuitive feature to travel towards the higher temperatures, totally confusing our concepts on how particles and quasiparticles normally behave.

The study of thermal gradient effects on skyrmions started in 2012 when it was discovered numerically that the skyrmion lattice can be rotated with spin torques and field or thermal gradient in bulk [91]. Soon after, it was reported that contrary to the conventional Brownian motion, the 2D skyrmions move towards a hotter region of the magnetic film [90]. The study of Kong and Zang [90] presented both the numerical simulations and a semi-quantitative analytical model, which proposed a magnon-scattering mechanism for this phenomenon. The idea of the calculation lies in the assumption that the difference in thermal-gradient magnon flow, while moving from hotter to colder region, scatters crucially on a skyrmion, which due to specifics of magnon-skyrmion scattering [183] leads to the anti-gradient-directed component of momentum (flow against thermal gradient), as also a weaker perpendicular component which indicates the skyrmion Hall effect [90]. Even though a similar calculation could be applied towards the dynamics of domain walls and magnetic bubbles, Kong and Zang argue that the effect under study is topologically-induced and thus depends crucially on the quantized topological charge [90].

The effect reported by Kong and Zang aspired further studies on the topic, as a direct application of it would be a low-dissipative control over dynamics of both individual

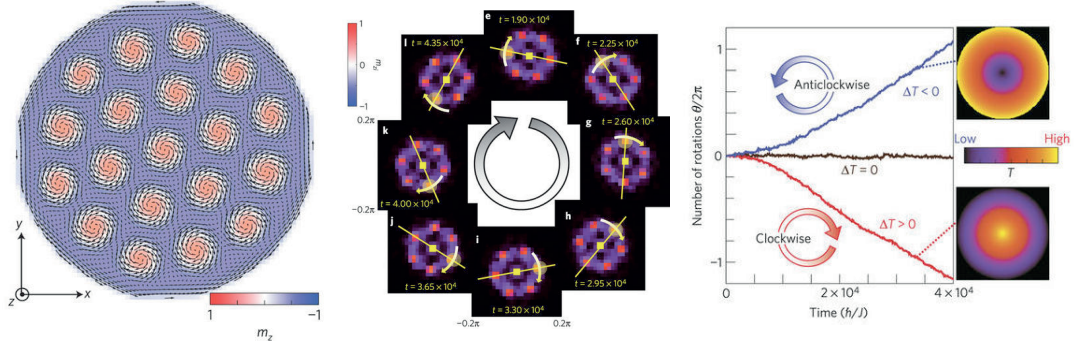


Figure 6.1: Thermally-driven ratchet motion of skyrmions under electron-flow induced radially-directed thermal gradient. The thermal gradient from the periphery of the skyrmion array to its center (and inverse) is induced by the electron-induced heating under operation of the Lorentz Transmission Electron Microscopy (LTEM). **Left:** Skyrmion array simulation for skyrmions confined in the circularly-shaped disk (shown the in-plane components of magnetization). **Center:** Ratchet motion of a skyrmion layer: skyrmions follow two rotational motions: a) clockwise rotation as a whole with respect to the center of the skyrmion array; b) each skyrmion itself makes a clockwise rotation with respect to its center. **Right:** Manifestation of the direct correlation between the rotation sense and thermal gradient direction. Figure from Ref.[152]

skyrmions and skyrmion arrays in insulating thin films.<sup>1</sup> In particular, an experimental observation of the "ratchet motion" of skyrmion arrays under radially-directed thermal gradients was shortly reported [152], see also Figure 6.1. Furthermore, in the other studies, a chiral magnetic bubble<sup>2</sup> was shown to also be subjected to an anti-gradient thermal motion [184], as also transverse skyrmion Seebeck effect was conjectured [185].

Even though the counterintuitive motion of skyrmions towards higher  $T$  was explained by a magnon-mediating mechanism, there is an alternative mechanism, which is at least equally important over a non-homogeneously heated sample. We thus propose a new elementary model underlying this feature, based on the variation of the skyrmion's "rest energy" as it goes from a colder to a warmer region. The resulting *thermogradients force* moves a skyrmion (or an array of skyrmions) towards a warmer zone depending on the parameters of the system.

To describe the force acting on a single skyrmion we use the axisymmetric model of a skyrmion as described in Chapter 2, that is with the coarse-grained magnetic moment varying as  $\mathbf{S} = (\sin\theta \cos\psi, \sin\theta \sin\psi, \cos\theta)$ , on top of the otherwise ferromagnetic background. We thus consider a rotationally-invariant 2D Bloch skyrmion with  $\theta = \theta(\rho)$  and  $\psi(\varphi) = \varphi + \gamma$ , – with  $m = 1$ ,  $\gamma = \pi/2$  and unitary topological charge  $Q = -1$ . On the microscopical level, the energy of a skyrmion in a thin film magnet is given by the interplay of

<sup>1</sup>In conductive thin films, the skyrmions are successfully moving under electric current.

<sup>2</sup>See next section on difference between a skyrmion and a magnetic bubble.

different spin interactions: the ferromagnetic Heisenberg exchange  $J$ , which prefers the parallel arrangement of spins, the Dzyaloshinskii-Moriya interaction  $D$ , which favours the mutual canting of the adjacent spins, and the Zeeman term stabilizing the skyrmion along the moderate external field  $\mathbf{H}$ , and anisotropies of different origin (including dipolar interactions). To calculate the "rest energy" of the skyrmion, we however use here the minimal model (2.25), as will capture the main features of the thermogradient motion,

$$W[\mathbf{M}(\mathbf{r})] = J \sum_{i,j} \left( \frac{\partial M_i}{\partial x_j} \right)^2 + D \mathbf{M} \cdot (\nabla \times \mathbf{M}) - \mathbf{M} \cdot \mathbf{H}, \quad (6.1)$$

We consider a skyrmion nucleated in the field-polarized (FP) phase, were its energy with respect to the FP background is

$$W[\theta(r)] = 2\pi M^2 \int dz \int d\rho \rho \left\{ J \left[ \left( \frac{d\theta}{d\rho} \right)^2 + \frac{\sin^2 \theta}{\rho^2} \right] + D \left( \frac{d\theta}{d\rho} + \frac{\sin 2\theta}{2\rho} \right) + \frac{H}{M} (1 - \cos \theta) \right\}, \quad (6.2)$$

For numerical calculations, we introduce dimensionless variables starting from  $x = \rho/a$ , and  $d = aD/J$  and  $h(M) = Ha^2/JM$ ,

$$w(M) = \frac{W(M)}{JM^2 a^2 z_0} = 2\pi \int_0^\infty dr r \left[ \theta_r^2 + \frac{\sin^2 \theta}{r^2} + d \left( \theta_r + \frac{\sin 2\theta}{2r} \right) + h(M)(1 - \cos \theta) \right], \quad (6.3)$$

( $z_0$  is thin film thickness). After that, we solve the variational problem with respect to the configuration  $\theta(x)$  which minimises the rest energy for given  $d$  and  $h$ . This leads us leads to the Euler-Lagrange equation to determine a skyrmion configuration,

$$\theta''(x) + \frac{1}{x} \theta'(x) - \frac{\sin 2\theta}{2x^2} + d \frac{\sin^2 \theta}{x} - \frac{h(M)}{2} \sin \theta = 0, \quad (6.4)$$

with boundary conditions:  $\theta(0) = \pi$ ,  $\theta(\infty) = 0$ , corresponding to the "spin down" in the center of a skyrmion and "spin up" far away. In general case, the solution of the nonlinear differential equation (6.4) can be done only numerically, however always should be verified that  $\theta(x)$  is controllably small at long distances (the long-scale asymptote is  $\theta(x) \sim \frac{e^{-\kappa x}}{\sqrt{\kappa x}}$ , with  $\kappa = \sqrt{h/2}$ , see Chapter 2 for details). To solve differential equation (6.4) with the Dirichlet boundary value problem, we first solve an auxillary Cauchy problem with boundary conditions  $\theta(0) = \pi$  and  $\theta'(0) = \alpha$ , choosing  $\alpha$  such as it gives  $\theta(\infty) = 0$ . This involves numerically finding a separatrix between the two attractors  $(0, \pi)$  and  $(0, -\pi)$  in the phase portrait. The value of  $\alpha$ , corresponding to the separatrix depends crucially on  $h$  that is a function of field and magnetization, and therefore temperature (meanwhile  $d$  is fixed for a given material). For details of this numerical technique, see Chapter 2.

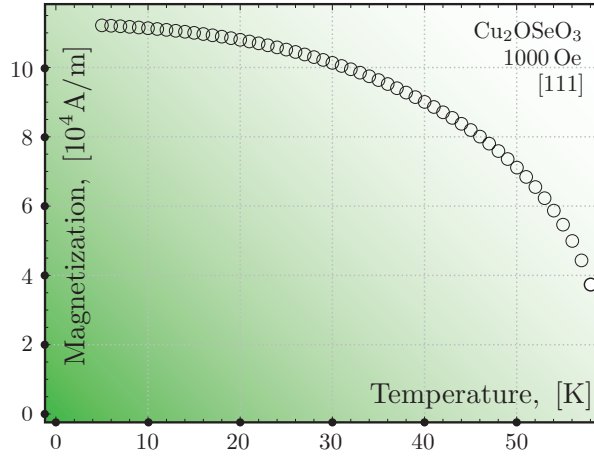


Figure 6.2: Magnetization of  $\text{Cu}_2\text{OSeO}_3$  along [111] in the external magnetic field 1000 Oe (slightly above saturation). Data extracted from Ref.[165].

Note that the dimensionless energy depend on the value of magnetization in non-trivial way: as  $w(M)$  is not a constant for the reason that  $\mathbf{h} = \mathbf{h}(M)$ , and in turn the length of magnetic moment is itself temperature-dependent. Moreover,  $M$  generally depends on magnetic field, that is dependence  $M = M(H, T)$  is defined on the underlying magnetic phase. Here we however consider a skyrmion in the field-polarized phase, with saturated magnetization  $M = M_S(T)$ . The renormalization group theory predicts this dependence to be scaled as  $M_S(T) \propto (1 - T/T_0)^n$ . In this study we consider for simplicity  $M_S(T) = M_0(1 - T/T_0)^n$ , where  $M_S \simeq M_S(0)$ ; for  $\text{Cu}_2\text{OSeO}_3$ , the exact dependence  $M_S(T)$  in field-polarized phase is known from experiment (see Figure 6.2).

We therefore solve (6.4) with the method described in Chapter 2 for given  $M_S(T)$  dependence and realistic bulk parameters for  $\text{Cu}_2\text{OSeO}_3$ , in particular: at the critical magnetic field  $H_C = 0.34$  T, Heisenberg exchange  $J = 4.85 \times 10^{-23}$  J m/A<sup>2</sup>, DMI strength  $D = 1.22 \times 10^{-14}$  J/A<sup>2</sup>, saturation magnetization  $M_S(0) = 1.11 \times 10^5$  A/m, and with lattice constant  $a = 8.91 \times 10^{-10}$  m. These numbers leads to dimensionless parameters  $d = Da/J = 0.224$  and  $h = Ha^2/MA = 0.050$ . We find for example that at  $T = 0$  the "rest energy" of a skyrmion is  $W = 3.16 \times 2\pi AM_S^2(0) = 1.19 \times 10^{-11}$  J. The detailed dependences  $W(M = M_S)$  are given on Figure 6.3.

As the "rest energy" of a skyrmion is changing with temperature, a skyrmion in regions with different temperature (for  $T < T_*$ ) exists with energy difference between colder and hotter regions. This, in turn, implies, that the potential energy  $W$  of the skyrmion depends on the position in non-homogeneously heated sample. Therefore there will be a gradential force  $F = -\nabla W$ , which will be in fact co-directed with temperature gradient,

$\mathbf{F}_\nabla = -\nabla W = -\frac{dW}{dM} \frac{dM}{dT} \nabla T$ . Thus we come to conclusion that this force is expressed by

$$\mathbf{F}_\nabla(T) = \mathfrak{f}(M(T)) \mathbf{grad} T, \quad (6.5)$$

with temperature-dependent mobility function

$$\mathfrak{f}(M(T)) = -4\pi JM \frac{dM}{dT} \int_0^\infty dr r \left[ \theta_r^2 + \frac{\sin^2 \theta}{r^2} + d \left( \theta_r + \frac{\sin 2\theta}{2r} \right) + \frac{h}{2} (1 - \cos \theta) \right], \quad (6.6)$$

Because local magnetization naturally decreases with temperature,  $\frac{dM}{dT} < 0$  (see Figure 6.2), after further algebra one deduces

$$\mathfrak{f}(M(T)) = 2JM(T) \left| \frac{dM}{dT} \right| \left( \frac{W}{JM^2} - \frac{h}{2} \int_0^\infty [1 - \cos \theta(r)] r dr \right), \quad (6.7)$$

Finally, we can rewrite the expression for the force acting on the skyrmion in the non-homogeneously heated sample

$$\mathbf{F}_\nabla = \left| \frac{dM}{dT} \right| \left( \frac{2W(T)}{M(T)} - \eta(T) a^2 H \right) \mathbf{grad} T, \quad (6.8)$$

where  $\eta = 2\pi \int_0^\infty (1 - \cos \theta) r dr$ ;  $\theta = \theta(d, h(T))$ .

Finally, we plot several temperature dependencies for numerical values as listed above, namely: (i) dependence of skyrmion "rest energy" on temperature; (ii) dependence of force on temperature for the unit temperature gradient, see Figure 6.4. As  $\nabla T$  points in the direction of the greatest increase of temperature, the skyrmion will move in the direction of the temperature gradient (i.e. from colder to hotter regions). Such a nontrivial feature of this calculations comes from the following model assumptions: (i) we place a skyrmion above the saturation field  $H_{C2}(T)$ , namely at the line  $H = 1000$  Oe, where we know the magnetization data [165]; (ii) the skyrmion is allowed to travel only along the line  $H = 1000$  Oe, thus at hotter temperatures the effective magnetic field  $H/H_{C2}$  increases with temperatures, and as we know from Chapter 2, single skyrmions become more stable in higher dimensionless magnetic fields  $\mathfrak{h}$ .

We conclude that even though magnon may cause the thermal-gradient motion of the skyrmion, there is an alternative effect based on variation of the skyrmion rest energy in differently-heated places of the sample. To our surprise, this effect is not in literature

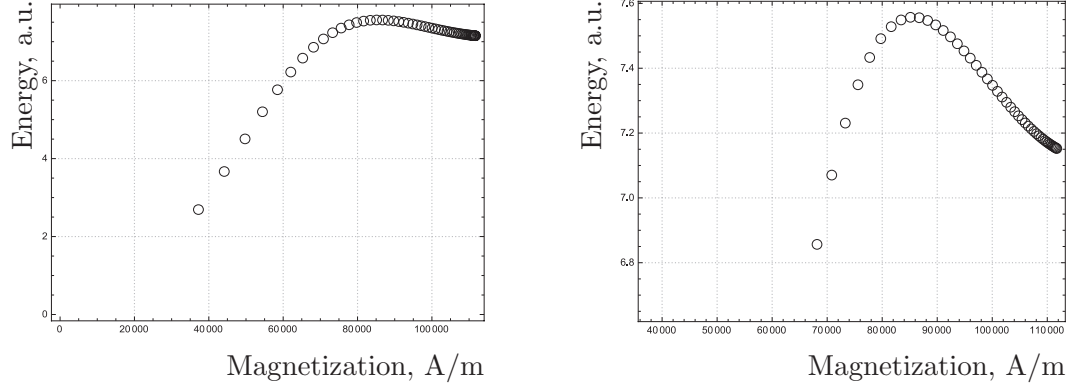


Figure 6.3: Rest energy of a skyrmion in the field-polarized background within the minimal model (2.25), calculated for experimental data from Figure 6.2. As we see, the slope of the function changes sign meaning that at different points of the sample the rest energy of a skyrmion can either increase or decrease. This in particular may take place if a skyrmion is embedded in a sample with different temperatures kept at it's end.

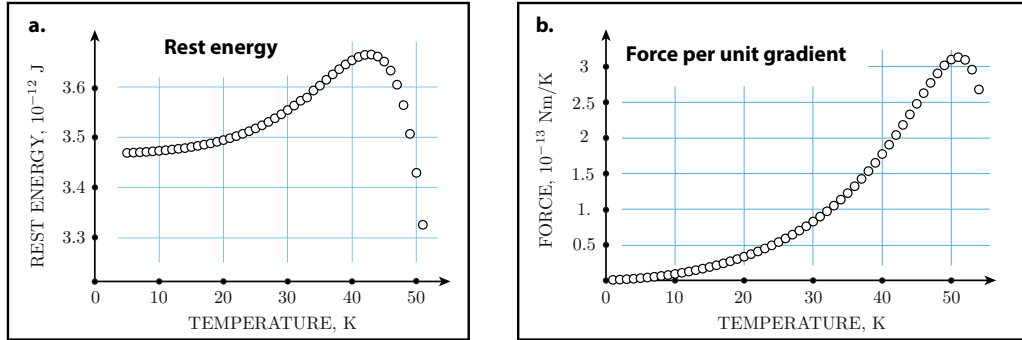


Figure 6.4: Calculated rest energy and gradiental force of a single skyrmion in the ferromagnetic background (above saturation field) for different temperatures, where the temperature-dependent magnetization data are available. (a) Skyrmion exists in a metastable state ( $E > 0$ ) above saturation field, with its maximum rest energy near the ordering temperature. (b) the resulting thermal-gradient force is co-directed with temperature gradient (i.e. skyrmions are moving from colder to hotter areas), as  $dM/dT < 0$  (see main text).

as most calculations are done for fixed length of magnetic moments. This apparently simple model however gives deeper insights on reasons why skyrmions can move against thermal gradient, and this reason is hidden in their topologically-dictated energetics.

## 6.2 TOPOLOGICALLY-PRESERVED CROSSOVER BETWEEN SKYRMIONS AND MAGNETIC BUBBLES IN THIN FILMS

While magnetic bubbles had been attracting attention in past as information carriers in promising bubble memory technology (see e.g. Ref[186] and references therein), they could not compete with other memory technologies, such as Flash RAM, because of the micrometer bubble size, which was too large for the industry. The discovery of magnetic skyrmions, a similar topological structures but of the nanoscale size, stabilized by the chiral interaction, gave a boost for studying skyrmions both in thin films and bulk materials. However, one of the intriguing observation is the broad dispersion in skyrmion sizes: from nanometers to micrometers, which may indicate a possible skyrmion-bubble crossover in systems with broken chiral symmetry.

The difference between skyrmions and magnetic bubbles is following: in skyrmions the points down at the very center, and then almost linearly evolves towards pointing up at the periphery of the skyrmion, and this rather linear progression comes essentially from the competition between Heisenberg exchange  $J(\nabla\mathbf{S})^2 \sim 1/x^2$  and chiral DMI coupling  $D\mathbf{S} \cdot (\nabla \times \mathbf{S})^2 \sim 1/x$ , thus for rather small  $x$  and without anisotropies  $\theta \propto x$  (see Figure 2.8). The chiral magnetic bubbles are another types of magnetic defects, with a wide spin-down plato forming the core of the bubble, – usually stabilized by interplay of anisotropies and dipolar interactions, – and the a rather thin wall where the spins rapidly twist as parallel to the field (see Figure 6.5). The bubbles are usually topologically trivial ( $Q = 0$ ), however there are indeed chiral bubbles where on the periphery spins manifest a fixed sense of rotation and thus the topological charge is finite.

The two objects, – magnetic skyrmions and chiral magnetic bubbles, – even though very different in key mechanisms leading to their stabilization, are however identical topologically speaking. The skyrmion and chiral magnetic bubble can have the same topological properties: they are both homeomorphic to a sphere with tilted spins, and one can obtain both the skyrmion and the bubble by using two different sphere-to-plane projectors (See Figure 6.5 ). Both the bubble and the skyrmion are topologically protected objects, and may be described within similar physical approaches, so one may expect to find a crossover. Because this crossover respects the topology of the magnetic skyrmions, one may hope to find it with a continuous change of parameters. This study shows that, indeed, the crossover between magnetic skyrmions and magnetic bubbles can happen with tuning either (uniaxial) anisotropy or stray field strength.

We consider both the magnetic bubbles and skyrmions in the quasiclassical continuous-field approximation, i.e. magnetization is a smoothly varying function from site to site.



For the convenience, we use the spherical parametrization for the local magnetization,  $\mathbf{M} = M_s (\sin\theta \cos\psi, \sin\theta \sin\psi, \cos\theta)$ , while the spatial coordinates are considered in cylindrical frame  $(\rho, \varphi, z)$  due to axial symmetry of a single skyrmion or magnetic bubble (see Chapter 2). As a reminder, the rotationally-invariant vortices are described by  $\theta = \theta(\rho)$  and  $\psi(\varphi) = m\varphi + \gamma$ , where  $m$  is an integer called vorticity, taken here as  $m = 1$ .

The main idea of the approach is to write down the energy functional, suitable for both skyrmions and (chiral) bubbles, and look for the stable spin configurations by solving a variational problem, i.e. minimizing the energy. We expect that for the same functional there are sets of parameters giving a skyrmion or a bubble as a stable solution. We consider a generalized energy functional of the form

$$W[\mathbf{M}(\mathbf{r})] = \int d^3 \mathbf{r} \left\{ J \sum_{i,j} \left( \frac{\partial M_i}{\partial x_j} \right)^2 + D \mathbf{M} \cdot (\nabla \times \mathbf{M}) - \mathbf{M} \cdot \mathbf{H} \right\} + W_A + W_{\text{str}}, \quad (6.9)$$

where  $J$  is the Heisenberg stiffness,  $D$  is Dzialoshkiy-Moriya interaction (DMI),  $\mathbf{H}$  is magnetic field,  $W_A$  is an anisotropic term and  $W_{\text{str}}$  is the energy of the stray field. The Dzialoshinskiy-Moriya interaction is responsible for stabilization of a skyrmion, however magnetic bubbles do not require this condition. In this study, we consider for definiteness the effect of the uniaxial anisotropy with the strength  $K$ .<sup>3</sup> The energy functional can be reduced to the functional of the azimuthal angle  $\theta(\rho)$ , that is

$$W = 2\pi z_0 \int_0^\infty dr \, r \left\{ J M_s^2 \left[ \left( \frac{d\theta}{dr} \right)^2 + \frac{\sin^2 \theta}{r^2} \right] + D M_s^2 \left( \frac{d\theta}{dr} + \frac{\sin 2\theta}{2r} \right) + K M_s^2 \sin^2 \theta + (M_s H - 2\pi M_s^2)(1 - \cos \theta) - 2\pi M_s^2 \cos \theta(r) I(r) \right\}, \quad (6.10)$$

with the stray field term

$$I(r) = \frac{1}{z_0} \iint (1 - e^{-kz_0}) J_0(kr) J_0(kr') [1 - \cos \theta(r')] r' dr' dk, \quad (6.11)$$

where the stray field energy is considered for the infinite plate of thickness  $z_0$ , see Refs. [187, 188], where  $J_0(x)$  are the zeroth-order Bessel functions. Some simplifications can be done by dropping the constant term and rewriting the functional in the following

---

<sup>3</sup>The lowest-order uniaxial anisotropy is of type constant  $+ K(\mathbf{M} \cdot \hat{e}_z)^2$ , thus effectively  $K \cos^2 \theta$ . This leads to term  $K \sin^2 \theta$  in Eq.(6.9) where the energy of a topological object is calculated with respect to the ferromagnetically-ordered background (e.g. in the field-polarized phase). The sign of  $K$  should be such that  $DK > 0$ .

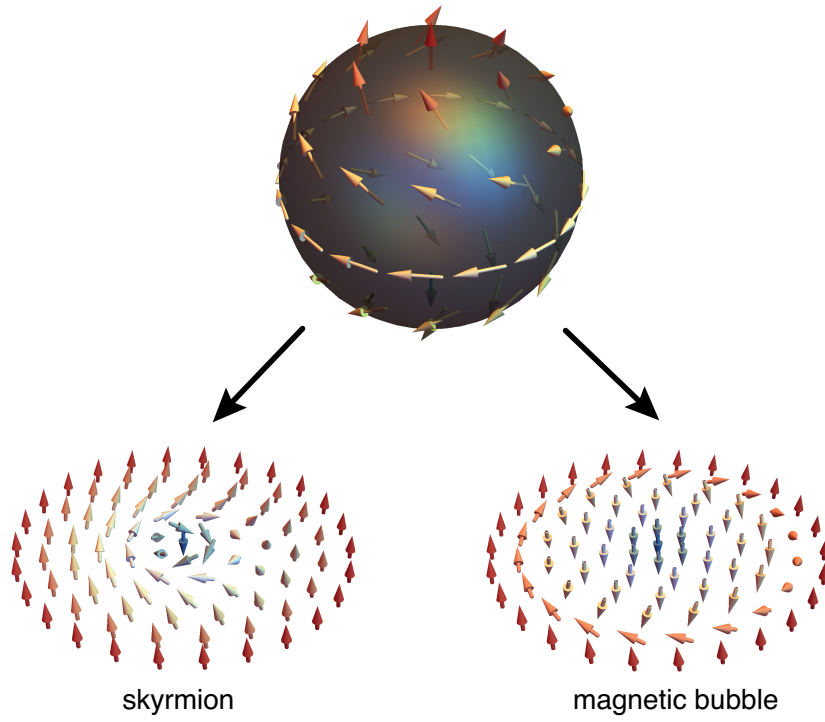


Figure 6.5: A sphere with tilted spins can be projected to the skyrmion (left) or a magnetic bubble (right) spin structure, both of them possess the same topological charge. [Here, the length scales are not kept as magnetic bubbles are usually much larger than skyrmions].

form

$$w = \frac{W}{M_s^2 z_0} = 2\pi \int_0^\infty dr \, r \left\{ J \left[ (\theta'_r)^2 + \frac{\sin^2 \theta}{r^2} \right] + D \left( \theta'_r + \frac{\sin 2\theta}{2r} \right) + K \sin^2 \theta + h(1 - \cos \theta) + 2\pi \cos \theta(r)(1 - f(r)) \right\}, \quad (6.12)$$

where we have introduced the dimensionless magnetic field  $h = H/M_s$ , and the stray functions

$$f(r) = \int_0^\infty G(r, r'; z_0) [1 - \cos \theta(r')] r' dr', \quad (6.13)$$

with the "Green function"

$$G(r, r'; z_0) = \frac{1}{z_0} \int_0^\infty (1 - e^{-kz_0}) J_0(kr) J_0(kr') dk. \quad (6.14)$$

it is useful to derive the (very) thin film asymptote, that is  $z_0 \ll 1/k_0 = J/Da$ ,

$$G(r, r'; z \ll k_0) \simeq \int_0^\infty J_0(kr) J_0(kr') k dk = \frac{\delta(r - r')}{r}, \quad (6.15)$$

and therefore

$$f(r)|_{z_0 \ll \lambda} \simeq \int_0^\infty \frac{[1 - \cos \theta(r')] \delta(r - r') r' dr'}{r} = 1 - \cos \theta(r). \quad (6.16)$$

The variational minimization of Equations (6.12), (6.16) gives the answer whether do we have a magnetic bubble ( $\theta(r)$  behaves as a smoothed step function) or a skyrmion ( $\theta(r)$  rapidly falls down and has an exponentially small tail).

Surprisingly, the crossover between the skyrmions and bubbles can be already seen even in the  $z_0/a \rightarrow \infty$  approximation, i.e. even if neglecting the stray field. (The dimensionless stray field strength  $\sigma$  is roughly  $\sigma \propto a/z_0$  for large  $z_0$ ). For this, the energy functional can be rewritten in dimensionless parameters as

$$W/(JM_s^2 a^2 z_0) = 2\pi \int_0^\infty dr \, r \left\{ \left( \frac{d\theta}{dr} \right)^2 + \frac{\sin^2 \theta}{r^2} + d \left( \frac{d\theta}{dr} + \frac{\sin 2\theta}{2r} \right) + \kappa \sin^2 \theta + h(1 - \cos \theta) \right\}, \quad (6.17)$$

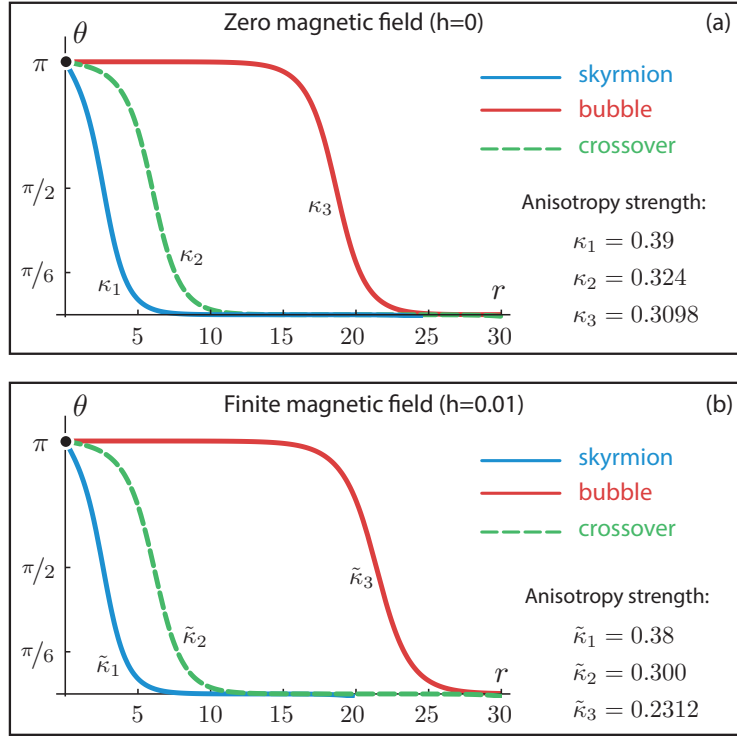


Figure 6.6: Crossover between magnetic skyrmions and magnetic bubbles in zero (a) and (b) finite magnetic fields, neglecting the stray field effect. x Surprisingly, the crossover can be seen even in the zero magnetic field by tuning the anisotropy strength  $\kappa$  by 25%, see inset (a). The moderate (for  $\text{Cu}_2\text{OSeO}_3$ ) magnetic field  $h = H/Ja^2M_s = 0.01$  affects mainly the bubble radius. For calculations, the dimensionless DMI is set  $d = 1$ .

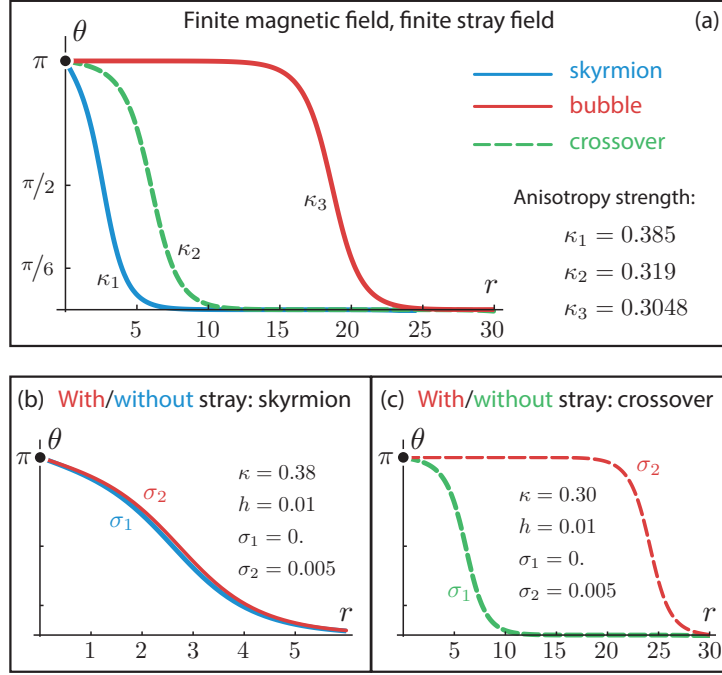


Figure 6.7: Influence of the stray field on the skyrmion-to-bubble crossover: (a) the qualitative picture holds the same; magnetic field  $h = 0.01$ , stray field strength  $\sigma = h/2$  (b) the stray field just slightly effects the skyrmion (b) however, for the given  $\kappa$ , the crossover skyrmion is very sensitive to the same stray field and it turns into a bubble.

where the dimensionless parameters are:

$$d = \frac{D}{Ja}, \quad \kappa = \frac{K}{Ja^2}, \quad h = \frac{H}{Ja^2 M_s}. \quad (6.18)$$

As an example, for  $\text{Cu}_2\text{OSeO}_3$ ,  $d \approx 0.23 \sim 1$ . In this study, we fix  $d = 1$ , and tune anisotropy and magnetic field to change. We solve the variational problem by applying the shooting method to Euler-Lagrange equation. For definiteness, throughout all the calculation we call the solutions satisfying  $\frac{1}{\pi}\theta'(0) = 0.1$ ,  $\frac{1}{\pi}\theta'(0) = 0.01$ , and  $\frac{1}{\pi}\theta'(0) = 10^{-6}$  as the skyrmion, the crossover, and the bubble correspondingly, and look how the tuning parameters changes.

The first set of results, corresponding to the skyrmion-to-bubble crossover if neglecting the stray field, is shown on Figure 6.6. The inset (a) shows the crossover between the skyrmion (blue solid line,  $\kappa_1 = 0.39$ ) and magnetic bubble (red solid line,  $\kappa_3 = 0.3098$ ). The crossover skyrmions are visually close to the skyrmion solution, however in terms of the tuned anisotropy ( $\kappa_2 = 0.324$ ), it is closer to the bubble solution ( $\kappa_3 = 0.3098$ ). Indeed, while increasing  $\kappa_2$  just slightly, the radius of the skyrmion-bubble grows abruptly. Note that the numerical method used is controllable both for the skyrmion and bubble

solution, however one needs a greater accuracy for  $\kappa_3$ . The inset (b) shows the similar results in the finite magnetic field  $h = 0.01$ . Qualitatively the physics of the crossover holds the same, however the magnetic bubble becomes larger and the required anisotropies now are shifted  $\tilde{\kappa}_1 = 0.38$ ,  $\tilde{\kappa}_2 = 0.300$ ,  $\tilde{\kappa}_3 = 0.2312$  (i.e. still corresponding to  $\frac{1}{\pi}\theta'(0) = 0.1$ ,  $\frac{1}{\pi}\theta'(0) = 0.01$ ,  $\frac{1}{\pi}\theta'(0) = 10^{-6}$ ).

The second set of results takes into account a moderate stray field  $\sigma$ . These results are summarized on Figure 6.7. The inset (a) shows the crossover between the skyrmion (blue) to the magnetic bubble (red) in finite magnetic field  $h = 0.01$  and stray field with strength  $\sigma = h/2$ . The qualitative physics of the crossover remains mainly the same, showing that the crossover-skyrmion is unstable towards the bubble, with  $\kappa_1 = 0.385$ ,  $\kappa_2 = 0.319$ ,  $\kappa_3 = 0.3048$  again for  $\frac{1}{\pi}\theta'(0) = 0.1$ ,  $\frac{1}{\pi}\theta'(0) = 0.01$ ,  $\frac{1}{\pi}\theta'(0) = 10^{-6}$ , correspondingly. The inset (b) shows that the stray strength  $\sigma = 0.005 = h/2$  almost does not affect the skyrmion solution, acting just like a small perturbation. This is however not true for a crossover region, see the inset (b): the same stray strength  $\sigma = 0.005$  pushes the crossover skyrmion (green) to a magnetic bubble (red). The stronger stray fields can even make the bubble solution unstable.

We highlight here briefly the main features of the skyrmion/bubble crossover: (I) the adiabatic (slow and continuous) tuning of  $\kappa$  reveals the abrupt behaviour in the skyrmion-bubble crossover, i.e. the radius of a skyrmion changes rapidly with just a tiny tuning of the control parameter  $\kappa$ ; (ii) surprisingly, the crossover seems to happen even when the stray field is neglected, as in the bulk systems. (iii) furthermore, the crossover can be observed even in the zero magnetic field, of course if the skyrmion has a sufficient lifetime. (iv) the qualitative picture with the moderate stray field remains similar, showing that the continuous crossover from a skyrmion to bubble is possible. However, the crossover region is very sensitive even to the small stray fields (large thickness of material), and it can happen that the solution becomes unstable if we try to push the skyrmion-bubble radius.

## A NOTE ON SCALING LENGTHS

DIMENSIONAL ARGUMENT. – We start for the effective quadratic form with second-order anisotropy

$$\mathcal{H}_{\text{eff}} = \int \frac{dV}{V} \left\{ J(\nabla \mathbf{S})^2 + D \mathbf{S} \cdot (\nabla \times \mathbf{S}) + K S_\rho^2 \right\}. \quad (6.19)$$

We now discuss the scaling arguments which follows from the natural length-scales which can be introduced in the system. First, we consider dimensionalities (denoted as [...]) of  $J$ ,  $D$ ,  $K$  (in SI):

$$[J] = \frac{J}{\text{m}^3} \times \text{m}^2 = \frac{J}{\text{m}}, \quad [D] = \frac{J}{\text{m}^3} \times \text{m} = \frac{J}{\text{m}^2}, \quad [K] = \frac{J}{\text{m}^3}, \quad (6.20)$$

We ask what are the most general scaling supported by the system. One would expect the domain-wall width  $\pi(J/K)^{1/2}$ , however as we shall see the result is more interesting. We are looking for a typical spatial parameter (in meters) which can be, in the most general case, a combination between  $J$ ,  $D$ ,  $K$ ,

$$J^\alpha D^\beta K^\alpha$$

where  $\alpha, \beta, \gamma$  are real numbers. We demand now that this combination has a dimensionality of length  $[L]$ ,

$$[J^\gamma D^\beta K^\alpha] \equiv [L], \quad \rightarrow \quad \left(\frac{J}{m}\right)^\gamma \times \left(\frac{J}{m^2}\right)^\beta \times \left(\frac{J}{m}\right)^\alpha = m, \quad (6.21)$$

Thus we obtain the system of coupled equations,

$$\alpha + \beta + \gamma = 0, \quad 3\alpha + 2\beta + \gamma = -1, \quad (6.22)$$

We have 2 equations and 3 unknowns. Thus we fix one of the unknowns as a parameter ( $\alpha$ ), and the solution is  $\gamma = \alpha + 1$ ,  $\beta = -1 - 2\alpha$ . Therefore the generalized scaling length is

$$L_\alpha \sim \frac{J^{\alpha+1} K^\alpha}{D^{2\alpha+1}}. \quad (6.23)$$

In particular, this qualitative scaling argument leads to the following length scales:

$$\text{Domain wall width } (\alpha = -1/2) \quad \rightarrow \quad L_{-1/2} \sim \left(\frac{J}{K}\right)^{1/2}, \quad (6.24)$$

$$\text{Skyrmion lattice } (\alpha = 0) \quad \rightarrow \quad L_0 \sim \frac{J}{D}. \quad (6.25)$$

Note that other scaling options are also possible. For example, for a skyrmion asymptote within model (6.19), numerical fit gives  $\alpha \approx -2$ .

#### SKYRMION-BUBBLE RADIUS VS. CROSSOVER PARAMETER

As we have seen previously, the skyrmion-to-(chiral)bubble crossover is already captured by a simple model in the absence of magnetic field and stray field. In this subsection, I present calculations for one of a very promising system where skyrmion-bubble crossover seems to have place [56]. We start from the effective energy density ( $H = 0$ ),

$$\mathcal{H}_{\text{eff}} = \int \frac{dV}{V} \left\{ J(\nabla \mathbf{S})^2 + D \mathbf{S} \cdot (\nabla \times \mathbf{S}) + K S_\rho^2 \right\}. \quad (6.26)$$

First, to estimate the characteristic parameters of the system, we choose the typical values of  $J, D, K$  as in Ref. [56],  $J = 2 \times 10^{-11} \frac{J}{m}$ ,  $D = 5 \times 10^{-4} \frac{J}{m^2}$ ,  $K = 2.8 \times 10^5 \frac{J}{m^3}$ . These numbers correspond to the following characteristics: domain wall width  $l_{DW} = \pi \sqrt{J/K} = 26.5 \text{ nm}$ , helix period  $\lambda = 4\pi J/D = 500 \text{ nm}$ , and critical DMI:  $D_c = \frac{4}{\pi} \sqrt{JK} = 3 \times 10^{-3} \frac{J}{m^2}$ . Note that the only dimensionless parameter in the system is  $\varkappa = JK/D^2 = 22.4$ . As the length scale for the size of a pure individual skyrmion in zero field is, as a general rule, comparable with DW width  $\pi \sqrt{J/K}$ , when we look at the inflation of a skyrmion to a chiral bubble, it would be better to separate this normal variation for a pure skyrmion due to changes in  $J$  or  $K$  from what is due to a transition to bubble. Thus we are looking at the transition at different  $D$  as  $\pi \sqrt{J/K}$  does not depend on  $D$ . For this, we rescale

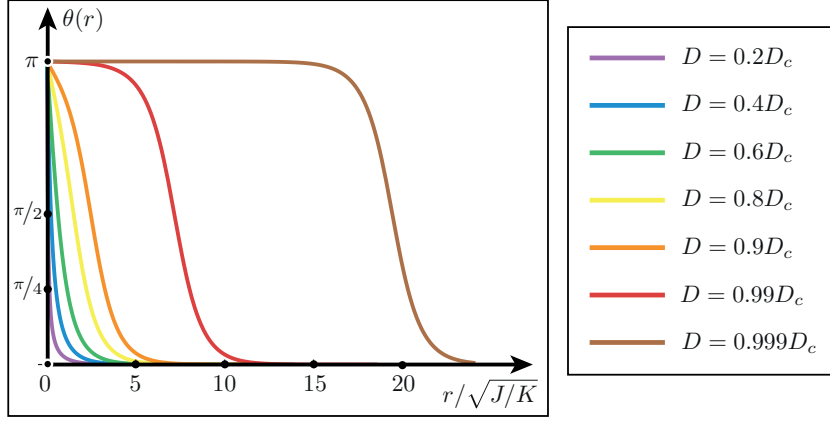


Figure 6.8: Crossover between skyrmions and magnetic bubbles in zero magnetic field and zero stray field, for different values of DMI parameter. Distance from the center of a skyrmion(bubble) is given in units  $\sqrt{J/K}$ . The skyrmion-to-(chiral)bubble crossover is very sensitive to the value of  $D$  and happens in the vicinity of  $D_c = \frac{4}{\pi}\sqrt{JK}$ .

the effective energy with  $r \rightarrow x = r/\sqrt{J/K}$ ,  $HM_s \rightarrow h = HM_s/K$ , and  $D \rightarrow d = \frac{\pi}{4}\frac{D}{\sqrt{JK}}$ . Thus, varying the energy, the dimensionless Euler-Lagrange equation takes shape

$$\frac{d^2\theta}{dx^2} + \frac{1}{x}\frac{d\theta}{dx} - \frac{\sin 2\theta}{2x^2} + \frac{4}{\pi}\frac{D}{D_c}\frac{\sin^2\theta}{x} - \frac{1}{2}\sin 2\theta = 0. \quad (6.27)$$

We solve this equation for boundary conditions  $\theta(0) = \pi$  (spin downwards in the center) and  $\theta(\infty) = 0$  (spins up at infinity). Several different solutions, including chiral bubbles, are shown on Figure 6.8. We notice that the crossover between skyrmions and magnetic bubbles is very sensitive to the DMI parameter. We thus introduce a more sensitive crossover parameter  $\sigma$ ,

$$\sigma = \ln\left(1 - \frac{D}{D_c}\right)^{-1}, \quad D_c = \frac{4}{\pi}\sqrt{JK}, \quad (6.28)$$

which is a dimensionless quantity in order of  $10^0 - 10^1$ , typically.<sup>4</sup>

The next step we plot the evolution of the skyrmion radius versus the crossover parameter  $\sigma$ . To be on the same foot for both the skyrmion and bubble branches, we define the radius  $R$  of a topological object under study as  $\theta(R) = \pi/2$ , that is the distance from the skyrmion center where spins are orthogonal to the external magnetic field (if a tiny one is present to define the skyrmion axis). After finding numerically for several  $\sigma$  the angular profile  $\theta(r)$  and solving the inverse problem  $2\theta(R)/\pi = 1$ , we plot

<sup>4</sup>Note that for extremely small  $D \rightarrow 0$ , the skyrmions-like topological objects can no longer exist (Derrick theorem, see [189]). Thus the skyrmionic solution of (6.27) naturally breaks down at very small  $D$  (corresponding to very small  $\sigma$ ). It would be interesting to address this minimal- $D$  criterion in future studies.



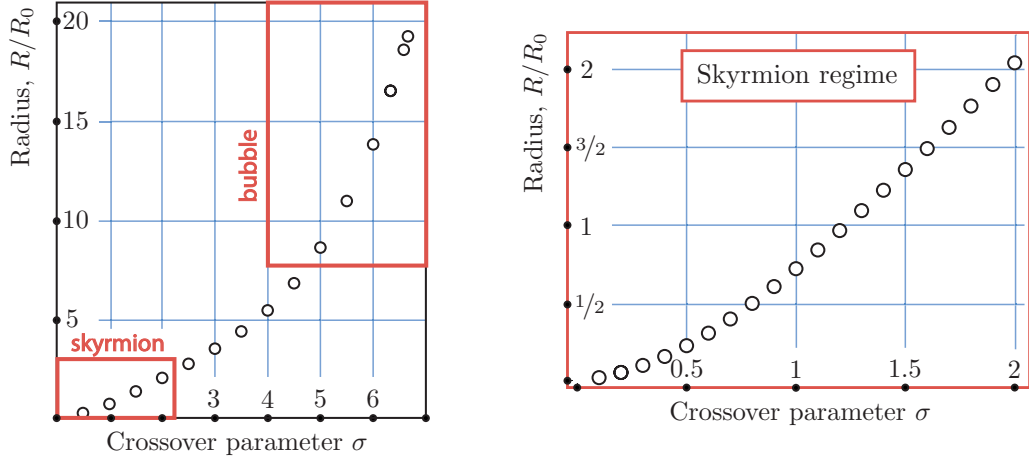


Figure 6.9: Radius of a topological object (skyrmion or chiral bubble) in units of  $R_0 = \sqrt{J/K}$  versus dimensionless crossover parameter  $\sigma = \ln(1 - D/D_c)^{-1}$  (see main text). The crossover from skyrmions to bubbles is assumed to take place around  $\sigma \approx 3$  where the radius of the crossover skyrmion is of order  $2 \times \sqrt{J/K}$ , and its profile is convex (see Figure 6.8). The "pure" chiral-bubble solution appears at around  $\sigma \approx 4$ , with radius two orders of magnitude larger than in the ultimate small-skyrmion limit  $\sigma \ll 1$ .

the dependence  $R(\sigma)$  on Fig.6.9. Remarkably, in the skyrmion regime, the skyrmion radius is non-vanishing even for  $D = 0$ , however is rather small, that is  $R_{\min} = 0.015 \times \sqrt{J/K}$  so they are (most likely) physically unstable with the radius less than the lattice constant; and then grows rather fast with  $\sigma$  as a nontrivial power law. It is still hard to distinguish where the "pure" skyrmion branch distinguished  $\sigma \lesssim 2$ , the radius is  $\approx 2\sqrt{J/K}$ , which visually looks more like a bubble (see Fig. 6.8). However, there is a rather clear crosser towards the chiral bubbles: at  $\sigma \approx 4$ , the radius of abruptly grows, indicating a pure bubble solution. For  $D/D_c > 1$  no radially symmetric, topologically nontrivial spin structures exist. This may or may not indicate a crossover towards a skyrmion lattice, as in this case  $\sqrt{J/K} \sim J/D$ , or a breakdown to other phase with topologically trivial (non-chiral) bubbles.

Another interesting question which rises here, is what is the nature of nearly power-law scaling  $R(\sigma)$  in the skyrmion regime. This needs further discussion and may be further addressed by considering the scaling flows. Even though not directly related to the crossover towards the chiral bubbles, this feature indicates that it is in fact impossible to introduce the universal length scale even in the limit  $D \ll D_c$ , where one would expect something simple as  $\sqrt{J/K}$ . The impossibility of introducing the universal length scale is usually a good hallmark for qualitatively different physics in the system.

Thus we numerically established that there are systems in which the same energy functional gives both skyrmionic and chiral-bubble solutions, which are topologically undistinguishable.

### 6.3 MERONS, BIMERONS AND TOY MODEL OF TOPOLOGICAL CHARGE SATURATION

Since I started studying magnetic skyrmions in early 2015, I was appealed on how come a topological magnetic phase abruptly emerges from what seems to be a topologically-trivial (helical or conical) phase. Granted, there are several both numerical and semi-analytical approaches on calculating magnetic phase diagram of skyrmion-hosting compounds, but to my experience none of them directly tackles this question. Thus to address the issue on how the topological charge appears from a trivial single-helix phase, I below propose a model which tracks the evolution of topological charge density under magnetic fields, and, indirectly, temperatures.

In an idealized situation, the helical phase is topologically trivial: it constitutes of infinitely long helical stripes, and the integrated scalar Berry field  $\mathfrak{B} = \frac{1}{2} \mathbf{m} \cdot \partial_x \mathbf{m} \times \partial_y \mathbf{m}$  vanishes for any chosen region. In reality nevertheless, it is not the ultimate truth, as the helical phase often constitutes from multiple helical domains. If one further zooms on how a helical stripes ends on the domain wall, one finds that it ends with a topologically-nontrivial object called a meron [190]. A meron is a half-skyrmion ( $Q = 1/2$ ) which is situated on the ends of a helix line (see Figure 6.10). To dissect a helix stripe into two stripes, one therefore needs to inject at least 2 merons. By definition, an object consisting of two merged merons is called a *bimeron*, and it is topologically equivalent to a skyrmion. The amount of helical domains, and thus, the number of merons in the system, is known to be related with the strength of applied magnetic field: in higher fields we have more merons within the helical phase. In this section I therefore propose a phenomenological model for topological charge saturation based on this observation.

The idea of the calculation is following: by applying the magnetic field the probability of nucleating more merons in the system increases. Therefore, the average topological charge density in the system is evolving from zero (in the ground state, i.e. the single-domain infinite helical phase) to a maximum (in the skyrmion phase). We expect that

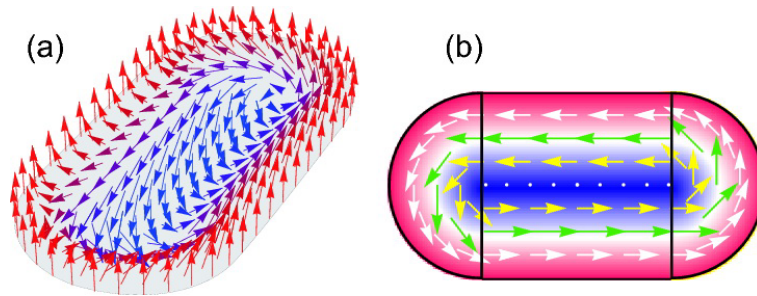


Figure 6.10: An illustration of a bimeron: a 3D scheme (a) and a top view (b). A single meron is a half-skyrmion as schematically separated on the left and right of subfigure (b). Several elongated bimerons piled parallel to each other constitute a helical domain with a non-zero topological charge on the edge. Figures from Ref.[190].

the helical-to-skyrmion phase transition happens when the topological charge density saturates to its maximum, thus representing an array of densely packed skyrmions. Even though the skyrmion phase in thin films reminds more of an (interacting) skyrmion liquid, to recognize the effect of topological charge saturation in its pure form we consider an idealized model of topological transition from the helical phase towards the ideal skyrmion gas (i.e. array of non interacting skyrmions).<sup>5</sup>

We start from considering an effective free energy of noninteracting meron gas. Merons are distributed in pairs through the helical phase. Adding more merons in the system breaks already existing helical channels into two parts. We therefore divide the space into  $N_i$  cells of a typical meron-pair size and consider the situation when the  $n_i$  meron pairs cannot overlap. The entropy of the meron gas is thus given by

$$S = \ln \mathfrak{P} = \ln \prod_i \frac{N_i!}{n_i!(N_i - n_i)!} \quad (6.29)$$

$$= \sum_i (\ln N_i! - \ln n_i! - \ln(N_i - n_i)!) \quad (6.30)$$

$$\simeq \sum_i (N_i \ln N_i - n_i \ln N_i - (N_i - n_i) \ln(N_i - n_i)), \quad (6.31)$$

where we used in (6.31) the Stirling's formula for factorial. We hence construct the free energy in conventional way  $F = E - TS$ , which upon substitution (6.31) yields

$$F = \sum_i [2(\epsilon_{\text{meron}} - \Delta_{\text{meron}}(H)) n_i - T(N_i \ln N_i - n_i \ln n_i - (N_i - n_i) \ln(N_i - n_i))], \quad (6.32)$$

where  $\Delta_{\text{meron}} = \alpha H$  is the Zeeman energy contributed by a meron with respect to the helical background, and  $\epsilon_{\text{meron}}$  is the field-independent energy contribution (in the helical phase,  $\epsilon_{\text{meron}} > 0$ ). Taking now a variation with respect to number of meron pairs  $n_i$ , one obtains

$$\frac{1}{T} \frac{\delta F}{\delta n_i} = \sum_i \left[ 2\beta(\epsilon_{\text{meron}} - \Delta_{\text{meron}}(H)) - \ln \frac{N_i - n_i}{n_i} \right] = 0, \quad (6.33)$$

which immediately gives the fluctuationally-averaged number of meron pairs in the system  $\bar{n}_i = n_i / N_i = \{1 + \exp[2\beta(\epsilon_{\text{meron}} - \Delta_{\text{meron}}(H))]\}^{-1}$ . As each of the meron pair in our model carries  $1/2 + 1/2$  topological charge, the fluctuationally-averaged topological charge in the helical phase upon increasing magnetic field evolves as

---

<sup>5</sup>Surprisingly, a qualitatively correct physics is captured already in the ideal-gas approximation for meron distribution [190].

$$Q(H) = Q_{\max} \left( \frac{1}{2} + \frac{1}{2} \tanh \frac{\epsilon_{\text{meron}} - \Delta_{\text{meron}}(H)}{T} \right), \quad (6.34)$$

and, more importantly, reaches the saturation around

$$\Delta_{\text{meron}}(H_*) \approx \epsilon_{\text{meron}}, \quad \rightarrow \quad \text{Topological Charge Saturation (TCS)}. \quad (6.35)$$

Note that formula catches several important features of the helical-to-skyrmion transition: (i) in ground-state helical phase  $\Delta_{\text{meron}}(H_*) \ll \epsilon_{\text{meron}}$ , the topological charge is vanishing,  $Q(H \approx 0) \approx 0$ , manifesting sufficiently large helical domains  $L^2 \gg J^2/D^2$ ; (ii) the topological charge goes from (almost) zero to a rapid saturation at some critical field  $H_* = \epsilon_{\text{meron}}/\alpha$ , thus reminding the first critical field  $H_{c1}$  determining the boundary between helical and skyrmion phase; we show below that for thin films  $H_* \propto D^2/J$ . For order-of-magnitude estimates, the "rest energy" (per thin-film thickness) of a meron confined by helical lines is of order  $\epsilon_{\text{meron}} \propto J$ , the dimensional analysis gives Zeeman energy roughly  $\Delta_{\text{meron}} \propto JH/D^2$ , thus  $\alpha \sim J^2/D^2$ ; here  $M = 1$ ,  $a = 1$  for simplicity. This, as we will see below, gives an estimate for the width of transition  $\Delta H/H_* \propto T/Jz_0$ , where  $z_0$  is the thickness of the thin film.

We introduce the normalized topological charge<sup>6</sup>  $q(H) = Q(H)/Q_{\max}$  and simplify the formula for TCS (6.35) as

$$q(H) = \frac{1}{2} + \frac{1}{2} \tanh \frac{H - H_*(T)}{\Delta H}. \quad (6.36)$$

This formula is sketched on Figure 6.11. We note that  $e^{-2Jz_0/T}$  is roughly a probability of spontaneous creation of a meron pair in the helical phase ( $H = 0$ ); in other words, it is of the same order as the density of merons in the system. As in the low fields this density is very low, we thus come to conclusion that  $\Delta H/H_* \ll 1$ . This simple estimate clearly indicates a rapid transition to the skyrmion phase near  $H = H_*(T)$ , which has the maximum topological charge among available thermodynamic phases. We also note that taking into account  $M = M(T)$ , both  $H_*$  and  $\Delta H$  are temperature-dependent.

We now estimate the energy of a single meron with respect to the helical phase. For this, we start from the minimal model

$$\langle W_{\text{meron}} \rangle \simeq M^2 \int_0^\pi d\varphi \int_0^R dr r \left\{ J \left[ \left( \frac{d\theta}{dr} \right)^2 + \frac{\sin^2 \theta}{r^2} \right] + D \left( \frac{d\theta}{dr} + \frac{\sin 2\theta}{2r} \right) - \frac{H}{M} \cos \theta \right\}, \quad (6.37)$$

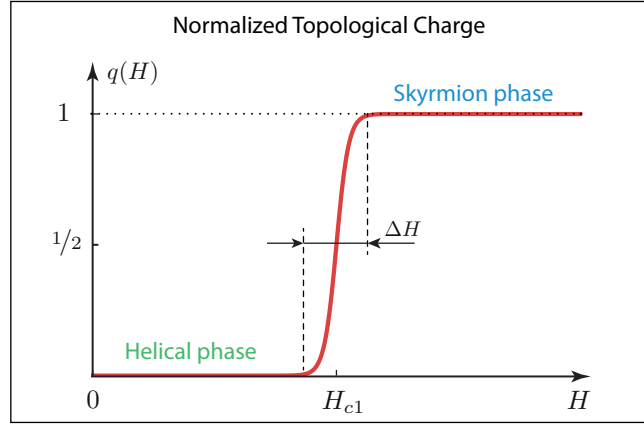


Figure 6.11: Normalized topological charge as the function of magnetic field  $H$ . In the helical phase ( $H < H_{c1}(T)$ ), the normalized topological charge is almost zero, while it goes to the saturation around  $H_{c1}$ . When the topological charge density is sufficient to create the Skyrmion lattice, the SkL phase becomes dominant for  $H > H_{c1}$ . This model however does not captures the skyrmion-to-field-polarized crossover ( $H_{c2}$ ), as the bimeron mechanism is no longer appropriate. For visualization, we adopt  $\Delta H = 0.05H_{c1}$ , while the numerical estimates give even more abrupt crossover,  $\Delta H/H_{c1} \sim 10^{-3} - 10^{-4}$ .

For numerical calculations, it is more convenient to introduce dimensionless variables by measuring rest energy of a skyrmion in units of  $JM^2$  ( $M^2 = M^2(T)$ ) and radial distance in units of lattice parameter  $x = r/a$ ,

$$\frac{\langle W_{\text{meron}} \rangle}{JM^2} \simeq \pi \int_0^{\lambda/2} dx x \left[ \theta_x'^2 + \frac{\sin^2 \theta}{x^2} + 2k_0 \left( \theta_x' + \frac{\sin 2\theta}{2x} \right) - 2\mathfrak{h} \cos \theta \right] \quad (6.38)$$

$$= \pi \int_0^{1/2k_0} dx x \left[ (\theta_x' + k_0)^2 - k_0^2 + \frac{\sin^2 \theta}{r^2} + k \frac{\sin \theta}{r} - 2\mathfrak{h} \cos \theta \right] \quad (6.39)$$

where we have introduced the dimensionless helical period  $\lambda = 2\pi/k_0$  (in units of  $a$ ), with  $k_0 = Da/2J$  (i.e. modulation vector  $D/2J$  times lattice constant  $a$ ), as also dimensionless magnetic field  $\mathfrak{h} = Ha^2/2JM$ . After that, we solve the variational problem with respect to the configuration  $\theta(r)$  which minimizes the meron energy for given  $k_0$  and  $\mathfrak{h}$ , as was discussed in Chapter 2.

The energy of a helical stripe per unit length is

$$\frac{\langle W_{\text{hel}} \rangle}{JM^2 \Delta l} \simeq \int_0^\lambda dx \left[ (\theta_x' + k_0)^2 - k_0^2 - 2\mathfrak{h} \cos \theta \right]. \quad (6.40)$$

<sup>6</sup>Below we consider for simplicity topological charge packing with effective occupancy  $\pi/4$ .

To compare the meron with the helical phase we consider a cell  $\lambda \times \lambda/2$ . The resulting energetics of a meron merged on the helical stripe roughly determines the self-adjusted quantities  $\epsilon_{\text{meron}}$ ,  $\Delta_{\text{meron}}(\mathfrak{h})$  as

$$\mathcal{E}(\mathfrak{h}) \equiv \epsilon_{\text{meron}} - \Delta_{\text{meron}}(\mathfrak{h}) \simeq 2JM^2 \left(1 - \frac{\mathfrak{h}}{\mathfrak{h}_*}\right), \quad \mathfrak{h}_* \approx k_0^2/4, \quad (6.41)$$

and thus restoring the dimensional units, one gets

$$\epsilon_{\text{meron}}(T) \simeq 2JM^2(T), \quad \Delta_{\text{meron}}(H) \simeq \frac{H}{H_*} \epsilon_{\text{meron}}(T), \quad H_*(T) \simeq \frac{D^2}{8J} M(T), \quad (6.42)$$

Thus according to (6.34), we have introduced  $\Delta H = T/\alpha = H_* T/\epsilon_{\text{meron}}$ , and hence for the relative width of topological-charge saturation (TCS width) in external magnetic fields we obtain estimate  $\Delta H/H_* = (\beta \epsilon_{\text{meron}})^{-1}$ ,  $\beta = 1/T$ , see (6.34). Taking now estimatively  $J \simeq 10^{-23} \text{ Jm/A}^2$ ,  $M_s \simeq 10^5 \text{ A/m}$ ,  $a \simeq 10^{-9} \text{ m}$  (we consider for simplicity a thin film with thickness  $z_0 \simeq 100a$ , without dipolar effects); for temperature  $T \approx 20 \text{ K}$ , one obtains  $\Delta H/H_* \approx 3\%$ , while for warmer conditions  $T = 50 \text{ K}$ , the TCS width is estimatively  $\Delta H/H_* \approx 7\%$ . Thus we have a reasonable agreement with available experimental signatures. We also come to conclusion that the TCS width is roughly proportional to temperature and drops inversely with the sample thickness (at least, if stray-field effects neglected). Thus the effect is expected to be rather crucial in the thin films than in the bulk crystals.

It is interesting to show that the topological charge saturation field  $H_*$  indeed corresponds to the first critical field  $H_{C1}$  which determines the helical-to-skyrmion phase transition if speaking energetically. Indeed, in the present model the energy of a skyrmion in the helical phase is given by  $\epsilon_{\text{skyrmion}} = 2(\epsilon_{\text{meron}} - \Delta_{\text{meron}}(H))$  (without interaction effects). We thus note that at  $H = H_*$  the skyrmion energy turns to zero with respect the helical phase, which qualitatively indicates the helical-conical phase transition [105, 190]. Therefore,  $H_*(T)$  is the first critical field  $H_{C1}(T)$  and the rapid saturation in topological charge described by (6.35) indeed reflects the topological phase transition.

Finally, I remind that the above calculations were done in approximation of non-interacting meron gas. In this approximation there is no difference between adding a skyrmion with a pair of merons or adding simply 2 pairs of merons [190]; however, because of interactions between topological charges, the energetics of the adding merons to the system is slightly perturbed. In particular, energetically 4 merons  $\neq$  2 merons + 1 skyrmion because of the skyrmion-meron interaction [150]. Of course, by including interactions one needs to consider the total accumulation of topological charge by all the (energetically different) players, – that is meron pairs, skyrmions, bimerons and other higher-order topological excitations. The qualitative physics however is the same even

in the later case, but it is less intuitive to distinguish what causes the rapid topological charge saturation and how it happens.

## 6.4 CONCLUSIONS

In this chapter I concluded with three different problems concerning physics of topological charges in thin films, namely: (i) moving magnetic skyrmion with thermal gradients, which is energetically cheap and easy; (ii) shown topologically-preserved crossover between (small) magnetic skyrmions and (huge) magnetic chiral bubbles, which is important because these objects are often confused in literature which apparently leads to a dissimilar reported data on both the sizes of "skyrmion-bubbles", their nucleation and mobilities; (iii) considered a problem of topological charge saturation during process of helical-to-conical phase transition; within the non-interacting model it was shown that the merons ( $Q = 1/2$  topological quasiparticles) are responsible for topological magnetic phase transition in this case. The merons can be to a good approximation considered as robust quasiparticles however they come in pairs in the form of helix-splitting meron couples, bimerons, skyrmions, and higher-order topological configurations.

Magnetic thin films is a very broad and exciting field of research, which potentially is more advantageous for skyrmionic applications than the bulk systems. In many cases it is possible to establish rather simple phenomenological models, and solve them analytically or semi-analytically, which is highly attractive for both fundamental and applied research, and I plan to focus on several eye-catching problems shortly.





# 7

## Conclusions and Overview

In this thesis, I thus presented theoretical results for application of different external stimuli to promote skyrmion stabilization and control, such as applying external electric fields, mechanical strains and uniform pressures, and thermal-gradient fields for skyrmion motion towards regions with enhanced stability. Different skyrmionic models as described in this thesis are taken under the umbrella title "Theories of the topologically-induced phenomena in skyrmion-hosting magnetoelectric insulators", as the papers which I co-author [95, 133, 157] and others under preparation consider experiments in the magnetoelectric insulator  $\text{Cu}_2\text{OSeO}_3$ . Thus one of the most intriguing results of this thesis (Chapter 4) is stabilization ("writing") and destabilization ("erasing") of the bulk skyrmion phase in magnetoelectric insulator  $\text{Cu}_2\text{OSeO}_3$  upon applying moderate electric fields of a few Volts per micrometer. Such electric fields are compatible with the modern microelectronic devices, which opens prospects for the further development of the skyrmion-based applications, in particular if room-temperature magnetoelectric skyrmion host is found. Importantly, many results of this thesis (such as e.g. Chapters 2,5,6) can be applied to a much broader class of (bulk) skyrmionic materials, namely chiral magnets without distinguishing in their conductive properties (e.g. both to metallic  $\text{MnSi}$  and insulating  $\text{Cu}_2\text{OSeO}_3$ ); a good twist on calculating the magnetic phase diagram is done comparing to the previously existed model of Ref.[38], See Chapter 3. The magnetic phase diagram, as had been already discussed, is a remarkably universal feature for all the bulk skyrmionic compounds, thus understanding of it in further details is important from the fundamental perspective. It is as a general rule very hard to simulate sufficiently large lattices to get critical fluctuations right. There-

fore my semi-quantitative analytic approach presented in Chapter 3 is valuable. For the skyrmions in bulk magnetoelectric insulator  $\text{Cu}_2\text{OSeO}_3$ , the summarized list of my contributions here is following: 1) I improved the "tail" solution of a single skyrmion; 2) I attempted a more consisted formulation of the variational solution; 3) I improved treatment of the critical fluctuations by taken into account recent experiments; 4) I proposed a new criterion for critical fluctuations regime in bulk phase diagrams; 5) From 2)-4) framework I developed a numerical technique for fast calculation of magnetic phase diagrams; 6) I developed phase diagrams in electric fields, and wrote code which allows relatively fast modification for change in  $\mathbf{E}$  and  $\mathbf{H}$  directions; 7) I have shown that a single skyrmion stabilizes under electric fields in field-polarized phase; 8) I have shown that the uniaxial mechanical strains lead to stabilization of individual skyrmions; 9) I have shown that applied pressure stabilizes the skyrmion lattice phase by modifying the anisotropy-induced mode-mode interaction; 10) I have shown that there is a new mechanism underlying the phenomenon of skyrmion motion under thermal gradients in thin films; 11) I have shown directly that there is a topology-preserving crossover between the thin-films skyrmions and magnetic bubbles, within the same energy formalism; 12) As a toy model which is still to be further explored, I proposed the meron-mediated mechanism for explaining the rapid topological charge saturation as the helical phase is turned into the skyrmion phase over the thin film.

In this thesis I thus presented several diverse both in their methods and goals calculations for magnetic skyrmions in chiral magnetoelectric insulators which I carried out since early 2015. Several other projects on which I was working on since starting my PhD in 2013, while being very successful, have not been included here for the reason that they are too distant from the content of the present thesis. Those are my single-author papers [191, 192] and earlier [193–195].

# Bibliography

- [1] G. Gamow. *Biography of physics*. Harper Torchbooks, New York, 1961.
- [2] G.E. Volovik. *The universe in a helium droplet*. Oxford University Press, 2003.
- [3] B. Bradlyn, L. Elcoro, J. Cano, M.G. Vergniory, Z. Wang, C. Felser, M.I. Aroyo, and B.A. Bernevig. Topological quantum chemistry. *Nature*, 547(7663):298–305, jul 2017. ISSN 0028-0836.
- [4] F.D.M. Haldane. O(3) nonlinear  $\sigma$  model and the topological distinction between integer-and half-integer-spin antiferromagnets in two dimensions. *Physical Review Letters*, 61(8):1029, 1988.
- [5] N.D. Mermin and H. Wagner. Absence of ferromagnetism or antiferromagnetism in one-or two-dimensional isotropic Heisenberg models. *Physical Review Letters*, 17(22):1133, 1966.
- [6] P.C. Hohenberg. Existence of long-range order in one and two dimensions. *Physical Review*, 158(2):383, 1967.
- [7] J.M. Kosterlitz and D.J. Thouless. Ordering, metastability and phase transitions in two-dimensional systems. *Journal of Physics C: Solid State Physics*, 6(7):1181, 1973.
- [8] V.L. Berezinskii. Destruction of long-range order in one-dimensional and two-dimensional systems having a continuous symmetry group I. Classical systems. *Sov. Phys. JETP*, 32(3):493–500, 1971.
- [9] V.L. Berezinskii. Destruction of long-range order in one-dimensional and two-dimensional systems possessing a continuous symmetry group. II. Quantum systems. *Soviet Journal of Experimental and Theoretical Physics*, 34:610, 1972.
- [10] A.J. Kruchkov. Reflections on the 66th Lindau Nobel Laureate Meeting. *Condensed Matter*, 1(1):13, 2016.
- [11] T.H.R. Skyrme. A new model for nuclear matter. In *Proceedings of the Royal Society of London A: Mathematical, Physical and Engineering Sciences*, volume 226, pages 521–530. The Royal Society, 1954.
- [12] T.H.R. Skyrme. The concept of a mesic fluid in relation to pseudoscalar meson theory. *Il Nuovo Cimento (1955-1965)*, 4:749–753, 1956.
- [13] T.H.R. Skyrme. A non-linear theory of strong interactions. In *Proceedings of the Royal Society of London A: Mathematical, Physical and Engineering Sciences*, volume 247, pages 260–278. The Royal Society, 1958.

- [14] T.H.R. Skyrme. A unified model of K-and  $\pi$ -mesons. In *Proceedings of the Royal Society of London A: Mathematical, Physical and Engineering Sciences*, volume 252, pages 236–245. The Royal Society, 1959.
- [15] T.H.R. Skyrme. A non-linear field theory. In *Proceedings of the Royal Society of London A: Mathematical, Physical and Engineering Sciences*, volume 260, pages 127–138. The Royal Society, 1961.
- [16] T.H.R. Skyrme. Particle states of a quantized meson field. In *Proceedings of the Royal Society of London A: Mathematical, Physical and Engineering Sciences*, volume 262, pages 237–245. The Royal Society, 1961.
- [17] T.H.R. Skyrme. A unified field theory of mesons and baryons. *Nuclear Physics*, 31:556–569, 1962.
- [18] T.H.R. Skyrme. The origins of skyrmions. *International Journal of Modern Physics A*, 3(12):2745–2751, 1988.
- [19] E. Witten. Baryons in the  $1/N$  expansion. *Nuclear Physics B*, 160(1):57–115, 1979.
- [20] E. Witten. Quarks, atoms, and the  $1/N$  expansion. *Physics Today*, 33(7):38–43, 1980.
- [21] W. Thomson. On vortex atoms. *The London, Edinburgh, and Dublin Philosophical Magazine and Journal of Science*, 34(227):15–24, 1867.
- [22] Y.M. Shnir. *Magnetic Monopoles*. Springer, 2005.
- [23] P. Dirac. Quantised singularities in the electromagnetic field. In *Proceedings of the Royal Society of London A: Mathematical, Physical and Engineering Sciences*, volume 133, pages 60–72. The Royal Society, 1931.
- [24] J. Preskill. Magnetic monopoles. *Annual Review of Nuclear and Particle Science*, 34(1):461–530, 1984.
- [25] C. Castelnovo, R. Moessner, and S.L. Sondhi. Magnetic monopoles in spin ice. *Nature*, 451(7174):42–45, 2008.
- [26] X. Wan, A. M. Turner, A. Vishwanath, and S.Y. Savrasov. Topological semimetal and Fermi-arc surface states in the electronic structure of pyrochlore iridates. *Physical Review B*, 83(20):205101, 2011.
- [27] P. Milde, D. Köhler, J. Seidel, L.M. Eng, A. Bauer, A. Chacon, J. Kindervater, S. Mühlbauer, C. Pfleiderer, S. Buhrandt, et al. Unwinding of a skyrmion lattice by magnetic monopoles. *Science*, 340(6136):1076–1080, 2013.
- [28] A.N. Bogdanov and D.A. Yablonski. Thermodynamically stable ”vortices” in magnetically ordered crystals. The mixed state of magnets. *Sov. Phys. JETP*, 68:101, 1989.
- [29] B.A. Ivanov and V.A. Stephanovich. On two-dimensional small radius topological solitons in magnets. *Sov. Phys JETP*, 64:376, 1986.

- [30] B.A. Ivanov, V.A. Stephanovich, and A.A. Zhmudskii. Magnetic vortices: The microscopic analogs of magnetic bubbles. *Journal of Magnetism and Magnetic Materials*, 88(1-2):116–120, 1990.
- [31] A.A. Belavin and A.M. Polyakov. Metastable states of two-dimensional isotropic ferromagnets. *JETP lett*, 22(10):245–248, 1975.
- [32] V.P. Voronov, B.A. Ivanov, and A.M. Kosevich. Two-dimensional dynamic topological solitons in ferromagnets. *Sov. Phys. JETP*, 57(6):1303, 1983.
- [33] A.V. Nikiforov and E.B. Sonin. Dynamics of magnetic vortices in a planar ferromagnet. *Sov. Phys. JETP*, 58(373):110, 1983.
- [34] B. Binz, A. Vishwanath, and V. Aji. Theory of the helical spin crystal: a candidate for the partially ordered state of MnSi. *Physical Review Letters*, 96(20):207202, 2006.
- [35] B. Binz and A. Vishwanath. Theory of helical spin crystals: Phases, textures, and properties. *Physical Review B*, 74(21):214408, 2006.
- [36] B. Binz and A. Vishwanath. Theoretical proposal predicting anomalous magnetoresistance and quadratic hall effect in the partially ordered state of MnSi. *Journal of Magnetism and Magnetic Materials*, 310(2):1062–1064, 2007.
- [37] B. Binz and A. Vishwanath. Chirality induced anomalous-hall effect in helical spin crystals. *Physica B: Condensed Matter*, 403(5):1336–1340, 2008.
- [38] S. Mühlbauer, B. Binz, F. Jonietz, C. Pfleiderer, A. Rosch, A. Neubauer, R. Georgii, and P. Böni. Skyrmion lattice in a chiral magnet. *Science*, 323(5916):915–919, 2009.
- [39] A. Tonomura, X. Yu, K. Yanagisawa, T. Matsuda, Y. Onose, N. Kanazawa, H.S. Park, and Y. Tokura. Real-space observation of skyrmion lattice in helimagnet mnsi thin samples. *Nano letters*, 12(3):1673–1677, 2012.
- [40] W. Münzer, A. Neubauer, T. Adams, S. Mühlbauer, C. Franz, F. Jonietz, R. Georgii, P. Böni, B. Pedersen, M. Schmidt, et al. Skyrmion lattice in the doped semiconductor  $\text{Fe}_{1-x}\text{Co}_x\text{Si}$ . *Physical Review B*, 81(4):041203, 2010.
- [41] X.Z. Yu, Y. Onose, N. Kanazawa, J.H. Park, J.H. Han, Y. Matsui, N. Nagaosa, and Y. Tokura. Real-space observation of a two-dimensional skyrmion crystal. *Nature*, 465(7300):901–904, 2010.
- [42] X.Z. Yu, N. Kanazawa, Y. Onose, K. Kimoto, W.Z. Zhang, S. Ishiwata, Y. Matsui, and Y. Tokura. Near room-temperature formation of a skyrmion crystal in thin-films of the helimagnet FeGe. *Nature Materials*, 10(2):106, 2011.
- [43] N. Kanazawa, Y. Onose, T. Arima, D. Okuyama, K. Ohoyama, S. Wakimoto, K. Kakurai, S. Ishiwata, and Y. Tokura. Large topological hall effect in a short-period helimagnet MnGe. *Physical Review Letters*, 106(15):156603, 2011.
- [44] S. Seki, S. Ishiwata, and Y. Tokura. Magnetoelectric nature of skyrmions in a chiral magnetic insulator  $\text{Cu}_2\text{OSeO}_3$ . *Physical Review B*, 86(6):060403, 2012.

- [45] T. Adams, A. Chacon, M. Wagner, A. Bauer, G. Brandl, B. Pedersen, H. Berger, P. Lemmens, and C. Pfleiderer. Long-wavelength helimagnetic order and skyrmion lattice phase in  $\text{Cu}_2\text{OSeO}_3$ . *Physical Review Letters*, 108(23):237204, 2012.
- [46] X.Z. Yu, N. Kanazawa, W.Z. Zhang, T. Nagai, T. Hara, K. Kimoto, Y. Matsui, Y. Onose, and Y. Tokura. Skyrmion flow near room temperature in an ultralow current density. *Nat. Comm.*, 3:988, 2012.
- [47] X.Z. Yu, Y. Tokunaga, Y. Kaneko, W.Z. Zhang, K. Kimoto, Y. Matsui, Y. Taguchi, and Y. Tokura. Biskyrmion states and their current-driven motion in a layered manganite. *Nature Communications*, 5:3198, 2014.
- [48] S. Heinze, K. Von Bergmann, M. Menzel, J. Brede, A. Kubetzka, R. Wiesendanger, G. Bihlmayer, and S. Blügel. Spontaneous atomic-scale magnetic skyrmion lattice in two dimensions. *Nature Physics*, 7(9):713, 2011.
- [49] N. Romming, C. Hanneken, M. Menzel, J.E. Bickel, B. Wolter, K. von Bergmann, A. Kubetzka, and R. Wiesendanger. Writing and deleting single magnetic skyrmions. *Science*, 341(6146):636–639, 2013.
- [50] H. Du, R. Che, L. Kong, X. Zhao, C. Jin, C. Wang, J. Yang, W. Ning, R. Li, and C. et al. Jin. Edge-mediated skyrmion chain and its collective dynamics in a confined geometry. *Nature Communications*, 6, 2015.
- [51] H. Du, D. Liang, C. Jin, L. Kong, M.J. Stolt, W. Ning, J. Yang, Y. Xing, J. Wang, and R. et al. Che. Electrical probing of field-driven cascading quantized transitions of skyrmion cluster states in MnSi nanowires. *Nature Communications*, 6, 2015.
- [52] X. Zhao, C. Jin, C. Wang, H. Du, J. Zang, M. Tian, R. Che, and Y. Zhang. Direct imaging of magnetic field-driven transitions of skyrmion cluster states in FeGe nanodisks. *Proceedings of the National Academy of Sciences*, 113(18):4918–4923, 2016.
- [53] S. Do Yi, S. Onoda, N. Nagaosa, and J.H. Han. Skyrmions and anomalous Hall effect in a Dzyaloshinskii-Moriya spiral magnet. *Physical Review B*, 80(5):054416, 2009.
- [54] A. Neubauer, C. Pfleiderer, B. Binz, A. Rosch, R. Ritz, P.G. Niklowitz, and P. Böni. Topological Hall effect in the A-phase of MnSi. *Physical Review Letters*, 102(18):186602, 2009.
- [55] G. Yin, Y. Liu, Y. Barlas, J. Zang, and R.K. Lake. Topological spin hall effect resulting from magnetic skyrmions. *Physical Review B*, 92(2):024411, 2015.
- [56] W. Jiang, X. Zhang, G. Yu, W. Zhang, X. Wang, M.B. Jungfleisch, J.E. Pearson, X. Cheng, O. Heinonen, K.L. Wang, et al. Direct observation of the skyrmion hall effect. *Nature Physics*, 13(2):162–169, 2017.
- [57] K. Litzius, I. Lemesch, B. Kruger, P. Bassirian, L. Caretta, K. Richter, F. Buttner, K. Sato, O.A. Tretiakov, J. Forster, R.M. Reeve, M. Weigand, I. Bykova, H. Stoll, G. Schutz, G.S.D. Beach, and M. Klau. Skyrmion Hall effect revealed by direct time-resolved X-ray microscopy. *Nat Phys*, 13(2):170–175, feb 2017.

- [58] S.L. Sondhi, A. Karlhede, S.A. Kivelson, and E.H. Rezayi. Skyrmions and the crossover from the integer to fractional quantum hall effect at small Zeeman energies. *Physical Review B*, 47(24):16419, 1993.
- [59] L. Brey, H.A. Fertig, R. Côté, and A.H. MacDonald. Skyrme crystal in a two-dimensional electron gas. *Physical Review Letters*, 75(13):2562, 1995.
- [60] T. Grover and T. Senthil. Topological spin hall states, charged skyrmions, and superconductivity in two dimensions. *Physical Review Letters*, 100(15):156804, 2008.
- [61] A. Knigavko, B. Rosenstein, and Y.F. Chen. Magnetic skyrmions and their lattices in triplet superconductors. *Physical Review B*, 60(1):550, 1999.
- [62] A. Knigavko and B. Rosenstein. Magnetic skyrmion lattices in Heavy Fermion superconductor UPt<sub>3</sub>. *Physical Review Letters*, 82(6):1261, 1999.
- [63] J. Garaud and E. Babaev. Skyrmionic state and stable half-quantum vortices in chiral  $p$ -wave superconductors. *Physical Review B*, 86(6):060514, 2012.
- [64] D.F. Agterberg, E. Babaev, and J. Garaud. Microscopic prediction of skyrmion lattice state in clean interface superconductors. *Physical Review B*, 90(6):064509, 2014.
- [65] E.-G. Moon. Skyrmions with quadratic band touching fermions: A way to achieve charge-4 $e$  superconductivity. *Physical Review B*, 85(24):245123, 2012.
- [66] T. Morinari. Mechanism of unconventional superconductivity induced by skyrmion excitations in two-dimensional strongly correlated electron systems. *Physical Review B*, 65(6):064513, 2002.
- [67] T. Yokoyama and J. Linder. Josephson effect through magnetic skyrmions. *Physical Review B*, 92(6):060503, 2015.
- [68] Q. Li, J. Toner, and D. Belitz. Elasticity and melting of skyrmion flux lattices in  $p$ -wave superconductors. *Physical Review Letters*, 98(18):187002, 2007.
- [69] T.-L. Ho. Spinor Bose condensates in optical traps. *Physical Review Letters*, 81(4):742, 1998.
- [70] U. Al Khawaja and H.T.C. Stoof. Skyrmions in a ferromagnetic Bose-Einstein condensate. *Nature*, 411(6840):918, 2001.
- [71] K.-P. Marzlin, W. Zhang, and B.C. Sanders. Creation of skyrmions in a spinor Bose-Einstein condensate. *Physical Review A*, 62(1):013602, 2000.
- [72] R.A. Battye, N.R. Cooper, and P.M. Sutcliffe. Stable skyrmions in two-component Bose-Einstein condensates. *Physical Review Letters*, 88(8):080401, 2002.
- [73] C.M. Savage and J. Ruostekoski. Energetically stable particlelike skyrmions in a trapped Bose-Einstein condensate. *Physical Review Letters*, 91(1):010403, 2003.
- [74] L.S. Leslie, A. Hansen, K.C. Wright, B.M. Deutsch, and N.P. Bigelow. Creation and detection of skyrmions in a Bose-Einstein condensate. *Physical Review Letters*, 103(25):250401, 2009.

- [75] J.-Y. Choi, W.J. Kwon, and Y.-I. Shin. Observation of topologically stable 2D skyrmions in an antiferromagnetic spinor Bose-Einstein condensate. *Physical Review Letters*, 108(3):035301, 2012.
- [76] V.P. Voronov and A.M. Kosevich. Two-dimensional solitons: magnetic vortices in a uniaxial antiferromagnet. *Zh. Eksp. Teor. Fiz*, 90:2145–2151, 1986.
- [77] M.E. Gouva, G.M. Wysin, A.R. Bishop, and F.G. Mertens. Vortices in the classical two-dimensional anisotropic heisenberg model. *Physical Review B*, 39(16):11840, 1989.
- [78] A. Abanov and V.L. Pokrovsky. Skyrmion in a real magnetic film. *Physical Review B*, 58(14):R8889, 1998.
- [79] A.N. Bogdanov, U.K. Rößler, M. Wolf, and K.-H. Müller. Magnetic structures and reorientation transitions in noncentrosymmetric uniaxial antiferromagnets. *Physical Review B*, 66(21):214410, 2002.
- [80] F. Jonietz, S. Mühlbauer, C. Pfleiderer, A. Neubauer, W. Münzer, A. Bauer, T. Adams, R. Georgii, P. Böni, R.A. Duine, et al. Spin transfer torques in MnSi at ultralow current densities. *Science*, 330(6011):1648–1651, 2010.
- [81] U.K. Rössler, A.N. Bogdanov, and C. Pfleiderer. Spontaneous skyrmion ground states in magnetic metals. *Nature*, 442(7104):797–801, 2006.
- [82] S. Rohart, J. Miltat, and A. Thiaville. Path to collapse for an isolated Néel skyrmion. *Physical Review B*, 93(21):214412, 2016.
- [83] J. Zang, M. Mostovoy, J.H. Han, and N. Nagaosa. Dynamics of skyrmion crystals in metallic thin films. *Physical Review Letters*, 107(13):136804, 2011.
- [84] T. Schulz, R. Ritz, A. Bauer, M. Halder, M. Wagner, C. Franz, C. Pfleiderer, K. Everschor, M. Garst, and A. Rosch. Emergent electrodynamics of skyrmions in a chiral magnet. *Nature Physics*, 8(4), 2012.
- [85] J. Iwasaki, M. Mochizuki, and N. Nagaosa. Current-induced skyrmion dynamics in constricted geometries. *Nature Nanotechnology*, 8(10):742–747, 2013.
- [86] J. Iwasaki, M. Mochizuki, and N. Nagaosa. Universal current-velocity relation of skyrmion motion in chiral magnets. *Nature Communications*, 4:1463, 2013.
- [87] A. Rosch. Skyrmions: moving with the current. *Nature Nanotechnology*, 8(3):160–161, 2013.
- [88] J. Sampaio, V. Cros, S. Rohart, A. Thiaville, and A. Fert. Nucleation, stability and current-induced motion of isolated magnetic skyrmions in nanostructures. *Nature Nanotechnology*, 8(11):839–844, 2013.
- [89] J. Kang and J. Zang. Transport theory of metallic B20 helimagnets. *Physical Review B*, 91(13):134401, 2015.
- [90] L. Kong and J. Zang. Dynamics of an insulating skyrmion under a temperature gradient. *Physical Review Letters*, 111(6):067203, 2013.



- [91] K. Everschor, M. Garst, B. Binz, F. Jonietz, S. Mühlbauer, C. Pfleiderer, and A. Rosch. Rotating skyrmion lattices by spin torques and field or temperature gradients. *Physical Review B*, 86(5):054432, 2012.
- [92] H.M. Hurst, D.K. Efimkin, J. Zang, and V. Galitski. Charged skyrmions on the surface of a topological insulator. *Physical Review B*, 91(6):060401, 2015.
- [93] W. Jiang, P. Upadhyaya, W. Zhang, G. Yu, M.B. Jungfleisch, F.Y. Fradin, J.E. Pearson, Y. Tserkovnyak, K.L. Wang, O. Heinonen, et al. Blowing magnetic skyrmion bubbles. *Science*, 349(6245):283–286, 2015.
- [94] M. Mochizuki and Y. Watanabe. Writing a skyrmion on multiferroic materials. *Applied Physics Letters*, 107(8):082409, 2015.
- [95] A.J. Kruchkov, J.S. White, M. Bartkowiak, I. Zivcovic, A. Magrez, and H.M. Rønnow. Direct control of the skyrmion phase stability by electric field in a magnetoelectric insulator. *arXiv preprint arXiv:1703.06081*, 2017.
- [96] M. Schott, A. Bernand-Mantel, L. Ranno, S. Pizzini, J. Vogel, H. Béa, C. Baraduc, S. Auffret, G. Gaudin, and D. Givord. The skyrmion switch: turning magnetic skyrmion bubbles on and off with an electric field. *Nano Letters*, 17(5):3006–3012, 2017.
- [97] Y. Liu, G. Yin, J. Zang, J. Shi, and R.K. Lake. Skyrmion creation and annihilation by spin waves. *Applied Physics Letters*, 107(15):152411, 2015.
- [98] G. Yin, Y. Li, L. Kong, R.K. Lake, C.-L. Chien, and J. Zang. Topological charge analysis of ultrafast single skyrmion creation. *Physical Review B*, 93(17):174403, 2016.
- [99] U.K. Rößler, A.A. Leonov, and A.N. Bogdanov. Chiral skyrmionic matter in non-centrosymmetric magnets. In *Journal of Physics: Conference Series*, volume 303, page 012105. IOP Publishing, 2011.
- [100] A.O. Leonov, T.L. Monchesky, J.C. Loudon, and A.N. Bogdanov. Three-dimensional chiral skyrmions with attractive interparticle interactions. *Journal of Physics: Condensed Matter*, 28(35):35LT01, 2016.
- [101] A.O. Leonov, T.L. Monchesky, N. Romming, A. Kubetzka, A.N. Bogdanov, and R. Wiesendanger. The properties of isolated chiral skyrmions in thin magnetic films. *New J. Phys.*, 18:065003, 2016.
- [102] L. Rózsa, A. Deák, E. Simon, R. Yanes, L. Udvardi, L. Szunyogh, and U. Nowak. Skyrmions with attractive interactions in an ultrathin magnetic film. *Physical Review Letters*, 117(15):157205, 2016.
- [103] W. Koshibae and N. Nagaosa. Theory of skyrmions in bilayer systems. *Scientific Reports*, 7, 2017.
- [104] C. Timm, S.M. Girvin, and H.A. Fertig. Skyrmion lattice melting in the quantum hall system. *Physical Review B*, 58(16):10634, 1998.
- [105] J.H. Han, J. Zang, Z. Yang, J.-H. Park, and N. Nagaosa. Skyrmion lattice in a two-dimensional chiral magnet. *Physical Review B*, 82(9):094429, 2010.

- [106] A. Fert, V. Cros, and J. Sampaio. Skyrmions on the track. *Nature Nanotechnology*, 8(3):152–156, 2013.
- [107] N. Nagaosa and Y. Tokura. Topological properties and dynamics of magnetic skyrmions. *Nature nanotechnology*, 8(12):899–911, 2013.
- [108] R. Tomasello, E. Martinez, R. Zivieri, L. Torres, M. Carpentieri, and G. Finocchio. A strategy for the design of skyrmion racetrack memories. *Scientific reports*, 4:6784, 2014.
- [109] X. Zhang, G.P. Zhao, H. Fangohr, J.P. Liu, W.X. Xia, J. Xia, and F.J. Morvan. Skyrmion-skyrmion and skyrmion-edge repulsions in skyrmion-based race-track memory. *Scientific Reports*, 5:7643, 2015.
- [110] X. Zhang, Y. Zhou, M. Ezawa, G.P. Zhao, and W. Zhao. Magnetic skyrmion transistor: skyrmion motion in a voltage-gated nanotrack. *Scientific reports*, 5:11369, 2015.
- [111] A. Fert, N. Reyren, and V. Cros. Magnetic skyrmions: advances in physics and potential applications. *Nature Reviews Materials*, 2:natrevmats201731, 2017.
- [112] C. Schütte. *Skyrmions and Monopoles in Chiral Magnets & Correlated Heterostructures*. PhD thesis, Universität zu Köln, 2014.
- [113] I. Dzyaloshinsky. A thermodynamic theory of “weak” ferromagnetism of antiferromagnetics. *Journal of Physics and Chemistry of Solids*, 4(4):241–255, 1958.
- [114] T. Moriya. Anisotropic superexchange interaction and weak ferromagnetism. *Physical Review*, 120(1):91, 1960.
- [115] I.E. Dzyaloshinskii. Theory of helicoidal structures in antiferromagnets. 1. non-metals. *Sov. Phys. JETP*, 19:960–971, 1964.
- [116] I.E. Dzyaloshinskii. The theory of helicoidal structures in antiferromagnets. ii. metals. *Sov. Phys. JETP*, 20(1), 1965.
- [117] I. Kézsmárki, S. Bordács, P. Milde, E. Neuber, L.M. Eng, J.S. White, H.M. Rønnow, C.D. Dewhurst, M. Mochizuki, K. Yanai, et al. Néel-type skyrmion lattice with confined orientation in the polar magnetic semiconductor GaV<sub>4</sub>S<sub>8</sub>. *Nature materials*, 14(11):1116–1122, 2015.
- [118] W. Li and J. Zang. Systematic search and a new family of skyrmion materials. *arXiv preprint arXiv:1502.03818*, 2015.
- [119] W. Li, C. Jin, R. Che, W. Wei, L. Lin, L. Zhang, H. Du, M. Tian, and J. Zang. Emergence of skyrmions from rich parent phases in the molybdenum nitrides. *Physical Review B*, 93(6):060409, 2016.
- [120] L.D. Landau and E.M. Lifshitz. *Theoretical Physics. Vol. 1: Mechanics*. Pergamon Press, 1969.
- [121] I.S. Lobanov, H. Jónsson, and V.M. Uzdin. Mechanism and activation energy of magnetic skyrmion annihilation obtained from minimum energy path calculations. *Phys. Rev. B*, 94:174418, Nov 2016.

- [122] D. Stosic, J. Mulkers, B. Van Waeyenberge, T. Ludermir, and M.V. Milošević. Paths to collapse for isolated skyrmions in few-monolayer ferromagnetic films. *Physical Review B*, 95:214418, 2017.
- [123] D. Cortés-Ortuño, W. Wang, M. Beg, R.A. Pepper, M.-A. Bisotti, R. Carey, M. Vousden, T. Kluyver, O. Hovorka, and H. Fangohr. Thermal stability and topological protection of skyrmions in nanotracks. *Scientific Reports*, 7, 2017.
- [124] A.B. Migdal. *Qualitative methods in quantum theory*. Addison-Wesley, 1977.
- [125] A.B. Migdal. *Qualitative methods in quantum theory*. Da Capo Press, 2000.
- [126] P.M. Morse and H. Feshbach. *Methods of theoretical physics*. Technology Press, 1946.
- [127] A. Bogdanov. New localized solutions of the nonlinear field equations. *JETP Letters*, 62(3):247–251, 1995.
- [128] N.S. Kiselev, A.N. Bogdanov, R. Schäfer, and U.K. Rößler. Chiral skyrmions in thin magnetic films: new objects for magnetic storage technologies? *Journal of Physics D: Applied Physics*, 44(39):392001, 2011.
- [129] I. Levatić, V. Šurija, H. Berger, and I. Živković. Dissipation processes in the insulating skyrmion compound  $\text{Cu}_2\text{OSeO}_3$ . *Physical Review B*, 90(22):224412, 2014.
- [130] M.S. Viazovska. The sphere packing problem in dimension 8. *Annals of Mathematics*, 185(3):991–1015, 2017.
- [131] H. Cohn, A. Kumar, S.D. Miller, D. Radchenko, and M. Viazovska. The sphere packing problem in dimension 24. *Annals of Mathematics*, 185:1017–1033, 2017.
- [132] J.S. White, K. Prša, P. Huang, A.A. Omrani, I. Živković, M. Bartkowiak, H. Berger, A. Magrez, J.L. Gavilano, G. Nagy, et al. Electric-field-induced skyrmion distortion and giant lattice rotation in the magnetoelectric insulator  $\text{Cu}_2\text{OSeO}_3$ . *Physical Review Letters*, 113(10):107203, 2014.
- [133] A.J. Kruchkov and H.M. Rønnow. Skyrmion lattices in electric fields. *arXiv preprint arXiv:1702.08863*, 2017.
- [134] M. Janoschek, M. Garst, A. Bauer, P. Krautscheid, R. Georgii, P. Böni, and C. Pfleiderer. Fluctuation-induced first-order phase transition in Dzyaloshinskii-Moriya helimagnets. *Physical Review B*, 87(13):134407, 2013.
- [135] S.A. Brazovskii. Phase transition of an isotropic system to a nonuniform state. *Sov. JETP*, 41:85, 1975.
- [136] P. Bak and M.H. Jensen. Theory of helical magnetic structures and phase transitions in MnSi and FeGe. *Journal of Physics C: Solid State Physics*, 13(31):L881, 1980.
- [137] Y.A. Izyumov. Modulated, or long-periodic, magnetic structures of crystals. *Soviet Physics Uspekhi*, 27:845–867, 1984.
- [138] H.S. Green. *Matrix mechanics*. P. Noordhoff, 1965.

- [139] S.A. Brazovskii, I.E. Dzyaloshinskii, and A.R. Muratov. Theory of weak crystallization. *Sov. JETP*, 93:1110–1124, 1987.
- [140] A.I. Akhiezer and S.V. Peletminskii. *Methods of statistical physics*. Pergamon, 1981.
- [141] P. Huang. Control of topological magnetic textures by magnetic and electric fields in magnetoelectric helimagnet  $\text{Cu}_2\text{OSeO}_3$ . 2017.
- [142] O. Janson, I. Rousochatzakis, A.A. Tsirlin, M. Belesi, A.A. Leonov, U.K. Rößler, J. Brink, and H. Rosner. The quantum origins of skyrmions and half-skyrmions in  $\text{Cu}_2\text{OSeO}_3$ . *Nature Communications*, 5:1–11, 2014.
- [143] S. Seki, X.Z. Yu, S. Ishiwata, and Y. Tokura. Observation of skyrmions in a multiferroic material. *Science*, 336(6078):198–201, 2012.
- [144] Y. Onose, Y. Okamura, S. Seki, S. Ishiwata, and Y. Tokura. Observation of magnetic excitations of skyrmion crystal in a helimagnetic insulator  $\text{Cu}_2\text{OSeO}_3$ . *Physical Review Letters*, 109(3):037603, 2012.
- [145] M. Mochizuki. Creation of skyrmions by electric field on chiral-lattice magnetic insulators. *Advanced Electronic Materials*, 2(1), 2016.
- [146] Y.H. Liu, Y.Q. Li, and J.H. Han. Skyrmion dynamics in multiferroic insulators. *Physical Review B*, 87(10):100402, 2013.
- [147] C. Jia, S. Onoda, N. Nagaosa, and J.H. Han. Microscopic theory of spin-polarization coupling in multiferroic transition metal oxides. *Physical Review B*, 76(14):144424, 2007.
- [148] M. Belesi, I. Rousochatzakis, M. Abid, U.K. Rößler, H. Berger, and J.P. Ansermet. Magnetoelectric effects in single crystals of the cubic ferrimagnetic helimagnet  $\text{Cu}_2\text{OSeO}_3$ . *Physical Review B*, 85(22):224413, 2012.
- [149] A.A. Omrani, J.S. White, K. Prša, I. Živković, H. Berger, A. Magrez, Y.-H. Liu, J.H. Han, and H.M. Rønnow. Exploration of the helimagnetic and skyrmion lattice phase diagram in  $\text{Cu}_2\text{OSeO}_3$  using magnetoelectric susceptibility. *Physical Review B*, 89(6):064406, 2014.
- [150] J. Müller, Ja. Rajeswari, P. Huang, H.M. Rønnow, F. Carbone, and A. Rosch. Magnetic skyrmions and skyrmion clusters in the helical phase of  $\text{Cu}_2\text{OSeO}_3$ . *arXiv preprint arXiv:1703.06989*, 2017.
- [151] J.S. White, I. Levatić, A.A. Omrani, N. Egetenmeyer, K. Prša, I. Živković, J.L. Gavilano, J. Kohlbrecher, M. Bartkowiak, H. Berger, et al. Electric field control of the skyrmion lattice in  $\text{Cu}_2\text{OSeO}_3$ . *Journal of Physics: Condensed Matter*, 24(43):432201, 2012.
- [152] M. Mochizuki, X.Z. Yu, S. Seki, N. Kanazawa, W. Koshibae, J. Zang, M. Mostovoy, Y. Tokura, and N. Nagaosa. Thermally driven ratchet motion of a skyrmion microcrystal and topological magnon Hall effect. *Nature materials*, 13(3):241–246, 2014.

- [153] H. Watanabe and A. Vishwanath. Electric field-induced skyrmion crystals via charged monopoles in insulating helimagnets. *Journal of the Physical Society of Japan*, 85(6):064707, 2016.
- [154] Y. Okamura, F. Kagawa, S. Seki, and Y. Tokura. Creation and annihilation of skyrmions by electric fields in a helimagnetic multiferroic. *Nature Communications*, 7:12669, 2016.
- [155] P. Upadhyaya, G. Yu, P.K. Amiri, and K.L. Wang. Electric-field guiding of magnetic skyrmions. *Physical Review B*, 92(13):134411, 2015.
- [156] Y. Tokunaga, X.Z. Yu, J.S. White, H.M. Rønnow, D. Morikawa, Y. Taguchi, and Y. Tokura. A new class of chiral materials hosting magnetic skyrmions beyond room temperature. *Nature Communications*, 6, 2015.
- [157] I. Levatić, P. Popčević, V. Šurija, A. Kruchkov, H. Berger, A. Magrez, J.S. White, H.M. Rønnow, and I. Živković. Dramatic pressure-driven enhancement of bulk skyrmion stability. *Scientific Reports*, 6:21347, 2016.
- [158] H. Wilhelm, M. Baenitz, M. Schmidt, U.K. Rößler, A.A. Leonov, and A.N. Bogdanov. Precursor phenomena at the magnetic ordering of the cubic helimagnet FeGe. *Physical Review Letters*, 107(12):127203, 2011.
- [159] A. Chacon, A. Bauer, T. Adams, F. Rucker, G. Brandl, R. Georgii, M. Garst, and C. Pfleiderer. Uniaxial pressure dependence of magnetic order in MnSi. *Physical Review Letters*, 115(26):267202, 2015.
- [160] Y. Nii, T. Nakajima, A. Kikkawa, Y. Yamasaki, K. Ohishi, J. Suzuki, Y. Taguchi, T. Arima, Y. Tokura, and Y. Iwasa. Uniaxial stress control of skyrmion phase. *Nature Communications*, 6:8539, 2015.
- [161] M. Belesi, I. Rousochatzakis, H.C. Wu, H. Berger, I.V. Shvets, et al. Ferrimagnetism of the magnetoelectric compound  $\text{Cu}_2\text{OSeO}_3$  probed by  $^{77}\text{Se}$  NMR. *Physical Review B*, 82(9):094422, 2010.
- [162] M. Bartkowiak, J.S. White, H.M. Rønnow, and K. Prša. Note: Versatile sample stick for neutron scattering experiments in high electric fields. *Review of Scientific Instruments*, 85(2):026112, 2014.
- [163] S.L. Zhang, A. Bauer, H. Berger, C. Pfleiderer, G. Van Der Laan, and T. Hesjedal. Resonant elastic x-ray scattering from the skyrmion lattice in  $\text{Cu}_2\text{OSeO}_3$ . *Physical Review B*, 93(21):214420, 2016.
- [164] K. Makino, J.D. Reim, D. Higashi, D. Okuyama, T.J. Sato, Y. Nambu, E.P. Gilbert, N. Booth, S. Seki, and Y. Tokura. Thermal stability and irreversibility of skyrmion-lattice phases in  $\text{Cu}_2\text{OSeO}_3$ . *Physical Review B*, 95(13):134412, 2017.
- [165] I. Živković, D. Pajić, T. Ivek, and H. Berger. Two-step transition in a magnetoelectric ferrimagnet  $\text{Cu}_2\text{OSeO}_3$ . *Physical Review B*, 85(22):224402, 2012.
- [166] K. Shibata, J. Iwasaki, N. Kanazawa, S. Aizawa, T. Tanigaki, M. Shirai, T. Nakajima, M. Kubota, M. Kawasaki, H.S. Park, et al. Large anisotropic deformation of skyrmions in strained crystal. *Nature Nanotechnology*, 10(7):589–592, 2015.

- [167] A.I. Figueroa, S.L. Zhang, A.A. Baker, R. Chalasani, A. Kohn, S.C. Speller, D. Gianolio, C. Pfleiderer, G. van der Laan, and T. Hesjedal. Strain in epitaxial MnSi films on Si (111) in the thick film limit studied by polarization-dependent extended X-ray absorption fine structure. *Physical Review B*, 94(17):174107, 2016.
- [168] R. Ritz, M. Halder, C. Franz, A. Bauer, M. Wagner, R. Bamler, A. Rosch, and C. Pfleiderer. Giant generic topological hall resistivity of MnSi under pressure. *Physical Review B*, 87(13):134424, 2013.
- [169] M.L. Plumer and M.B. Walker. Magnetoelastic effects in the spin-density wave phase of MnSi. *Journal of Physics C: Solid State Physics*, 15(35):7181, 1982.
- [170] L.D. Landau and E.M. Lifshitz. *Course of Theoretical Physics Vol 7: Theory and Elasticity*. Pergamon Press, 1959.
- [171] P.H. Mott and C.M. Roland. Limits to Poisson’s ratio in isotropic materials. *Physical review B*, 80(13):132104, 2009.
- [172] A.E. Petrova, V.N. Krasnorussky, W.M. Yuhasz, T.A. Lograsso, and S.M. Stishov. Elastic properties of MnSi, FeSi and CoSi. In *Journal of Physics: Conference Series*, volume 273, page 012056. IOP Publishing, 2011.
- [173] A.B. Butenko, A.A. Leonov, U.K. Röbller, and A.N. Bogdanov. Stabilization of skyrmion textures by uniaxial distortions in noncentrosymmetric cubic helimagnets. *Physical Review B*, 82(5):052403, 2010.
- [174] Y. Li, N. Kanazawa, X.Z. Yu, A. Tsukazaki, M. Kawasaki, M. Ichikawa, X.F. Jin, F. Kagawa, and Y. Tokura. Robust formation of skyrmions and topological hall effect anomaly in epitaxial thin films of mnsi. *Phys. Rev. Lett.*, 110(11):117202, 2013.
- [175] C. Pfleiderer, S.R. Julian, and G.G. Lonzarich. Non-fermi-liquid nature of the normal state of itinerant-electron ferromagnets. *Nature*, 414(6862):427–430, 2001.
- [176] N. Doiron-Leyraud, I.R. Walker, L. Taillefer, M.J. Steiner, S.R. Julian, and G.G. Lonzarich. Fermi-liquid breakdown in the paramagnetic phase of a pure metal. *Nature*, 425(6958):595–599, 2003.
- [177] P. Pedrazzini, H. Wilhelm, D. Jaccard, T. Jarlborg, M. Schmidt, M. Hanfland, L. Akselrud, H.Q. Yuan, U. Schwarz, Y. Grin, et al. Metallic state in cubic FeGe beyond its quantum phase transition. *Physical Review Letters*, 98(4):047204, 2007.
- [178] C.L. Huang, K.F. Tseng, C.C. Chou, S. Mukherjee, J.L. Her, Y.H. Matsuda, K. Kindo, H. Berger, and H.D. Yang. Observation of a second metastable spin-ordered state in ferrimagnet Cu<sub>2</sub>OSeO<sub>3</sub>. *Physical Review B*, 83(5):052402, 2011.
- [179] V.A. Sidorov, A.E. Petrova, P.S. Berdonosov, V.A. Dolgikh, and S.M. Stishov. Comparative study of helimagnets MnSi and Cu<sub>2</sub>OSeO<sub>3</sub> at high pressures. *Physical Review B*, 89(10):100403, 2014.
- [180] P.W. Anderson. *Basic notions of condensed matter physics*. Benjamin-Cummings, 1984.

- [181] S. Buhrandt and L. Fritz. Skyrmion lattice phase in three-dimensional chiral magnets from monte carlo simulations. *Phys. Rev. B*, 88(19):195137, 2013.
- [182] I. Kézsmárki, S. Bordács, P. Milde, E. Neuber, L.M. Eng, J.S. White, H.M. Rønnow, C.D. Dewhurst, M. Mochizuki, K. Yanai, et al. Néel-type skyrmion lattice with confined orientation in the polar magnetic semiconductor  $\text{GaV}_4\text{S}_8$ . *Nature materials*, 14(11):1116–1122, 2015.
- [183] J. Iwasaki, A.J. Beekman, and N. Nagaosa. Theory of magnon-skyrmion scattering in chiral magnets. *Physical Review B*, 89(6):064412, 2014.
- [184] S.-Z. Lin, C.D. Batista, C. Reichhardt, and A. Saxena. AC current generation in chiral magnetic insulators and skyrmion motion induced by the spin Seebeck effect. *Physical Review Letters*, 112(18):187203, 2014.
- [185] A.A. Kovalev. Skyrmionic spin Seebeck effect via dissipative thermomagnonic torques. *Physical Review B*, 89(24):241101, 2014.
- [186] A.P. Malozemoff and J.C. Slonczewski. *Magnetic Domain Walls in Bubble Materials: Advances in Materials and Device Research*, volume 1. Academic press, 2016.
- [187] Y.-O. Tu. Determination of magnetization of micromagnetic wall in bubble domains by direct minimization. *Journ. Appl. Phys.*, 42(13):5704–5709, 1971.
- [188] Y.S. Lin and Y.O. Tu. Micromagnetic solutions for bubble domains. *Appl. Phys. Lett.*, 18(6):247–249, 1971.
- [189] G.H. Derrick. Comments on nonlinear wave equations as models for elementary particles. *Journal of Mathematical Physics*, 5(9):1252–1254, 1964.
- [190] M. Ezawa. Compact merons and skyrmions in thin chiral magnetic films. *Phys. Rev. B*, 83(10):100408, 2011.
- [191] A.J. Kruchkov. One-dimensional Bose-Einstein condensation of photons in a microtube. *Physical Review A*, 93(4):043817, 2016.
- [192] A. Kruchkov. Bose-Einstein condensation of light in a cavity. *Physical Review A*, 89(3):033862, 2014.
- [193] A. Kruchkov and Y. Slyusarenko. Bose-Einstein condensation of photons in an ideal atomic gas. *Physical Review A*, 88(1):013615, 2013.
- [194] Y. Slyusarenko and A. Kruchkov. Mechanism of collisionless sound damping in dilute Bose gas with condensate. *Condensed Matter Physics*, 16(2):23004:1–17.
- [195] A. Kruchkov. Radiation spectrum of systems with condensed light. *arXiv preprint arXiv:1404.2561*, 2014.





**Full name** Oleksandr Jura Kriuchkov  
**a.k.a.** **Alex Kruchkov**  
**Address** av. de Montoie 6, 1007 Lausanne, Switzerland  
**Date of Birth** 24<sup>th</sup> October 1989  
**Nationality** Ukraine  
**Languages** English, French, Ukrainian, Russian  
**Mobile Phone** +41 (78) 841 1333  
**Email** alex.kruchkov@epfl.ch  
**Website** alexkruchkov.com  
**Google Scholar** Alex J. Kruchkov  
**Orcid** orcid.org/0000-0003-3850-8590  
**ResearcherID** N-3950-2013



**Summary.** – I am a theoretical physicist in a very broad sense, currently working on cutting-edge topics in Condensed Matter. By submitting this thesis I am 27 years old, and I published my first single-author paper being 24. During past years I received a number of academic honors and awards as listed below. In November 2017 I am starting my postdoctoral training at Harvard.

## Education and Training

- 2013-2017** Docteur ès Sciences (Ph.D.)  
 at EPFL (École Polytechnique Fédérale de Lausanne)  
 Thesis: "Theories of topologically-induced phenomena in skyrmion-hosting magnetoelectric insulators"
- 2011-2013** M.Sc. with Honors (Physics)  
 at University of Kharkiv  
 Thesis: "Mechanism of collisionless sound damping in Bose-Einstein condensates"
- 2007-2011** B.Sc. with Honors (Physics)  
 at University of Kharkiv  
 Thesis: "Dynamics of long-scale fluctuations in dilute Bose gases with condensate"

## Honors, Fellowships, Awards

- 2017-2019** SNSF Early PostDoc Fellowship for Harvard University
- 2016** 66th Lindau Nobel Laureate Meeting
- 2016** Bayer Science & Education Foundation Fellowship (Lindau Meeting)
- 2015** EPFL Teaching excellence reward
- 2013** Master of Science degree with High Honors, University of Kharkiv
- 2011** First Prize Award at International Physicists' Tournament, Moscow
- 2011** Bachelor of Science degree with High Honors, University of Kharkiv
- 2010/2011** Sapronov's Fellowship for outstanding students/ Sapronov Foundation
- 2009/2010** Tarapov's Fellowship for outstanding students / National Academy of Sciences of Ukraine

**Other:** Enlarged stipend for excellent studies/ University of Kharkiv (Spring 2011), Enlarged stipend for excellent studies/ University of Kharkiv (Fall 2010), Enlarged stipend for excellent studies/ University of Kharkiv (2009 Spring), Enlarged stipend for excellent studies/ University of Kharkiv (Fall 2008), Enlarged stipend for excellent studies/ University of Kharkiv (Spring 2008), Freshman's stipend for studies / University of Kharkiv (Fall 2007), Serdiuk's Award/ University of Odessa & National Academy of Sciences of Ukraine (2007).

## Research Experience

**Sep 2013 - Nov 2017:** Doctoral Assistant at Laboratory for Quantum Magnetism (LQM), EPFL.

**Mar 2013 - Aug 2013:** Junior Research Fellow at at Laboratory for Nuclear Reactor Materials, University of Kharkiv.

## Teaching Record

- Substitute Lecturer (Quantum Physics IV, EPFL, Apr-May 2016)
- Substitute Lecturer (Solid State Physics IV, EPFL, Apr 2015)
- Substitute Lecturer (General Physics III, EPFL, Oct-Dec 2014)
- Teaching Assistant (Quantum Physics IV, EPFL, Feb-May 2016)
- Teaching Assistant (General Physics III, EPFL, Sept-Dec 2016)
- Teaching Assistant (General Physics III, EPFL, Sep 2015 - Jan 2016)
- Teaching Assistant (General Physics III, EPFL, Oct-Dec 2014)
- Teaching Assistant (Solid State Physics IV, EPFL, Feb-May 2014)
- Teaching Assistant (General Physics III, EPFL, Sep 2013 - Jan 2014)
- Independent Expert on exam for Solid State Physics III, EPFL, Jan 2015
- Independent Expert on exam for Solid State Physics III, EPFL, Jan 2014

## Publications

Summary: 5 published research papers including 2 single-author papers; 3 preprints; 2 manuscripts in preparation; 1 outreach paper.

### Published peer-reviewed papers [5]

- [1] A. **Kruchkov**, One-dimensional Bose-Einstein condensation of photons in a microtube, Phys. Rev. A 93, 043817 (2016).
- [2] I. Levatic, P. Popcevic, V. Suriya, A. **Kruchkov**, H. Berger, A. Magrez, J. S. White, H. M. Rønnow & I. Zivkovic, Dramatic pressure-driven enhancement of bulk skyrmion stability, Scientific Reports 6, 21347 (2016).
- [3] A. **Kruchkov**, Bose-Einstein condensation of light in a cavity, Phys. Rev. A 89, 033862 (2014).
- [4] A. **Kruchkov**, Y. Slyusarenko, Bose-Einstein condensation of photons in an ideal atomic gas, Phys. Rev. A 88, 013615 (2013).
- [5] Y. Slyusarenko, A. **Kruchkov**, Mechanism of collisionless sound damping in dilute Bose gas with condensate, Cond.Mat.Phys., vol. 16, No. 2, 23004, (2013).

### Outreach [1]

Alex **Kruchkov**, Editorial: Reflections on the 66th Lindau Nobel Laureate Meeting, Condensed Matter (ISSN 2410-3896) [in press].

### Preprints [3]

- [1] A.J. **Kruchkov** and H.M. Rønnow, Skyrmion Lattices in Electric Fields. arXiv preprint: 1702.08863.
- [2] A.J. **Kruchkov**, J.S. White, M. Bartkowiak, I. Zivkovic, A. Magrez, and H.M. Rønnow, Direct control of the skyrmion phase stability by electric field in a magnetoelectric insulator, manuscript in preparation. arXiv preprint: 1703.06081
- [3] A. **Kruchkov**, Radiation spectrum of systems with condensed light. arXiv preprint:1404.2561

### Manuscripts in preparation [2]

- [1] Alex **Kruchkov**, Henrik Rønnow, and Albert Fert, Topological Transition between Skyrmions and Magnetic Bubbles in Thin Films, manuscript in preparation.
- [2] A. J. **Kruchkov** and H. M. Rønnow, Thermogradient Force Moving Skyrmions in Helimagnets, manuscript in preparation.

## Talks

11 talks, including 5 invited:

- A. Kruchkov, "Creating Skyrmions with Electric Fields: Theory and Experiment", Joint Annual Meeting of SPS and ÖPG (2017), 25 Aug 2017, Geneva, Switzerland.
- A. Kruchkov, "Creating Skyrmions with Electric Fields: Theory and Experiment", SKYMAG-2017, 5 May 2017, Paris, France.

- A. Kruchkov, "Creating Skyrmions with Electric Fields: Theory and Experiment", APS March Meeting, 16 Mar 2017, New Orleans, USA.
- **[invited]** A. Kruchkov, "A quantum lightsaber: condensation of light in a microtube", invited by Prof. Dr. A. Rosch, University of Cologne, 14 Oct 2016, Cologne (Köln), Germany
- **[invited]** A. Kruchkov, "A quantum lightsaber: condensation of light in a microtube", invited by Prof. Dr. M. Weitz, University of Bonn, 1 Sep 2016, Bonn, Germany
- A. Kruchkov, "Increasing Skyrmion Lattice Stability: Theory and Experiment", SPS Annual Meeting, 25 Aug 2016, Lugano, Switzerland
- A. Kruchkov, "Increasing Skyrmion Lattice Stability: Theory and Experiment", APS March Meeting, 17 Mar 2016, Baltimore, USA
- A. Kruchkov, , "Increasing Skyrmion Lattice Stability: Theory and Experiment", Winter School in Mathematical Physics, 13 Jan 2016, Les Diablerets, Switzerland
- **[invited]** A. Kruchkov, , "Condensation of Light", seminar at EPFL Photonics Chapter, invited by Dr. M. Reinke, EPFL, June 2014, Lausanne, Switzerland
- **[invited]** A. Kruchkov, , "From Maxwell equations to Bose-Einstein condensation of light", invited by Prof. P. Leiman, EPFL, December 2014, Lausanne, Switzerland
- **[invited]** A. Kruchkov, , "Bose-Einstein condensation of photons in an ideal gas", invited by Prof. H. Rønnow (before I joined EPFL), May 2013, Lausanne, Switzerland

## Conferences

- Joint Annual Meeting of SPS and ÖPG, 21-25 Aug 2016, Geneva, Switzerland
- APS March Meeting 2017, 12-17 March 2017, New Orleans, USA
- Swiss Physical Society Annual Meeting, 23-25 Aug 2016, Lugano, Switzerland
- APS March Meeting 2016, 13-18 March 2016, Baltimore, USA
- 20th International Conference on Magnetism, 5-10 July 2015, Barcelona, Spain
- International Conference on Strongly Correlated Electron Systems, 7-11 July 2014, Grenoble, France
- Mott Physics Beyond the Heisenberg Model, Oct 27-31 2013, Monte Verita, Switzerland

## Summer and Winter Schools

- Winter School in Mathematical Physics, Les Diablerets, Jan 10-15 2016, Les Diablerets, Switzerland
- New Physics due to Spin-Orbit Coupling (CORSO2015), August 4-14 2015, Cargese (Corsica), France
- Les Houches Doctoral Training in Statistical Physics, 22 Jun 22 - 3 Jul 3 2015, Les Houches (Chamonix), France
- 6th MaNEP Winter School: "Shedding light on correlated electrons", 18-23 Jan 2015, Saas-Fee, Switzerland
- Les Houches Doctoral Training in Statistical Physics, 27 Aug 27 - 7 Sep 2012, Les Houches (Chamonix), France

## Media

My research results were highlighted by different media outlets, including **EPFL main page** and **Daily Mail** newspaper:

- Light can be almost stopped at room temperature (2016)  
<http://actu.epfl.ch/news/light-can-be-almost-stopped-at-room-temperature>
- Alex Kruchkov qualifies for 2016 Lindau Nobel Laureate Meeting  
<https://actu.epfl.ch/news/alex-kruchkov-qualifies-for-2016-lindau-nobel-la-2/>
- A new state of light (2014)  
<http://www.dailymail.co.uk/sciencetech/article-2620823>
- New state of light revealed with photon-trapping method (2014)  
[http://www.huffingtonpost.com/2014/05/05/new-state-of-light-photon\\_n\\_5266415.html](http://www.huffingtonpost.com/2014/05/05/new-state-of-light-photon_n_5266415.html)
- Trapping photons: a model for containing light (2014)  
<http://actu.epfl.ch/news/trapping-photons-a-model-for-containing-light/>
- Pièges à photons: création d'un modèle pour retenir la lumière (2014)  
<http://actu.epfl.ch/news/pieges-a-photons-creation-d-un-modele-pour-retenir/>
- New state of light revealed with photon-trapping method (2014)  
<http://www.livescience.com/45287-how-to-trap-light.html>

## Reference

Recommendation letters are available upon request:

<b>Name</b>	Prof. Dr. Henrik M. Rønnow
<b>Affiliation</b>	EPFL, Switzerland
<b>Contact</b>	henrik.ronnow@epfl.ch

<b>Name</b>	Prof. Dr. Vincenzo Savona
<b>Affiliation</b>	EPFL, Switzerland
<b>Contact</b>	vincenzo.savona@epfl.ch



